Association of CK2 with Polycomb complexes and its functional implications

Hollie Chandler

University College London

and

Cancer Research UK London Research Institute

PhD Supervisor: Dr Gordon Peters

A thesis submitted for the degree of

Doctor of Philosophy

University College London

January 2013

Declaration

I, Hollie Chandler, confirm that the work presented in this thesis is my own. Where information has been derived from other sources, I confirm that this has been indicated in the thesis.

Abstract

Polycomb group (PcG) proteins are important for establishing the patterns of gene expression in different cell types and are critical for the maintenance of pluripotency. They participate in multi-component complexes, such as Polycomb repressive complex 1 (PRC1), which modify, and bind to, histone tails. A number of auxiliary proteins consistently associate with PRC1, including the three subunits of protein kinase CK2 (CK2). The work described in this thesis investigates the interaction of CK2 with PRC1 components and the implications for PRC1 function.

The data suggest that CK2 can directly bind to members of the CBX family, the mammalian orthologues of Polycomb in Drosophila. In the case of CBX7, residues within the conserved Pc box, near the C-terminus, were critical for this interaction. Interestingly, these residues were also required for the interaction between CBX7 and RING2, another core component of mammalian PRC1. Whether CBX7 is phosphorylated by CK2 remains equivocal and likewise, it has been difficult to demonstrate a role for CK2 in the ability of CBX7 to function as a transcriptional repressor.

In addition to their role as regulators of gene expression, PcG proteins have been recently implicated in the DNA damage response (DDR). Moreover, several proteins involved in the DDR are known to be CK2 substrates. To explore the link between CK2 and PRC1 in the context of DNA damage, a cell system was established in which multiple sequence-specific double-strand breaks (DSBs) could be induced in human diploid fibroblasts. Interestingly, detection of PRC1 proteins by both immunofluorescence and genome-wide ChIP-seq suggests that they are not recruited to DSBs in this system. Furthermore, the data indicate that extensive DNA damage does not mobilise PRC1 complexes from known binding sites.

Acknowledgements

Firstly, and most importantly, I would like to thank my supervisor, Gordon Peters. I feel incredibly fortunate to have been a PhD student in your lab Gordon and especially privileged to have been your last. Thank you for your advice, patience, guidance and encouragement over the years and particularly over the last few months, whilst I've been writing up.

I would also like to thank all of the past and present members of the Molecular Oncology laboratory. Marc, I cannot thank you enough for training me as a summer student and igniting my enthusiasm for bench research. Julie, Helen and Emma, I feel so fortunate that I was able to work with, and learn from, such good friends. Thank you for teaching me so much and for always being so supportive (even after you all left me!). Sharon, your longstanding knowledge of the laboratory and your generosity in sharing that knowledge has been invaluable. Thank you so much for all of your help and advice. Ana and Richard, thank you for keeping me sane and dosed up on caffeine during the write up! I'm so glad you both joined the lab and I'm really looking forward to getting back to the bench to work with you.

Thank you to Emily Bernstein and Mooki Wu for such an enjoyable collaboration. Especially for your unfailing enthusiasm Mooki and for my favourite quote of the PhD: "Let's rock these PTMs!" I would like to acknowledge members of my thesis committee, Caroline Hill and David Ish-Horowicz, for guiding my project and going through the horror of UCL E-Logs. I am also very grateful to Helen Walden for helping me to understand the world of protein crystallography.

There are many LRI services that have contributed to the work presented in this thesis. Special thanks goes to Nicola O'Reilly and the Peptide Synthesis lab, Nik Matthews and the Advanced Sequencing facility, Harshil Patel and the Bioinformatics and Biostatistics group, the Protein Analysis and Proteomics group, and everyone in the Equipment Park. I would also like to thank our lab aide, Mark, for keeping the 2nd floor, organised, tidy, stocked and clued up on the football.

I am also grateful for the opportunity that I had to work as a CRUK fellow in the Parliamentary Office of Science and Technology. This fellowship was only made possible by the support of Sally Leevers, Ava Yeo, and Gordon; thank you so much for this. I would also like to thank Sally, Sophie, Sabina and David, for making the LRI graduate program work so seamlessly and for creating such a great student community.

Thank you to all of my friends for helping me to work and play in equal measure. Special thanks go to my PhD buddy, Franzi, my lovely flat mates, Ashleigh Christina, Mel, Meghan and Hannah, and to Suzi; this PhD would have been so tough without you guys. Thank you for everything.

Thank you to my family for trying to understand my experiments, for teasing me mercilessly over “my cells”, taking care of me when I needed some respite and for all of your support and encouragement.

Finally, I would like to thank CRUK for funding my placement as a graduate student and the generosity of the public for donating to such an amazing charity.

Table of Contents

Abstract 3
Acknowledgements 4
Table of Contents 6
Table of figures 11
List of tables 13
Abbreviations 14
Chapter 1. Introduction 17
1.1 Polycomb group (PcG) protein complexes 18
1.1.1 Composition of PcG complexes 19
1.2 PcG complex recruitment to target genes 22
1.2.1 Sequence-specific recruitment of PcG complexes 22
1.2.2 PcG complex recruitment by non-coding RNAs 23
1.2.3 Recruitment of PRC1 to H3K27me3 23
1.3 PRC1 repression of target genes 24
1.3.1 PcG-mediated chromatin compaction 25
1.3.2 Higher-order regulation of chromatin by PcG proteins 27
1.4 PcG proteins in stem cell maintenance and differentiation 27
1.4.1 Regulation of pluripotency and cell fate 27
1.4.2 Regulation of the self-renewal capacity of stem cells 29
1.5 The *INK4a-ARF-INK4b* locus and cellular senescence 29
1.5.1 The *INK4a-ARF-INK4b* locus 29
1.5.2 Cellular senescence 30
1.5.3 Characteristics of senescent cells 32
1.5.4 Role of senescence in tumour suppression 33
1.6 PcG complexes in cancer 34
1.7 Changes in PcG proteins at senescence 35
1.8 Association of PcG complexes with *INK4a-ARF-INK4b* 36
1.9 The DNA damage response (DDR) 37
1.9.1 An overview of the DDR 37
1.9.2 Proteins involved in the DDR 38

1.10 Evidence implicating PcG proteins in the DDR 41
1.10.1 Recruitment of PcG proteins to DSBs 41
1.10.2 Importance of PcG proteins for DNA damage repair 42
1.11 Protein kinase CK2 (CK2) 42
1.11.1 Auxiliary proteins that co-purify with PRC1 complexes 42
1.11.2 Interaction of CK2 with PRC1 complexes 43
1.11.3 CK2 complex composition 43
1.11.4 Regulation of CK2 activity and substrate specificity 44
1.11.5 CK2 consensus sites 45
1.11.6 Importance of CK2 for cell viability and its role in tumorigenesis 47
1.11.7 CK2 in the DNA damage response 49
1.12 Thesis aims 50
Chapter 2. Materials & Methods 51
2.1 Molecular biology 51
2.1.1 Oligonucleotides 51
2.1.2 Plasmid vectors 52
1.1.1 Amplification of DNA by PCR 53
2.1.3 Site-directed mutagenesis by over-lap extension 54
2.1.4 Cloning shRNA expression vectors 56
2.1.5 Restriction digests and ligation of plasmids 56
2.1.6 Agarose gel electrophoresis and gel extraction 57
2.1.7 DNA sequencing 57
2.1.8 Production of chemically competent bacteria 58
2.1.9 Transformation of chemically competent bacteria 59
2.1.10 Small-scale preparation of plasmid DNA (miniprep) 59
2.1.11 Large-scale preparation of plasmid DNA (maxiprep) 59
2.2 Cell culture 60
2.2.1 Cell lines and primary fibroblasts 61
2.2.2 Storage and recovery of cells 61
2.2.3 Transfection of cell lines 62
2.2.4 Viral infection of human diploid fibroblasts (HDFs) 62
2.2.5 Chemical treatment of cells in culture 63

2.2.6 Harvesting cells 63
2.3 RNA techniques 64
2.3.1 Preparation of total cellular RNA 64
2.3.2 Reverse transcription PCR (RT-PCR) 64
2.3.3 Quantitative Real-Time PCR (qPCR) of cDNA 65
2.3.4 qPCR of DNA purified from ChIP 66
2.4 Biochemistry 67
2.4.1 Preparation of total cell lysate 67
2.4.2 SDS-PAGE 68
2.4.3 Gel Coomassie staining 69
2.4.4 Immunoblotting and stripping 69
2.4.5 Antibodies 70
2.4.6 Phosphoenrichment assay 72
2.4.7 Immunoprecipitation 72
2.4.8 Gel filtration 73
2.4.9 Fixed chromatin immunoprecipitation (ChIP) 75
2.4.10 Production of recombinant protein 77
2.4.11 GST pull-down assay 78
2.4.12 Peptide array synthesis 78
2.4.13 Peptide array kinase assay 79
2.4.14 Peptide array binding assay 80
2.4.15 *In vitro* kinase assay and analysis by ^{32}P incorporation 80
2.4.16 *In vitro* kinase assay and analysis by mass spectrometry 80
2.4.17 β-galactosidase assay 81
2.4.18 Immunofluorescence 81
2.4.19 Confocal microscopy 82
2.4.20 Solutions 83
Chapter 3. Interaction of CK2 with PRC1 89
3.1 Introduction 89
3.2 Association of CK2 with PRC1 complexes 89
3.2.1 Association of CK2 and PRC1 proteins 89
3.2.2 Interaction of CK2 and CBX7 in a high molecular weight complex 92

3.3 Interaction of CK2 with the Pc box domain of CBX proteins 96
3.3.1 Binding of CK2α to C-terminal peptides representing the Pc box of CBX7 96
3.3.2 CK2 binding to the Pc box of other CBX proteins 100
3.4 Mapping the critical CK2 binding residues within the Pc box of CBX7 102
3.4.1 Identifying CBX7 Pc box residues that interact with CK2 102
3.4.2 Designing CBX7 point mutants 103
3.4.3 Testing the CK2 binding potential of mCbx7 point mutants 108
3.5 Conclusions 109
Chapter 4. Phosphorylation of CBX7 113
4.1 Introduction 113
4.1.1 CK2 phosphorylation of mCbx7 *in vitro* 114
4.1.2 Identifying CK2 phosphorylated peptides within CBX7 118
4.2 Evidence for phosphorylation of endogenous CBX7 122
4.3 CK2-independent phosphorylation of mCbx7 126
4.4 Conclusions 132
Chapter 5. Importance of CK2 for PRC1 repression of target genes 136
5.1 Introduction 136
5.2 CK2 levels at senescence 137
5.3 Expression from *INK4a* following CK2 knockdown 139
5.4 Repression of PcG protein targets following CK2 inhibition 143
5.5 Conclusions 144
Chapter 6. PRC1 recruitment to double strand breaks 146
6.1 Introduction 146
6.2 Establishing an inducible DNA damage system in HDFs 147
6.3 Co-localisation of PcG proteins at DSBs 150
6.4 ChIP-seq analysis of CBX7 in HDFs following genome-wide DNA damage 154
6.5 Conclusions 156
Chapter 7. Discussion 161
7.1 The interaction of CK2 with PRC1 161
7.2 Phosphorylation of CBX7 by CK2 166
7.3 Influence of CK2 on PRC1-repression of target genes 168

7.4 PcG proteins in the DDR.....171
Chapter 8. Appendix 175
Reference List 181

Table of figures

Figure 1.1 DNA damage response at double strand breaks 40
Figure 2.1 Schematic diagram of site-directed mutagenesis by over-lap extension 55
Figure 3.1 Co-immunoprecipitation of CK2 with FLAG-tagged CBX proteins and endogenous RING2..... 91
Figure 3.2 Gel filtration of 293T cell lysate and CBX7-FLAG complexes..... 95
Figure 3.3 Binding of CK2α to peptide arrays of HPH2, RING2 and BMI1 98
Figure 3.4 Binding of CK2α to a peptide array of CBX7 99
Figure 3.5 Binding of CK2α to peptide arrays of CBX6, CBX8, and RYBP 101
Figure 3.6 Binding of CK2α to a substitution array of CBX7(218-237) 104
Figure 3.7 CK2 interacting residues of CBX7 in the context of a CBX7-RING2 complex 106
Figure 3.8 Conservation of Pc box residues important for CK2 binding..... 107
Figure 3.9 GST pull-down of mutant mCbx7 proteins from 293T cell lysate 111
Figure 3.10 Thermal denaturation of mCbx7 (wild-type) and mCbx7 point mutants 112
Figure 4.1 Candidate CK2 phosphorylation sites within mCbx7 and CBX7 114
Figure 4.2 *In vitro* phosphorylation of CBX7 by CK2..... 116
Figure 4.3 CK2 phosphorylation of mCbx7 (wild-type, T140D and V137DV139DV140D) and Cdc37 117
Figure 4.4 *In vitro* kinase assay of CBX7 peptide array with CK2..... 120
Figure 4.5 *In vitro* kinase assay of CBX7 peptide array in the absence of CK2... 121
Figure 4.6 Phosphorylation status of CBX7 following CK2 inhibition 124
Figure 4.7 Lambda phosphatase treatment of cell lysate..... 125
Figure 4.8 $p16^{INK4a}$ levels in HDFs following expression of mCbx7 mutants..... 129
Figure 4.9 *INK4a* RNA levels in HDFs following expression of mCbx7 mutants.. 130
Figure 4.10 ChIP of mCbx7 (wild-type, T119A or T119E) at *INK4a-ARF-INK4b* . 134
Figure 4.11 Life span chart of HDFs following expression of mCbx7 mutants..... 135
Figure 5.1 CK2 levels in senescent fibroblasts 138
Figure 5.2 Levels of *INK4a* mRNA and $p16^{INK4a}$ following CK2 knockdown..... 141

Figure 5.3 H3K27me3 enrichment at *INK4a-ARF-INK4b* following *CSNK2A1* knockdown 142
Figure 5.4 Expression of PRC1 target genes following CK2 inhibition..... 145
Figure 6.1 Immunofluorescence of γH2AX foci following 4OHT induction of DNA damage by *Asi*SI. 149
Figure 6.2 Detecting co-localisation of PcG proteins with γH2AX foci following 4OHT induction of DNA damage by *Asi*SI..... 153
Figure 6.3 HCHA1 antibody detection of FLAG-tagged CBX7 157
Figure 6.4 CBX7 enrichment across *INK4a-ARF-INK4b* following ChIP of CBX7 using Ab21873 or HCHA1 antibodies..... 158
Figure 6.5 ChIP-seq analysis of CBX7 in HDFs before and after DNA damage.. 160
Figure 8.1 Calibration of Superose 6 column 176
Figure 8.2 Bacterial expression of GST-mCbx7 177
Figure 8.3 Bacterial expression of GST-mCbx7 point mutants 179
Figure 8.4 Purification of mCbx7 180

List of tables

Table 1.1 PcG proteins of *Drosophila*, mouse and human PRC1 and PRC2. 21
Table 1.2 Number of CK2 consensus sites within the human PcG proteins 47
Table 2.1 Oligonucleotides 52
Table 2.2 Description of cell lines and primary fibroblasts 61
Table 2.3 List of primers used to amplify cDNA (previously generated from mature mRNA) 66
Table 2.4 List of primers used to amplify DNA (purified by ChIP) 67
Table 2.5 List of commonly used primary antibodies 71

Abbreviations

4OHT	4-hydroxytamoxifen
ATP	Adenosine 5'-triphosphate
bp	Base pair(s)
BSA	Bovine serum albumin
C-terminus	Carboxy terminus
CDK	Cyclin dependent kinase
cDNA	Complimentary DNA
ChIP	Chromatin immunoprecipitation
ChIP-chip	ChIP followed by microarray hybridisation
ChIP-seq	ChIP followed by highthroughput sequencing
CRUK	Cancer Research UK
CTD	C-terminal domain (of RNA polymerase II)
DMEM	Dulbecco's modified Eagle's medium
DMSO	Dimethyl sulphoxide
DNA	Deoxyribonucleic acid
DNMT	DNA methyltransferase
dNTP	Deoxyribonucleoside 5-triphosphate
dPc	Drosophila Polycomb
DRB	5,6-Dichlorobenzimidazole 1-β-D-ribofuranoside
DSB	Double-strand break
DTT	Dithiothreitol
E. coli	Escherichia Coli
E(z)	Enhancer of zeste
ECL	Enhanced chemiluminescence
EED	Embryonic ectoderm development
ESC	Embryonic stem cell
Esc	Extra sex combs
EZH	Enhancer of zeste homologue
FBS	Foetal bovine serum
Fwd	Forward
GBM	Glioblastoma multiforme

GFP	Green fluorescent protein
GST	Glutathione-S-transferase
GST-mCbx7	N-terminal GST-tagged mCbx7
GTF	General transcription factor
H2AK119Ub	Monoubiquitinated histone H2A at lysine 119
H3K27me3	Trimethylated histone H3 at lysine 27
HA	Hemagglutinin
HDF	Human diploid fibroblast
HDFs	Human diploid fibroblasts
HK3K9me3	Trimethylated histone H3 at lysine 9
Hox	Homeobox
hTERT	human telomerase reverse transcriptase
INK4	Inhibitor of CDK4
IP	Immunoprecipitation
Kb	Kilobase
kDa	Kilo Daltons
lncRNA	Long non-coding RNA
LRI	London Research Institute
LTR	Long-terminal repeat
mCbx7	Mouse Cbx7
MDM2	Murine double minute 2
MEF	Mouse embryonic fibroblast
mESC	Mouse embryonic stem cell
MS	Mass spectrometry
MW	Molecular weight
N-terminus	Amino terminus
ncRNA	Non-coding RNA
NEB	New England Biolabs
OIS	Oncogene-induced senescence
^{o}C	Degrees Centigrade
PAGE	Polyacrylamide gel electrophoresis
Pc	Polycomb
PcG	Polycomb group
PCR	Polymerase chain reaction

PD	Population doubling
Ph	Polyhomeotic
Pho	Pleiohomeotic
PhoRC	Pleiohomeotic repressive complex
PIC	Pre-initiation complex
Pol II	RNA polymerase II
PRC	Polycomb repressive complex
PRE	Polycomb responsive element
Psc	Posterior sex combs
Rb	Retinoblastoma
Rev	Reverse
RNA	Ribonucleic acid
Sce	Sex combs extra
SDS	Sodium dodecyl sulphate
shRNA	Short hairpin RNA
siRNA	Short interfering RNA
SSB	Single-strand break
Su(z)12	Suppressor of zeste 12
TAP	Tandam affinity purification
TBB	4,5,6,7-tetrabromobenzotriazole
TCA	Trichloroacetic acid
TrxG	Trithorax group

Chapter 1. Introduction

Multicellular organisms are composed of a variety of cell types that have specialised functions. Although these cells contain the same genetic information, their differences are established by individual patterns of gene expression. DNA is packaged into a highly organised structure known as chromatin. This involves the wrapping of DNA around histone octamers, which are composed of two copies each of histone H2A, H2B, H3 and H4, to form a nucleosome. Nucleosomes are further organised to form chromatin. Regions of open chromatin (euchromatin), and regions of condensed chromatin (heterochromatin), generally correspond to transcriptionally active (or potentially active) and transcriptionally silenced genes respectively (Khorasanizadeh, 2004).

Regulation of gene expression can be mediated by changes in the chromatin structure, which are typically associated with specific modifications to histone tails. Histone tails are unstructured N-terminal regions of the core histones that protrude from the nucleosome. These histone tails can be chemically modified, for example, by acetylation, methylation, ubiquitination and phosphorylation. Some of these modifications can directly affect the state of chromatin. For example, *in vitro* studies of histone acetylation suggest that this modification neutralises the positive charge of histone tails and therefore reduces their affinity for negatively charged phosphate groups of DNA (Hong et al., 1993). This can result in a more relaxed and open chromatin conformation; lending itself more readily to transcription. Other histone modifications are specifically recognised by certain proteins that can remodel the chromatin or promote/repress transcription directly. The terminology for these modifications describes both the type of modification, and the histone and residue at which it occurs. For example, tri-methylation of lysine 27 on histone H3 is denoted: H3K27me3. Together, these modifications are thought to generate a code that defines the chromatin state, the associated proteins, and the transcriptional status of a region of DNA; this is the histone code hypothesis (Jenuwein and Allis, 2001).

Both H3K27me3 and H3K9me3 are markers of transcriptionally silenced chromatin. H3K9me3 is associated with constitutive and facultative heterochromatin (Bannister

et al., 2001, Lachner et al., 2001, Nakayama et al., 2001, Peters et al., 2002). Constitutive heterochromatin is principally found within centromeric, pericentromeric (Gilbert and Allan, 2001) and telomeric regions (Schoeftner and Blasco, 2009) that contain highly repetitive DNA sequences. Facultative heterochromatin forms in the euchromatin environment to stably repress target genes. The most extensively studied example of facultative chromatin is at the inactive X chromosome in somatic cells of female mammals (Chow and Heard, 2009).

Gene silencing within euchromatic regions is generally associated with the H3K27me3 mark. This mark is both catalysed and recognised by members of the Polycomb group (PcG) of proteins. By maintaining patterns of transcriptionally silenced genes, PcG proteins preserve the memory of cellular identity. These proteins are also clearly relevant to pluripotency and to senescence, largely because of effects on the *CDKN2A* locus.

1.1 Polycomb group (PcG) protein complexes

Polycomb group (PcG) proteins were originally identified in *Drosophila* as regulators of the *Hox* genes. *Hox* gene expression determines body segment patterning of the developing *Drosophila* embryo. In cooperation with Trithorax group (TrxG) proteins, which are positive regulators of transcription, PcG proteins are responsible for maintaining patterns of *Hox* gene expression and therefore the lineage commitment of specific cells (reviewed in (Kennison, 1995) and (Ringrose and Paro, 2004)). Most PcG proteins have been ascribed names based on phenotypes that arise from dominant or recessive PcG gene mutations in *Drosophila*. For example, *Extra sex combs* (*Esc*) (Slifer, 1942) and *Polycomb* (*Pc*) mutants (Lewis, 1947) have sex combs on their second and third legs that are absent in wild-type *Drosophila*. There are 18 documented PcG genes in *Drosophila* (Ringrose and Paro, 2004). *Drosophila* PcG proteins pertinent to this thesis are outlined in Table 1.1.

1.1.1 Composition of PcG complexes

The co-localisation of several *Drosophila* PcG proteins on polytene chromosomes suggested that PcG proteins might associate in complexes (Franke et al., 1992, Martin and Adler, 1993, Rastelli et al., 1993, Lonie et al., 1994). The first direct evidence for a PcG complex was the purification of the *Drosophila* Polycomb repressive complex 1 (PRC1). PRC1 contains four core PcG proteins, Pc, Ph, Posterior sex combs (Psc), and Sex combs extra (Sce), and sub-stoichiometric amounts of Sex Combs on Midleg (SCM) (Francis et al., 2001, Shao et al., 1999). The core components of PRC1 were shown to be sufficient to block the remodelling of nucleosomes by SWI/SNF *in vitro* (Francis et al., 2001). Three further multi-PcG protein complexes have been described in *Drosophila*: Polycomb repressive complex 2 (PRC2), pleiohomeotic (Pho) repressive complex (PhoRC) and dRAF (dRING-associated factors). PRC2 contains three core PcG proteins, Enhancer of zeste (E(z)), Suppressor of zeste 12 (Su(z)12) and Extra sex combs (Esc) (Czermin et al., 2002, Muller et al., 2002). PhoRC contains two core PcG proteins, Pho and dSfmbt (Klymenko et al., 2006). dRAF is a non-canonical PRC1, comprising Sce, Psc and the histone demethylase KDM2 (Lagarou et al., 2008).

Analogous complexes have been described in mammals, with most attention focused on PRC1 and PRC2 (Levine et al., 2002, Cao et al., 2002, Kuzmichev et al., 2002). Mammalian PRC2 contains a highly conserved homologue of each *Drosophila* PRC2 protein, two in the case of E(z): Enhancer of zeste homologue 1 (EZH1) and EZH2, Embryonic ectoderm development (EED) and Suppressor of zeste 12 (SUZ12). However, there has been a substantial expansion of the PcG genes during evolution and mammals encode multiple homologues of each *Drosophila* PRC1 protein. There are five Pc homologues (CBX2, 4, 6, 7 and 8), three Ph homologues (HPH1, 2 and 3), six Psc homologues (NSPC1, MEL18, RNF3, BMI1, RNF159 and MBLR) and two Sce homologues (RING1 and 2). Virtually all of these proteins have alternative names, in different studies and species (summarised in Table 1.1), and there is currently no accepted consensus. Throughout this thesis, human proteins/genes will be in upper case whereas mouse proteins/gene and *Drosophila* equivalents will be in mixed case.

Importantly, just one representative of each PcG protein family appears to be present in any one mammalian PRC1 complex (Dietrich et al., 2007, Gao et al., 2012, Maertens et al., 2009, Sanchez et al., 2007, Vandamme et al., 2011). Currently, there is limited evidence of preferential interactions between specific components (Gao et al., 2012). Allowing for free assortment, there could be as many as 180 different permutations of PRC1. This has led to speculation that different PRC1 subtypes may have functional specificity, perhaps operating in different cell types or at a subset of PcG repressed genes. Indeed, CBX7 appears to be the predominant Pc component in embryonic stem cells (ESCs). During ESC differentiation, CBX7 expression is downregulated, resulting in the upregulation of CBX2, 4 and 8 (O'Loghlen et al., 2012, Morey et al., 2012). In addition, chromatin immunoprecipitation followed by high-throughput sequencing (ChIP-seq) in ESCs suggested CBX7 and CBX6 occupy different target genes (Morey et al., 2012). However, ChIP-seq analyses in human fibroblasts (Pemberton et al., Submitted) have shown that CBX6, 7 and 8 invariably occupy the same loci.

PcG proteins have also been detected in other types of affinity purified complex based on proteins such as E2F6, L3MBTL2, BcoR, FBXL10 and RYBP (Trojer et al., 2011, Trimarchi et al., 2001, Gearhart et al., 2006, Sanchez et al., 2007). Functional characterisation of these complexes has been limited, a notable exception being a set of PRC1-like complexes that comprise representatives from the Sce and Psc families bound to either RYBP (RING and YY1 binding protein) or YAF2 (YY1-associated factor 2) instead of Pc. Interestingly, RYBP and CBX7 form nearly identical intermolecular beta sheet structures with the C-terminus of RING2 (Wang et al., 2010) and biochemical analysis suggest that CBX7 and RYBP bind to RING proteins in a mutually exclusive manner (Tavares et al., 2012, Gao et al., 2012). These complexes will hereafter be referred to as CBX-PRC1 and RYBP-PRC1.

PRC1

Drosophila	Mouse	Human
Polycomb (Pc)	**Cbx2**/M33/pc **Cbx4**/MPc2 **Cbx6** Cbx7/**mCbx7** **Cbx8**/Pc3	**CBX2**/M33/PC **CBX4**/hPC2 **CBX6** **CBX7** **CBX8**/HPC3
Polyhomeotic (Ph)	**Mph1**/Phc1/Rae28/Edr1 **Mph2**/Phc2/Edr2 **Mph3**/Phc3/Edr3	**HPH1**/PHC1/EDR1/RAE28 **HPH2**/PHC2/EDR2/PH2 **HPH3**/PHC3/EDR3
Sex combs extra (Sce)	**Ring1a**/Ring1 **Ring1b**/Ring2	RING1A/**RING1**/RNF1 RING1B/**RING2**/RNF2
Posterior sex combs (Psc)	**Nspc1**/Pcgf1 **Mel18**/Pcgf2/Rnf110/Zfp144 Pcgf3/**Rnf3**/RNF3A **Bmi1**/Pcgf4/Rnf51 Pcgf5/**Rnf159** **Mblr**/Pcgf6/Rnf134	**NSPC1**/PCGF1/RNF68 **MEL18**/PCGF2/RNF110 PCGF3/**RNF3**/RNF3A **BMI1**/PCGF4/RNF51 PCGF5/**RNF159** **MBLR**/PCGF6/RNF134

PRC2

Drosophila	Mouse	Human
Extra sex combs (Esc)	**Eed**/17Rn5	**EED**/HEED/WAIT1
Enhancer of zeste (E(z))	**Ezh1** **Ezh2**/Enx-1/KMT6	**EZH1** **EZH2**/ENX-1/KMT6
Suppressor of zeste (Su(z))	**Suz12**	**SUZ12**/CHET9/JJAZ1

Table 1.1 PcG proteins of *Drosophila*, mouse and human PRC1 and PRC2.

Alternative PcG protein names are shown. The PcG protein names used in this thesis are in bold.

1.2 PcG complex recruitment to target genes

1.2.1 Sequence-specific recruitment of PcG complexes

Drosophila PcG complexes associate with cis-regulatory DNA sequences termed Polycomb responsive elements (PREs) that are required for PcG-mediated repression (Muller and Kassis, 2006). The few PREs that have been characterised to date show limited sequence conservation, apart from binding sites for proteins such as Pho, Zeste and GAGA factor. Pho is the only PcG protein that has sequence-specific DNA binding activity (Brown et al., 1998), and, as it has been shown to interact with both PRC1 and PRC2 *in vitro*, it is implicated in the recruitment of these complexes to PREs (Wang et al., 2004b, Mohd-Sarip et al., 2002). Other PRE-binding proteins, for example Zeste (Saurin et al., 2001), also interact with PcG proteins. The role of other PRE-binding proteins is less clear as *Drosophila* with null-mutations in the corresponding genes do not demonstrate PcG phenotypes (Goldberg et al., 1989)

Because of the lack of sequence conservation, it has proved difficult to identify PREs in mammals, but two candidates have recently been described. The first of these, PRE-*kr*, regulates PcG repression of *MafB/Kreisler* gene in mouse F9 cells (Sing et al., 2009). The second, D11.12, lies between *HOXD11* and *HOXD12* in human ESCs (Woo et al., 2010). Both PRE-*kr* and D11.12 contain binding sites for YY1, the mammalian homologue of *Drosophila* Pho (Brown et al., 1998). Although it is tempting to speculate that YY1 is involved in the recruitment of PcG complexes to PREs, perhaps via interactions with RYBP or YAF2, there is currently no evidence that this is the case (Tavares et al., 2012). Recently Bmi1 was shown to directly bind the Runx1/CBFβ transcription factor complex. Furthermore, this study also demonstrated similar patterns of chromatin occupancy between Ring1b and Runx1/CBFβ (Yu et al., 2012). Other sequence-specific DNA binding proteins such as Oct4, Sox2 and Nanog have been implicated in PcG complex recruitment because of their similar chromatin localisation (Boyer et al., 2006, Lee et al., 2006b). However there is little evidence for an interaction between these transcription factors and PcG proteins.

1.2.2 PcG complex recruitment by non-coding RNAs

While a role for sequence-specific DNA binding proteins in PcG recruitment is by no means excluded, studies in both *Drosophila* and mammalian cells have suggested an alternative possibility. For example, in *Drosophila*, non-coding RNAs (ncRNAs) of the *bithoraxoid* complex are critical for PcG-mediated regulation, although there is some debate about the mechanism. One school of thought is that antisense transcription through PREs prevents PcG binding and repression, while other studies suggest that ncRNAs are essential for recruitment of PcG complexes and long-range interactions between PREs (Grimaud et al., 2006, Petruk et al., 2006, Schmitt et al., 2005, Sanchez-Elsner et al., 2006). In mammalian systems, the classical example is the silencing of the inactive X chromosome, which relies on recruitment of PcG complexes by the *Xist* ncRNA. The discovery of literally thousands of long ncRNAs (lncRNAs), such as *HOTAIR, HOTTIP, TUG1*, suggests this may be a much more widespread phenomenon. *HOTAIR* is transcribed from within the *HOXC* locus and appears to function in *trans* to promote PcG repression of *HOXD* genes (Rinn et al., 2007). Given the inherent sequence specificity of lncRNAs, these would serve as elegant PcG complex recruiters. However, some lncRNAs, such as *HOTTIP*, appear to have the opposite effect and promote transcription by recruiting TrxG complexes (Schuettengruber, 2011). Others, such as the *ANRIL* transcript from the *INK4a-ARF-INK4b* locus and short RNAs expressed from CpG island/promoter regions, are viewed as acting in *cis* rather than *trans* (Kanhere et al., 2010, Yap et al., 2010, Kotake et al., 2011). Most of these studies conclude that the ncRNAs interact directly with PRC2 components, such as SUZ12 and EZH2. However, the chromodomains of Pc proteins have also been shown to interact with RNA (Akhtar et al., 2000) and the recruitment of Cbx proteins to target genes depends, in part, on this interaction (Bernstein et al., 2006b).

1.2.3 Recruitment of PRC1 to H3K27me3

Importantly, the Pc chromodomain has been shown to bind trimethylated histone tails at lysine 9 and 27 on histone H3 (H3K9me3 and H3K27me3)(Min et al., 2003, Fischle et al., 2003, Cao et al., 2002, Bernstein et al., 2006b, Ringrose et al., 2004).

As the PRC2 complex is an H3K27me3-specific methyltransferase, catalysed by the SET domain in the E(z) protein, an attractive model has been proposed in which the trimethylation of H3K27 by PRC2 is responsible for recruitment of PRC1. In support of this idea, mutations in the chromodomain of Pc abolish the ability of Pc to bind chromatin *in vivo* (Cao et al., 2002, Czermin et al., 2002, Fischle et al., 2003, Kuzmichev et al., 2002, Messmer et al., 1992, Min et al., 2003, Muller et al., 2002). Furthermore, the methyltransferase activity of PRC2 is important for the binding of PRC1 at PREs (Cao et al., 2002), but PRC1 binding to regions of H3K27me3 does not require the continued presence of PRC2 (Wang et al., 2004b). In addition, the H3K27-specific demethylases, UTX and JMJD3, have been shown to reduce the binding of PRC1 to target genes (Agger et al., 2007, Lee et al., 2007). However, although genome-wide mapping of H3K27me3 in *Drosophila* has shown this mark to be largely coincidental with both binding of PRC1 and PRC2, the domain of H3K27me3 is broader than that bound by PRC1, suggesting this mark is not sufficient for recruitment (Schwartz et al., 2006). It has also been argued that the binding affinity between Pc and H3K27me3 is too low to account for locus-specific recruitment. Importantly, at some loci, PRC1 binding can occur in the absence of a functional PRC2 complex, suggesting that at least in some instances the H3K27me3 mark is not necessary for PRC1 recruitment (Pasini et al., 2007, Schoeftner et al., 2006, Vincenz and Kerppola, 2008).

1.3 PRC1 repression of target genes

Chromodomains are also present in the HP1 proteins (α, β, and γ), which bind preferentially to H3K9me3 and are necessary for the formation of heterochromatin. Interestingly HP1γ is found within euchromatin, whereas HP1α and HP1β are predominantly found at pericentromeric sites (Minc et al., 1999, Vakoc et al., 2005). Although heterochromatin and PcG-mediated repression are generally considered separate modes of transcriptional silencing (Beisel and Paro, 2011), the compaction of chromatin is common to both. Compact chromatin has the potential to limit access to the transcriptional machinery and to impede the progression of RNA polymerase II (Pol II) through nucleosomes, which requires the loosening of histone-DNA interactions (Lorch et al., 1987, Bondarenko et al., 2006).

Regulation of gene transcription by Pol II can occur at the initiation, elongation and termination stages. Pol II is assembled at promoters with multiple general transcription factors (GTFs), forming a large protein complex known as the pre-initiation complex (PIC). PIC comprises a minimal set of GTFs, including TFIIE and TFIID (containing the TATA-binding protein TBP). Recruitment of Pol II is also greatly influenced by the Mediator complex, nucleosome remodelling complexes, histone modifying enzymes and DNA-binding transcriptional activators. A tightly controlled exchange of factors accompanies the transition from transcriptional initiation to early elongation. This, in part, is orchestrated by the phosphorylation of the C-terminal domain (CTD) of Pol II, which contains multiple heptad repeats with the consensus sequence YSPTSPS. Phosphorylation of CTD at serine 5, by the CDK7 subunit of TFIIH, is thought to destabilise the interaction of Pol II with promoter-bound factors and thereby facilitate promoter escape. The transition from early to productive elongation is triggered by recruitment of p-TEFb, which phosphorylates the CTD at serine 2. p-TEFb recruitment leads to the release of pausing factors and association of factors that promote productive elongation (reviewed in (Nechaev and Adelman, 2011)). Recent *in vitro* work has shown that PRC1 inhibits the binding of Mediator and assembly of PIC, although TFIID promoter binding is unaffected (Lehmann et al., 2012). However, ChIP studies have demonstrated that poised Pol II (phosphorylated at serine 5) can be enriched at PcG targets in mouse ESCs. Such targets lack the form of Pol II associated with active transcription (phosphorylated at serine 2). Importantly, Ring1b was required to maintain this poised state of transcription (Stock et al., 2007).

1.3.1 PcG-mediated chromatin compaction

The ability of PRC1 to compact chromatin was first demonstrated by Francis and colleagues. Using electron microscopy, they visualised PRC1-dependent nucleosome compaction *in vitro* (Francis et al., 2004). *In vivo*, chromatin compaction at the *Hoxb* and *Hoxd* loci is dependent on Ring1b and contributes to transcriptional repression of the *Hox* genes (Eskeland et al., 2010).

The only catalytic function attributed to the PRC1 complex is E3 ubiquitin ligase activity, based on the concerted action of the RING domains of Psc and Sce proteins. Importantly, the purified complexes have been shown to catalyse the monoubiquitination of histone H2A at lysine 119 (H2AK119Ub) (Buchwald et al., 2006, de Napoles et al., 2004, Wang et al., 2004a). H2AK119Ub is invariably found at PcG target genes (Endoh et al., 2012, Kallin et al., 2009) and is regarded as the histone mark that promotes chromatin condensation and/or affects protein-nucleosome interactions to directly to repress transcription. Indeed, depletion of Ring1a and Ring1b from mESCs results in loss of H2AK119Ub and de-repression of PcG targets (Stock et al., 2007). Moreover, a recent study in mouse ESCs suggested that the catalytic activity of Ring1b is important for repression of PcG targets, albeit to varying degrees (Endoh et al., 2012). However, nucleosome compaction by PRC1 *in vitro* is independent of histone-tails (Francis et al., 2004). Furthermore, the catalytic activity of Ring1b is dispensable for both chromatin compaction and gene repression at the *Hox* loci (Eskeland et al., 2010).

Recent data from Tavares and colleagues, has questioned whether canonical PRC1 complexes are responsible for H2AK119Ub at target genes. In $Eed^{-/-}$ mESCs, the enrichment of H2AK119Ub at PcG target genes is equivalent to that in wild-type mESCs. Ring1b was also enriched at these PcG target genes, but to a greatly reduced extent in $Eed^{-/-}$ mESCs, whereas H3K27me3 and CBX7 could only be detected at PcG targets in the wild-type cells. RYBP was enriched at PcG targets to a similar extent in both wild-type and $Eed^{-/-}$ mESCs (Tavares et al., 2012). These data have suggested that RYBP is recruited independently of PRC2 and that RYBP-PRC1 may be responsible for H2AK119Ub at PcG targets, at least in mESCs. Indeed, there is evidence that RYBP-PRC1 has stronger enzymatic activity towards H2AK119 than CBX2- or CBX8-PRC1, although these complexes demonstrate an equivalent potential to compact nucleosomes *in vitro* (Gao et al., 2012). Thus, the extent to which H2AK119Ub is mediated by canonical PRC1 complexes, and its importance for PcG repression, remains controversial (Gutierrez et al., 2012).

1.3.2 Higher-order regulation of chromatin by PcG proteins

In addition to chromatin compaction, PcG-mediated repression is likely to involve higher-order chromatin configurations. Long-range interactions have been observed between *Drosophila* PREs, which assemble with multimeric PcG complexes called Polycomb bodies. These can be observed by immunofluorescence as discrete nuclear foci (Buchenau et al., 1998). There is evidence that Ph and Pc both have the propensity to self-associate (Kim et al., 2002, Kyba and Brock, 1998, Min et al., 2003, Reijnen et al., 1995). This characteristic may serve to promote the assembly of multimeric PRC1 complexes. Importantly, Polycomb bodies co-localise with PcG repressed genes that are maintained in a silent transcriptional state and disruption of long-range PRE interactions can result in derepression of PcG targets (Bantignies et al., 2011, Lanzuolo et al., 2007). In *Drosophila* therefore, it seems that higher-order chromatin structure can be important for PcG repression.

In mammalian cells, PcG proteins have also been observed in nuclear speckles by immunofluorescence. Human fibroblasts contain approximately 100 nuclear PcG protein speckles, which are evenly distributed throughout the nucleus (Voncken et al., 1999, Buchenau et al., 1998, Saurin et al., 1998). However, the composition of these assemblies and their importance for PcG repression remains to be established. In human tumour cell lines, PRC1 proteins are typically found in a few (~5-15 per cell) large nuclear bodies that associate with pericentromeric heterochromatin (Alkema et al., 1997, Saurin et al., 1998, Cmarko et al., 2003, Hernandez-Munoz et al., 2005). Whether these more prominent PRC1 foci reflect changes in PRC1 genome-wide binding patterns or changes in PRC1-PRC1 complex interactions remains to be established.

1.4 PcG proteins in stem cell maintenance and differentiation

1.4.1 Regulation of pluripotency and cell fate

Embryonic stem (ES) cells are derived from the inner cell mass (ICM) of the mammalian blastocyst. They are pluripotent, having the potential to differentiate

into all derivatives of the three primary germ layers, and have limitless replicative potential (Nishikawa et al., 2007). These characteristics of ES cells are ensured by a specialised chromatin-state that is maintained by epigenetic regulators such as the PcG and TrxG proteins. Bivalent domains, regions of chromatin containing both H3K27me3 and H3K4me3, are a primary feature of the ES chromatin landscape. Such domains are typically found at the promoters of genes encoding lineage-specific transcription factors (Bernstein et al., 2006a). As discussed above, H3K27me3 is a repressive mark with implications for PcG protein recruitment. Conversely, H3K4me3 is an active mark that is responsible for recruiting nucleosome remodelling proteins (Santos-Rosa et al., 2003) and histone deacetylases (Pray-Grant et al., 2005) to promote transcription. H3K4me3 is catalysed by TrxG proteins (Schuettengruber et al., 2011). These opposing modifications result in a poised state of transcription at bivalent promoters (Stock et al., 2007). Ring1b is required to maintain this poised state of transcription (Stock et al., 2007). As cells differentiate, bivalent domains tend to be resolved into transcriptionally active or silent states, marked by H3K4me3 or H3K27me3 respectively (Bernstein et al., 2006a).

Among the most prevalent PcG targets in ES cells are genes that encode proteins involved in cell fate determination. During differentiation and cellular commitment to a specific lineage there is selective de-repression of PcG targets. For example, during neuronal differentiation, PcG targets *ZIC1* and *MEIS1* (transcription factors required for neurogenesis) are expressed and PcG proteins are displaced from these genes (Bracken et al., 2006). However, PcG repression is also more dynamic than originally appreciated. For example, neuronal progenitors have been shown to acquire PcG repression (described by detection of H3K27me3) at genes that are not PcG targets in ES cells. Furthermore, PcG repression of these “new” targets is subsequently lost during terminal differentiation, repression in the progenitor having been a transient, poised state of PcG repression (Mohn et al., 2008).

1.4.2 Regulation of the self-renewal capacity of stem cells

Like ES cells, somatic stem cells (SCCs) have the capacity to self-renew and to differentiate into a variety of cell types, depending on the tissue of origin. Somatic stem cells have been identified in a number of tissues including the nervous system, the haematopoietic system, lung, intestine and skin (reviewed in (Snippert and Clevers, 2011)) and are important for maintaining tissue homeostasis. Evidence implicating PcG proteins in stem cell self-renewal has mostly come from studies on Bmi1 knockout mice. The mice that survive to adulthood have neural and haematopoietic defects that reflect a deficiency in stem cell numbers rather than their failure to differentiate (Iwama et al., 2004, Jacobs et al., 1999a, Lessard and Sauvageau, 2003, Leung et al., 2004, Molofsky et al., 2003, Park et al., 2003). Although the analyses of other PcG gene knockouts have been much less extensive, a number appear to impair some aspects of stem cell renewal, including Mph1, Ring1b, Cbx2 and Ezh2 (Kamminga et al., 2006, Ohta et al., 2002, Cales et al., 2008, Core et al., 1997). Remarkably, where tested, the proliferative defects in the PcG knockout mice can be largely rescued by concomitant inactivation of *INK4a-Arf.*

1.5 The *INK4a-ARF-INK4b* locus and cellular senescence

1.5.1 The *INK4a-ARF-INK4b* locus

The *INK4a-ARF-INK4b* locus is found on human chromosome 9p21, and the equivalent region of mouse chromosome 4. *INK4a* and *INK4b* are thought to have arisen by gene duplication. Between these genes lies an additional exon, exon 1β. Transcription from the promoter of exon 1β results in an RNA product that incorporates exons 2 and 3 of *INK4a*. This RNA is translated in an alternative reading frame from *INK4a* and was therefore named *ARF* (Quelle et al., 1995).

The products of *INK4a* and *INK4b* are commonly referred to as $p16^{INK4a}$ and $p15^{INK4b}$. These INK4 proteins are cyclin-dependent kinase inhibitors, which directly bind to CDK4 and CDK6 and block the assembly of catalytically active cyclin D-CDK4/6 complexes (Pavletich, 1999). In addition, by sequestering CDK4 and

CDK6, the INK4 proteins increase the availability of the CIP/KIP family of CDK inhibitors to bind and inhibit cyclin E-CDK2 and cyclin A-CDK2 (Sherr and Roberts, 1999). As these cyclin-CDK complexes orchestrate progression through the cell cycle, at least in part by phosphorylating and inactivating the retinoblastoma gene product (pRb) and its relatives, elevated expression of $p16^{INK4a}$ or $p15^{INK4b}$ results in a G1 phase cell cycle arrest (reviewed in (Sherr, 2000, Ortega et al., 2002)).

Importantly, ARF is not a CDK inhibitor and bears no structural similarities to the INK4 family, which are composed of ankyrin type repeats (Pavletich, 1999). As well as its unusual genomic organisation, ARF has an unusual amino acid composition and the primary sequence is poorly conserved. It is also credited with binding to a wide variety of cellular proteins but its best-characterised function is its interaction with MDM2 (Bothner et al., 2001). MDM2 is an E3 ubiquitin ligase that catalyses the polyubiquitination of p53, resulting in its proteasome-mediated degradation. Binding of ARF to MDM2 inhibits this activity leading to the accumulation of a transcriptionally active pool of p53 (Sherr, 2000, Michael and Oren, 2003). Although the situation is complicated by feedback loops, through which, p53 activates the expression of MDM2 and represses that of ARF, events that cause up-regulation of ARF generally induce a p53-dependent cell cycle arrest in G1 and G2, presumably mediated by p21 (Lowe and Sherr, 2003).

It is clear, therefore, that all three proteins encoded by the *INK4a-ARF-INK4b* locus are able to cause cell cycle arrest. However, the balance of evidence suggests these proteins are not involved in regulating the cell cycle *per se*. Instead, the expression of these proteins seems to be important for establishing a state of permanent cell-cycle arrest, termed senescence.

1.5.2 Cellular senescence

Hayflick and colleagues originally proposed the concept of senescence when they observed that human diploid fibroblasts (HDFs) had a limited replicative potential when propagated under cell culture conditions. The number of population doublings achieved by a particular cell strain was consistent, suggesting a counting

mechanism (Hayflick and Moorhead, 1961). One factor governing this limited replication potential is the loss of telomeric DNA at each cell division, which occurs due to the incomplete replication of the lagging strand by DNA polymerase (Olovnikov, 1971, Watson, 1972). Telomeres are repetitive sequences at chromosome ends that protect the loss of coding genomic information. In stem cells, telomere length is maintained by telomerase which catalyses telomere elongation (reviewed in (Hiyama and Hiyama, 2007)). When telomeres reach a critical length, their structure is disrupted causing a persistent DNA damage response (DDR) that can induce permanent cell-cycle arrest (Fumagalli et al., 2012). This is known as replicative senescence. Ectopic expression of human telomerase reverse transcriptase (hTERT), the catalytic subunit of telomerase, can extend the lifespan of normal somatic cells in culture (Bodnar et al., 1998).

Both the p53 and pRB pathways are key regulators of senescence (reviewed in (Campisi and d'Adda di Fagagna, 2007)). Senescent cells show marked changes in gene expression patterns, although it is difficult to separate those involved in causing senescence and those that result from the senescent cell state. These changes include the striking accumulation of $p16^{INK4a}$, preceded by $p21^{CIP1}$ (Alcorta et al., 1996). Curiously expression of $p18^{INK4c}$, another member of the INK4 family of proteins, is downregulated (Gagrica et al., 2012). Human cells do not demonstrate any appreciable differences in *ARF* RNA levels, but the situation is very different in mouse fibroblasts where ARF accumulates. Although the reasons behind the species difference are not entirely clear, laboratory mice have exceptionally long telomeres. Consequently, the senescence of MEFs in culture is a reflection of oxidative stress rather than eroded telomeres, and can be alleviated by growing cells in low oxygen conditions (Parrinello et al., 2003).

In addition to telomere erosion and oxidative stress, other forms of cellular stress will also induce premature senescence, including the activation of oncogenes. For example, in primary cells, expression of oncogenic RAS is a potent inducer of senescence (Serrano et al., 1997). Such oncogene-induced senescence (OIS) is generally accompanied by upregulation of p53 and increased expression from *INK4a-ARF-INK4b*. Interestingly, the contribution of *INK4a-ARF-INK4b* to this arrest is attributable to $p16^{INK4a}$ in HDFs, whereas ARF plays the predominant role

in MEFs (Brookes et al., 2002, Kamijo et al., 1997). OIS is thought to result from a DDR triggered by oncogene-induced replication stress (Bartkova et al., 2006, Di Micco et al., 2006).

1.5.3 Characteristics of senescent cells

Senescence is often described as being irreversible, largely distinguishing it from quiescence, which can be reversed by addition of the appropriate growth signals. In culture, senescent cells remain metabolically active and viable without increasing in number. These cells acquire a number of phenotypic characteristics, such as enlarged and flattened morphology, and single, prominent nucleoli (Campisi and d'Adda di Fagagna, 2007). Senescent cells also have an increased lysosomal content that results in high levels of lysosomal β-galactosidase (Lee et al., 2006a). This feature, referred to as senescence-associated β-galactosidase (SA-β-Gal) activity, is commonly used as a marker for senescence. For this assay, 5-bromo-4-chloro-3-indolyl-β-D-galactoside (X-gal) is used to detect β-galactosidase activity at a suboptimal pH (Dimri et al., 1995).

Dramatic changes in chromatin can also be a feature of senescent cells. Senescent-associated heterochromatin foci (SAHF) are DAPI-dense, subnuclear structures that are enriched with heterochromatic proteins and histone modifications, such as H3K9me3, that are associated with heterochromatin (Narita et al., 2003, Zhang et al., 2007). SAHF have been observed in replicative senescence but are a more prominent feature of oncogene-induced senescence (Di Micco et al., 2011). It has been proposed that the formation of SAHF facilitates the transcriptional silencing of E2F target genes (Narita et al., 2003). However, the observation that senescence can be established in the absence of SAHF formation, questions the extent to which SAHF play a causative role in senescence (Di Micco et al., 2011). Another feature of senescent cells is that they have a specialised secretory programme, termed the senescence-associated secretory phenotype (SASP) (Coppe et al., 2008). This includes the increased expression of inflammatory cytokines and cognate receptors that appear to enhance the senescence phenotype in culture (Acosta et al., 2008, Kuilman et al., 2008).

Furthermore, there are indications that, *in vivo*, the SASP could act as a mechanism for clearance of incipient cancer cells by the innate immune system (Kang et al., 2011).

1.5.4 Role of senescence in tumour suppression

Importantly, OIS is not confined to cultured cells but has been observed in pre-malignant lesions in both humans and mice. An example of this is human naevi. Human naevi are benign tumours of melanocytes that frequently contain oncogenic mutations in BRAF or RAS and display classical hallmarks of senescence, including SA-β-Gal activity and $p16^{INK4a}$ expression (Michaloglou et al., 2005). This lends credence to the idea that senescence is an important tumour suppressive mechanism that prevents the expansion of cells that have sustained oncogenic mutations. Indeed, bypass, or escape from senescence, has been described as one of the "Hallmarks of Cancer" (Hanahan and Weinberg, 2000, Hanahan and Weinberg, 2011).

This would explain the importance of *INK4a* in human cancer. *INK4a* was identified as a melanoma susceptibility gene in 1994 (Nobori et al., 1996, Kamb et al., 1994). Recent meta-analyses have indicated that the region around *CDKN2A* is the most frequently altered genomic locus in human cancer (Beroukhim et al., 2010, Bignell et al., 2010). The COSMIC database implies that of over 25,000 human tumour samples analysed, 14% have somatic mutations in *CDKN2A* (Forbes et al., 2008). Furthermore, *CDKN2A* is frequently hypermethylated in tumours (Esteller et al., 2001), causing transcriptional silencing of this locus. The majority of point mutations and intragenic alterations in this region, in both sporadic and familial human tumours, target *INK4a* rather than *ARF* or *INK4b* (Sharpless, 2005, Ruas and Peters, 1998). In mice, ARF seems to play a more important role in tumour suppression. Individual knockout of either *Ink4a* or *Arf* predisposes mice to spontaneous tumour formation and this effect is amplified in double knockout mice (Sharpless et al., 2004). Furthermore, studies in MEFs have shown that although Arf and $p16^{Ink4a}$ accumulate after passaging, spontaneous escape from senescence occurs in $ARF^{-/-}$ MEFs but not $Inka^{-/-}$ MEFs (Krimpenfort et al., 2001).

1.6 PcG complexes in cancer

As discussed in more detail in Chapter 1.8, there is compelling evidence that *INK4a-ARF-INK4b* is regulated by PcG complexes. The seminal observation in this regard was that Bmi1$^{-/-}$ MEFs undergo premature senescence as a consequence of de-repression of *Ink4a/Arf* (Jacobs et al., 1999a). Conversely, BMI1 and CBX7 can extend replicative lifespan, when ectopically expressed, by down-regulating p16^{INK4a} (Gil et al., 2004, Itahana et al., 2003).

The oncogenic potential of Cbx7 was shown when transgenic mice, in which Cbx7 is expressed from the Eμ promoter, developed follicular lymphoma (Scott et al., 2007). Bmi1 was originally identified as an oncogene that collaborates with Myc in MuLV-induced lymphomas (van Lohuizen et al., 1991, Haupt et al., 1991). Although, Bmi1 can also have *INK4a*-independent effects in cancer, the oncogenic co-operation of Bmi1 and Myc during lymphomagenesis is dependent on Bmi1 repression of *CDNK2A* (Jacobs et al., 1999b). Furthermore, BMI1 is amplified in B cell lymphoma and breast cancer (Bea et al., 2001) and EZH2 is over-expressed in a number of tumour types (van Kemenade et al., 2001, Varambally et al., 2002, Bachmann et al., 2006, Bracken et al., 2003, Kleer et al., 2003).

A frequent epigenetic change observed in tumour cells is the hypermethylation of PcG target genes (Ohm et al., 2007, Widschwendter et al., 2007, Schlesinger et al., 2007). Indeed, PcG target genes are up to 12-times more likely to have cancer-specific promoter DNA hypermethylation than non-PcG genes (Widschwendter et al., 2007). This DNA methylation may be promoted at PcG targets by the interaction of EZH2 and CBX7 with DNA methyltransferases (DNMTs) (Vire et al., 2006, Mohammad et al., 2009). The effect of aberrantly silenced PcG target genes is thought to favour stem cell-like properties such as increased proliferative potential and a dedifferentiated cell state. Cancer cells that exhibit such properties, “cancer stem cells”, have been proposed to drive the formation and growth of tumours (Reya et al., 2001).

In addition to global upregulation of PcG proteins, alterations in PcG recruitment at specific targets could account for aberrant transcriptional programmes in cancer (Sparmann and van Lohuizen, 2006). Indeed factors implicated in PcG recruitment, including certain transcription factors and ncRNAs, are often dysregulated in primary and metastatic tumours. For example, the transcription factor OCT4, which occupies a significant proportion of PcG targets in human ES cells (Lee et al., 2006b), is highly expressed in human germ cell tumours and required for their growth (Gidekel et al., 2003, Looijenga et al., 2003). Elevated expression of OCT4 could therefore impair differentiation of cancer-associated stem cells. The ncRNA *HOTAIR,* which has been shown to recruit PRC2 complexes at specific target loci, is also expressed at elevated levels in primary breast tumours and is associated with a more metastatic phenotype (Gupta et al., 2010).

1.7 Changes in PcG proteins at senescence

Remarkably little is known about how various stress signals induce expression from *CDKN2A* to implement senescence. Although many signalling pathways are reputed to regulate *CDKN2A* (reviewed in (Gil and Peters, 2006)), our understanding of their integration and how they impact on PcG-associated mechanisms is sparse. Some PcG proteins are downregulated during replicative senescence (Itahana et al., 2003, Gil et al., 2004) but it is not clear that the decreased levels can account for derepression of *CDKN2A*. Interestingly, oncogenic RAS causes up-regulation of the H3K27me3 demethylase JMJD3 and down-regulates the EZH2 H3K27 methyltransferase. This results in a global reduction of H3K27me3 and activation of *INK4a,* leading to increased expression of $p16^{INK4a}$ (Barradas et al., 2009). However, it is not clear how locus specificity is achieved, as the related H3K27me3 demethylase UTX has no effect on *INK4a* expression.

One possibility that has been suggested is that recruitment of either PRC2 or PRC1 to the *CDKN2A* locus is specified by the lncRNA *ANRIL* (Yap et al., 2010, Kotake et al., 2011). *ANRIL* is transcribed in the antisense direction relative to *INK4a* and *ARF* and initiates at a site that is approximately 300 bp upstream of the

transcriptional start site of *ARF*, suggesting that *ARF* and *ANRIL* share a bidirectional promoter. As one report suggests that the levels of *ANRIL* decrease during replicative senescence in IMR90 cells, this could potentially release PcG repression specifically at *CDKN2A* (reviewed in (Aguilo et al., 2011)).

1.8 Association of PcG complexes with *INK4a-ARF-INK4b*

As alluded to above, several lines of evidence suggested a link between various PcG proteins and *INK4a-ARF-INK4b.* For example, *Bmi1*-null mice show proliferative defects that can be rescued by the concurrent knockout of *CDKN2A* (Jacobs et al., 1999a). Furthermore, overexpression of BMI1, CBX7 or CBX8 in human and mouse fibroblasts can delay the onset of senescence by repressing *CDKN2A* (Bracken et al., 2007, Dietrich et al., 2007, Gil et al., 2004, Itahana et al., 2003). However, the first evidence for a direct connection was ChIP data from Bracken and colleagues, showing Bmi1, Cbx8, Ezh2 and H3K27me3 enrichment across the locus. In human and mouse fibroblasts, PcG protein binding peaks at the promoter and first exon of *INK4a*. Very little binding of PRC1 proteins is seen at the *ARF* and *INK4b* promoters. ChIP for H3K27me3 shows a much broader binding profile, although the peak still centres on *INK4a* (Bracken et al., 2007). Subsequent genome wide ChIP (both ChiP-on-chip and ChIP-seq) has shown that the *INK4b* and *ARF* promoter are also occupied by PcG complexes in mouse and human ES cells (Ku et al., 2008).

Further ChIP studies in human fibroblasts have demonstrated that CBX4, CBX6, CBX7, CBX8, BMI1, MEL18, RING1, RING2, HPH1, HPH2, and HPH3, all bind at the *INK4a* locus (Dietrich et al., 2007, Bracken et al., 2007, Maertens et al., 2009, Pemberton et al., Submitted). Remarkably, the binding patterns are very similar if not identical, implying that many different types of PRC1 complex are associating with a relatively small region of DNA. Moreover, sequential ChIP studies with antibodies against different members of the Pc, Ph and Sce families, suggest that multiple variants of PRC1 associate simultaneously with the same DNA (Maertens et al., 2009, Pemberton et al., Submitted). This is thought to reflect the presence of Polycomb bodies in mammalian cells that comprise many different permutations of

PRC1 (Pemberton et al., Submitted). Conversely, the equivalent structures in *Drosophila* consist of multimers of the same PRC1. Such a scenario would explain why shRNA-mediated knockdown of any one of several mammalian PRC1 proteins (e.g. BMI1, MEL18, CBX6, CBX7, CBX8, RING1 and RING2) causes up-regulation of p16 and a senescent-like growth arrest (Maertens et al., 2009, Dietrich et al., 2007, Pemberton et al., Submitted).

1.9 The DNA damage response (DDR)

1.9.1 An overview of the DDR

Recent evidence has emerged that in addition to their well-established role as transcriptional repressors, PcG proteins are involved in the DNA damage response (DDR). The DDR refers to DNA damage signalling and repair networks that are crucial for maintaining genome integrity. Thousands of DNA lesions arise in human cells each day, typically caused by errors in DNA replication or by oxidative stress but also by environmental factors such as ultraviolet light and toxic chemicals. Failure to repair these lesions, or prevent their transmission to daughter cells, can result in the types of mutations and chromosomal aberrations that contribute to developmental defects, cancer and aging (reviewed in (Jackson and Bartek, 2009))

The nature of the DDR is determined by the type of DNA damage, and the cell cycle state in which it occurs. Double strand breaks (DSBs) are repaired by two main pathways: homologous recombination (HR) and non-homologous end-joining (NHEJ). HR is restricted to the S and G2 phases as it requires a homologous template, typically a sister chromatid, that is only available following DNA replication. NHEJ (the predominant pathway in higher eukaryotes) does not require a template and so can operate throughout the cell cycle (albeit with a higher mutagenic frequency) (Hartlerode and Scully, 2009). Single strand breaks (SSBs) elicit their own repair pathway (Caldecott, 2008).

Various experimental strategies are used to introduce DNA damage and they have different outcomes. Exposing cells to genotoxic drugs, ionising radiation (IR), and ultraviolet (UV) radiation can induce global DNA damage consisting of both DSBs

and SSBs. These breaks occur randomly and their positions will differ between cells in the population, although less condensed regions of chromatin can be more susceptible to DNA damage (Elia and Bradley, 1992, Costes et al., 2007), More targeted DNA damage can be induced by laser microirradiation. Importantly, the laser wavelength, and energy output will all affect the type and density of DNA lesions (Polo and Jackson, 2011). This approach offers control over the physical location of the damage within a cell nucleus but not the genomic location of the DNA lesions. To generate site-specific breaks, it is necessary to use sequence specific endonucleases such as I-*Sce*I, I-*Ppo*I and *Asi*SI, but these agents also have limitations. For example, as there are no I-*Sce*I cut sites in the human genome they have to be artificially introduced (Rouet et al., 1994). I-*Ppo*I cuts more frequently but typically within repeated sequences in the ribosomal genes (Berkovich et al., 2007). The *Asi*SI restriction enzyme has 1219 target sites (consensus GCGATCGC) in the human genome (Hg19 release; personal communication from Harshil Patel, LRI Bioinformatics and Biostatistics service). However, CpG methylation of the consensus can inhibit *Asi*SI cleavage (Roberts et al., 2010). Nucleases can also be targeted to specific loci by fusing the nuclease domain to a sequence-specific zinc finger protein (Miller et al., 2007). However, these zinc finger nucleases (ZFN) are generally designed to cut at a single defined site. Finally, it is possible to induce artificial telomere uncapping and a localised DDR by depletion of components that protect chromosome ends (d'Adda di Fagagna et al., 2003, Takai et al., 2003).

1.9.2 Proteins involved in the DDR

Proteins involved in the DDR can be categorised as DNA damage sensors, transducers, mediators and effectors. In mammalian cells, DSBs are detected by the MRN complex (MRE11-RAD50-NBS1), which contributes to the recruitment and activation of ATM (Falck et al., 2005, Lavin, 2007, Lee and Paull, 2005, Uziel et al., 2003). ATM is a transducer kinase, which, with the aid of mediator proteins such as 53BP1, BRCA1 and MDC1, activates the effector kinases CHK1 and CHK2 (Harper and Elledge, 2007) (Figure 1.1). The ultimate targets of this signalling cascade include DNA repair factors, cell cycle regulators, transcription

factors and regulators of apoptosis. This cascade involves many additional proteins. Among these, are a number of histone modifying enzymes, chromatin remodelling complexes and histone chaperones, highlighting the importance of the chromatin context for an effective DDR (Misteli and Soutoglou, 2009, van Attikum and Gasser, 2009). The phosphorylation of the histone variant H2AX on serine 139 (γH2AX) has been the most widely studied histone modification induced by DSBs. γH2AX spreads from DSBs into large domains of surrounding chromatin and can be visualised as cytologically discernible foci by immunofluorescence (Haaf et al., 1995, Maser et al., 1997, Scully et al., 1997). These foci are thought to be important for the accumulation and retention of DDR proteins. Histone ubiquitination is also important for orchestrating the assembly of DDR proteins at DNA breaks. The ubiquitination of H2A and H2AX by RNF8 and RNF168 promotes the recruitment of various DDR proteins, such as 53BP1 and BRCA1, to DSBs (Huen et al., 2007, Kolas et al., 2007, Mailand et al., 2007). Ubiquitination of H2AX is thought to cause local changes in chromatin structure revealing methylated lysine residues in core histones. Exposure of methylated histones may aid 53BP1 recruitment by its tudor domain (Stewart, 2009). The SUMO E3 ligases PIAS1 and PIAS4 rapidly accumulate at sites of DNA damage. These E3 ligases promote the association of BRCA1 and 53BP1 with DSBs, and PIAS4 is important for the effective ubiquitination of H2A at these sites (Galanty et al., 2009).

The E3 ubiquitin ligase activity of PRC1 and SUMO E3 ligase activity of CBX4 have both been implicated in the DDR. Interestingly, the function of CBX4 in this response may be to promote PRC1 recruitment to DSBs by sumoylating BMI1 (Ismail et al., 2012).

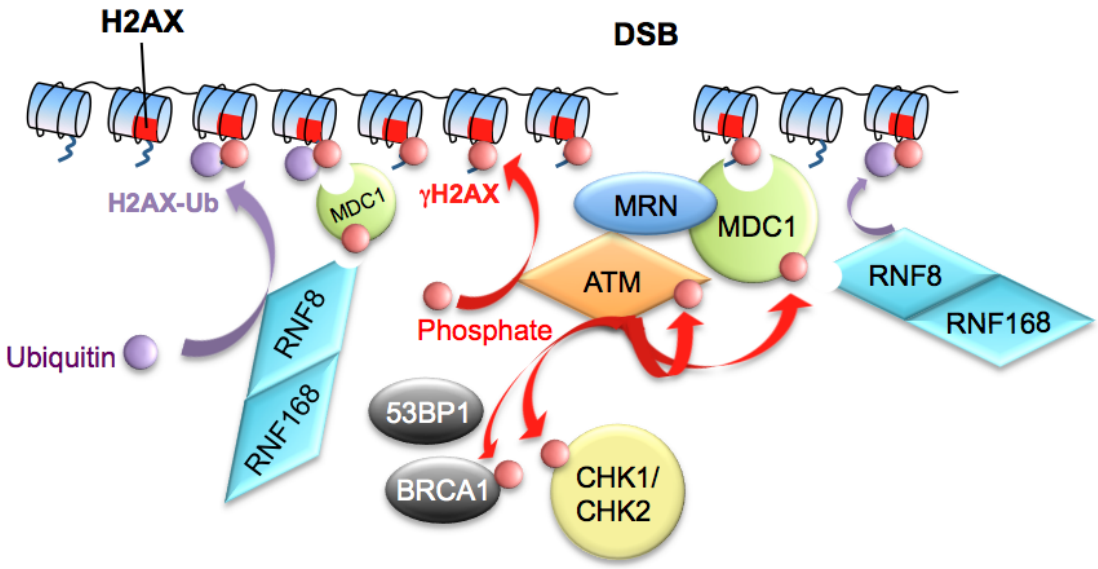

Figure 1.1 DNA damage response at double strand breaks

Schematic illustrating the key proteins recruited to DSBs and the protein modifications they facilitate. Upon sensing a DSB the MRN complex recruits and actives the ATM kinase. Activated ATM has a number of substrates including CHK1, CHK2, p53, BRCA1, MDC1 and histone H2AX. MDC1 recognises and binds γH2AX. Phosphorylated MDC1 serves to recruit RNF8 to DSBs. RNF8 and RNF168 can catalyse the ubiquitination of H2A and H2AX, which is important for the recruitment of both 53BP1 and BRCA1 (reviewed in (Bohgaki et al., 2010)).

1.10 Evidence implicating PcG proteins in the DDR

1.10.1 Recruitment of PcG proteins to DSBs

The earliest indications that PcG proteins might be involved in the DDR came from studies of PHF1 and EZH2. PHF1, a human homologue of Polycomblike (PCL), which associates with PRC2 complexes (Cao et al., 2008), was detected at sites of laser microirradiation in HeLa cells (Hong et al., 2008). ChIP experiments revealed EZH2 and H3K27me3 enrichment at an I-SceI cut site (O'Hagan et al., 2008). Subsequent studies have extended these observations, demonstrating the co-localisation of various PRC1 components with sites of DNA damage by visualising either endogenous proteins (BMI1, MEL18, RING2, CBX4) or GFP-tagged proteins (CBX4, CBX6, CBX7, CBX8, RING1, RING2, HPH1 and 2) in different contexts (Ismail et al., 2010, Chou et al., 2010, Facchino et al., 2010, Ginjala et al., 2011). Together these studies provide strong evidence that PRC1 proteins are recruited to sites of DNA damage in response to a variety of damage stimuli including IR, laser microirradiation and nucleases. However, it is of note that the majority of these studies have been conducted in either MEFs or human cancer cells lines.

A number of DDR proteins interact with PRC1 proteins and these interactions are often enhanced following DNA damage. For example, in GBM cells, BMI1 binds endogenous phospho-ATM only after irradiation (Facchino et al., 2010). Furthermore, the interaction of H2AX with BMI1 and RING2 was enhanced following IR treatment (Pan et al., 2011). These interactions are probably not important for the initial recruitment of PRC1 proteins but may be required for their sustained localisation at sites of DNA damage (Chou et al., 2010, Ismail et al., 2010, Ismail et al., 2012, Ginjala et al., 2011). The kinetics of PRC1 recruitment to sites of microirradiation are comparable to those of early DNA damage response proteins, such as RNF8, NBS1 and MRE11, but the details differ in the published studies (Ismail et al., 2010, Chou et al., 2010, Ginjala et al., 2011). Likewise, there are varied opinions about how long the association of PRC1 proteins is sustained in different contexts.

1.10.2 Importance of PcG proteins for DNA damage repair

Studies in Bmi1$^{-/-}$ MEFs have implicated PcG proteins in the recruitment of 53BP1 and BRCA1 to DNA breaks, particularly at early points after microirradiation (Ismail et al., 2010). However, the recruitment of Mre11, Rnf8, Nbs1 and phospho-ATM to DSBs is normal in BMI$^{-/-}$ MEFs. In addition, neither MEL18 nor BMI1 are required for H2AX phosphorylation at sites of DNA damage (Chou et al., 2010, Ismail et al., 2010). However, IR-induced ubiquitination of H2AX is significantly reduced in Bmi1$^{-/-}$ MEFs or in U2OS cells following BMI1 knockdown (Ismail et al., 2010). Rnf8$^{-/-}$ MEFs still contain considerable amounts of mono-ubiquitinated H2AX following irradiation but these levels are reduced by around 80% following knockdown of Bmi1. These data demonstrate a role for BMI1-RING2 in the mono-ubiquitination of H2AX that is independent of RNF8 (Ismail et al., 2010).

Depletion of DDR proteins decreases the effectiveness of the DDR and thereby sensitises cells to DNA damage. Cell survival following IR treatment can be assessed by clonogenic assays. Depletion of BMI1, CBX4 or RING2 in different cell backgrounds increases the sensitivity of these cells to IR (Ginjala et al., 2011, Pan et al., 2011, Ismail et al., 2010, Facchino et al., 2010, Ismail et al., 2012). Bmi1$^{-/-}$ MEFs and Rnf8 $^{-/-}$ MEFs show similar sensitivity to IR. Importantly, the knockdown of Bmi1 in Rnf8$^{-/-}$ MEFs or of Rnf8 in Bmi1$^{-/-}$ MEFs increases the sensitivity of these cells to IR, suggesting BMI1-RING2 and RNF8 have individual contributions to the DDR (Ismail et al., 2010).

1.11 Protein kinase CK2 (CK2)

1.11.1 Auxiliary proteins that co-purify with PRC1 complexes

It is over 10 years since the first description of a mammalian PRC1 complex. In the ensuing decade there have been several descriptions of affinity purified complexes based on different tagged PRC1 proteins (Dietrich et al., 2007, Gao et al., 2012, Maertens et al., 2009, Sanchez et al., 2007, Vandamme et al., 2011). PRC1 proteins have also been found in other types of complex as discussed in Chapter 1.1.1. Moreover, a number of auxiliary proteins that are not encoded by recognised

PcG genes consistently co-purify with PRC1 complexes. Examples include WDR68, MOV10, USP7, USP11 and CK2 (formerly known as casein kinase 2) (Maertens et al., 2010, Nicholls, 2006). Curiously, CK2 appears to be the only auxiliary protein that has a connection to the DDR.

1.11.2 Interaction of CK2 with PRC1 complexes

CK2 is a heterotetramer with two catalytic subunits, α and/or α', and two regulatory β subunits. Peptides representing all three subunits were detected by mass spectrometry analysis of proteins that co-purify with mCbx7 from 293T cells (Nicholls, 2006, El Messaoudi-Aubert et al., 2010). These observations have been confirmed in several independent studies that collectively imply that CK2 associates with complexes based on CBX2, CBX4, CBX7, CBX8, RING2, RNF3 and RNF159 (El Messaoudi-Aubert et al., 2010, Dietrich et al., 2007, Vandamme et al., 2011, Sanchez et al., 2007, Gao et al., 2012). CK2 has also been found in non-canonical PRC1 complexes. For example, CK2 subunits were identified by mass spectrometry analysis of affinity purified Fblx10 (Sanchez et al., 2007), RYBP and YAF2 (Gao et al., 2012). However, until recently, there has been no documented validation of the interaction by, for example, immunoblotting, mapping of interaction domains, or binding between recombinant proteins (Vandamme et al., 2011, Sanchez et al., 2007).

1.11.3 CK2 complex composition

CK2 has been identified in all eukaryotic organisms investigated, in most tissues of higher eukaryotes, and in nearly every cellular compartment (Guerra and Issinger, 1999, Faust and Montenarh, 2000). The CK2 holoenzyme is a heterotetramer that consists of two catalytic subunits (α) that bind a central dimer of non-catalytic of regulatory subunits (β) (Niefind et al., 2001). In contrast to other kinases, CK2 can efficiently use either ATP or GTP as a phosphoryl donor (Niefind et al., 1999). CK2α and α' are encoded by the *CSNK2A1* and *CSNK2A2* genes respectively, which are located on different chromosomes (Pyerin and Ackermann, 2003). CK2β is encoded by *CSNK2B*. CK2α and α' have very similar protein sequences except

for their C-termini, which vary in sequence and length (Bischoff et al., 2011). CK2α is reported to have an approximately 12-fold higher affinity for CK2β than CK2α' (Olsen et al., 2008).

Although CK2 tetramers are very stable, there is evidence that CK2 catalytic and regulatory subunits can act independently *in vivo* (Bibby and Litchfield, 2005). For example, immunofluorescence has identified subcellular populations of CK2β that do not co-localise with CK2α or α' (Krek et al., 1992), and populations of CK2α and α' that do not co-localise with CK2β (Faust et al., 2001). Furthermore, live cell imaging of GFP-CK2α and GFP-CK2β, has demonstrated that CK2 subunits are independently imported into the nucleus and can move independently within the nucleus (Martel et al., 2001, Filhol et al., 2003). These findings suggest that interactions between CK2 catalytic and regulatory subunits are more dynamic *in vivo* then previously appreciated. Furthermore, CK2β has been shown to associate with, and regulate the activity of, other kinases, including c-Mos (Chen et al., 1997) and A-Raf (Hagemann et al., 1997).

1.11.4 Regulation of CK2 activity and substrate specificity

Unlike most protein kinases, CK2 is constitutively active. The isolated and holoenzyme-bound forms of CK2α have conserved active segment conformations and are both catalytically active (Boldyreff et al., 1994, Grankowski et al., 1991, Niefind et al., 2001). CK2β can modulate the basal activity of the catalytic subunits but the effects appear to be context dependent. For most substrates CK2β increases the basal activity of CK2α but there are examples, such as calmodulin, where the presence of CK2β can be inhibitory to substrate phosphorylation (Marin et al., 1999a). In addition to the positive regulatory domain within its C-terminus of CK2β, CK2β contains an acidic loop towards its N-terminus. This acidic loop might negatively regulate CK2 by inhibiting binding of potential substrates; the CK2 consensus is acidic. Alternatively, as this loop binds polyamines that can increase the basal activity of CK2α *in vitro*, in certain contexts, it could positively regulate CK2 activity (Niefind et al., 2001, Litchfield, 2003).

In addition to modulating CK2 catalytic activity, CK2β can be important for mediating substrate interactions and specificity. For example, CK2 associates with p53 via the CK2β, which binds the C-terminus of p53. Interestingly, phosphorylation of p53 by CK2 repels the interaction between these proteins (Filhol et al., 1992). There are situations in which the action of the holoenzyme can be influenced by interactions with other proteins. For example, the FACT complex, which facilitates transcription through nucleosomes (Orphanides et al., 1998), has been shown to bind CK2 following exposure to UV radiation. This interaction can modulate the specificity of CK2 and promote phosphorylation of p53 over other CK2 substrates (Keller et al., 2001). Another example is the association of CK2α with Pin1, which catalyses prolyl cis/trans isomerisation at pSer/Thr-Pro motifs and thereby regulates the conformation of its substrates (Lu and Zhou, 2007). Pin1 has been shown to inhibit CK2 phosphorylation of topoisomerase IIα (Messenger et al., 2002).

CK2α and CK2β are phosphorylated by CDK1 during mitosis (Litchfield et al., 1995, Litchfield et al., 1992) and these modifications can regulate cell-cycle phase-specific substrate interactions. For example, the association of Pin1 with CK2α is dependent on the phosphorylation of CK2α at its C-terminus, which occurs in mitosis (Messenger et al., 2002). Phosphorylation of CK2 can also affect CK2 stability. Both CK2α and CK2β contain autophosphorylation sites and autophosphorylation of CK2β can prevent ubiquitination and proteasome-mediated degradation of CK2β (Zhang et al., 2002). Interestingly CK2β contains a sequence with similarity to the destruction box of cyclin B, which confers mitosis-specific proteolysis to cyclin B. However, this putative destruction box alone does not affect CK2β stability (Zhang et al., 2002, Glotzer et al., 1991, King et al., 1996).

1.11.5 CK2 consensus sites

The minimal consensus sequence described for CK2 is S/T-x-x-D/E/pS/pT (where underlining denotes the residue targeted by CK2 (serine being more common than threonine) and pS/pT describes a phosphorylated serine or threonine serving as a specificity determinant) (Marin et al., 1986, Meggio and Pinna, 2003, Meggio et al.,

1984). CK2 can also phosphorylate tyrosine *in vitro* (Marin et al., 1999b). Although any acidic amino acid or pS at position n+3 is the best predictor of a CK2 target site, the majority also have a negatively charged side chain at n+1 and multiple acidic residues are commonly found in region n-4 to n+7 (Meggio and Pinna, 2003). There are limitations to using the minimal consensus for the identification of novel CK2 target. For example, p53 is efficiently phosphorylated at Ser392 by CK2 despite the fact that it does not conform to the consensus sequence, although there is an aspartic acid at n-1 and n+1 (Meggio et al., 1994).

Almost any protein sequence is likely to contain the CK2 consensus (Litchfield, 2003). Given this, its constitutive activity, and ubiquitous expression, it is not surprising that CK2 has an extensive repertoire of substrates – over 300 were documented in a recent comprehensive review (Meggio and Pinna, 2003). The catalogue of CK2 substrates includes transcription factors, proteins affecting the structure of DNA/RNA, proteins implicated in RNA synthesis or translation, signalling proteins, viral proteins and a few metabolic enzymes. However, the catalogue compiled by Meggio and colleagues has been criticised due to the lack of rigorous testing to determine whether the substrates are phosphorylated *in vivo* (Litchfield, 2003).

Each mammalian PcG protein contains multiple CK2 consensus sequences (Table 1.2), but there is currently no evidence that CK2 phosphorylates these proteins. Several PcG proteins are phosphorylated. For example, MBLR is phosphorylated at Ser32 during mitosis, probably by CDK7 (Akasaka et al., 2002). EZH2 is phosphorylated by CDK1 and CDK2 at Thr350 and this phosphorylation is important for effective recruitment of PRC2 to target loci (Zeng et al., 2011). Moreover, BMI1 is phosphorylated at mitosis and the phosphorylation of BMI1 correlates with its dissociation from chromatin (Voncken et al., 1999). Interestingly, Mel18 is phosphorylated at multiple sites, one of which, Ser 254, lies within a CK2 consensus (Elderkin et al., 2007).

Human PcG protein	N° of CK2 consensus sites
HPH1	10
HPH2	9
HPH3	10
NSCP1	5
MEL18	8
RNF3	5
BMI1	8
RNF159	4
MBLR	3
CBX2	16
CBX4	9
CBX6	6
CBX7	3
CBX8	8
RING1	9
RING2	13

Table 1.2 Number of CK2 consensus sites within the human PcG proteins

1.11.6 Importance of CK2 for cell viability and its role in tumorigenesis

Many studies in mammalian cells have demonstrated that CK2 is required for cell-cycle progression (Pepperkok et al., 1991, Lorenz et al., 1993, Pepperkok et al., 1994). It is hardly surprising, therefore, that elevated levels of CK2, which typically correlate with increased CK2 activity, are associated with both highly proliferative, normal and cancerous tissue (Faust and Montenarh, 2000, Faust et al., 1999). Indeed, CK2 is reported to be upregulated in all cancers examined to date and expression can relate to disease severity and serve as a prognostic indicator (Tawfic et al., 2001, Guerra and Issinger, 1999, Faust et al., 1996, Laramas et al., 2007, Gapany et al., 1995, O-Charoenrat et al., 2004). Although CK2 is not an oncogene in the classical sense, its upregulation contributes to the transformation potential of oncogenes such as c-myc and Tal-1, and loss of p53 (Kelliher et al., 1996, Landesman-Bollag et al., 1998, Channavajhala and Seldin, 2002). Conversely, CK2 levels are low in brain tissue preparations from neurodegenerative disorders such as in Alzheimer's disease (Iimoto et al., 1990). Furthermore, there is evidence that CK2 levels decrease at senescence.

Specifically, CK2 activity and levels of CK2α decrease during replicative and H_2O_2-induced senescence and CK2 inhibition can induce senescence in human fibroblasts and mesenchymal stem cells (Ryu et al., 2006, Wang and Jang, 2009).

The ability of CK2 to promote cellular transformation may result from its capacity to protect cells from apoptosis. Normal cells overexpressing CK2α show resistance to chemical-mediated apoptosis (Guo et al., 2001) and siRNA of CK2α promotes apoptosis of cells following IR treatment (Yamane and Kinsella, 2005). In cancer cells, chemical inhibition or siRNA-mediated knockdown of CK2 has been shown to induce apoptosis (Wang et al., 2005). A number of compounds have been used to inhibit CK2 including DRB (Blaydes and Hupp, 1998), emodin, apigenin (Channavajhala and Seldin, 2002) and TBB (Sarno et al., 2001). Of these, TBB demonstrates the highest selectivity for CK2. CK2 inhibitors are currently in clinical trials for treatment of various cancer types (for example: (Pierre et al., 2011)). There is evidence that the anti-apoptotic function of CK2 is at least in part due to its phosphorylation of proteins such as Max (Krippner-Heidenreich et al., 2001), Bid (Desagher et al., 2001) and HS1 (Ruzzene et al., 2002). The phosphorylation of these proteins by CK2 protects them from caspase cleavage. Furthermore, phosphorylation of ARC (apoptosis repressor with caspase recruitment domain) is required for ARC to exert its inhibition of caspase 8 (Li et al., 2002).

CK2$\alpha^{-/-}$ mouse embryos have a marked reduction in CK2 activity despite the presence of CK2α' and die in mid-gestation (Lou et al., 2008). CK2β is also essential for mouse development; knockout of CK2β causes postimplantation lethality (Buchou et al., 2003). Conditional knockout studies have shown that CK2β is essential for viability of mouse ES cells and primary MEFs (Buchou et al., 2003). In contrast deletion of CK2α' is well tolerated. CK2$\alpha'^{-/-}$ mice are viable but the males have defects in spermatogenesis and are infertile (Xu et al., 1999). This probably reflects the restricted expression of CK2α', which is predominantly found in the brain and testes of mice, contrasting the ubiquitous expression of CK2α (Guerra et al., 1999, Faust and Montenarh, 2000).

1.11.7 CK2 in the DNA damage response

The importance of CK2 for cell viability and for protection against apoptosis may also be partly explained by its function in the DDR. Phosphorylation of XRCC1 by CK2 stabilises the interaction of XRCC1 with DNA ligase IIIα, a complex involved in the DNA ligation stage of both base-excision repair (BER) and SSB repair (Parsons et al., 2010). A recent study has shown that CK2 is involved in promoting HR. Phosphorylation of Rad51 (a recombinase that catalyses homologous pairing and strand transfer during HR) by Polo-like kinase 1 (Plk1), primes Rad51 for phosphorylation by CK2 during the cell cycle and in response to DNA damage. CK2 phosphorylation of Rad51 promotes binding of Rad51 to Nbs1, facilitating Rad51 recruitment to sites of DNA damage (Yata et al., 2012). Furthermore, CK2 has been shown to directly phosphorylate HP1β during the DDR. The phosphorylation of HP1β disrupts its interaction with H3K9me3 and serves to mobilise HP1β from chromatin. Mobilisation of HP1β from chromatin appears to facilitate the phosphorylation of H2AX (Ayoub et al., 2008). CK2 phosphorylates threonine 51 (T51) within the chromodomain of HP1β, which lies within an atypical but highly acidic consensus (TXEXEE). Interestingly, T51 of HP1β is conserved in the chromodomains of CBX4, 6, 7 and 8 and is replaced with a serine in CBX2. This raises the tantalising possibility that CK2 might phosphorylate the CBX chromodomains and disrupt their interaction with H3K27me3.

1.12 Thesis aims

At the inception of this thesis, CK2 had been identified as a prominent auxiliary protein that co-purified with mCbx7 (Nicholls, 2006). The aim of this thesis was to investigate the functional relevance of this interaction. Specifically, we set out to answer the following questions:

- Which PRC1 component is responsible for the interaction with CK2?
- Does CK2 phosphorylate components of the PRC1 complex?
- Is CK2 required for the ability of PRC1 proteins to repress target genes such as *INK4a* and to extend the lifespan of HDFs?
- Is CK2 important for the role of PRC1 proteins in the DDR?

Chapter 2. Materials & Methods

2.1 Molecular biology

2.1.1 Oligonucleotides

All oligonucleotides were ordered from Sigma and are listed in Table 2.1. Oligonucleotides were supplied with –OH groups at both the 5' and 3' ends. Melting temperatures (T_m) of oligonucleotides were calculated by the suppliers. Oligonucleotides were used as primers for polymerase chain reaction (PCR) amplification or DNA sequencing.

Name	**Sequence (5' - 3')**
CK2α shRNA1 forward (fwd)	GATCCCCGTGTGTCTTAGTTACATCATTCAAGAGATGATGTAACTAAGACACACTTTTTGGAAA
CK2α shRNA1 reverse (rev)	AGCTTTTCCAAAAAGTGTGTCTTAGTTACATCATCTCTTGAATGATGTAACTAAGACACACGGG
CK2α shRNA2 fwd	GATCCCCCCGTTGCTTGTGGATTTATTTCAAGAGAATAAATCCACAAGCAACGGTTTTTGGAAA
CK2α shRNA2 rev	AGCTTTTCCAAAAACCGTTGCTTGTGGATTTATTCTCTTGAAATAAATCCACAAGCAACGGGGG
CK2α' shRNA1 fwd	GATCCCCGGGAATCATGCACAGGGATTTCAAGAGAATCCCTGTGCATGATTCCCTTTTTGGAAA
CK2α' shRNA1 rev	AGCTTTTCCAAAAAGGGAATCATGCACAGGGATTCTCTTGAAATCCCTGTGCATGATTCCCGGG
CK2α' shRNA2 fwd	GATCCCCGATCCTGACAGACTTTGATTTCAAGAGAATCAAAGTCTGTCAGGATCTTTTTGGAAA
CK2α' shRNA2 rev	AGCTTTTCCAAAAAGATCCTGACAGACTTTGATTCTCTTGAAATCAAAGTCTGTCAGGATCGGG
CK2β shRNA1 fwd	GATCCCCGCCATGGTGAAGCTCTACTTTCAAGAGAAGTAGAGCTTCACCATGGCTTTTTGGAAA
CK2β shRNA1 rev	AGCTTTTCCAAAAAGCCATGGTGAAGCTCTACTTCTCTTGAAAGTAGAGCTTCACCATGGCGGG
CK2β shRNA2 fwd	GATCCCCGGAGTCGTTATTGTGGTGGTTCAAGAGACCACCACAATAACGACTCCTTTTTGGAAA
CK2β shRNA2 rev	AGCTTTTCCAAAAAGGAGTCGTTATTGTGGTGGTCTCTTGAACCACCACAATAACGACTCCGGG
mCbx7-T140A fwd	AACTCCGTCACCGTCGCCTTCCGCGAGGCTCAA
mCbx7-T140A rev	TTGAGCCTCGCGGAAGGCGACGGTGACGGAGTT
mCbx7-T140D fwd	AACTCCGTCACCGTCGACTTCCGCGAGGCTCAA

mCbx7-T140D rev	TTGAGCCTCGCGGAAGTCGACGGTGACGGAGTT
mCbx7-V137A fwd	ATCACCGCCAACTCCGCCACCGTCACCTTCCGC
mCbx7-V137A rev	GCGGAAGGTGACGGTGGCGGAGTTGGCGGTGAT
mCbx7-V137AT140A fwd	AACTCCGCCACCGTCGCCTTCCGCGAGGCTCAA
mCbx7-V137AT140A rev	TTGAGCCTCGCGGAAGGCGACGGTGGCGGAGTT
mCbx7-V137AV139AT140A fwd	GCCAACTCCGCCACCGCCGCCTTCCGCGAGGCT
mCbx7-V137AV139AT140A rev	AGCCTCGCGGAAGGCGGCGGTGGCGGAGTTGGC
mCbx7-V137D fwd	ATCACCGCCAACTCCGACACCGTCACCTTCCGC
mCbx7-V137D rev	GCGGAAGGTGACGGTGTCGGAGTTGGCGGTGAT
mCbx7-V137DT140D fwd	AACTCCGACACCGTCGACTTCCGCGAGGCTCAA
mCbx7-V137DT140D rev	TTGAGCCTCGCGGAAGTCGACGGTGTCGGAGTT
mCbx7-V137DV139DT140D fwd	GCCAACTCCGACACCGACGACTTCCGCGAGGCT
mCbx7-V137DV139DT140D rev	AGCCTCGCGGAAGTCGTCGGTGTCGGAGTTGGC
mCbx7-V139A fwd	GCCAACTCCGTCACCGCCACCTTCCGCGAGGCT
mCbx7-V139A rev	AGCCTCGCGGAAGGTGGCGGTGACGGAGTTGGC
mCbx7-V139D fwd	GCCAACTCCGTCACCGACACCTTCCGCGAGGCT
mCbx7-V139D rev	AGCCTCGCGGAAGGTGTCGGTGACGGAGTTGGC
pBABE fwd	CGTCTCTCCCCCTTGAACC
pBABE rev	CTGCCTGCTGGGGAGGCC
pcDNA6 fwd (T7)	AATACGACTCACTATAG
pcDNA6 rev (BGH)	TAGAAGGCACAGTCGAGG
pGEX-6P1 fwd	GGGCTGGCAAGCCACGTTTGGTG
pGEX-6p1 rev	CCGGGAGCTGCATGTGTCAGAGG
pRetroSuper fwd	TACATCGTGACCTGGGAAGC
pRetroSuper rev	TAAAGCGCATGCTCCAGACT

Table 2.1 Oligonucleotides

2.1.2 Plasmid vectors

Plasmid vectors were propagated from laboratory stocks and used to clone new constructs. In addition, constructs were kindly provided by other laboratories, as acknowledged in the relevant sections. Commonly used vectors are described below.

pBABE This vector is based on the Moloney leukaemia virus (Morgenstern and Land, 1990). When transfected into a packaging cell line this vector allows for the production of ecotropic retroviruses. The gene of interest is under the control of a long-terminal repeat (LTR) promoter. The vector contains an

ampicillin resistance gene for selection in bacteria, and puromycin, hygromycin or bleomycin resistance genes for selection of mammalian cells.

pRetroSuper This vector is based on the pMSCV retroviral plasmid and the pSUPER shRNA plasmid for expression of shRNAs (Brummelkamp et al., 2002). shRNA targeting the gene of interest is expressed from an RNA polymerase III-dependent promoter. The vector contains an ampicillin resistance gene for selection in bacteria and a puromycin resistance gene for selection of mammalian cells.

pcDNA6/V5-HisB This vector is derived from pcDNA3.1. It is designed for stable or transient expression of the gene of interest in mammalian cells. The gene of interest is under the control of a CMV promoter allowing for high levels of expression. The vector contains an ampicillin resistance gene for selection in bacteria, and a blasticidin resistance gene for selection of mammalian cells.

pGEX-6P1 This vector allows for the expression a protein attached to the C-terminus of GST. Between the protein and GST lies a prescission protease cleavage site, allowing for the removal of the GST tag if required. An internal lactose repressor gene allows for control of high level gene expression from the tac promoter. Chemical induction of gene expression occurs when IPTG releases lac repressor from the tac promoter. The vector contains an ampicillin resistance gene for selection in bacteria.

1.1.1 Amplification of DNA by PCR

DNA was routinely amplified using the following 50µl PCR reaction mix: 1x Pfu Ultra HF Reaction buffer (Agilent), 0.2mM deoxynucleotide triphosphates (dNTPs) (Pharmacia Biotech), 1µM Primer 1, 1µM Primer 2, 50ng DNA, 2.5 units Pfu Ultra HF polymerase (Agilent). The 'basic' PCR cycle program used was as follows:

1. 94^{o}C for 5 minute (denaturation (denaturation of plasmid DNA and primer:template complexes))

2. 94°C for 30 seconds (cyclical denaturation)
3. T_{ann} (primers) for 30 seconds (primer annealing (annealing of primers to template))
4. 72°C for 2 minutes (extension (amplification of plasmid in a template-directed manner by DNA polymerase))
5. Cycle steps 2-4, 34 more times

Annealing temperature of primers (T_{ann}) was approximated at 3-4°C less than the T_m of the primers. The elongation time of the reaction at 72°C was adjusted according the length of expected product (2 minutes/kb).

2.1.3 Site-directed mutagenesis by over-lap extension

The cloning strategy for site-directed mutagenesis by over-lap extension is outlined in Figure 2.1. PCR 1 used the routine PCR reaction mix and the basic PCR cycle program. DNA fragments were separated by gel electrophoresis and visualised using a UV transilluminator as described below. PCR 2 used the following 50µl PCR reaction mix: 1x Pfu Ultra HF Reaction buffer (Agilent), 2.5 units Pfu Ultra HF polymerase (Agilent), 0.2mM dNTPs (Pharmacia Biotech), 1µM Primer 1, 1µM Primer 2, 1/10th PCR 1 product AB and 1/10th PCR 1 product BC. PCR 2 used the following '2cycles3' program:

1. 94°C for 3 minutes (denaturation)
2. 94°C for 30 seconds (cyclical denaturation)
3. Ramp to 45°C for 1 minute (0.1°C/second) (annealing)
4. 72°C for 5 minutes (extension)
5. Cycle steps 2-4, 4 more times
6. 94°C for 30 seconds (denaturation)
7. T_{ann} (Primers) for 30 seconds (Primer annealing)
8. 72°C for 5 minutes (extension)
9. Cycle steps 6-9, 29 more times
10. 72°C for 15 minutes

The DNA fragment product of PCR 2 was separated by gel electrophoresis and visualised using a UV transilluminator before being subject to restriction enzyme digestion and ligation into cut vector as described below.

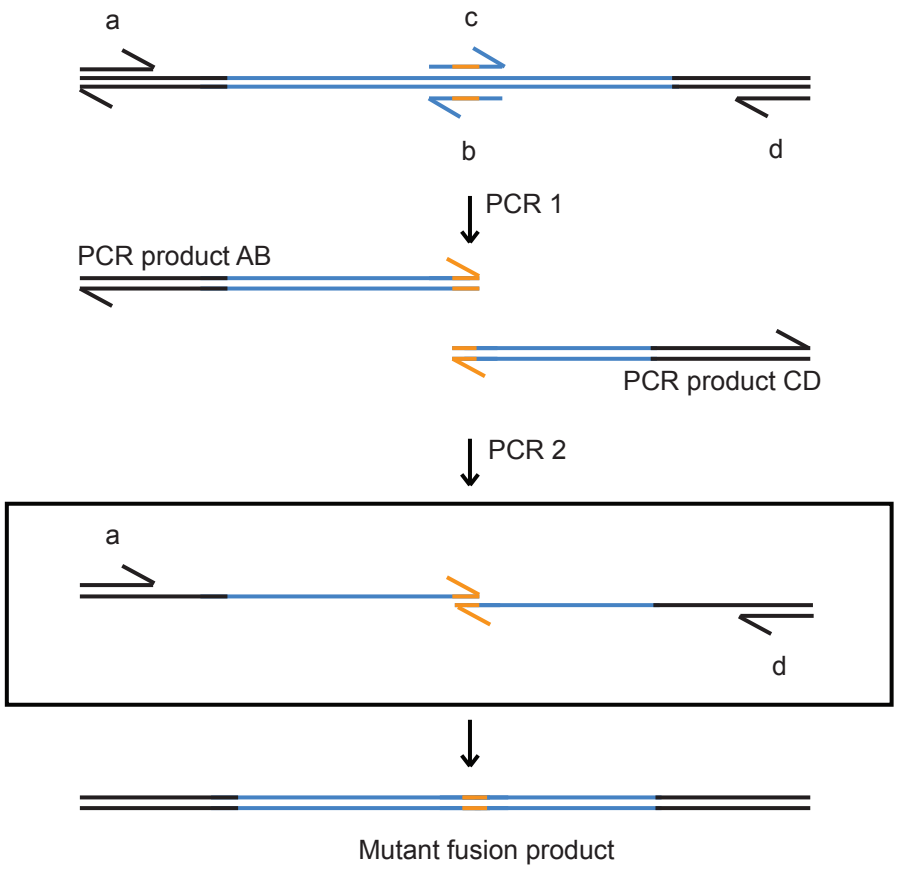

Figure 2.1 Schematic diagram of site-directed mutagenesis by over-lap extension DNA and synthetic oligonucleotides are represented by lines with half arrows indicating the 5' to 3' orientation. Black lines represent the pGEX-6P1 vector, blue lines represent the mCbx7 sequence and the orange lines represent the site of mutagenesis. Oligonucleotides are denoted by lower-case letters and PCR products are denoted by pairs of upper-case letter corresponding to the oligonucleotide primers used to generate that product. The boxed portion represents the intermediate step taking place during PCR 2, where the denatured fragments anneal at the overlap for extension by DNA polymerase to form the mutant fusion product, which is amplified in the presence of primers a and d.

2.1.4 Cloning shRNA expression vectors

Short hairpin RNA (shRNA) template inserts were created by annealing complementary oligonucleotides to create a synthetic DNA duplex for cloning. Unique siRNA target sites within mRNA nucleotides were identified using the GenScript siRNA Target Finder. Accession numbers used were: NM_001895 (CK2α), NM_001896 (CK2α') and NM_001320 (CK2β). The unique 19 nucleotide siRNA target sequence (SeqA1) generated by the GenScript program and its reverse-compliment counterpart (SeqA2) were entered into a template oligonucleotide sequence as follows:

shRNA fwd: .....GATCCCC(SeqA1)TTCAAGAGA(SeqA2)TTTTTGGAAA

shRNA rev:. AGCTTTTCCAAAAA(SeqA1)TCTCTTGAA(SeqA2)GGG……

SeqA1 and SeqA2 were separated by a loop region, which facilitated short hairpin structure folding upon expression. The sticky ends at the periphery of the oligonucleotide, allowed for ligation into the pRetroSuper vector. Oligonucleotides used to clone shRNAs against CK2α, CK2α' and CK2β are specified in Table 2.1.

Oligonucleotides were diluted to 1µg/µl in water. 3µl shRNA fwd primer and 3µl shRNA rev primer were mixed with 44µl annealing buffer heated to 94^{o}C for 4 minutes and then incubated ay 70^{o}C for 10 minutes. 3µl annealed primers were mixed with 50ng pRetroSuper vector previously cut with restriction enzymes HindIII and BglII (New England Biolabs (NEB)), 1µl 10x T4 DNA ligase buffer and 400 units T4 DNA ligase (NEB). This ligation mix was incubated at room temperature for 30 minutes before transformation of competent bacteria (described below)

2.1.5 Restriction digests and ligation of plasmids

Plasmid DNA or PCR products were digested with restriction enzymes to produce DNA fragments. These fragments were subsequently used in ligation reactors, either as the recipient vector or insert DNA. Digestion was set up in a total volume of 30µl using 1 unit restriction enzyme (NEB) for 1µg DNA (typically 2µg was used), 100µg/ml BSA (NEB) and 1x digestion buffer (NEB) chosen to provide optimal conditions for the restriction enzymes in question. Digests were incubated for between 30 minutes and 1 hour at 37^{o}C. Fragments were resolved by agarose gel

electrophoresis, purified from the gel, and DNA concentration was determined (described below).

Ligation reactions were set up in a total volume of 10µl with 1µl 10x T4 DNA ligase buffer, 400 units T4 DNA ligase (NEB) and a 3:1 ratio of insert:vector DNA e.g. 150ng insert DNA and 50ng vector DNA (although this did vary depending on fragment size). Ligation reactions were left for 1 hour at room temperature or overnight at 16^{o}C and 5µl was subsequently used to transform bacteria. A control reaction containing cut vector only was set up to determine background colony formation as a consequence of self-ligated plasmid.

2.1.6 Agarose gel electrophoresis and gel extraction

0.5-2% agarose gels (Invitrogen) (depending on the size of DNA fragment to be resolved) containing 50ng/ml ethidium bromide (Sigma) were cast using the Hoefer system. Once set, the gel was placed in an electrophoresis tank containing 1x TAE running buffer and samples were loaded alongside 10µl of pre-diluted molecular weight markers (Trackit 1Kb plus (Invitrogen)). 6x DNA loading buffer was added to DNA samples to allow visualisation of the gel front and assist sinking of samples into the wells. Electrophoresis was performed at 100V. Following sufficient separation, DNA fragments were visualised by a UV transilluminator (UVP BioDoc-IT). Relevant DNA fragment sizes were excised and recovered using the QIAquick Gel Extraction kit (Qiagen) according to manufacturer's instructions. DNA was typically eluted in 30µl EB.

2.1.7 DNA sequencing

DNA sequencing was performed by LRI Equipment Park using ABI PRISM Dye Terminator Cycle Sequencing kit (Applied Biosystems). PCR reactions contained low-level dye-labelled dideoxynucleotide triphosphate (ddNTP) terminators in a pool of dNTPs. Random incorporation of these ddNTP terminators caused premature termination of DNA polymerase. The products of such a PCR varied in length and were each labelled with one of the four ddNTPs. Sequencing reactions

contained 8µl big-dye terminator (BDT) 3.1 mix (Applied Biosystems), 3.2pmol sequencing primer and 250ng DNA, made up to a final volume of 20µl. The PCR cycling program used was as follows:

1. 96°C for 1 minute (denaturation)
2. 96°C for 10 seconds (cyclical denaturation)
3. Ramp to 50°C for 5 seconds (1°C/second)
4. Ramp to 60°C for 4 minutes (1°C/second)
5. Cycle steps 2-4, 24 more times

PCR products were purified using DyeEx 2.0 Spin kit (Qiagen), according to manufacturers instructions, to remove unincorporated dye-labelled ddNTPs. 30µl elute containing purified DNA was dried in a vacuum centrifuge (DNA Speed Vac Savant) and pellets were then processed by the LRI Equipment Park. This processing involved separation of PCR products using the Applied Biosystems Prism 3730 system. Sequences were analysed using MacVector software (Accelrys) and ddNTP fluorescence traces were confirmed manually. DNA sequencing was analysed using MacVector software (Accelrys).

2.1.8 Production of chemically competent bacteria

DH5α competent *E. coli* bacteria were thawed from -80°C stocks on ice. 20µl competent DH5α were inoculated into 10ml L-Broth (LB) and incubated, shaking at 200rpm overnight at 37°C alongside 10ml LB without DH5α (control). If the control 'culture' was clear of bacteria the following day then 100ml LB was inoculated with 1ml overnight DH5α culture and incubated shaking at 200rpm, at 37°C until it reached an optical density measured at a wavelength of 600nm (OD_{600}) of 0.5. Bacteria were pelleted at 3000rpm for 10 minutes at 4°C and supernatant was discarded. Cells were gently resuspended in 50ml ice-cold 100mM $MgCl_2$ and then pelleted at 3000rpm for 10 minutes at 4°C. After supernatant had been discarded, DH5α cells were gently resuspended in 100ml ice-cold 100mM $CaCl_2$ and left on ice for 60-90 minutes. After the cells were pelleted at 3000pm for 10 minutes at 4°C, the supernatant was discarded and cells were resuspended in 8ml ice-cold 85mM

$CaCl_2$ with 15% glycerol. 100µl aliquots were snap frozen in liquid nitrogen and stored at -80°C.

2.1.9 Transformation of chemically competent bacteria

Top10 One Shot (Invitrogen) or DH5α chemically competent bacteria (stored at -80°C) were thawed on ice. 10-50ng DNA in a total volume of 5µl was added to 50µl thawed bacteria and flicked to mix. The bacteria/DNA mix was incubated on ice for 30 minutes then transferred to a 42°C water bath for 45 seconds and immediately transferred back to ice for 2 minutes. Bacteria were subsequently incubated shaking at 200rpm with 500µl LB for 1 hour at 37°C. 50µl-250µl bacteria were spread on LB agar plates containing the selective drug (100µg/ml ampicillin) (LB AMP) and incubated overnight at 37°C.

2.1.10 Small-scale preparation of plasmid DNA (miniprep)

Small-scale preparation of plasmid DNA was used to screen bacterial colonies to identify those expressing successfully ligated plasmids. Single colonies picked from the transformation plate were inoculated in 5ml LB AMP and incubated overnight shaking at 200rpm, at 37°C. Bacteria were pelleted by centrifugation at 6000g for 10 minutes and supernatant was discarded. Plasmid preparation was then performed using the QIAprep Spin Miniprep kit (Qiagen) by following the manufacturers protocol and using the solutions provided. Bacterial cells were lysed under alkaline conditions. The lysate was subsequently neutralised and adjusted to high-salt binding conditions. the lysate was cleared by centrifugation (13,200rpm) and applied to a silica-gel membrane, which adsorbed DNA but not RNA, cellular proteins or metabolites. This membrane was washed in buffer containing 80% ethanol to remove salt. Pure plasmid DNA was eluted with 50µl EB.

2.1.11 Large-scale preparation of plasmid DNA (maxiprep)

100ml LB AMP was inoculated with 200µl overnight mini-culture and incubated overnight shaking at 200rpm, at 37°C. Alternatively, a scrape sample of a glycerol

stock of bacteria was inoculated in 100ml LB AMP and incubated overnight shaking at 200rpm at 37°C. This glycerol stock was made by mixing 500µl 60% filtered glycerol with 500µl of overnight mini-culture and snap freezing the mix in liquid nitrogen for subsequent storage at -80°C. Bacteria in the 100ml culture that had been incubated overnight shaking at 200rpm, at 37°C, were pelleted at 6000g for 15 minutes and supernatant was discarded.

Large-scale preparation of plasmid DNA was performed using the QIAfilter Plasmid Maxi kit (Qiagen) by following the manufacturer's protocol and using the solutions provided. Bacterial cells were lysed under alkaline conditions. Lysate was subsequently neutralised and debris removed using a QIAfilter cartridge (Qiagen). The remaining solution was loaded into a pre-equilibrated QIAGEN-tip by gravity flow. Salt and pH conditions ensured only DNA was adsorbed. The QIAGEN-tip was washed with medium-salt buffer to remove any remaining contaminants. Plasmid DNA was then eluted with high-salt buffer. Eluted plasmid DNA was desalted, concentrated by isopropanol precipitation and washed with 70% ethanol at room temperature. Purified DNA was briefly air-dried and re-dissolved in 500µl-1ml TE. Plasmid DNA concentration was determined using a spectrophotometer (Nanodrop (Thermo Scientific)), which measured absorbance of 260nm wavelength light in 1µl of eluted DNA.

2.2 Cell culture

All cell types used were cultured in Dulbecco's Modified Eagle Medium (DMEM) (GIBCO) supplemented with 10% foetal bovine serum (FBS) (PAA) and the antibiotics penicillin and streptomycin, which will together be referred to as 'medium'. *Asi*SI-ER-HA-U20S cells were grown in the continued presence of 1µg/ml puromycin. Cells were grown as monolayers in plastic tissue culture dishes at 37°C in 5% CO_2. Just prior to confluency, cells were washed in 37°C PBSA and incubated with diluted trypsin (between 1:2 and 1:10 trypsin (0.25% Trypsin-EDTA (Gibco)):PBSA depending on cell type) at 37°C. When cells began to detach from the plate medium was added to neutralise the trypsin and cells were seeded into new culture dishes. For cell lines, cells were generally split at a ratio 1:4 and 1:8.

For primary human fibroblasts, cells were split either 1:2 or 1:4 and new passage numbers (+1 or +2 respectively) were recorded accordingly.

2.2.1 Cell lines and primary fibroblasts

293T	Ad5/SV40 large T-transformed HEK293 (ATCC number CRL-1573)
U2OS	Human osteosarcoma cell line (ATCC number HTB-96)
*Asi*SI-ER-HA-U20S	Clonal U20S cell line that stably expressed *Asi*SI-ER fusion protein ((Iacovoni et al., 2010))
FDF	Human foetal dermal fibroblasts (Brookes et al., 2004)
Hs68	Human neonatal foreskin fibroblasts (ATCC number CRL-1635) (Ohtani et al., 2001)
IMR90	Foetal lung fibroblast strain (ATCC number CCL-186) (Nichols et al., 1977)
TIG3	Foetal lung fibroblast strain (ATCC number CRL-9609) (Provided by E.Hara)
ESC	Human endometrial stromal cells (fibroblast) (Brookes et al., 2004)

Table 2.2 Description of cell lines and primary fibroblasts

2.2.2 Storage and recovery of cells

Prior to storage, cells were released from the tissue culture dish using trypsin, as previously described, and resuspended in medium. Cells were pelleted at 750g for 5 minutes and resuspended in freezing medium (50% FCS, 10% DMSO and 40% medium) before being transferred to Cryovials (Corning Incorporated). Cryovials were placed in a freezing container (Nalgene) containing isopropanol, which ensured cells were gradually frozen (-1^{o}C/minute) when placed at -80^{o}C. Once frozen, cells were transferred to liquid nitrogen tanks. Cells were recovered from liquid nitrogen storage by placing the Cryovial directly in a 37^{o}C water bath to thaw (typically 1 minute). Cells were then transferred into 10ml medium and pelleted at

750g to remove DMSO. Cell pellets were resuspended in medium and seeded into a culture dish.

2.2.3 Transfection of cell lines

12 hours prior to transfection, approximately $4x10^6$ cells were seeded into a 100mm-diameter culture dish (BD Falcon) in a total volume of 10ml medium.

2.2.3.1 Lipofectamine 2000 transfection

Transfection Mix A (1.5ml OptiMem (Gibco) and 10µg plasmid DNA) and Transfection Mix B (1.5ml OptiMem and 30µl Lipofectamine 2000 (Invitrogen)) were incubated alone for 5 minutes and then mixed together and incubated at room temperature for a further 20 minutes. During this incubation, the medium bathing 293T cells was replaced with DMEM only. Transfection Mix A/B was then added to the cells. Cells were harvested for protein or RNA extraction 24 hours after transfection.

2.2.3.2 Calcium phosphate transfection for production of amphotropic virus

10µg of plasmid DNA was combined with 2µg pCG-VSV-G and 8µg pCG-Gag-Pol DNA (for retrovirus) or pCMV Δ8.2 (for lentivirus), mixed with 60µl 2M $CaCl_2$, and made up to 500µl with water. 500µl 2x HBS was added to the DNA mix in a drop-wise manner and solution was incubated at room temperature for 30 minutes without mixing. The solution was added to 293T cells in a drop-wise manner evenly over the plate. Cells were incubated under normal conditions for 10-14 hours before the medium was replaced with 10ml fresh medium. 24 hours later virus was harvested and used to infect HDFs.

2.2.4 Viral infection of human diploid fibroblasts (HDFs)

HDFs were split 1:4, 24 hours prior to infection into a 100mm-diameter culture dish. Amphotropic virus was collected from medium bathing 293T cells and filtered

through a 0.45µm Millex-HV filter (Millipore). For retroviral infection the total 10ml of virus-containing medium was added directly to the HDFs (with previous medium removed). For lentiviral infection the harvested virus was first diluted 1:5. 32-48 hours post-infection HDFs were washed and fresh medium was applied containing 0.75µg/ml Puromycin (Invitrogen). Selection efficiency was monitored against a plate of uninfected HDFs.

2.2.5 Chemical treatment of cells in culture

2.2.5.1 Tamoxifen (4OHT) *induction of ER-fusion protein translocation*

4OHT causes the translocation of ER-fusion proteins from the cytosol to nucleus. 4OHT (300µM in methanol) was diluted to a working concentration of 300nM in cell medium. Control medium contained an equivalent volume of methanol. *Asi*SI-ER-HA-U20S cell line and *Asi*SI-ER-HA-Hs68 HDF cells (both stably expressing HA-tagged *Asi*SI-ER fusion protein) were grown to near confluency and incubated with 4OHT or control medium for 4 hours. After this incubation, cells were fixed for immunofluorescence or chromatin immunoprecipitation (see below).

2.2.5.2 TBB and DRB inhibition of CK2

TBB and DRB are chemical inhibitors of protein kinase CK2. TBB (Sigma-Aldrich) (60mM in DMSO) was diluted to a working concentration of 300µM in cell medium. Control medium contained an equivalent volume of DMSO. HDF cells were incubated with TBB or control medium for 6 or 12 hours before harvesting.

DRB (Sigma-Aldrich) (30mM in ethanol) was diluted to 75µM in cell medium. Control medium contained an equivalent volume of ethanol. 293T cells were incubated with DRB for 3 hours before harvesting.

2.2.6 Harvesting cells

Cells were released from the culture dish using trypsin, as previously described, and resuspended in medium. Cells were pelleted at 750g for 5 minutes and

washed twice in 10ml ice-cold PBSA. The washed cell pellet was resuspended in 1ml ice-cold PBSA, transferred to a 1.5ml microcentrifuge tube and pelleted. The cell pellet was then either snap frozen in liquid nitrogen and stored at -80^{o}C or immediately lysed for protein or RNA extraction.

2.3 RNA techniques

2.3.1 Preparation of total cellular RNA

Total RNA was purified using the Qiagen RNeasy kit according to the manufacturer's protocol for mammalian cells. Harvested cells were lysed in 600µl lysis buffer containing 2-Mercaptoethanol to inactivate RNases. Lysates were homogenised by passing them through a QIAshredder spin column (Qiagen) at 13,200rpm for 1 minute. 70% ethanol was added to the samples, which were then transferred to RNeasy spin columns. RNA was bound to the silica gel of the RNeasy spin column by centrifugation at 13,200rpm, washed to remove contaminants and eluted in RNase-free water. The Nanodrop spectrometer was used to determine the RNA concentration (by measuring sample absorbance at a wavelength of 260nm) and to check the purity of the RNA.

2.3.2 Reverse transcription PCR (RT-PCR)

RNA was reverse-transcribed using the High Capacity cDNA Reverse Transcription kit (Applied Biosystems) according to the manufacturers instructions. Random hexamers were used, as opposed to oligo(dT)$_{16}$, to prime cDNA synthesis. 2µg RNA was used in a 50µl reaction mix that contained RNase inhibitors. The reaction mix was heated to 65^{o}C for 10 minutes to initiate the reaction, held at 42^{o}C for 30 minutes for reverse transcription and then heated to 95^{o}C for 5 minutes to inactivate the reverse transcriptase. The cDNA product was used for Quantitative Real-Time PCR (see below).

2.3.3 Quantitative Real-Time PCR (qPCR) of cDNA

Primers were typically designed to be 20-24mers with 50-60% GC content, a $T_m \geq 60^oC$ and no more than three consecutive repeats of the same base. Exonic regions where forward and reverse primers anneal were either separated by a large intron in genomic sequence or spanned an intron/exon boundary. This prevented potential amplification of cDNA in the PCR. Products were designed to be around 150bp. Correct product size was verified by agarose gel electrophoresis alongside a H_2O control qPCR. High specificity of a qPCR reaction corresponded to a single sharp peak in the dissociation curve at a temperature above 80^oC in the presence of cDNA but not in an H_2O control. These curves were also assessed to ensure primer-dimers were not formed during the qPCR reaction. Primers used are detailed in Table 2.3.

Every cDNA:Primer mix reaction combination was performed in triplicate. A primer set measuring changes of a reference gene invariant under experimental condition (β tubulin or RPS17) was used as an internal control so as to allow relative quantification of mRNA levels between samples. Each well of a MicroAMP fast optical 96-well Reaction plate (Applied Biosystems) contained the follow reaction mix: 1µl cDNA, 11µl sterile water, 0.5µl Primer mix (10µM fwd primer and 10µM rev primer), and 12.5µl Express qPCR Supermix with Premixed ROX (Invitrogen), which is based on SYBR green incorporation and includes ROX passive reference dye. Reaction mixes were transferred from master mixes of A) cDNA and sterile water and B) Express qPCR Supermix and Primer mix. Wells were sealed with MicroAMP Optical Adhesie Film (Applied Biosystems), centrifuged to remove any bubbles and PCR cycling was carried out in a 7500 FAST Real-Time PCR machine (Applied Biosystems). The following cycling protocol was used:

1. 95^oC for 15 seconds (hotstart of the polymerase)
2. 95^oC for 3 seconds (cyclical denaturation)
3. 60^oC for 30 seconds (primer anneal and extension)
4. Fluorescence read
5. Cycle steps 2-4, 39 times
6. Dissociation stage

Data were analysed using SDS software (Applied Biosystems) and exported to Excel.

Name	Sequence (5' – 3')
CBX7 fwd	CGGAAGGGTAAAGTCGAGTATC
CBX7 rev	TCGGACCTCTCTTCCTATACCC
CK2α fwd	CTTCTCAGGGGAGGCAGGA
CK2α rev	CACACTTCCACAAGAGCCACT
CK2α' fwd'	CACTTTTCCATAAGCAGAACAAGA
CK2α' rev	TACATTCGGAAGTGAGGTTTGATA
CK2β fwd	AAAAGTACCAGCAAGGAGACTTTG
CK2β rev	GTGTCTTGATGACTTGGGTGTGTA
Cyclin D2 fwd	ATTGCTCTGTGTGCCACCGAC
Cyclin D2 rev	GGCATCACAAGTGAGCGAGCT
GAS1 fwd	TCTCGACAGCTGTTCATTTCC
GAS1 rev	GCAGAAGGTCCCCTTTCG
IGFBP5 fwd	GGTTTGCCTCAACGAAAAGA
IGFBP5 rev	AGATCTTGGGGGAGTAGGTCTC
p16 fwd	CGGTCGGAGGCCGATCCAG
p16 rev	GCGCCGTGGAGCAGCAGCAGC
RPS17 fwd	GCACCAAAACCGTGAAGAAG
RPS17 rev	TCTTGTTGCGGAGCTTTTTG
TGFB2 fwd	CCAAAGGGTACAATGCCAAC
TGFB2 rev	CAGATGCTTCTGGATTTATGGTATT
β tubulin fwd	ATGGATCCCCAACAATGTCA
β tubulin rev	TCCTGGATGGCTGTGCTATT

Table 2.3 List of primers used to amplify cDNA (previously generated from mature mRNA)

2.3.4 qPCR of DNA purified from ChIP

DNA purified from ChIP assays (Chapter 2.4.9) was also analysed by qPCR in essentially the same way as cDNA prepared from cellular mRNA (Chapter 2.3.3). However, 2µl DNA was used per well and therefore only 10µl sterile water. Primer sets to measure reference gene expression were not included on the plate. Primers to amplify genomic DNA had been verified previously in the lab, these are detailed in Table 2.4. In addition, dissociation curves were checked for each qPCR reaction as described for qPCR of cDNA.

Name	Sequence (5' – 3')
CDKN2A-1 fwd	GGAACCTAGATCGCCGATGTA
CDKN2A-1 rev	TGTTTTACGCGTGGAATGCAC
CDKN2A-2 fwd	GTGGGTCCCAGTCTGCAGTTA
CDKN2A-2 rev	CCTTTGGCACCAGAGGTGAG
CDKN2A-3 fwd	GGAGCGATGTGATCCGTTATC
CDKN2A-3 rev	TGAAATCCCAATCGTCTTCCAC
CDKN2A-5 fwd	CTCAAAGCGGATAATTCAAGAGC
CDKN2A-5 rev	AAGCCTTAAGAACAGTGCCACAC
CDKN2A-7 fwd	AGAGGGTCTGCAGCGG
CDKN2A-7 rev	TCGAAGCGCTACCTGATTCC
CDKN2A-9 fwd	CAAGCTTCCTTTCCGTCATGC
CDKN2A-9 rev	GCCAGAGAGAACAGAATGGTCAGAGCCA

Table 2.4 List of primers used to amplify DNA (purified by ChIP)

2.4 Biochemistry

2.4.1 Preparation of total cell lysate

Harvested cells were lysed with approximately 10 x cell pellet volume ice-cold NP40 lysis buffer (1) for 10 minutes on ice. The lysate was cleared of nuclear debris by centrifugation at 13,200rpm for 10 minutes at 4^{o}C and supernatant was collected on ice. Protein concentration was determined by Bradford assay. Protein Assay Dye Reagent (Bio-Rad) was diluted 1:5 in water and 995µl was transferred to a microcentrifuge. 5µl protein lysate or BSA standard of known concentration (0.125-20µg/µl) was added to the diluted Dye Reagent, the solution was vortexed and transferred to a plastic cuvette (Sarstedt). The solution was then incubated for 15 minutes at room temperature before absorbance was measured at a wavelength of 595nm using an Ultrospeco-2000 spectrometer (Pharmacia Biotech). Protein lysate concentrations were estimated from a standard curve calculated from absorbance values of BSA standards of known concentration.

2.4.1.1 Phosphatase treatment of cell lysates

Harvested cells were lysed with approximately 10 x cell pellet volume ice-cold Tween lysis buffer, incubated for 15 minutes on ice and sheared by passing

through a 23G gauge needle. The lysate was cleared of nuclear debris by centrifugation at 13,200rpm for 10 minutes at 4^{o}C and the supernatant was collected on ice. Protein concentration was determined by Bradford assay as described above. The lysate was treated with 4,000 units Lambda Protein Phosphatase NEB) per mg protein in 1x NEBuffer and 1mM $MnCl_2$, for 45 minutes at 30^{o}C and was then fractionated by SDS-PAGE prior to immunoblotting.

2.4.2 SDS-PAGE

Polyacrylamide gels (8x10x1.5cm (small) or 15x15x1.5cm(large)) were poured using the Protean system (Bio-Rad) or the Hoefer system respectively. Running gels were cast from a mix of 375mM TrisHCl pH 8.8, 0.1% SDS, 0.1% APS, 0.04% TEMED and 8-15% acrylamide (type) depending on the molecular weight of the protein of interest. Following polymerisation of the running gel, the stacking gel containing 5% acrylamide in 375mM TrisHCl pH 6.8, 0.1% SDS, 0.1% APS and 0.1% TEMED was poured. A comb was inserted before polymerisation to create wells to hold protein samples. Protein samples were boiled for 5 minutes in 1x Laemmli buffer and loaded into the wells of a cast polyacrylamide gel. Molecular weight markers (12-225kDa) (Amersham) were loaded into a well alongside protein samples to later identify proteins of interest according to their molecular weight. For small gels, electrophoresis was performed in 1x running buffer in a Protean tank (BioRad) at a constant current of 30mA per gel until desired fractionation was achieved. For large gels, electrophoresis was performed in 1x running buffer in a Hoefer tank at a constant current of 80mA at 4^{o}C until desired fractionation was achieved.

For fractionation of ^{32}P-containing samples and for samples to be subsequently analysed by mass spectrometry, the NuPAGE system (Invitrogen) was used. Samples were loaded into a precast 10%, 12% or 4-12% NuPAGE Bis-Tris gel (Invitrogen) and run in 1x NuPAGE MOPS running buffer (Invitrogen). Gels were run at a constant current of 30mA per gel until desired fractionation was achieved.

2.4.3 Gel Coomassie staining

Following SDS-PAGE, gels were fixed in fixing solution for 30 minutes before being submerged in Coomassie stain solution overnight, at room temperature. The gel was destained in destaining solution until the gel background was clear. Gels were stored in 3% acetic acid.

2.4.4 Immunoblotting and stripping

Following fractionation by SDS-PAGE, protein was transferred from small acrylamide gels to Protran nitrocellulose membrane (Whatman) using the Protean system (BioRad). The membrane was soaked in transfer buffer, placed on top of the running gel and sandwiched between 3mm filter paper (Whatman) and sponge pads (Biorad) within a cassette (Biorad). The closed cassette was inserted into the Protean transfer module. Proteins were transferred at room temperature at 100V for 60-90 minutes depending on the size of the protein of interest, or at 4^{o}C at 30V overnight. Protein from large acrylamide gels was transferred to Protran nitrocellulose membrane (Whatman) using semi-dry transblot apparatus (Atto Corp). The membrane was soaked in transfer buffer and placed on top of 3mm filter paper. The acrylamide gel was laid on top of the membrane and 3mm filter paper was laid on top of the gel. This sandwich was placed between the electrode plates. Proteins were transferred at 270mA for 60 minutes.

Following transfer, the nitrocellulose membrane was incubated with Blocking buffer for 1 hour at room temperature or overnight at 4^{o}C. Primary antibodies used are listed in Table 2.5. Blocked membranes were incubated with primary antibodies against the protein/epitope of interest that were diluted in Blocking buffer. These incubations were either overnight at 4^{o}C or for 1 hour at room temperature depending on the antibody. Membranes were then subject to 3 x 10 minute washes in PBST. The relevant secondary antibody (HRP-conjugated anti-rabbit, anti-mouse or anti-goat IgG (Amersham)) was then applied to the washed membrane (1:2,000, previously diluted in Blocking buffer) and left to incubate for 1 hour at room temperature. The membrane was then subjected to further 3 x 10 minute washes in PBST. Excess PBST was blotted from the membrane, which was then laid on

flattened Saran Wrap (Dow). Antibody complexes on the membrane were detected by the addition of a 1:1 mix of enhanced chemiluminescence (ECL) reagents 1 and 2 (Amersham Pharmacia Biotech). ECL was left on the membrane sandwiched between Saran Wrap for one minute before excess was blotted off and the membrane was placed in a Hypercassette (Amersham Pharmacia Biotech) within fresh Saran Wrap. Hyperfilm (GE Healthcare) was then exposed to the membrane in the cassette for anywhere between 20 seconds and 24 hours depending on the amount of protein of interest and the sensitivity of the antibody. After exposure, the film was developed in an automatic x-ray film processor (model JP-33 (JPI Healthcare Solutions). A ^{14}C-labelled ruler strip within the cassette was used to position the developed film relative to the membrane. Occasionally it was necessary to remove the previous primary antibody signal before re-probing the membrane with a different primary antibody. On these occasions, the membrane was incubated with stripping buffer at 50^{o}C for 30 minutes, washed extensively with PBST before being re-blocked in Blocking buffer.

2.4.5 Antibodies

2.4.5.1 Antibody generation

A peptide representing the C-terminus of CBX7 was synthesised on a branched lysine core (MAP) by the LRI Peptide Synthesis facility. This peptide sequence was FREAQAAEGFFRDRSGKF. This antigen was used by Pettingill Technology Ltd (PTL) to immunize a pair of rabbits. The terminal bleed was collected 77 days after immunisation. The terminal bleed was subsequently IgG purified by LRI Cell services.

2.4.5.2 Commonly used antibodies

Primary antibodies that were used for the work presented in this thesis are listed in Table 2.5.

Antigen	Origin / Source	Product number	Species and Type	Dilution for Immunoblotting and Immuno-fluorescence
BMI1	Cell Signalling	6964	Rabbit mAb	1:500
BMI1	Millipore	05-637	Mouse mAb	1:500
β-tubulin	Santa Cruz	sc-9140	Rabbit pAb	1:1000
CK2a	Cell Signalling	2656	Rabbit pAb	1:1000
CK2a	Bethyl	A300-198A	Rabbit pAb	1:1000
CK2a	Santa Cruz	sc-12738	Mouse mAb	1:100
CK2a'	Santa Cruz	sc-6481	Goat pAb	1:500
CK2b	Santa Cruz	sc-12739	Mouse mAb	1:100
FLAG (HRP)	Sigma	A8592	Mouse mAb	1:4000
Histone H3K27me3	Millipore	07-449	Rabbit pAb	1:1000
HA	Santa Cruz	sc-805	Rabbit pAb	1:1000
HPH2	LRI	1615	Rabbit pAb	1:500
CBX7	Abcam	21873	Rabbit pAb	1:1000
Histone H3	Abcam	1791	Rabbit pAb	1:4,000
p16	LRI	JC8	Mouse mAb	1:5
p18	Novus Biologicals	NB120-3216	Mouse mAb	1:200
RING2	Haruhiko Koseki (Atsuta et al., 2001)	MAb3-3	Mouse mAb	1:500
RING1	Cell Signalling	2820	Rabbit pAb	
Mel18	Santa Cruz	10744	Rabbit pAb	1:500
Phospho-Pol II (Ser2)	Covance	MMS-129R	Mouse mAb	1:500
IgG	Abcam	46540	Rabbit pAb	
IgG	Abcam	18413	Mouse	
γH2AX	Millipore	05-636	Mouse mAb	1:1000
γH2AX	Cell Signalling	9718	Rabbit mAb	1:1000
53BP1	Santa Cruz	sc-22760	Rabbit pAb	1:200
Phospho-MEK (Ser217/221)	Cell Signalling	9121S	Rabbit pAb	1:1000
PARP	Cell Signalling	9532	Rabbit mAb	1:1000
Phospho-CBX7 (Thr119)	Emily Bernstein (Mount Sinai School of Medicine)		Rabbit pAb	1:1000
β-actin	Sigma	A5441	Mouse mAb	1:2000

Table 2.5 List of commonly used primary antibodies

2.4.6 Phosphoenrichment assay

Harvested cells were lysed and the lysate was fractionated to separate phosphorylated and non-phosphorylated proteins using the TALON PMAC Phosphoprotein Enrichment kit (Clontech) according to the manufacturers instructions. Harvested cells were lysed by incubating in 30µl Buffer A (Clontech) for each mg of cells, on ice for 10 minutes. The lysate was cleared at 10,000g for 20 minutes at 4^{o}C to pellet any insoluble material. Some cleared lysate was reserved for later analysis (Input). A maximum of 8mg cleared lysate was loaded into an equilibrated Phosphoprotein Affinity column (Clontech) and was incubated rotating end-over-end for 20 minutes at 4^{o}C. This allowed phosphorylated proteins in the lysate to bind the Phosphate Metal Affinity Chromatography (PMAC) resin (Clontech) of the column. The column was then left to stand upright for 5 minutes at room temperature to allow the resin to settle. The column top and end caps were then removed and non-phosphorylated proteins, that had not bound the resin, were collected in the flow-through. The column was washed four times with Buffer A (Clontech). 4 x 1ml Buffer B (Clontech) were added to the column to elute phosphorylated proteins from the resin. Elutes were pooled and stored on ice immediately after elution. Flow-through and eluted samples were fractionated by SDS-PAGE alongside input samples equivalent to 2% volume of cell lysate loaded on the PMAC column.

2.4.7 Immunoprecipitation

Harvested cells were lysed in 10 x NP40 lysis buffer 2 on ice for 10 minutes. The lysate was cleared at 13,200rpm for 15 minutes. 60µl equilibrated beads (previously resuspended to a 50% slurry) per 1ml of lysate, were added to the cleared lysate and incubated rotating end-over-end for 1 hour at 4^{o}C. The beads used were dependent on the primary antibody to be used for immunoprecipitation of the protein of interest. Pierce Protein G agarose (ThermoScientific) beads were used for mouse monoclonal antibodies and Pierce Protein A agarose (ThermoScientific) beads were used for rabbit polyclonal antibodies. Following this incubation, beads (and any bound proteins) were pelleted at 13,200rpm for 5 minutes at 4^{o}C and pre-cleared lysate was transferred to a fresh microcentrifuge

tube. Pre-cleared lysate was incubated with 5µg primary antibody rotating end-over-end at 4^{o}C overnight. Typically 1mg (at a concentration of around 1mg/ml) pre-cleared protein was used per immunoprecipitation. 10% of the input was set aside for later analysis. Non-specific Rabbit control IgG ChIP-grade or Mouse control IgG ChIP-grade antibodies (Abcam) were used to immunoprecipitate lysate as a negative control. Antibody amounts per immunoprecipitation are detailed in table 4. Following the overnight incubation, 60µl fresh equilibrated beads (previously resuspended to a 50% slurry), per 1ml of lysate, were added to the lysate containing immune complexes and incubated rotating end-over-end for 2-3 hours. The beads were then pelleted (along with any immune complexes) at 2,000rpm, washed four times in 1ml ice-cold lysis buffer and then once in ice-cold PBSA. Immune complexes were eluted from beads by boiling for 5 minutes in 100µl 2x Laemmli sample buffer, pelleting beads at 13,200rpm and removing the supernatant. Input and immunoprecipitated proteins were fractionated by SDS-PAGE prior to immunoblotting.

For the immunoprecipitation of HA/FLAG epitope-tagged proteins, no pre-clearing of the lysate was required. 30µl of a 50% slurry of anti-FLAG M2-agarose affinity gel (Sigma) or anti-HA-agarose (Sigma) beads were added directly to cleared lysate and incubated rotating end-over-end for 2 hours and 30 minutes. The beads were subsequently washed four times in 1ml lysis buffer before eluting with 200µg/ml FLAG or HA peptide in a total volume of 150µl, by rotating end-over-end for 30 minutes at 4^{o}C. Beads and peptide were pelleted at 13,200rpm before removing eluted protein and boiling this in 1x Laemmli sample buffer.

2.4.8 Gel filtration

Whole cell lysate and immune complexes were fractionated using Superose 6 High-Resolution (HR) 10/30 Gel Filtration Column (GE Healthcare) according to the manufacturer's instructions. Gel filtration separates molecules according to size as they pass through gel filtration medium packed within a column. Smaller molecules will diffuse into pores of the matrix and therefore take longer to travel the length of the column. The molecular weight (MW) range over which molecules are efficiently

separated is determined by the choice of gel filtration medium. Superose 6 HR 10/30 gel filtration column (GE Healthcare), enables high-resolution fractionation of protein complexes between 5 kDa and 5 MDa. This column was initially calibrated using the HMW and LMW calibration kit (GE Healthcare) according to the manufacturer's instructions.

For analysis of whole cell lysate, harvested cells were lysed in CHAPS lysis buffer for 20 minutes on ice. The lysate was subjected to two rounds of clearing at 13,200rpm to remove any aggregates of insoluble material. The protein concentration of the lysate was measured and adjusted to a maximum of 12.5mg/ml. For analysis of immune complexes, it was necessary to amend the immunoprecipitation protocol (detailed above) slightly to perform the final wash steps with 1ml CHAPS lysis buffer and to elute the immune complexes in this buffer (the Superose 6 column may not be compatible with NP40 containing buffer (Goedele Maertens (personal communication)). Immunoprecipitation was performed with starting material equating to approximately 5 x confluent 100mm-diameter culture dishes of 293T cells.

200µl of eluted immune complexes or 200µl whole cell lysate (≤ 12.5µg/ml) was loaded onto the Superose 6 HR 10/30 Gel Filtration Column (GE Healthcare) that had been previously equilibrated with CHAPS lysis buffer. Protein run through the column was collected in 0.5ml fractions at 4^{o}C. 10% Trichloroacetic acid (TFA) was added to each 500µl fraction and incubated overnight rotating at 4^{o}C to precipitate proteins. The following day, samples were centrifuged at 13,200rpm for 30 minutes at 4^{o}C, supernatant was removed and the pellet of precipitated protein was vortexed with 500µl ice-cold acetone. This acetone wash was repeated twice more. After the final wash, acetone was removed and the pellet was vacuum dried for 5 minutes. The pellet was subsequently boiled for 5 minutes in 2x Laemmli sample buffer. Proteins were fractionated by SDS-Page prior to immunoblotting.

2.4.9 Fixed chromatin immunoprecipitation (ChIP)

Cells to be used for chromatin immunoprecipitation (ChIP) were treated with formaldehyde, a reversible DNA-protein cross-linking agent, before they were harvested. Cells were incubated by rocking with 1% formaldehyde at room temperature for 10 min. The reaction was then quenched by addition of glycine to a final concentration of 125 mM and incubation at room temperature for 5 min. Cells were scraped from culture dishes and transferred to 225ml conical tube (BD Falcon). Cells were pelleted at 2,000rpm for 5 minutes at 4^{o}C. The pellets were resuspended in 10 x pellet volume of ice-cold ChIP swelling buffer (containing the following inhibitors: 5mM NaF, 1mM PMSF, 1x protease inhibitor cocktail (Roche), 25mM β-glycerophosphate and 1mM Na_3VO_4), incubated on ice, rocking for 10 minutes and homogenised with 50 strokes of a tight pestle (Wheaton). Nuclei were pelleted at 4,400rpm for 5 minutes at 4^{o}C. The supernatant was discarded and nuclei were resuspended in 5 x pellet volume of ChIP sonication buffer (containing the following inhibitors: 5mM NaF, 1mM PMSF, 1x protease inhibitor cocktail, 25mM β-glycerophosphate and 1mM Na_3VO_4). The chromosomal DNA was then sheared using a BioRuptor waterbath sonicator (Diagenode). Sonication was performed at the high setting for intervals of 30 seconds of sonication followed by 30 seconds rest (to keep samples cool) over three 12 min periods. Ice in the waterbath was replaced after each 12-minute cycle. After the first cycle, the concentration of DNA was roughly estimated by adding 2µl chromatin to 98µl 0.1M NaOH and using the Nanodrop sepctrometer to estimate the DNA concentration of the sample (as described previously). Following this measurement, samples were adjusted to equivalent concentrations to ensure equivalent sonication efficiency between different conditions. After the sonication cycles were complete, chromatin was centrifuged at 13,200rpm for 15 minutes at 4^{o}C and supernatant was transferred to a fresh 2ml microcentrifuge tube. DNA concentration was again measured using the Nanodrop spectrometer and samples were adjusted to a DNA concentration of 1.667µg/µl.

Immunoprecipitation of the protein of interest was performed using 300µg chromatin by essentially the same protocol as previously described. However, immunoprecipitation was carried out in ChIP sonication buffer and following

incubation of the relevant agarose beads with immune complexes, beads were washed with 1 x 1ml ChIP sonication buffer, 1 x 1ml ChIP wash buffer A, 1 x 1ml ChIP wash buffer B and 2 x 1ml ChIP TE buffer. Following these washes, the beads were resuspended in 100µl ChIP elution buffer, incubated at 65^{o}C for 5 minutes and then rotated end-over-end for 15 minutes. The beads were then pelleted at 2,000rpm for 3 minutes and the elute was transferred to a fresh 1.5ml microcentrifuge tube. This elution step was repeated once more, with the spin being performed at 13,200rpm to collapse the beads, and elutes were pooled. Inputs were brought up to 200µl with ChIP TE buffer. 6.4µl 5M NaCl and 4µl 1mg/ml DNase-free RNase A (Qiagen) was added to both the elutes and input samples, which were subsequently incubated at 65^{o}C overnight to reverse the formaldehyde-induced protein-DNA cross-linking.

Reverse cross-linked samples were cooled and DNA was purified using the QIAquick PCR Purification kit (Qiagen) according to the manufacturer's instructions. DNA was typically eluted in 30-60µl EB buffer (Qiagen). DNA was subject to qPCR analysis as previously described. The sonication efficiency of chromatin was confirmed by analysing DNA fragment sizes on a 1% agarose gel. The target DNA fragment size range was 0.5 – 1 kb.

2.4.9.1 ChIP-seq and bioinformatics analysis

Library preparation and Solexa genome-wide sequencing was performed by the LRI Advanced Sequencing Facility. Typically 60µl of DNA was submitted to the LRI Advanced Sequencing Facility at a minimum concentration of 0.2µg/µl. To obtain enough DNA, parallel ChIPs were performed and DNA elutes were subsequently pooled and concentrated. Input DNA was used as a control for the ChIP seq analysis. Sequence alignments were performed using Novoalign (version 2.07.14) allowing for a single base mismatch per read. Reads were mapped to the human genome (assembly hg19). Peak calling was performed using MACS (version 1.4.0rc2).

2.4.10 Production of recombinant protein

BL21 *E. coli* were transformed with pGEX-6P1 vector contain the gene of interest. To check the efficiency of protein production following IPTG induction, 3-4 clones were analysed by the small-scale protein production protocol. Large-scale protein production was performed for successful clones.

2.4.10.1 Small-scale production of recombinant protein

20ml LB AMP was inoculated with a single colony and incubated at 37^{o}C overnight, with shaking at 200rpm. Subsequently, 50ml LB AMP was inoculated with 1ml of the overnight culture and incubated at 37^{o}C, with shaking at 200rpm, until culture reached an OD_{600} between 0.4 and 0.6 (log growth phase). 1ml culture was removed, pelleted at 4,400rpm and resuspended in 2x Laemmli sample buffer (SB). 1mM IPTG was added to the remaining culture to induce protein expression. The culture was subsequently incubated at 37^{o}C, shaking at 200rpm, and 2ml samples were removed after 2, 3 and 4 hours. These 1ml samples were pelleted at 4,400rpm, and resuspended in Xml 2x Laemmli sample buffer (where X is 100x(OD post-IPTG/OD pre-IPTG). Samples were fractionated by SDS-PAGE and evaluated by Coomassie staining.

2.4.10.2 Large-scale production of recombinant protein

500ml LB AMP was inoculated with 10ml overnight culture and incubated at 37^{o}C, with shaking at 200rpm, until culture reached an OD_{600} between 0.4 and 0.6 (log growth phase). 1mM IPTG was added to induce protein expression and culture was incubated shaking at 200rpm, at 37^{o}C for a further 2 hours. Bacteria were pelleted at 4,400rpm at 4^{o}C for 10 minutes. The bacterial pellet was resuspended in 5 volumes GST lysis buffer, incubated for 10 minutes on ice and sonicated on ice at medium intensity (Soniprep 150) for 3 cycles of 20 seconds on/20 seconds off. The lysate was cleared at 13,200pm for 10 minutes. Cleared lysate was incubated with equilibrated glutathione sepharose 4B beads (GE Healthcare) (100µl per 100ml culture) for 30 minutes at room temperature. The beads were washed 4 times with 10 x bead volume of ice-cold GST lysis buffer (beads were pelleted at 500g).

Protein was eluted in 3 x 500µl GST elution buffer (containing 10mM reduced glutathione) for every 1ml beads. The elute was concentrated with microcon filter devices (Ultracel YM-10 membrane) (according the manufacturer's instructions), which also removed any excess glutathione. Alternatively, protein was eluted from beads using PreScission protease (GE Healthcare) to cleave the GST tag from the protein. In this case, beads were equilibrated with GST cleavage buffer before incubation with 80 units PreScission protease per 1ml beads, and GST cleavage buffer to a total volume of 1ml. The beads were incubated for 4-24 hours at 4^{o}C. Beads, GST and PreScission protease were pelleted at 500g, whilst purified protein was recovered in solution. Purified protein was analysed by SDS-PAGE alongside a series of BSA standards of known concentration (0.1-6mg/ml). This gel was subsequently stained by the Coomassie staining protocol described previously.

2.4.11 GST pull-down assay

Whole cell lysates were prepared from harvested cells NP40 lysis buffer 1, as described previously. 5mg lysate was precleared by incubation with 60µl GST glutathione sepharose 4B (GS4B) beads (GE Healthcare) (previously washed in lysis buffer and resuspended to a 50% slurry), rotating end-over-end for 1 hour at 4^{o}C. Beads were pelleted at 13,200rpm and 5mg precleared lysate was incubated with 10µg purified GST-tagged protein and 50µl fresh 50% slurry of GS4B beads for 2 hours, rotating end-over-end at 4^{o}C. 10% of the input was set aside for later analysis. The beads were pelleted at 500g, washed four times in 1ml GST lysis buffer, and the proteins were eluted in 60µl GST elution buffer (containing 10mM reduced glutathione). The beads were pelleted at 13,200rpm and the elute was boiled with 1x Laemmli sample buffer. Input and proteins recovered from the GST pull-down were fractionated by SDS-PAGE prior to immunoblotting.

2.4.12 Peptide array synthesis

Peptide arrays were generated by the LRI Peptide Synthesis facility. Peptide arrays were made from 20mer peptides. For peptide-scanning arrays, each peptide in the

array was advanced from the previous by 1 or 2 residues (as specified in the figure legend) in the C-terminal direction of the protein being represented. For peptide substitution arrays each peptide had an amino acid of the wild-type peptide substituted for one of the 20 common amino acids. Peptide arrays were comprised of 600 or 777 peptides spots (the latter spot diameters being smaller than the former). Peptide arrays were synthesised on an Intavis Multipep Peptide Synthesiser (Intavis Bioanalytical Instruments AG, Cologne, Germany). Each amino acid was coupled by activating its carboxylic acid group with diisopropylcarbodiimide in the presence of hydroxybenzatriazole. Individual aliquots of the 20 common amino acids (which are N-terminally protected) were spotted onto a cellulose membrane (100mm x 150mm) that had been derivatised to have 8-10 ethylene glycol spacers between the cellulose and an amino group. Peptide synthesis was accomplished by cycles of coupling amino acids, washing and then removing the temporary N-terminal protecting group. Once the required number of cycles was complete, the membrane was subjected to various wash steps to remove side chain protecting groups and TFA salts. Loading was 400nmol/cm^2. For a 4mm diameter spot this equates to 50nmol peptide per spot. Membranes were dried and stored at -20^oC before use.

2.4.13 Peptide array kinase assay

The peptide array was hydrated in 50% methanol and blocked for 2 hours in 1ml Kinase assay buffer at room temperature. Blocking solution was drained and the peptide array was incubated with 6125 units of recombinant CK2α or CK2a' (Calbiochem) and 3.75µCi [γ-^{32}P] ATP (PerkinElmer) in 1ml Kinase assay buffer for 2 hours at 37^oC. 1 unit of CK2α is defined as the amount of enzyme that will catalyse the transfer of 1.0pmol phosphate from ATP to the synthetic CK2 substrate RRRDDDSDDD per minute at 37^oC, pH 8.5. The membrane was subsequently washed by 5 x 10 minute incubations with 75mM H_3PO_4 and 5 x 10 minute incubations with PBSA before exposing for autoradiography.

2.4.14 Peptide array binding assay

The peptide array was hydrated in 50% methanol and blocked for 2 hours in 1ml Binding assay buffer at room temperature. Blocking solution was drained and the peptide array was incubated with 2µg recombinant CK2α (Calbiochem) in 1ml Binding assay buffer, or Binding assay buffer alone as a negative control. This incubation was carried out at room temperature for 2 hours. The membrane was subsequently washed by 5 x 10 minute incubations with TBST and subjected to immunoblotting.

2.4.15 *In vitro* kinase assay and analysis by ^{32}P incorporation

2µg recombinant protein substrate was incubated with 100 units of CK2 holoenzyme (Calbiochem) and 1.5µCi [γ-^{32}P] ATP in 20µl Kinase assay buffer for 30 minutes at 30^{o}C. 1 unit of CK2 holoenzyme is defined as the amount of enzyme that will catalyse the transfer of 1.0pmol phosphate from ATP to the synthetic CK2 substrate RRRDDDSDDD per minute at 30^{o}C, pH 7.5. The reaction was boiled in 1x Laemmli buffer for 5 minutes to stop the reaction. Proteins were fractionated by SDS-PAGE. Subsequently, the gel was subjected to Coomassie staining and then vacuum dried. ^{32}P labelled proteins were detected by autoradiography.

2.4.16 *In vitro* kinase assay and analysis by mass spectrometry

2µg recombinant protein substrate was incubated with 100 units of CK2 holoenzyme (Calbiochem) in 20µl Kinase assay buffer for 30 minutes at 30^{o}C. The reaction was boiled in 1x Laemmli buffer for 5 minutes to stop the reaction. Proteins were fractionated by SDS-PAGE. The gel was then subjected to Coomassie staining as described previously. The band of recombinant protein substrate, made visible by the Coomassie stain, was excised and added to a 1.5ml microcentrifuge tube with 50µl HPLC water. These samples were kept at 4^{o}C and analysed by the LRI Protein Analysis and Proteomics service. Samples were digested using Trypsin or Asp-N endoproteases. LC-MS/MS analysis of the resulting peptides was performed using an LTQ-Orbitrap XL (Thermo Scientific) machine. MASCOT

software was used for database searching for identification of peptides. Scaffold software was used for data analyses.

2.4.17 β-galactosidase assay

HDFs in culture dishes were washed twice in 37°C PBSA and then incubated for 3-5 minutes with 37°C fixing solution at room temperature. Cells were then washed twice with 37°C PBSA and incubated with staining solution at 37°C for 12-16 hours in the culture dish sealed with parafilm. After staining, cells were washed twice in PBSA and once in methanol. Cells were then stored dry in sealed culture dishes at room temperature and submerged in PBSA for visualisation using a Ziess Axiovert 25 inverted microscope microscopy.

2.4.18 Immunofluorescence

Approximately 10^3 cells were seeded into each well of a 12-well culture plate (BD Falcon) containing N° 1.5 coverslips. 24 hours after cells were seeded they were washed once in 37°C PBSA for 1 minute and then fixed in 37°C 3.7% formaldehyde in PBSA for 15 minutes at room temperature. Cells were then subjected to 4 x 20 second washes in 37°C PBSA (hereafter referred to as 'wash'). Cells were permeabilised in 0.1% Triton X-100 in PBSA for 15 minutes at room temperature before washing. Four drops of Image-iT FX Signal Enhancer (Molecular Probes) was added to each well and incubated for 30 minutes at room temperature in a humid atmosphere. After incubation, cells were washed and blocked for one hour in 3% BSA in PBSA. Cells were then incubated with primary antibody (previously diluted in 3% BSA in PBSA) overnight at 4°C or for 1 hour at room temperature. After washing, the relevant fluorescein-coupled (Alexa Fluor 488 or 555), highly cross-adsorbed, secondary antibody (previously diluted in 3% BSA in PBSA) was applied and incubated for 30-60 minutes at room temperature in the dark. Cells were washed and coverslips were mounted onto glass microscopy slides (76x26x1mm) using ProLong Gold Antifade reagent with DAPI (Invitrogen). Coverslips were left to cure before confocal microscopy analysis.

2.4.19 Confocal microscopy

Images were acquired using a 40x/1.3 DIC Plan Apochromat lens under oil immersion and a Zeiss LSM *invert* 710 microscope using sequential scanning. Zen 2009 software (Zeiss) was used. DAPI was excited using a 405nm laser line, Alexa Fluor 488 was excited using a 488nm laser line and Alexa Fluor 555 was excited using a 561nm laser line. Spatial sampling was 0.04µm per pixel in the X/Y plane and between 0.2µm and 0.3µm per pixel in the Z plane. The pinhole aperture was set to 1 airy unit. Images were deconvoluted using Huygens Essential software (Scientific Volume Imaging (SVI)). Imaris 7.6 software (Bitplan) was used for colocalisation analysis of deconvoluted images. Colocalisation analysis was performed using automatically selected intensity thresholds within a region of interest (set by the DAPI channel) to generate Pearson's correlation coefficient values.

2.4.20 Solutions

Solutions were made up to the appropriate concentration in water (unless otherwise stated). To sterilise solutions (if required) they were either autoclaved or filtered though 0.22µm Stericup Filter Units (Millipore). LRI Media services provided clean glassware, PBSA, L-Broth (LB), and LB-Agar. Chemicals were generally purchased from Sigma-Aldrich. Water was purified using a Millipore reverse osmosis system.

Molecular biology solutions

1x TAE running buffer	40mM Tris acetate (pH 7.6) 5mM Sodium acetate 1mM EDTA
6x DNA loading buffer	60% Sucrose 0.1% Bromophenol blue
Annealing buffer	30mM HEPES-KOH (pH 7.4) 100mM Potassium acetate 2mM Magnesium acetate
L-Broth (LB)	1% NaCl 0.5% yeast extract 1% NP40

Cell culture solutions

2x HBS	50mM HEPES (pH 7.0) 280mM NaCl 10mM KCl 1.5mM Na_2PO_4 12mM dextrose

Biochemistry solutions

SDS-PAGE running buffer	25mM Trizma base 192mM Glycine 0.1% SDS
Transfer buffer	25mM Trizma base 192mM Glycine 20% Methanol
6x Laemmli sample buffer	375mM TrisHCl (pH 6.8) 10% SDS 10% 2-Mercaptoethanol 0.04% bromophenol blue 50% glycerol
Coomassie stain solution	0.1% Coomassie Brilliant Blue R250 50% Methanol 10% Acetic acid
Gel fixing/destaining solution	50% Methanol 10% Acetic acid
PBSA	8.06 mM Na_2HPO_4 0.8% NaCl 1.47 mM KH_2PO_4 0.025% KCl (pH 7.2)
PBSA-Tween (PBST)	PBSA 0.2% Tween
Blocking buffer	PBSA

	0.2% Tween 5% dried milk (Marvel) or bovine serum albumin (BSA) (Sigma)
Stripping buffer	62.5mM TrisHCl (pH 6.8) 5% 2-Mercaptoethanol 2% SDS
NP40 lysis buffer (1)	50mM TrisHCl (pH 7.5) 120mM NaCl 5mM EDTA 0.5% NP40 1mM PMSF (added fresh) 1mM DTT (added fresh) 2mM Na_3VO_4 (added fresh) 100mM NaF 1x protease inhibitor cocktail (Roche) (added fresh)
NP40 lysis buffer (2)	50mM TrisHCl (pH 8.0) 150mM NaCl 1mM EDTA 1% NP40 1x protease inhibitor cocktail (Roche) (added fresh)
CHAPS lysis buffer	50mM TrisHCl (pH 8.0) 0.5% CHAPS 150mM NaCl 1mM EDTA 1mM PMSF (added fresh) 1x protease inhibitor cocktail (Roche) (added fresh)

Tween lysis buffer	20mM HEPES (pH 7.5) 150μM NaCl 0.1% Tween 1mM EDTA 10% Glycerol 1mM DTT (added fresh) 1x protease inhibitor cocktail (Roche) (added fresh)
ChIP swelling buffer	25mM HEPES pH 7.9 1.5mM $MgCl_2$ 10mM KCl 0.1% NP-40
ChIP sonication buffer	50mM HEPES pH 7.9 140mM NaCl 1mM EDTA 1% Triton X-100 0.1% Na-deoxycholate 0.1% SDS
ChIP wash buffer A	50mM HEPES pH 7.9 500mM NaCl 1mM EDTA 1% Triton X-100 0.1% Na-deoxycholate 0.1% SDS
ChIP wash buffer B	20mM Tris pH 8.0 1mM EDTA 250mM LiCl 0.5% NP-40 0.5% Na-deoxycholate

ChIP TE buffer	10mM Tris pH 8.0 1mM EDTA
ChIP elution buffer	50mM Tris pH 8.0 1mM EDTA 1% SDS
GST lysis buffer	10mM TrisHCl pH 7.6 500mM NaCl 0.5% NP40 5mM EDTA
GST elution buffer	50mM TrisHCl pH 8.0 10mM reduced glutathione
GST cleavage buffer	50mM TrisHcl pH 7.5 150mM NaCl 1mM EDTA 1mM DTT (added fresh)
Kinase assay buffer	20mM TrisHCl pH 7.5 5mM EGTA 1mM DTT (added fresh) 20mM $MgCl_2$ 100μM ATP 25mM β-glycerophosphate
Binding assay buffer	20mM TrisHCl pH 7.5 0.1% Tween 5mM EGTA 1mM DTT (added fresh)

Microscopy solutions

β-galactosidase staining solution	1mg/ml X-gal in dimethylformamide 40mM Citric acid/Sodium phosphate buffer (pH 6.0) 5mM Potassium ferricyanide 5mM Potassium ferrocyanide 150mM NaCl 2mM MgCl
Citric acid/ Sodium phosphate buffer	2:1 ratio of 0.1M Citric acid solution:0.2M Sodium phosphate solution

Chapter 3. Interaction of CK2 with PRC1

3.1 Introduction

As discussed in Chapter 1.1.1, several auxiliary proteins, which are not encoded by recognised PcG genes, consistently co-purify with the core PRC1 components. Although some of these auxiliary proteins have been shown to contribute to the function or regulation of PRC1 (El Messaoudi-Aubert et al., 2010, Maertens et al., 2010), it is not clear that they are present in stoichiometric amounts. CK2 is an interesting example, because the enzyme is itself a complex and all three subunits have been identified in PRC1-like complexes. Specifically, mass spectrometry identified CK2 subunits in PRC1-like complexes affinity purified via CBX2, CBX4, CBX7, CBX8, RING2, RNF3 and RNF159, (El Messaoudi-Aubert et al., 2010, Dietrich et al., 2007, Vandamme et al., 2011, Sanchez et al., 2007, Gao et al., 2012). However, CK2 is a relatively abundant and ubiquitous protein that has been detected in a number of other types of complex, including those involved in the DNA damage response (Keller et al., 2001).

At the inception of this thesis, only one study had sought to confirm the mass spectrometry data by immunoblotting for CK2 in a RING2-based complex (Sanchez et al., 2007). We therefore set out to confirm the presence of CK2 in PRC1 complexes and to explore the direct protein-protein interactions that might be responsible.

3.2 Association of CK2 with PRC1 complexes

3.2.1 Association of CK2 and PRC1 proteins

A previous graduate student in the lab, James Nicholls, had identified all three CK2 subunits in a complex purified from 293T cells transduced with TAP-tagged mouse Cbx7 (Nicholls, 2006). To confirm and extend this observation, FLAG tagged (C-terminal) versions of human CBX2, CBX4, CBX6, CBX7 and CBX8 were expressed in 293T cells and the cell lysates were immunoprecipitated with anti-FLAG agarose, fractionated by SDS-PAGE, and immunoblotted for CK2 subunits. FLAG-tagged

CBX proteins were mostly resolved as two or more differently migrating bands (Figure 3.1A). This may reflect the use of different methionines as alternative translation start sites as each CBX protein contains two or more methionines within its sequence. Although there was some variability in the levels of the CBX proteins achieved by transient transfection, it was clear that both the α and α' subunits of CK2 co-precipitated with all five CBX proteins (Figure 3.1A). As expected, endogenous RING2 was also detected in the immunoprecipitates. It was difficult to draw conclusions regarding differential binding affinities between CK2 and CBX-complexes. It appeared that more CK2 was co-precipitated with CBX2-FLAG than any of the other CBX-FLAG proteins. This was especially striking considering the relatively low level of RING2 that co-precipitated with CBX2-FLAG. However, not only was there some variability in the expression of the CBX proteins but the levels of endogenous RING2, used as a positive control in this experiment, varied substantially in the transfected 293T cells. This is unlikely to reflect differences in loading, as the CK2 signals appear well balanced. A more likely explanation is that overexpression of CBX proteins affects the stability of RING2, perhaps to varying degrees. Although interesting, this issue would be difficult to resolve by standard approaches that rely on transient over-expression and the analyses of endogenous proteins is very dependent on the efficacy of the available antibodies.

Endogenous co-IP is the gold standard for demonstrating a biologically relevant interaction between two proteins. Although attempted, it was not possible to recover CK2 subunits from IPs of endogenous CBX7 (data not shown). Of the laboratory's panel of antibodies against PRC1 proteins, anti-RING2 (gifted by Haruhiko Koseki) has demonstrated the greatest efficiency for purifying its target (personal communication with various members of the Molecular Oncology laboratory). Anti-RING2 was therefore used to immunoprecipitate RING2-complexes from 293T lysate. Purified proteins were fractionated by SDS-PAGE and immunoblotted for CK2 subunits. Figure 3.1B shows that all three endogenous CK2 subunits co-precipitated with endogenous RING2.

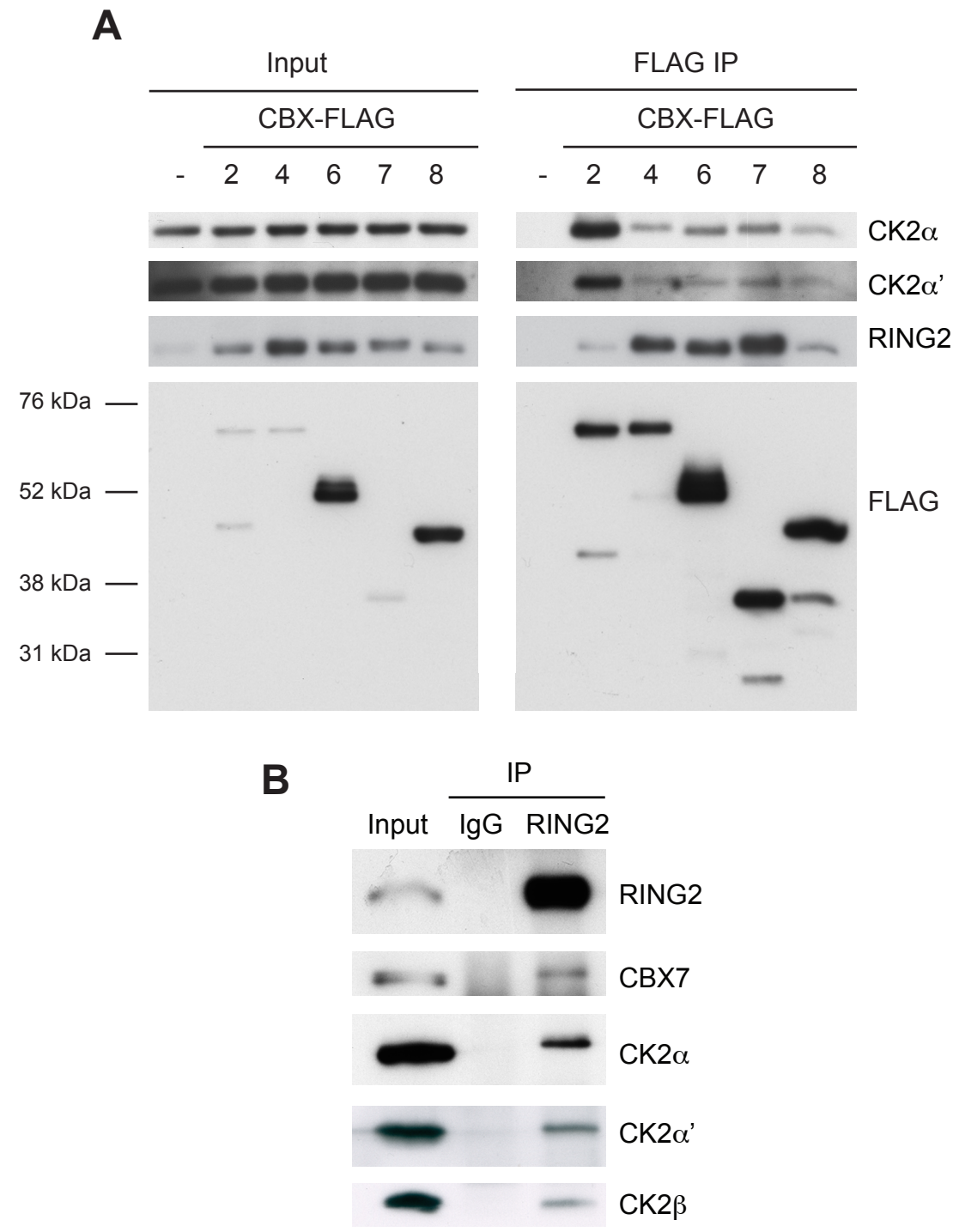

Figure 3.1 Co-immunoprecipitation of CK2 with FLAG-tagged CBX proteins and endogenous RING2

A) pcDNA6 plasmids encoding FLAG-tagged CBX2, 4, 6, 7 or 8 (generated by Marc Rodriguez-Niedenfuhr) were transfected into 293T cells using lipofectamine. After 24 hours cells were harvested and cell lysate was subject to immunoprecipitation (IP) using anti-FLAG M2 agarose (Sigma). Purified proteins were fractionated by SDS-PAGE alongside input samples equivalent to 1/10th volume of lysate used for the IP. Immunoblotting was performed against

CK2α, CK2α', RING2, and FLAG. The image is representative of two biological replicates **B)** 293T cells were harvested and lysate was subject to IP using anti-RING2 antibody and Protein G agarose (Thermoscientific). Purified proteins were fractionated by SDS-PAGE alongside an input sample equivalent to 1/10th volume of lysate used for the IP. Immunoblotting was performed against CK2α, CK2α', CK2β, RING2, and CBX7. The image is representative of three biological replicates.

3.2.2 Interaction of CK2 and CBX7 in a high molecular weight complex

The co-precipitation data were consistent with reports from other groups showing CK2 to purify with CBX2, CBX4, CBX8 and RING2 complexes (Dietrich et al., 2007, Vandamme et al., 2011, Sanchez et al., 2007). However, these studies did not indicate whether the interaction between CK2 and PcG proteins takes place in the context of a PRC1 complex. To address this issue, and exclude the possibility that CK2 interacts with free, monomeric PcG proteins, gel filtration was used to estimate the molecular weight of CK2-CBX7 protein complexes.

A Superose 6 HR 10/30 gel filtration column (GE Healthcare), which enables high-resolution fractionation of protein complexes between 5 kDa and 5 MDa, was calibrated using a series of protein standards whose elution was monitored by UV (Appendix: Figure 8.1). Although these protein standards were those recommended for the calibration of this column, it is important to note that the largest monomeric protein was thyroglobulin (669 kDa). As a consequence, the size of protein complexes larger than 669 kDa cannot be estimated with any confidence. To analyse the endogenous complexes, a sample of 293T whole cell lysate, containing approximately 2mg of protein, was applied to the Superose 6 column. The proteins in each fraction were concentrated by precipitation with trichloroacetic acid (TCA) fractionated by SDS-page, and detected by immunoblotting. As shown in Figure 3.2A, endogenous CBX7 was recovered in a size range between 43 and 440 kDa, with the majority in a peak at approximately 200 kDa. The apparent CBX7 doublet will be discussed in Chapter 4.2. The predicted molecular weight of human CBX7 is 28 kDa and that of a canonical PRC1 complex comprising CBX7, MEL18, HPH2 and RING2 is 194 kDa.

Interestingly, endogenous RING2 also shows a peak at about 200 kDa although its distribution suggests that it is also present in much larger complexes.
The predicted molecular weight of the human CK2 holoenzyme is between 132 kDa and 140 kDa, depending on the contributing subunits. However, the majority of the endogenous CK2 eluted in a peak at around 550 kDa and extended into a much higher size range (Figure 3.2A). There was little if any signal equivalent to free holoenzyme but some of the protein was clearly detectable in the fractions containing CBX7 and RING2. These data would be consistent with the idea that CK2 associates with CBX7 in the context of a PRC1 complex but is not definitive.

A number of studies have used a similar approach to characterise the molecular weight of complexes containing endogenous PcG proteins (Gao et al., 2012, Sanchez et al., 2007, Vandamme et al., 2011, Tavares et al., 2012, Maertens et al., 2010). For example, endogenous CBX7 has been observed in complexes of around 75-158 kDa in mESCs (Tavares et al., 2012) and 158-500 kDa in HDFs (Maertens et al., 2010), whereas CBX8 complexes appear to be somewhat larger (Dietrich et al., 2007, Maertens et al., 2010). There is broad agreement that endogenous RING proteins are distributed in two different sizes of complex, although the composition of these complexes has not been determined (Sanchez et al., 2007, Vandamme et al., 2011, Tavares et al., 2012).

One of the problems with this approach is that the endogenous proteins are rarely present in sufficient quantities to allow further analysis of potential complexes, for example by immunoprecipitation and immunoblotting of individual fractions. An alternative strategy is to perform the immunoprecipitation prior to gel filtration. Unfortunately, it was not possible to recover CK2 subunits from IPs of endogenous RING2 in sufficient quantities for such analysis (data not shown). However, this approach was possible using CBX7-FLAG precipitates from transiently transfected 293T cells. Figure 3.2B shows that the majority of CBX7-FLAG was present in large complexes in excess of 669 kDa. Some CBX7-FLAG was also found in smaller complexes around 440 kDa. Importantly, the endogenous RING2 that co-precipitated with FLAG-CBX7 showed the same distribution as FLAG-CBX7. All three CK2 subunits co-purified with the larger species of CBX7 complexes but were not detected in the 440 kDa size range.

It was surprising that FLAG-CBX7 complexes were much larger than endogenous CBX7 given that the FLAG epitope only adds 1 kDa. However, others have observed a similar phenomenon (Vandamme et al., 2011). It is possible that endogenous CBX7 can also form these larger complexes but that levels were too low to detect. In light of these discrepancies, it is unclear how biologically relevant the FLAG-tagged complexes are and the size of endogenous CBX7-CK2 complexes remains undetermined. However, these data do suggest that the interaction of CK2 with CBX7 can take place within the context of a high molecular weight complex above 669 kDa, a size consistent with PRC1-like complexes.

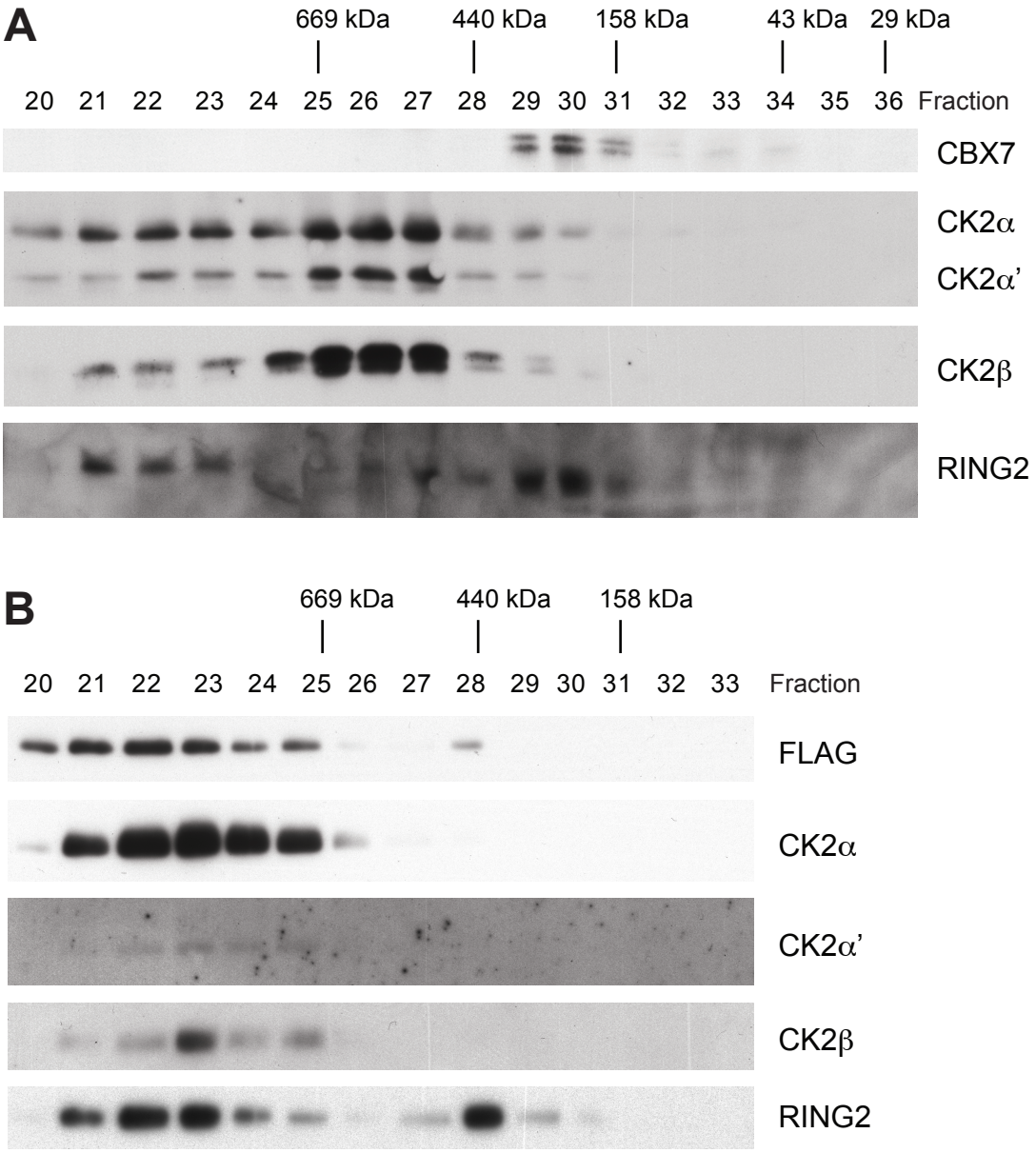

Figure 3.2 Gel filtration of 293T cell lysate and CBX7-FLAG complexes

A) 2mg 293T cell lysate was applied to a Superose 6 column and flow through was collected in 500µl fractions. Protein was precipitated from fractions 20-36 using TCA, fractionated by SDS-PAGE and immunoblotting was performed against CK2α, CK2α', CK2β, RING2, and CBX7. The image is representative of three biological replicates **B)** Purified CBX7-FLAG complexes were applied to the Superose 6 column. Flow though was collected in 500µl fractions. Protein was precipitated from fractions 20-33 with TCA, fractionated by SDS-PAGE and immunoblotting was performed against CK2α, CK2α', CK2β, RING2, and FLAG. The image is representative of two biological replicates.

3.3 Interaction of CK2 with the Pc box domain of CBX proteins

3.3.1 Binding of CK2α to C-terminal peptides representing the Pc box of CBX7

Although CK2 has been found in a variety PcG complexes, little attention has been paid to the protein(s) responsible for the direct interaction with CK2. To address this question, recombinant CK2α (Calbiochem) was used to probe synthetic peptide arrays of CBX7, BMI1, HPH2 and RING2 (examples representing the Pc, Psc, Ph, and Sce protein families respectively). These arrays represented the protein of interest as a series of overlapping 20-mers. Peptide arrays can be used to test whether a direct interaction is possible between protein A and a peptide representing a domain of protein B. The result can suggest that protein A and B directly interact, and also, the domain of protein B wherein this interaction occurs. Duplicate arrays were incubated with or without recombinant CK2α and the bound protein was detected by immunoblotting.

Low-level signals of CK2α were detected on all four arrays (Figure 3.3 and Figure 3.4). However, these signals were generally confined to discrete peptides scattered throughout the entire protein and, although we cannot rule out some contribution to CK2 binding, they are not consistent with a defined interaction domain. The notable exception was a series of 20 consecutive peptides (spots H1-H20 in Figure 3.4A) that correspond to amino acids 210-249 of CBX7. This C-terminal region of CBX7 contains the conserved Pc box domain (Figure 3.4B) and peptides that contain the complete Pc box are highlighted by the blue bar (Figure 3.4A). One amino acid, Ile230, was common to all peptides bound by CK2α.

Four other regions of the CBX7 peptide array demonstrated binding to CK2 that could be consistent with these also representing CK2 interaction domains: I) Peptides A23-30, corresponding to amino acids 23-49 within the conserved chromodomain of CBX7, II) Peptides C21-30, corresponding to amino acids 80-108 of CBX7, III) Peptides E25-30 corresponding to amino acids 145-169 of CBX7, IV) Peptides F7-18 corresponding to amino acids 157-187 of CBX7. Although the signals were generally weaker relative to the C-terminal domain, it is possible that

there are multiple binding sites for CK2 within the CBX7 protein or that, in the context of the tertiary CBX7 structure, CK2 may contact these regions simultaneously.

Taken together, the peptide array data suggest that CK2 interacts directly with CBX7 via the C-terminal Pc box but does not make stable contacts with other components of the PRC1 complex when tested in isolation. This would be consistent with recently published observations that CK2 does not interact directly with BMI1 or RING2 and that the Pc box of CBX4 is necessary for the direct interaction with CK2 (Vandamme et al., 2011). However, these authors concluded that the interaction involved the β rather than the α subunit of CK2, which will be discussed further in Chapter 7.

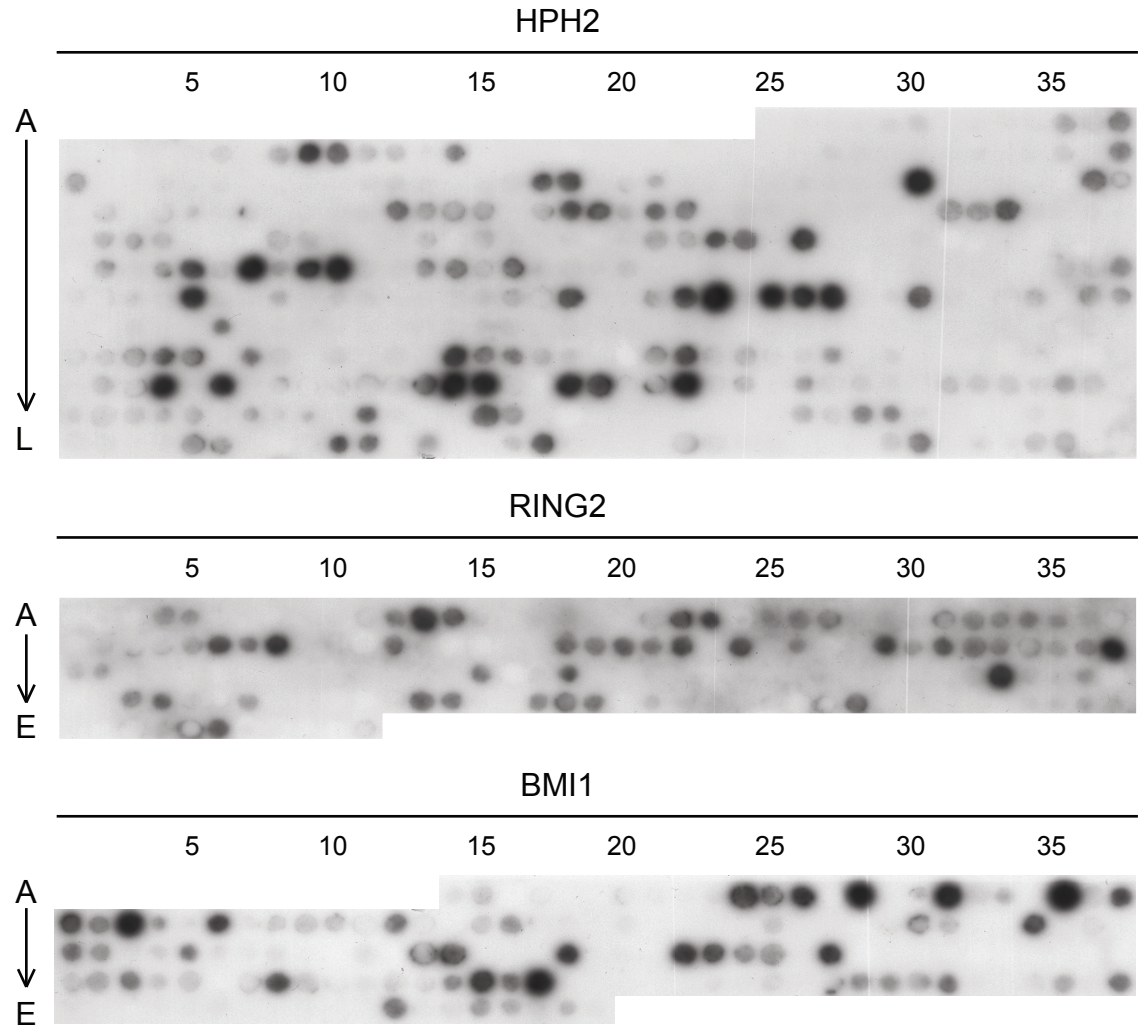

Figure 3.3 Binding of CK2α to peptide arrays of HPH2, RING2 and BMI1

Peptide arrays of HPH2, RING2 and BMI1 were incubated with recombinant CK2α. After extensive washing, immunoblotting was performed against CK2α to detect CK2α bound to array peptides. Position A1 of each array corresponds to N-terminal amino acids 1-20 of each protein. Each 20-mer peptide in the array was advanced from the previous by two residues in the C-terminal direction. The last peptide corresponds to the 20 amino acids at the C-terminus of each protein.

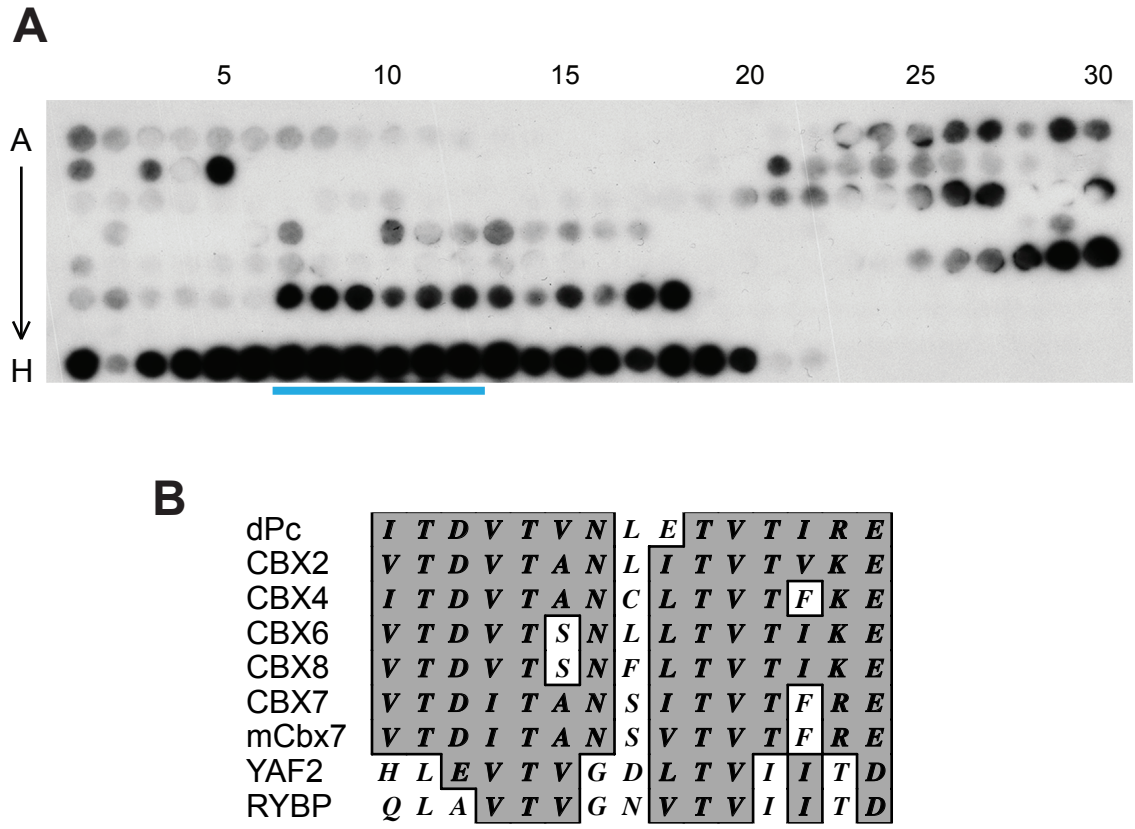

Figure 3.4 Binding of CK2α to a peptide array of CBX7

A) A peptide array of CBX7 was incubated with recombinant CK2α. After extensive washing, immunoblotting was performed against CK2α to detect CK2α bound to array peptides. Position A1 of the array corresponds to N-terminal amino acids 1-20 of CBX7. Each 20-mer peptide in the array was advanced from the previous by one residue in the C-terminal direction. The last peptide, at position H22, corresponds to the C-terminal amino acids 232-251. The image is representative of two biological repeats. **B)** A schematic alignment of the Pc box in CBX proteins and conserved domains found within RYBP and YAF2.

3.3.2 CK2 binding to the Pc box of other CBX proteins

To investigate whether CK2α also binds to the Pc box of other CBX proteins, additional peptide arrays were generated to represent CBX6 and CBX8. As before, the arrays were incubated with recombinant CK2α and the bound CK2α was detected by immunoblotting. Although the data were less compelling than the original CBX7 array, binding of CK2α was observed at peptides containing the complete Pc box, highlighted by the blue bar in Figure 3.5. These data suggest that the ability of the Pc box to interact directly with CK2 is conserved among the CBX proteins.

RYBP (RING1 and YY1 interacting protein) has recently been shown to bind to the same surface of RING2 as the CBX proteins (Wang et al., 2010) and it has been proposed that RYBP-PRC1 and CBX-PRC1 represent functionally distinct complexes (Tavares et al., 2012, Gao et al., 2012). Although RYBP and CBX proteins share little sequence homology (11% identity between CBX7 and RYBP at the amino acid level), some residues in the CBX Pc box are conserved in RYBP (Figure 3.4B) and the corresponding domains in each protein are predicted to interact with RING2 via similar structural folds (Wang et al., 2010). To test whether CK2 can also interact with the relevant domain in RYBP, a peptide array of RYPB was generated and used in a binding assay with recombinant CK2α. Figure 3.5 shows that CK2α was able to bind peptides at the N-terminus of RYBP and also peptides sharing conserved residues with the Pc box of CBX proteins. The blue bar highlights peptide spots containing the domain of RYPB similar to the Pc box of CBX proteins. These data suggest that CK2 might directly interact with RYBP as well as CBX proteins and are consistent with work showing that CK2 co-purifies with TAP-tagged versions of RYBP and YAF2 from 293T cells (Gao et al., 2012).

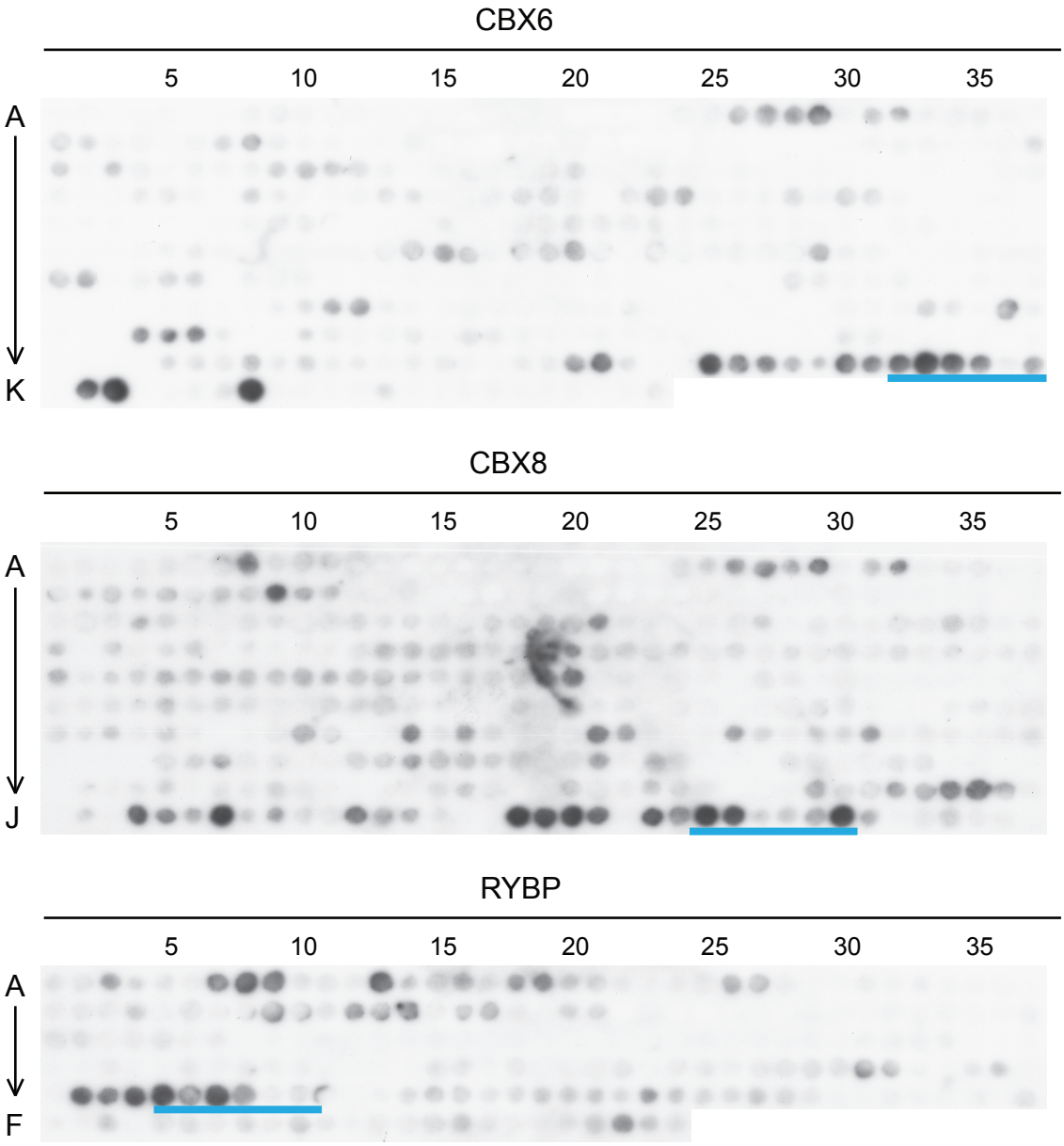

Figure 3.5 Binding of CK2α to peptide arrays of CBX6, CBX8, and RYBP

Peptide arrays of CBX6, CBX8 and RYBP were incubated with recombinant CK2α. After extensive washing, immunoblotting was performed against CK2α to detect CK2α bound to array peptides. Position A1 of each array corresponds to N-terminal amino acids 1-20 of each protein. Each 20-mer peptide in the array was advanced from the previous by one residue in the C-terminal direction. The last peptide corresponds to the 20 amino acids at the C-terminus of each protein.

3.4 Mapping the critical CK2 binding residues within the Pc box of CBX7

3.4.1 Identifying CBX7 Pc box residues that interact with CK2

To identify residues in the Pc domain of CBX7 that are critical for the interaction with CK2, a peptide array was generated in which amino acids 218-237 (SEVTVTDITANSITVTFREA) of CBX7, encompassing the entire Pc box domain, were individually substituted in turn with one of the 20 common amino acids. A binding assay was performed, with or without recombinant CK2α, and the bound protein was detected by immunoblotting. Binding of CK2 to the SEVTVTDITANSITVTFREA peptide was largely unaffected by the substitution of the first twelve residues (Ser218-Ser229) and the last three residues (Arg235-Ala237) in this sequence, suggesting that these residues were not important for the interaction of CBX7 with CK2 (Figure 3.6). Notable exceptions were the replacement of some of the residues with either proline (Row P) or cysteine (Row C), which resulted in a loss of CK2α binding. Proline is unable to occupy many of the main-chain conformations adopted by other amino acids and is often found within very tight turns in protein structures. The substitution of a residue to proline is therefore likely to have introduced a kink in the peptide structure. The propensity of cysteine to form disulphide bonds could also have meant that cysteine substitutions altered peptide conformation. Loss of CK2 binding, to peptides containing proline or cysteine substitutions, may therefore be due to a significant change in the structure of these peptides, as opposed to the importance of the substituted residue for the interaction with CK2.

A notable feature of the data was that replacing certain residues in the peptide with different alternatives seemed to have a consistent effect on the binding of CK2α. Most strikingly, the substitution of Val232 with any of 15 different amino acids resulted in reduced or loss of CK2α binding. The only exceptions are proline and asparagine, and the aliphatic amino acids leucine and isoleucine, which are biochemically similar to valine. Substitutions of Ile230, Thr233, and to a certain extent Phe234, also resulted in the disruption of CK2α binding to the peptide. In particular mutating these residues to charged amino acids, such as histidine and

aspartic acid resulted in a loss of CK2α binding. Taken together these results indicate that four residues within this peptide are important for CK2 binding: Ile230, Val232, Thr233 and Phe234.

3.4.2 Designing CBX7 point mutants

The peptide binding data suggested that it might be possible to design a minimally mutated version of full length CBX7 that is unable to bind to CK2. This would obviously be an ideal tool for testing the functional importance of the interaction between these proteins. However, before introducing mutations into the full-length cDNA, it was important to consider how the four residues identified in the context of a 20-mer peptide (Ile230, Val232, Thr233 and Phe234) relate to the 3-dimensional structure of CBX7. Specifically, would these residues be available to interact with CK2 and how might they affect the interaction between CBX7 and RING2?

The crystal structure of the C-terminus of CBX7 bound to the C-terminal domain of RING2 has been solved at a resolution of 1.7Å (PDB ID 3GS2, (Wang et al., 2010)). Interestingly, residues 218-237 of CBX7 form an antiparallel beta sheet that, in combination with residues in RING2, generates an extended intermolecular beta sheet that packs against the central helix in the C-terminal domain of RING2 (see Figure 3.7). Critically, Phe234 of CBX7 participates in a key hydrophobic stacking interaction with residue Tyr262 of RING2. Mutation of this residue was therefore likely to disrupt the interaction between CBX7 and RING2 and negate the participation of CBX7 in a functional PRC1 complex. Similarly, Val232 is one of four residues clustered around Phe234 that pack against a hydrophobic pocket in RING2. The side chain of Val232 can also be seen to point towards RING2, making it likely that is involved in the interaction (Figure 3.7). In contrast, the side chains of both Ile230 and Thr233 point out from the CBX7-RING2 interface suggesting they are not involved in the interaction between these proteins and in principle could be available to make additional protein contacts. Hydrophobic amino acids such as isoleucine are generally buried within protein structures and it is unusual to find a surfaced exposed aliphatic side chain unless it is involved in an inter-molecular interaction.

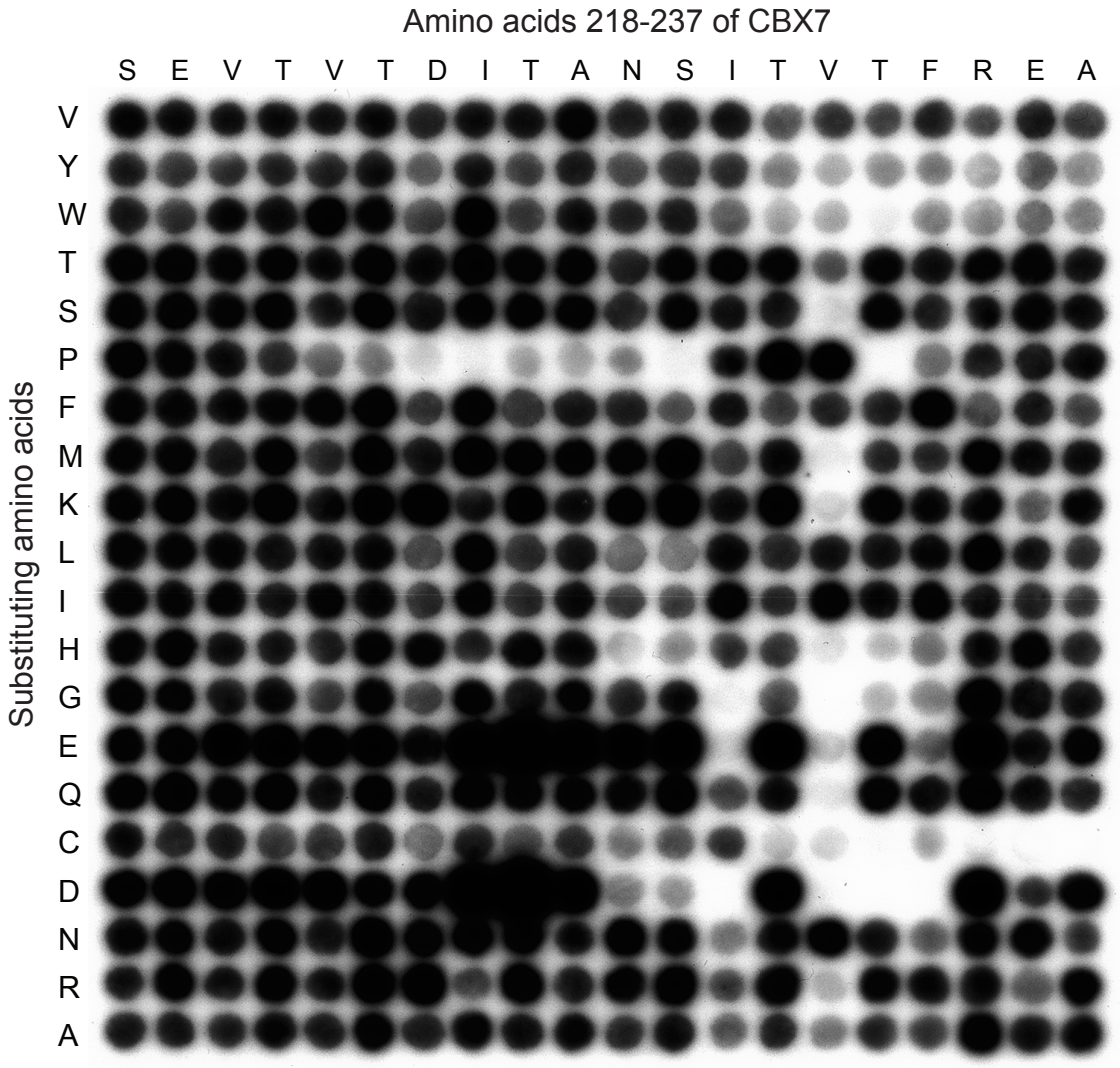

Figure 3.6 Binding of CK2α to a substitution array of CBX7(218-237)

A peptide array in which residues 218-237 of CBX7 (left-right axis) were individually changed to one of the 20 common amino acids (top-bottom axis). This array was incubated with recombinant CK2α. After extensive washing, immunoblotting was performed to detect CK2α bound to array peptides.

Together, these considerations suggested that Ile230 and Thr233 could contribute to a docking site for CK2 and that mutation of these residues might abrogate binding of CBX7 to CK2 while maintaining its ability to interact with RING2. They were therefore selected as targets for mutagenesis. Although the substitution of Val232 was predicted to affect the interaction of CBX7 with RING2, given the strength of the peptide array data implying a role for this residue in the interaction with CK2, it was also included as a target.

Recombinant human CBX7 has proved difficult to produce in bacteria (personal communication from Jesus Gil, Janice Rowe and Lucas de Breed) and is less stable than mouse Cbx7 (mCbx7) (personal communication from Marc Rodriguez-Neidenführ). The human protein contains a stretch of 92 amino acids that is not present in mCbx7 but otherwise there is 89% sequence identity between the two homologues. Importantly, the C-terminal Pc box is highly conserved (Figure 3.7).
Because of these considerations, it was decided to generate mutations in mCbx7 rather than the human protein, and to use mCbx7 for further functional investigation of the interaction with CK2. Previous work in the lab has shown that mCbx7 can extend the lifespan of human fibroblasts by repressing *INK4a* (Maertens et al., 2009) and can interact with human PRC1 proteins when expressed in 293T cells (El Messaoudi-Aubert et al., 2010). As depicted in Figure 3.8, the critical residues in human CBX7 identified in the peptide arrays (Ile230, Val232 and Thr233) correspond to Val137, Val139 and Thr140 in mCbx7.

The wild-type mCbx7 cDNA was cloned into the pGEX-6P1 vector to introduce an N-terminal GST tag. Using this plasmid as a template, PCR-based site-directed mutagenesis (Chapter 2.1.3) was used to make the following substitutions:
1) V137A/D
2) V139A/D
3) T140A/D
4) V137A/D T140A/D
5) V137A/D V139A/D T140A/D

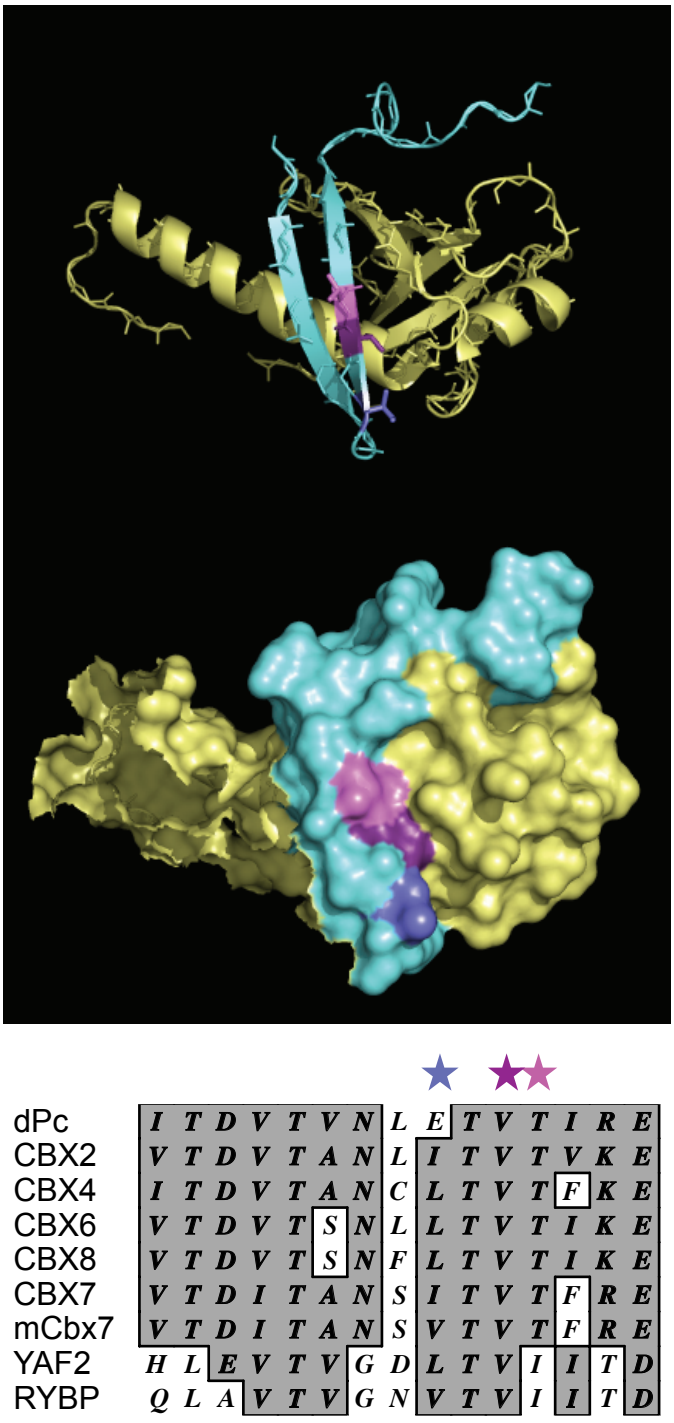

Figure 3.7 CK2 interacting residues of CBX7 in the context of a CBX7-RING2 complex

The crystal structure of the C-terminus of CBX7 (cyan) and the C-terminus of RING2 (yellow). Key residues important for an interaction with CK2 are highlighted, Ile230 (indigo), Val232 (purple), Thr233 (pink). Images were created using PyMol from PDB ID 3GS2 (Wang et al., 2010). The conservation of these residues between the human CBX proteins, mCbx7, dPc, YAF2 and RYBP is shown in the ClustalW sequence alignment below.

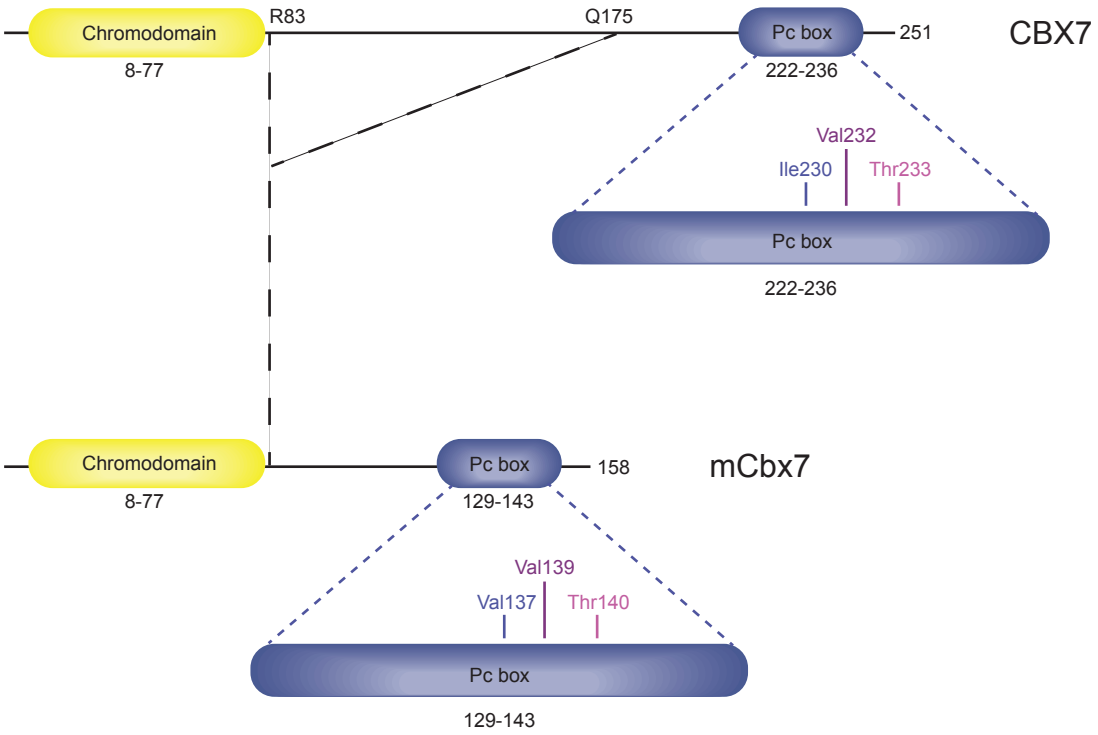

Figure 3.8 Conservation of Pc box residues important for CK2 binding

Schematic diagram of the chromodomain and Pc box of human CBX7 and the conservation of these domains in mouse Cbx7 (mCbx7). The stretch of 92 amino acids unique to CBX7 (Arg83-Gln175) is indicated. CK2 interacting residues in the Pc box of CBX7 (Ile230, Val232, Thr233) and mCbx7 (Val137, Val139 and Thr140) are highlighted.

3.4.3 Testing the CK2 binding potential of mCbx7 point mutants

The plasmids encoding the GST-mCbx7 variants were transduced into an appropriate strain of *E. coli* and protein expression was induced by addition of IPTG (Appendix: Figure 8.2 and Figure 8.3). The fusion proteins were purified on glutathione sepharose beads and their concentrations were adjusted to 0.1mg/ml. The ability of these fusion proteins to interact with CK2 subunits and RING2 was analysed in a standard GST pull-down assay with 293T cell lysate.

Wild-type mCbx7 showed the expected interaction with the α, α' and β of CK2 and with RING2 (Figure 3.9). The V137A, V139A and T140A single substitutions and even the V137AT140A double substitution had no discernible effect on the binding of CK2 to mCbx7. However, the V137AV139AT140A triple substitution showed a reduced ability to bind to CK2. Interestingly, the single substitutions in which Val137, Val139 and Thr140 were replaced with aspartic acid rather than alanine (V137D, V139D and T140D) did cause a decrease in the binding of CK2 to mCbx7, with V139D demonstrating the strongest effect. CK2 binding to the V137DT140D double mutant was very weak and with the triple substitution, V137DV139DT140D, binding to CK2 was essentially abolished. The different effects of the alanine and aspartic acid substitutions are consistent with peptide array data (Figure 3.6) and can be explained by the properties of these residues. As alanine is non-polar and only weakly hydrophobic, replacing a wild-type residue with alanine will test whether the physiochemical properties of that particular amino acid are critical for the tested function. In contrast, aspartic acid is a negatively charged, hydrophilic amino acid with very different physiochemical properties compared to valine and threonine. Thus, aspartic acid is a more disruptive substitution that could have a stronger effect on the interface involved in intra-molecular interactions.

To ensure that the loss of CK2 binding to mCbx7-V137DT140D and mCbx7-V137DV139DT140D was not due to protein misfolding, the melting point (Tm) of the variants was compared to that of wild-type mCbx7 by differential scanning fluorimetry (DSF) (Figure 3.10). All of the proteins had a Tm within one degree centigrade of each other, giving high confidence that the mutant proteins are folded in the same manner as wild-type mCbx7 (Helen Walden, personal communication).

Collectively, the data suggested that residues Val137, Val139 and Thr140 in mCbx7 are indeed important for its interaction with CK2 and that it is possible to abrogate binding to CK2 by changing all three of these residues to aspartic acid. Unfortunately, the substitutions also disrupted the interaction of mCbx7 with RING2 and BMI1, although not with HPH2 (Figure 3.9). This is an interesting distinction that warrants further investigation and is discussed in more detail in Chapter 7. It is also important to note that these experiments did not determine whether the mutated residues are absolutely required for the direct interaction between mCbx7 and either CK2 or RING2. It is possible that they disrupt the interaction with an, as yet, unspecified protein or domain that promotes the formation of the CBX7-CK2 or CBX7-RING2 complex (see discussion in Chapter 7).

3.5 Conclusions

The results described in this chapter demonstrate that CK2 can associate with all five members of the CBX family and that, in the case of CBX7, this interaction takes place in high molecular weight complexes that would be consistent with PRC1. It was further shown that CK2 could directly interact with residues in the C-terminus of CBX proteins that coincide with the conserved Pc box domain. Three residues within the Pc box of mCbx7, Val137, Val139 and Thr140, were shown to be necessary for the interaction with endogenous CK2. Interestingly, these three residues were also necessary for the interaction of mCbx7 with both BMI1 and RING2. The specific interaction of CK2 with CBX proteins suggested that CK2 might phosphorylate these proteins. The next chapter describes efforts to investigate this possibility.

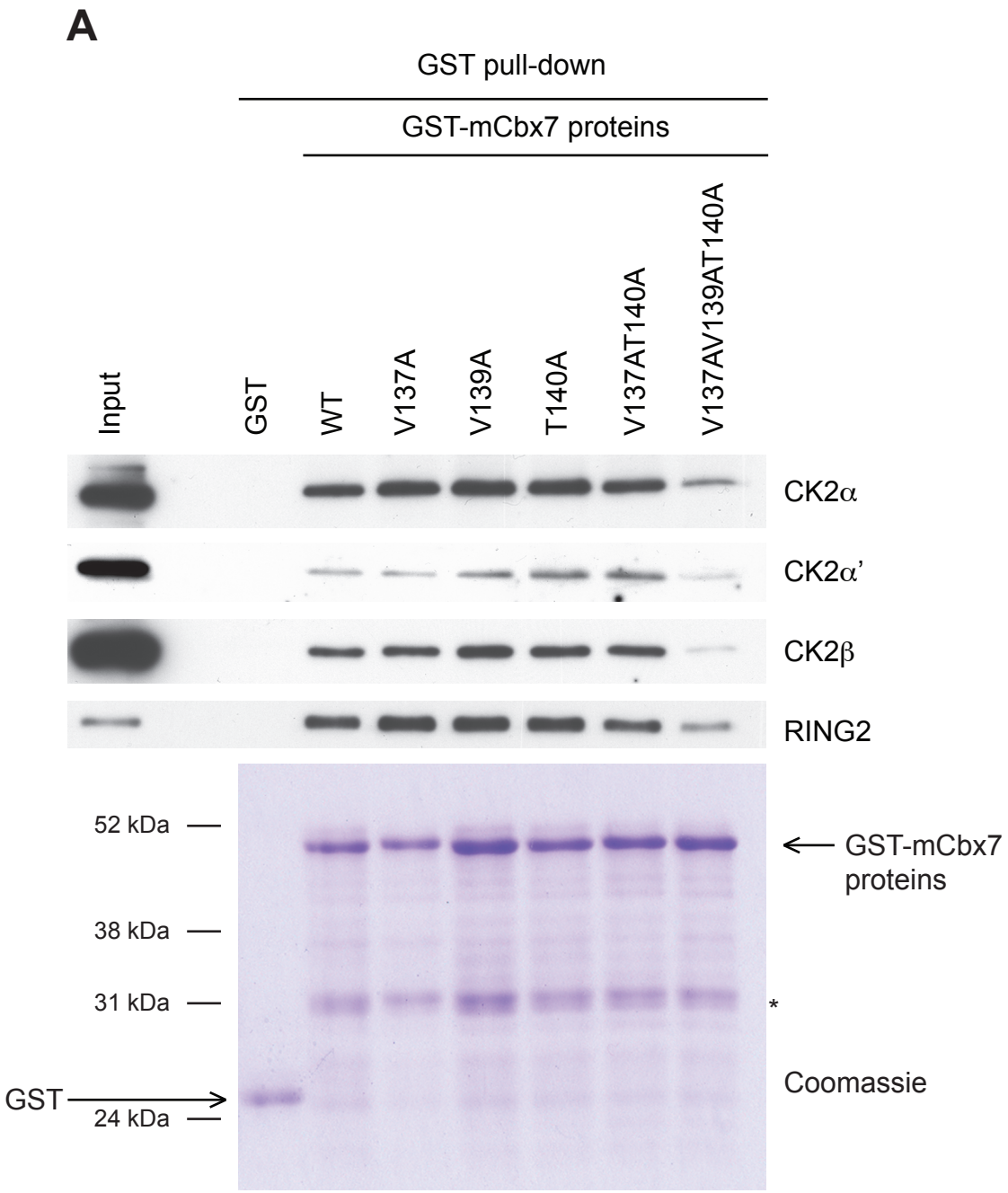
A
GST pull-down
GST-mCbx7 proteins
Input
GST
WT
V137A
V139A
T140A
V137AT140A
V137AV139AT140A
CK2α
CK2α'
CK2β
RING2
52 kDa
38 kDa
31 kDa
GST
24 kDa
GST-mCbx7 proteins
*
Coomassie

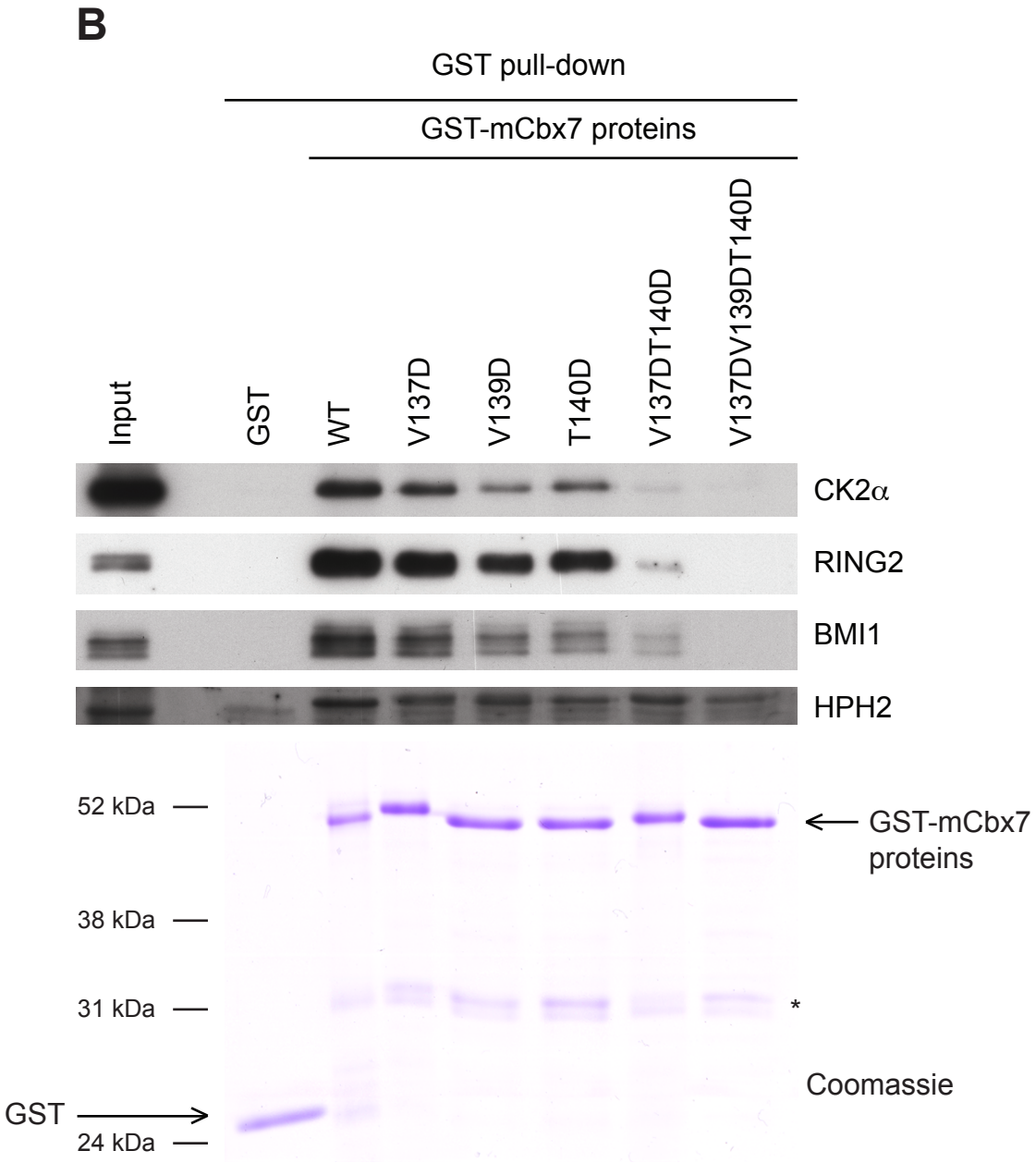

Figure 3.9 GST pull-down of mutant mCbx7 proteins from 293T cell lysate

5mg pre-cleared 293T cell lysate was incubated with 10µg GST, GST-mCbx7, or GST-mCbx7 mutant proteins (**A)** alanine mutants **B)** aspartic acid mutants), as indicated. GST pull-down was performed as described in methods. Proteins recovered from the pull-down were fractionated by SDS-PAGE alongside input samples equivalent to 1/100th of the volume of cell lysate used for the pull-down. Immunoblotting was performed against CK2α, CK2α', CK2β, RING2, BMI1 and HPH2. GST and GST-mCbx7 proteins are indicated and asterisks highlight suspected degradation products. Images are representative of two biological repeats.

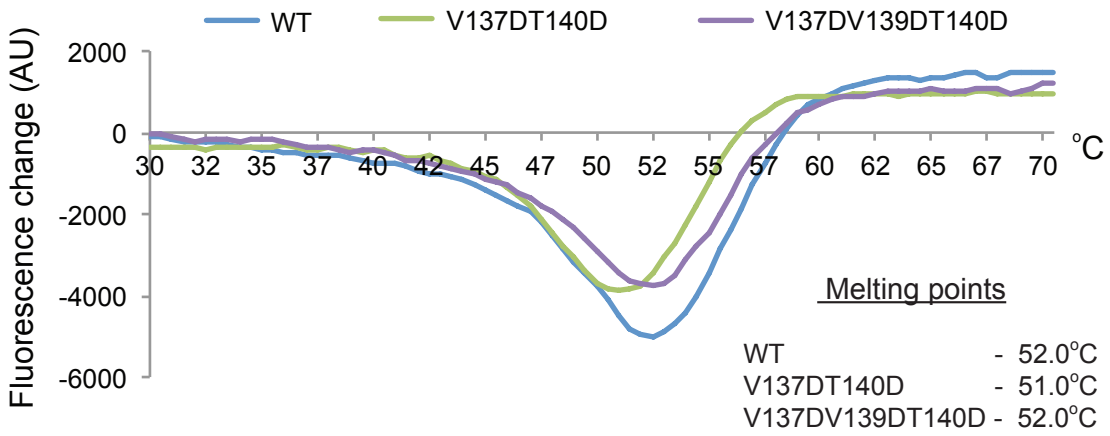

Figure 3.10 Thermal denaturation of mCbx7 (wild-type) and mCbx7 point mutants

Differential scanning fluorimetry (DSF) was used to determine thermal denaturation curves for GST-mCbx7 (wild-type, V137DT140D, and V137DV139DT140D). Data are representative of three technical repeats. Each thermal denaturation curve is coloured according to the key, and the melting point (Tm) of each protein is noted in the figure.

Chapter 4. Phosphorylation of CBX7

4.1 Introduction

Phosphorylation can enhance or disrupt protein-protein and protein-DNA interactions. The association of CK2 with CBX proteins suggested that CK2 could influence the function of PRC1 complexes, either by phosphorylating a component of PRC1 or acting in conjunction with PRC1 to phosphorylate a protein at its site of action. However, as discussed in Chapter 1.11.5, investigating candidate CK2 substrates is challenging due to their large number. The CK2 consensus sequence, S/T-x-x-D/E (Marin et al., 1986, Meggio and Pinna, 2003, Meggio et al., 1984), is present in most protein sequences (Litchfield, 2003)). Indeed, each human PRC1 protein contains multiple CK2 consensus sequences (Table 1.2). Importantly, although an interaction between CK2 and the PRC1 complex has been extensively reported, no CK2 substrates have been identified among the known PcG proteins.

CK2 is constitutively active and although this activity can be modulated by the CK2β subunits, in a substrate and context dependent manner, a main facet its regulation is via substrate interactions (Chapter 1.11.4). Given the specific interaction between CK2 and the Pc box domain of CBX proteins described in Chapter 3, we hypothesised that the CBX proteins might be phosphorylated by CK2. Within CBX7, there are three residues that lie within CK2 consensus sequences: Ser40, Thr221 and Thr233 (Figure 4.1). The Thr233 residue is a particularly interesting candidate because of its location in the Pc box of CBX7. The equivalent residue in mCbx7, Thr140, (Figure 3.8) is one of the three residues in the Pc box that are important for the interaction of mCbx7 with CK2 and RING2. A fourth residue, Thr41, was also of interest as a candidate CK2 target. Although Thr41 does not lie within a CK2 consensus, the equivalent residue in the chromodomain of HP1β, Thr51, is phosphorylated by CK2 during the DNA damage response. Phosphorylation of Thr51 disrupts the interaction of HP1β with H3K9me3 and serves to mobilise HP1β from chromatin (Ayoub et al., 2008). Thr41 of CBX7 may therefore be an atypical CK2 target site and its phosphorylation could affect the interaction of CBX7 with chromatin. Given these precedents, we decided to investigate whether CBX7 itself is a substrate for CK2 phosphorylation.

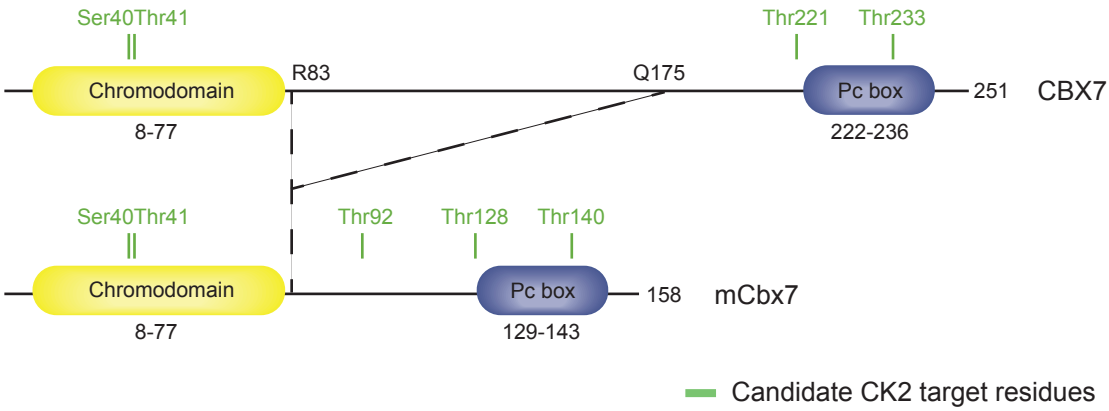

Figure 4.1 Candidate CK2 phosphorylation sites within mCbx7 and CBX7

CBX7 (251 amino acids) and mCbx7 (158 amino acids) proteins are represented by this schematic. Regions containing the chromodomains and Pc boxes are indicated (yellow and blue boxes, respectively). Dashed lines show the 92 amino acid stretch of CBX7 (Arg83-Gln175) that is not conserved in mCbx7. Candidate CK2 target residues are indicated.

4.1.1 CK2 phosphorylation of mCbx7 *in vitro*

To determine whether CBX7 could be phosphorylated by CK2 *in vitro*, purified recombinant mCbx7 was used as a substrate in a kinase assay with recombinant CK2 and [γ-^{32}P]ATP. The wild-type GST-mCbx7 fusion protein was expressed in *E. coli* using the pGEX-6P1 plasmid as described in Chapter 3. Following purification on glutathione sepharose beads, the intact mCbx7 protein was released from the beads by cleavage with PreScission protease. The production and recovery of recombinant proteins was assessed by SDS-PAGE and Coomassie staining of the gel. The purified mCbx7 appeared as a band of the expected size at around 24kDa and its provenance was confirmed by immunoblotting with an antibody that recognises mCbx7 (Appendix: Figure 8.4).

Incubation of purified mCbx7 with recombinant CK2 and [γ-^{32}P]ATP resulted in the incorporation of radioactive label, suggesting that CK2 was able to phosphorylate mCbx7 *in vitro* (Figure 4.2). Importantly, incorporation of ^{32}P was dependent on the addition of CK2, demonstrating that other kinases, which might have been present as contaminants of the purification, were not responsible for the phosphorylation of

mCbx7. ^{32}P was also incorporated into CK2α as expected; the α and β subunits of the CK2 holoenzyme are known to be autophosphorylated (Zhang et al., 2002). However, under the conditions used, autophosphorylation of the β-subunit was not detectable.

Substrate interactions can be important for the regulation of CK2 activity (Chapter 1.11.4). We therefore set out to test whether mCbx7 variants, which show impaired binding to CK2 (Chapter 3.4.3), could be phosphorylated. Two mCbx7 mutants, mCbx7-T140D and mCbx7-V137DV139DT140D were expressed in *E. coli*, purified, and subsequently cleaved from their N-terminal GST-tag, as described above for wild-type mCbx7. Purified mCbx7 (Wild-type, T140D and V137DV139DT140D) or recombinant Cdc37 (ProSpec), were incubated with recombinant CK2 and [γ-^{32}P]ATP, and proteins were subsequently fractionated by SDS-PAGE. Coomassie staining of the gel revealed equivalent loading of wild-type and mutant mCbx7 species. ^{32}P incorporation of wild-type mCbx7 was comparable to ^{32}P incorporation of Cdc37, a known target of CK2 phosphorylation (Miyata and Nishida, 2005) (Figure 4.3). ^{32}P incorporation of mCbx7-T140D was slightly less than that of wild-type mCbx7. This could be a consequence of the slightly abrogated binding of CK2 to this mutant (Chapter 3.4.3). Alternatively, it could also suggest that Thr140 is a CK2 target. However, as ^{32}P incorporation was not completely abolished by the T140D mutation, this result would suggest that CK2 is able to phosphorylate additional residues under these conditions. Surprisingly, ^{32}P incorporation into mCbx7-V137DV139DT140D was greater than wild-type mCbx7. Evidence in Chapter 3.4.3 suggested this mutant would be unable to bind CK2. It is possible that the increased ^{32}P incorporation could be a consequence of phosphorylation at a novel CK2 consensus site, Ser136, found in this mutant. These data suggest that either CK2 binds mCbx7-V137DV139DT140D under these conditions, or that the binding of CK2 to mCbx7 is uncoupled from its ability to phosphorylate mCbx7. These points will be discussed further in Chapter 7.

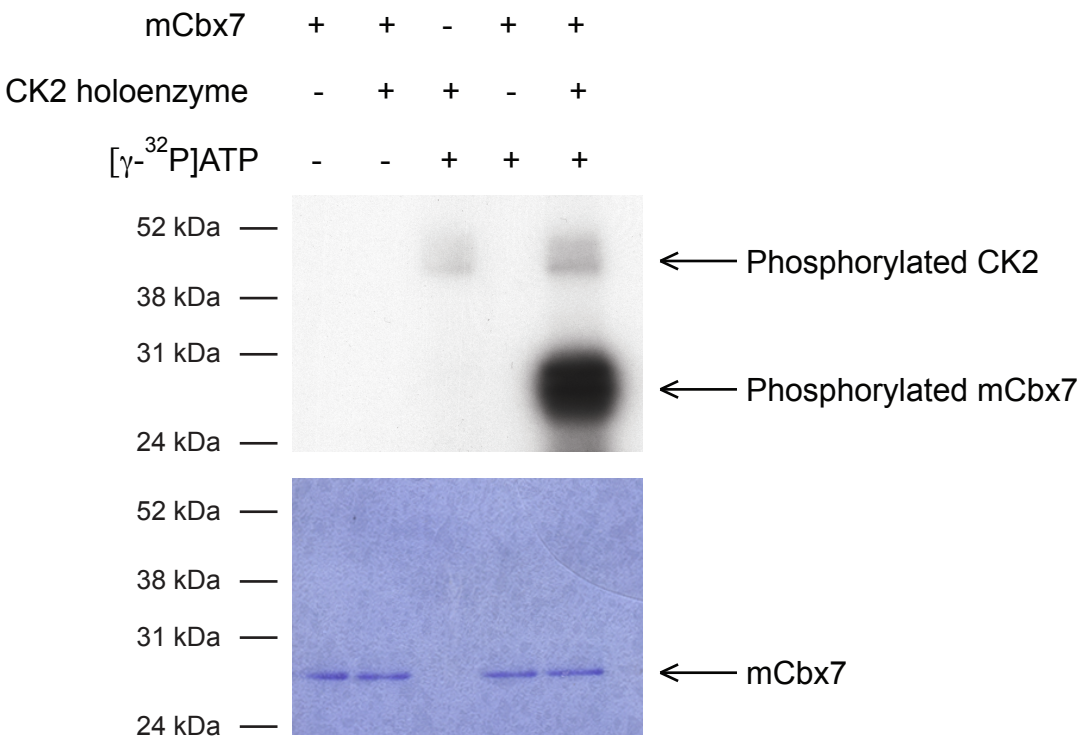

Figure 4.2 *In vitro* phosphorylation of CBX7 by CK2

Kinase assays were performed using purified mCbx7, CK2 holoenzyme and [γ-^{32}P]ATP in the combinations indicated. Kinase assay products were fractionated by SDS-PAGE and Coomassie stained overnight. Autoradiography was used to detect ^{32}P in the Coomassie stained gel. Arrows indicate phosphorylated CK2α and mCbx7. Image is representative of three biological repeats.

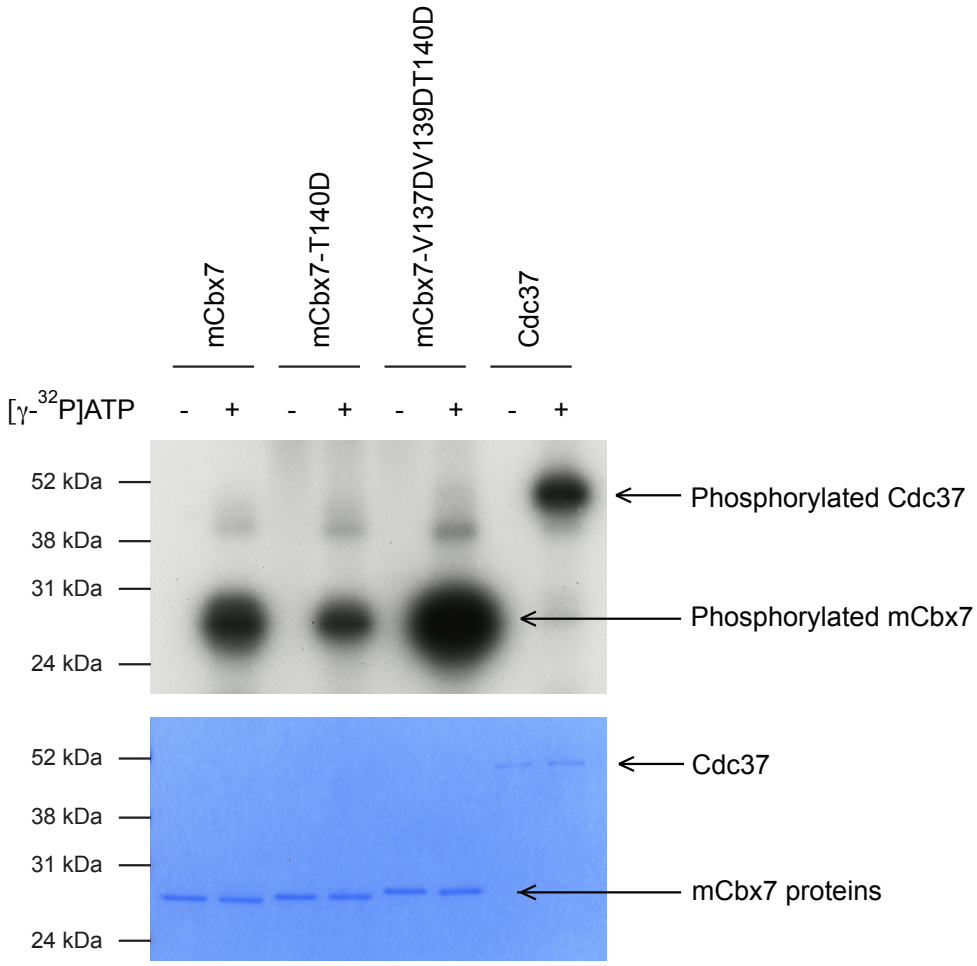

Figure 4.3 CK2 phosphorylation of mCbx7 (wild-type, T140D and V137DV139DV140D) and Cdc37

Kinase assays were performed using purified mCbx7 (wild-type, T140D and V137DV139DT140D) or Cdc37 (ProSpec), CK2 holoenzyme and [γ-^{32}P]ATP when indicated. Kinase assay products were fractionated by SDS-PAGE and Coomassie stained overnight. Autoradiography was used to detect ^{32}P in the Coomassie stained gel. Arrows indicate phosphorylated mCbx7 proteins and Cdc37. Image is representative of two biological repeats.

4.1.2 Identifying CK2 phosphorylated peptides within CBX7

To try to identify the residue(s) in mCbx7 phosphorylated by CK2, the *in vitro* kinase assay was repeated in the presence of unlabelled ATP and the products were submitted for analysis by mass spectrometry (MS). Samples that had been treated with or without CK2 were submitted and two enzymatic digestions were performed on each. Although the coverage of mCbx7-derived peptides was good, the MS analyses did not identify any phosphorylated residues within mCbx7. This was disappointing, given the clear evidence for ^{32}P labelling of mCbx7 in the *in vitro* kinase reaction. However, if only a small percentage of the mCbx7 was phosphorylated in the reaction, the MS analyses may not have been sufficiently sensitive to identify sub-stoichiometric amounts of phosphopeptides.

As the MS analysis was inconclusive, it was decided to take an alternative approach. A synthetic peptide array, representing the sequence of human CBX7 as a series of overlapping 20-mers, was used as the substrate in an *in vitro* kinase assay with [γ-^{32}P]ATP and recombinant CK2. Autoradiography was used to detect ^{32}P-bound to the array (Figure 4.4A). Interestingly, ^{32}P labelling was observed in four discrete regions of the array, in patterns consistent with phosphorylation of adjacent peptides. However, these ^{32}P-labelled peptide spots did not contain candidate CK2 target residues. Furthermore, some of the ^{32}P-bound peptides did not contain a serine or threonine residue (A17-21), and although these peptides did contain tyrosine, it is very rare to find tyrosine phosphorylation attributable to CK2 (Meggio and Pinna, 2003). Taken together, these data suggested that ^{32}P incorporation did not reflect phosphorylation of the peptides by CK2.

As ATP is negatively charged, it was conceivable that the signals on the array represented direct binding of [γ-^{32}P]ATP to positively charged peptides. A crude estimate of the charge was obtained by simply counting the difference between the number of acidic (aspartate and glutamate) and basic (histidine, arginine and lysine) residues in each peptide. As represented in Figure 4.4B, there was a striking correlation between the peptides with an excess of positively charged residues and those labelled by [γ-^{32}P]ATP on the array. To confirm this interpretation, a duplicate array was used in an *in vitro* kinase assay in the absence

of CK2. The ^{32}P signal was detected on the same positively charged peptides implying that it did not represent phosphorylation by CK2 (Figure 4.5).

This was an unexpected finding as, in other studies, peptide arrays have been successfully used to identify sites of phosphorylation. For example, similar peptide arrays were used at the LRI to determine the CK2 phosphorylation site in TEL2 (Horejsi et al., 2010). Importantly, the conditions used in the TEL2 study were adopted here for the *in vitro* kinase assay on the CBX7 array. Presumably, the signal to noise ratio for a true phosphorylation event would be great enough to negate the background signal obtained from binding of [γ-^{32}P]ATP to positively charged peptides. A positive control peptide on these arrays would have been useful to test this hypothesis. The implication is either that CK2 can only phosphorylate CBX7 in the context of the full-length protein or that CBX7 is not a substrate for phosphorylation by CK2.

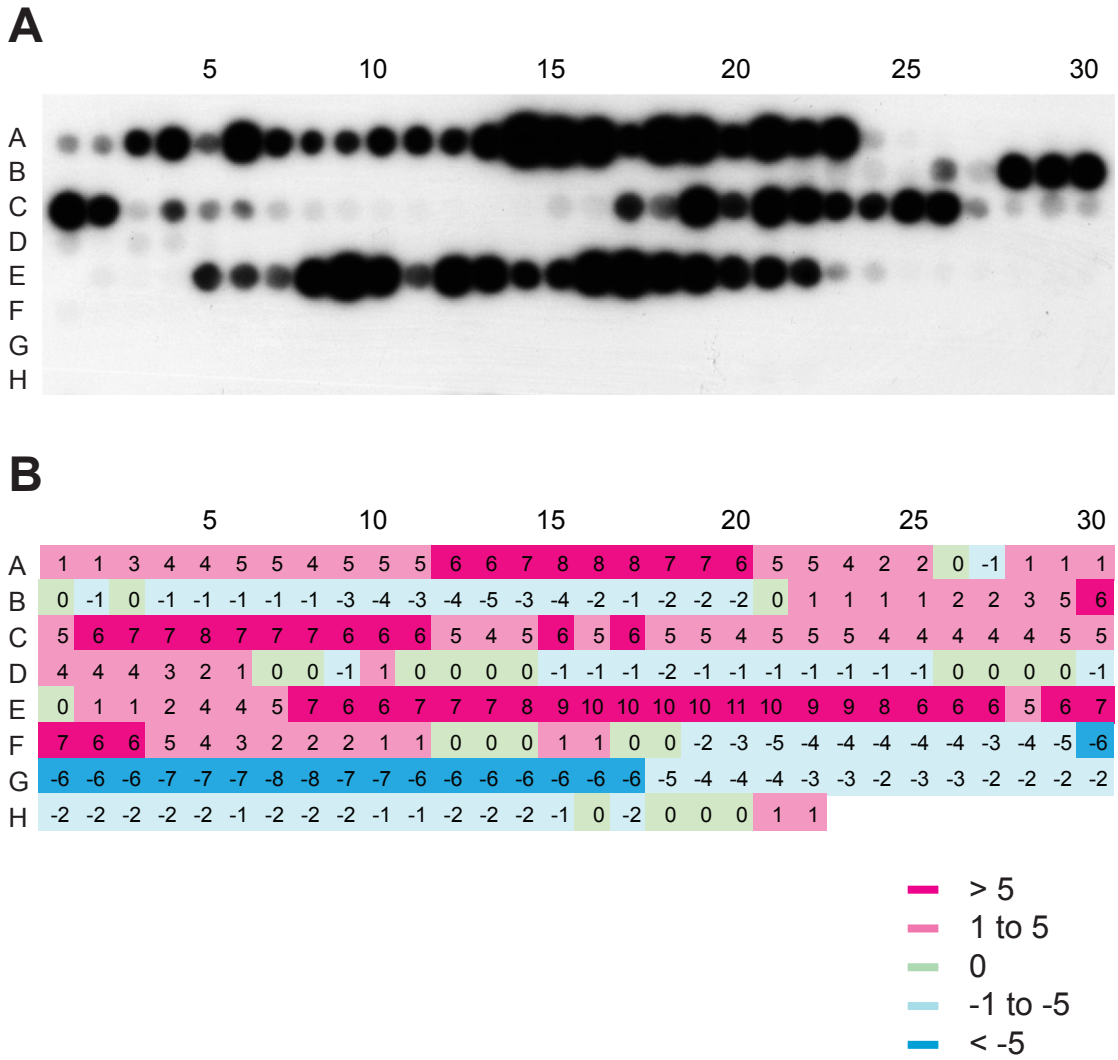

Figure 4.4 *In vitro* kinase assay of CBX7 peptide array with CK2

A) A peptide array of CBX7 was incubated under kinase assay conditions with recombinant CK2α and [γ-^{32}P]ATP. After extensive washing, autoradiography was used to detect ^{32}P bound to the array. Position A1 of the array corresponds to N-terminal amino acids 1-20 of CBX7. Each 20-mer peptide in the array was advanced from the previous by one residue in the C-terminal direction. The last peptide, at position H22, corresponds to the C-terminal amino acids 232-251. **B)** A diagram showing the number of positive side-chains minus the number of negative side chains within each peptide of the CBX7 array used in A. Peptide positions are coloured according to the key shown in the diagram.

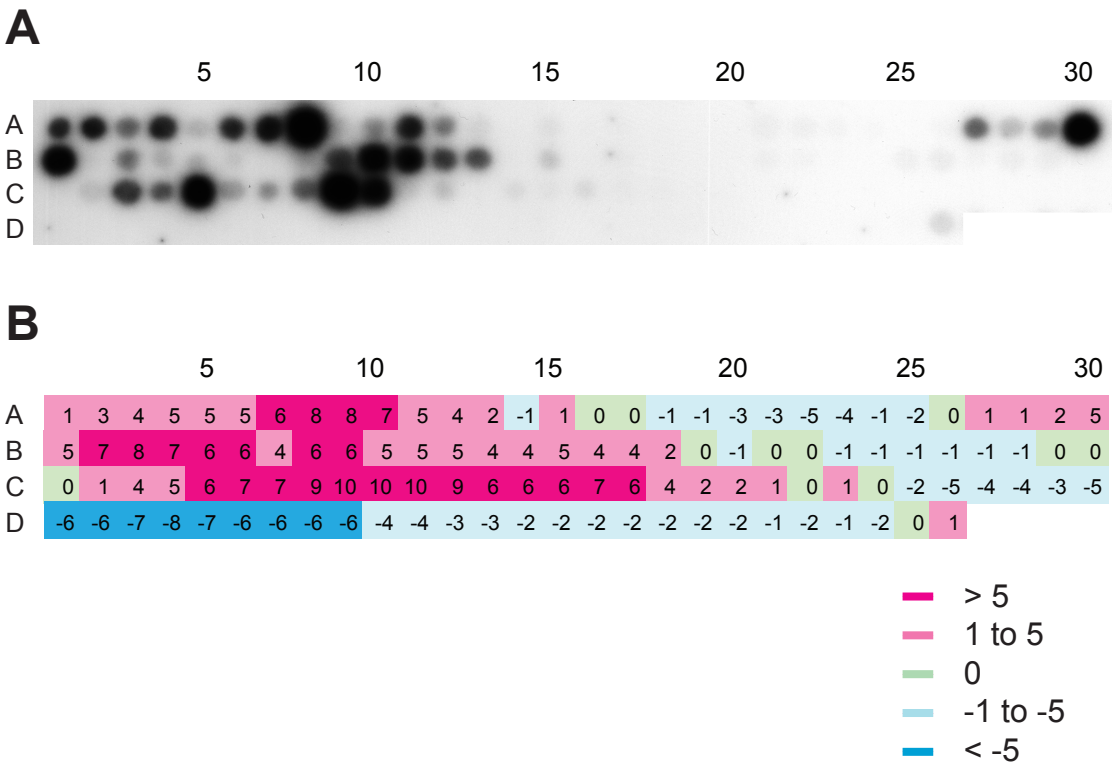

Figure 4.5 *In vitro* kinase assay of CBX7 peptide array in the absence of CK2

A) A peptide array of CBX7 was incubated under kinase assay conditions with [γ-^{32}P]ATP but in the absence of recombinant CK2. After extensive washing, autoradiography was used to detect ^{32}P bound to the array. Position A1 of the array corresponds to N-terminal amino acids 1-20 of CBX7. Each 20-mer peptide in the array was advanced from the previous by two residues in the C-terminal direction. The last peptide, at position D26, corresponds to the C-terminal amino acids 232-251. **B)** A diagram showing the number of positive side-chains minus the number of negative side chains within each peptide of the CBX7 array used in A. Peptide positions are coloured according to the key shown in the diagram.

4.2 Evidence for phosphorylation of endogenous CBX7

To assess whether endogenous CBX7 is phosphorylated, the TALON phosphate metal affinity chromatography (PMAC) resin was used to separate cell lysates into fractions containing phosphorylated proteins (that had bound to the resin) and fractions containing non-phosphorylated proteins (which did not bind to the resin). Phospho-enrichment was performed on lysates from control cells (treated with ethanol) and from cells treated with the CK2 inhibitor DRB, to investigate whether CBX7 phosphorylation status was dependent on CK2 activity.

In addition to CK2, DRB is known to target additional kinases, such as P-TEFb. Inhibition of P-TEFb by DRB blocks transcriptional elongation by Pol II; leading to a decrease in the Ser2-phosphorylated form of RNA polymerase II (phospho-Pol II (Ser2)) levels (Nechaev and Adelman, 2011). As expected, β-actin was recovered exclusively in the non-binding fraction whereas phospho-Pol II (Ser2) was exclusively in the bound fraction (Figure 4.6). Less phospho-Pol II (Ser2) was recovered in the bound fraction from DRB-treated cells, confirming DRB had blocked transcriptional elongation.

Figure 4.6 shows that endogenous CBX7 was bound to the PMAC resin in both the control and DRB-treated samples. Moreover, the amount of phosphorylated CBX7 recovered under both conditions was equivalent. This result suggests that if endogenous CBX7 is indeed phosphorylated by CK2, as implied by the *in vitro* kinase assay, then CK2 is not the only kinase to do so. RING2 was also recovered as a phosphorylated protein in both the presence and the absence of DRB, and therefore similar conclusions apply. One caveat in this experiment is the discrepancy between the amount of CBX7 recovered in the phosphorylated fraction and the input. Although CBX7 was not detected in the flow-through, it could have been lost during the extensive washing of the column between loading and elution. This did not appear to be an issue with RING2 and phospho-Pol II (Ser2) but it is conceivable that the extent of phosphorylation and the position of these modifications in the protein can affect the affinity of the protein for PMAC resin.

Endogenous CBX7 is resolved into two differently migrating bands when fractionated by SDS-PAGE under optimal conditions. This doublet is apparent in Figure 4.6 but is more convincing in Figure 4.7. To investigate whether the doublet reflected a phosphorylation event, 293T cell lysate was treated with lambda phosphatase to remove this modification from all cellular proteins. Following SDS-PAGE and immunoblotting, CBX7 was still resolved as a doublet (Figure 4.7). Phosphorylated-MEK served as a positive control to show that lambda phosphatase treatment had been effective. This result suggests that the endogenous CBX7 doublet is not due to phosphorylation. Overexpressed mCbx7-FLAG and mCbx7-HA are resolved as doublets but the bands are markedly different in size as opposed to those of endogenous CBX7. CBX7-FLAG can also be resolved as two differentially migrating bands, although the smaller of these, migrating to around 26 kDa, is often only visible after FLAG-immunoprecipitation (Figure 3.1). Following lambda phosphatase treatment, the higher migrating bands of mCbx7-FLAG, mCbx7-HA and CBX7-FLAG were detected at equivalent amounts to untreated lysate, suggesting that they are not a consequence of phosphorylation. As mCbx7 and CBX7 have a conserved methionine position 55, and CBX7 has an additional methionine at position 86, the different sizes of these C-terminally tagged proteins probably reflect translation from alternative start codons.

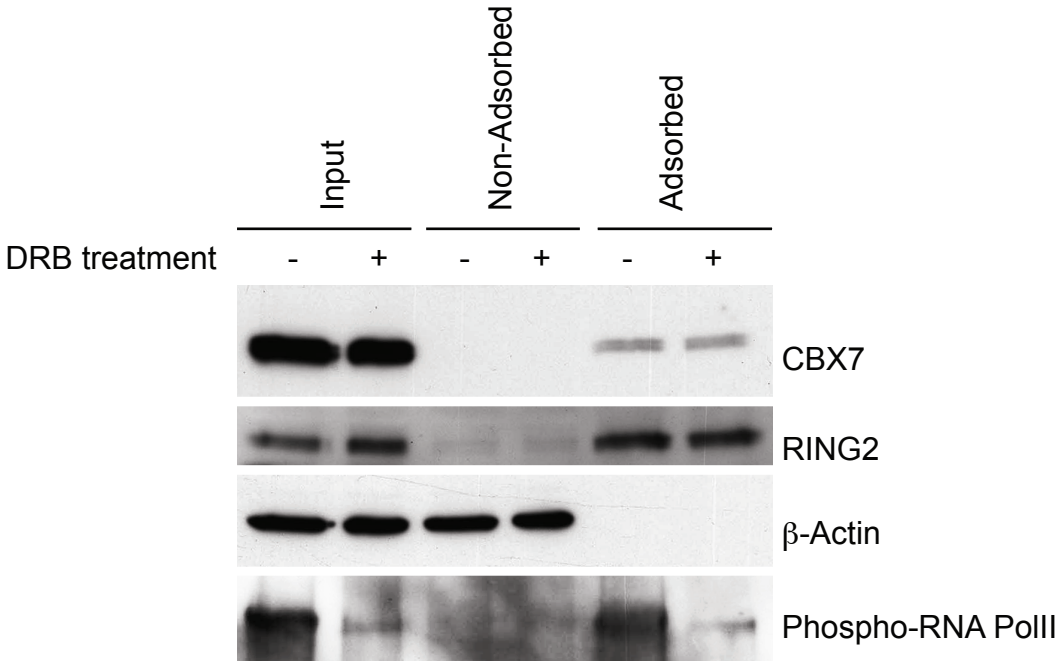

Figure 4.6 Phosphorylation status of CBX7 following CK2 inhibition

293T cells were treated with ethanol or 75mM DRB for 3h and then lysed. Lysate was loaded into phosphate metal affinity chromatography (PMAC) resin columns. Non-phosphorylated proteins did not bind to the resin and were collected in the flow-thorough. After extensive washing of the column, phosphorylated proteins bound to the resin were eluted. Flow-through and eluted samples were fractionated by SDS-PAGE alongside input samples equivalent to 2% volume of cell lysate loaded on the PMAC column. Immunoblotting against CBX7, RING2, β-Actin and phospho-Pol II (Ser2) was performed. Image is representative of two biological repeats.

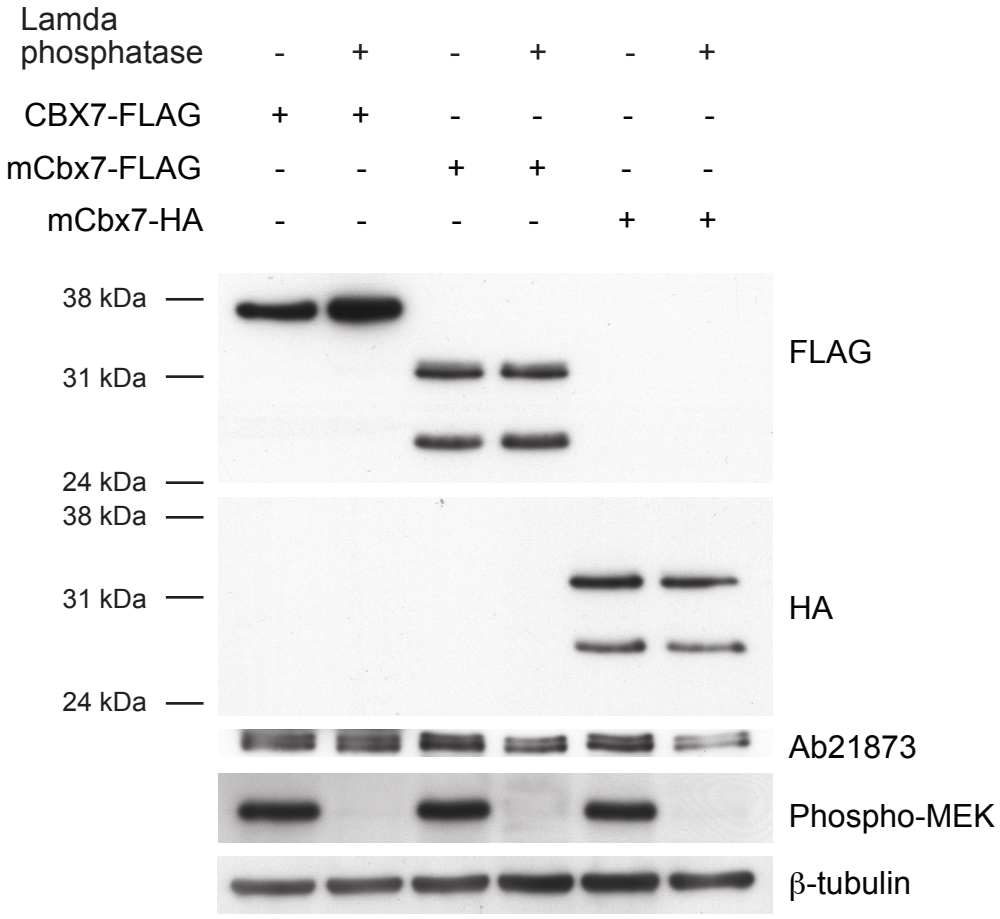

Figure 4.7 Lambda phosphatase treatment of cell lysate

pcDNA6 plasmids encoding CBX7-FLAG, mCbx7-FLAG or mCbx7-HA (generated by Marc Rodriguez-Niedenfuhr) were transfected into 293T cells using lipofectamine. After 24 hours, cells were lysed and treated with lambda phosphatase (4,000 U per mg protein lysate) for 45 minutes at 30°C. The untreated and lambda phosphatase treated lysates were fractionated by SDS-PAGE. Immunoblotting was performed against FLAG, HA, CBX7 (Ab21873), phospho-MEK(Ser217/221) and β-tubulin.

4.3 CK2-independent phosphorylation of mCbx7

Figure 4.6 suggested that endogenous CBX7 is phosphorylated and that some level of phosphorylation can occur independently of CK2 activity. In agreement with this, residue Thr119 of mCbx7, which does not lie within a CK2 consensus site, was found to be phosphorylated when mCbx7 was expressed in 293T cells (Emily Bernstein, personal communication). Phosphorylation of Thr119 was determined by mass spectrometry and the Bernstein laboratory developed a phospho-specific antibody against this residue of mCbx7. The phospho-specific antibody developed by the Bernstein laboratory was validated in two ways. Firstly, a peptide competition assay was performed using unphosphorylated or phosphorylated mCbx7 peptides. This assay showed that the antibody was specifically blocked by the phosphorylated mCbx7 peptide. Secondly, the antibody was validated by its failure to detect Cherry-tagged mCbx7 following lambda phosphatase treatment of the cell lysate. These experiments to validate the phospho-specific antibody were performed by the Bernstein laboratory; the data is not shown in this thesis. It is important to note that the mass spectrometry analysis of mCbx7, carried out by the Bernstein laboratory, did not reveal any phosphorylation at putative CK2 target residues.

A collaboration was established with the Bernstein laboratory to investigate the functional implications of Thr119 phosphorylation. Our work specifically focused on understanding whether Thr119 phosphorylation affected the ability of mCbx7 to repress the *INK4a* tumour suppressor gene. Over-expression of mCbx7, including the TAP-tagged version, can extend the replicative lifespan of HDFs via the repression of *INK4a* (Nicholls, 2006). Conversely, shRNA-mediated knockdown of CBX7 causes up-regulation of *INK4a* and premature senescence (Maertens et al., 2009).

Retrovirus-based vectors encoding phospho-ablating and phospho-mimicking mutants of mCbx7 at Thr119 (mCbx7T119A-FLAG-Cherry-LPC and mCbx7T119E-FLAG-Cherry-LPC respectively) were provided by the Bernstein laboratory. They were packaged into amphotropic particles and used to infect the TIG3 and ESC strains of human fibroblasts (Brookes et al., 2004). Previous studies in the

laboratory have shown that ectopic expression of PRC1 components can have variable effects, depending on the strain of human fibroblasts, and TIG3 and ESC are two distinctive examples (Sharon Brookes, personal communication). As both the LPC vector and the Cherry tag had not been previously tested in the lab, cells were also infected with mCbx7-FLAG in pBABE, and the pBabe vector alone, which had both been previously validated (data not shown).

Following infection and drug selection, the expression of the different versions of mCbx7 was assessed by immunoblotting with an antibody against the C-terminal FLAG epitope. As shown in Figure 4.8, similar levels of expression were achieved with each construct and in both cell backgrounds. Immunoblotting with an antibody that recognises mCbx7 identified the relevant bands on the gel and their sizes were consistent with the addition of FLAG and Cherry epitopes. Full-length protein species are indicated in Figure 4.8. The provenance of lower migrating bands detected by the anti-FLAG antibody have not resolved but may be a consequence of translation from alternative start codons as previously discussed (Chapter 4.2) Importantly, immunoblotting with an antibody against phospho-Thr119 confirmed the phosphorylation of wild-type Cbx7, expressed from either vector (lanes 2 and 4), but was not sensitive enough to detect endogenous CBX7. The phospho-mimicking and phospho-ablating mutants were not detected by the phospho-Thr119 antibody.

The cell lysates were also analysed for the expression of $p16^{INK4a}$ at both the protein and RNA level. Wild-type mCbx7, expressed from either the pBABE or LPC vectors, caused the expected down-regulation of endogenous $p16^{INK4a}$ in both TIG3 and ESC cells, and comparable effects, relative to the loading control, were observed with the T119A and T119E mCbx7 mutants (Figure 4.8). *INK4a* RNA levels were also reduced to equivalent amounts following the overexpression of mCbx7-T119A, -T119E and wild-type mCbx7 proteins (Figure 4.9). The ability of mCbx7 to repress transcription of *INK4a* therefore appears to be intact in mCbx7-Thr119 phospho-mimicking and phospho-ablating mutants.

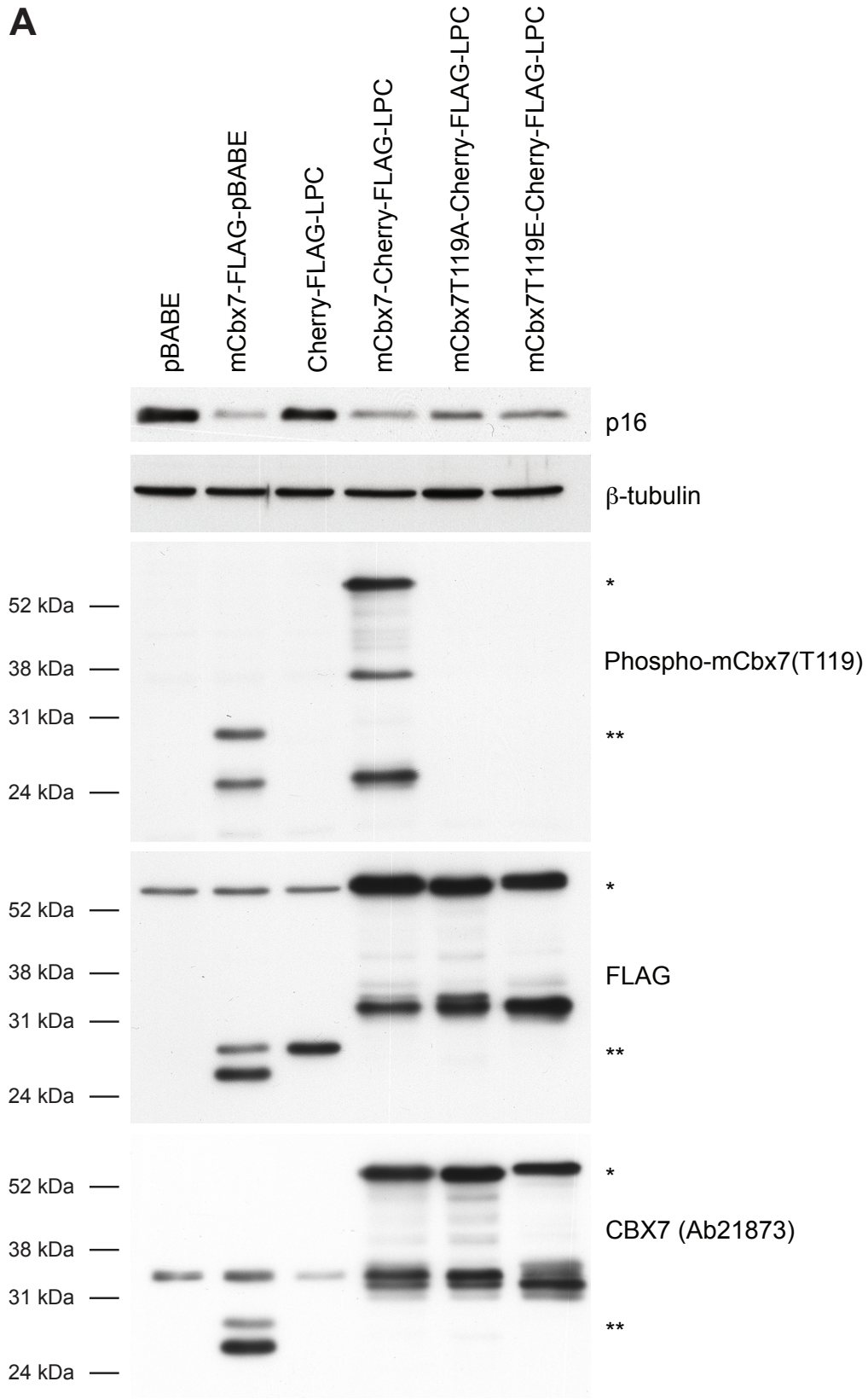
A
pBABE
mCbx7-FLAG-pBABE
Cherry-FLAG-LPC
mCbx7-Cherry-FLAG-LPC
mCbx7T119A-Cherry-FLAG-LPC
mCbx7T119E-Cherry-FLAG-LPC
p16
β-tubulin
52 kDa
38 kDa
31 kDa
24 kDa
*
Phospho-mCbx7(T119)
**
52 kDa
38 kDa
31 kDa
24 kDa
*
FLAG
**
52 kDa
38 kDa
31 kDa
24 kDa
*
CBX7 (Ab21873)
**

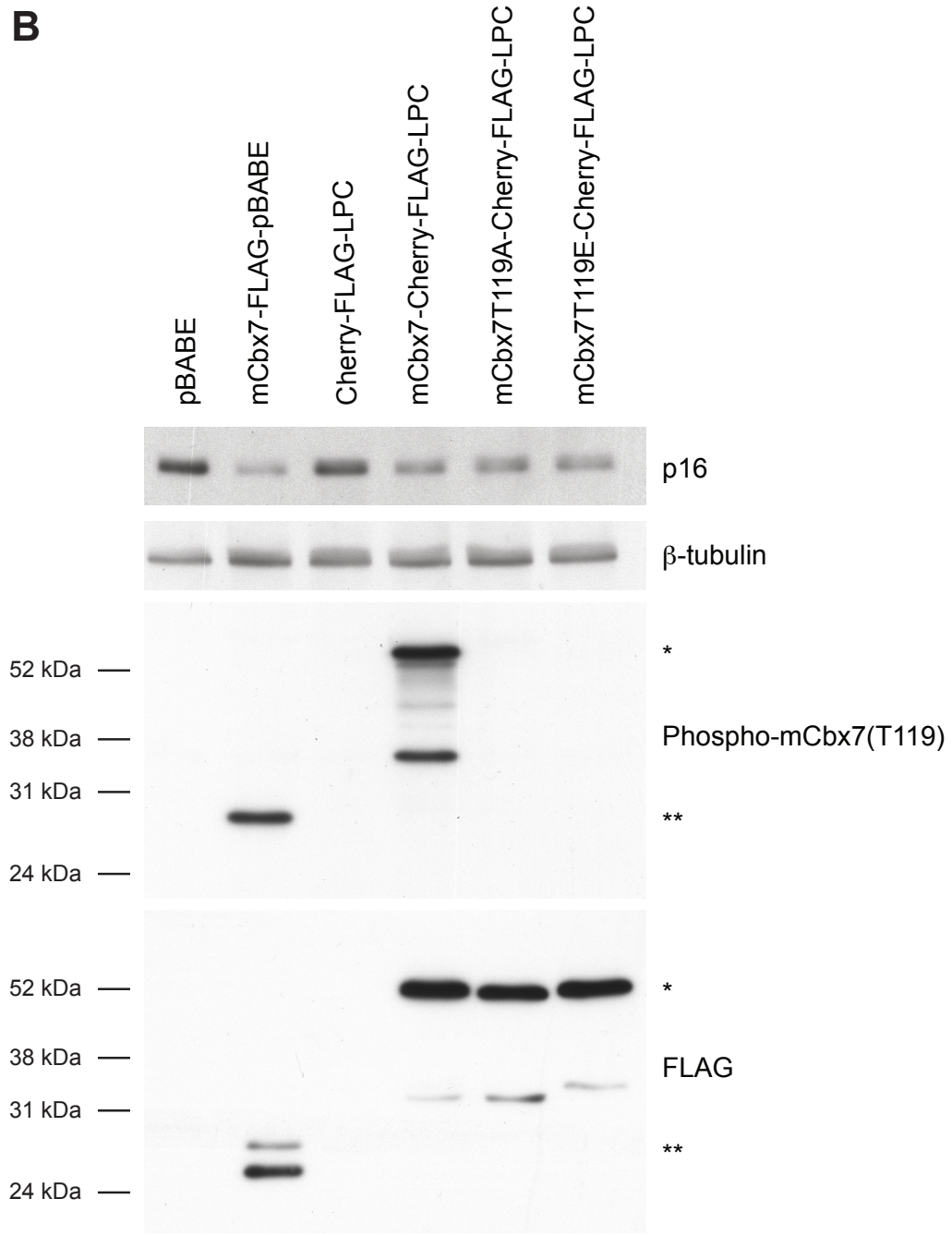

Figure 4.8 p16^{INK4a} levels in HDFs following expression of mCbx7 mutants

Retrovirus-based vectors (pBABE, mCbx7-FLAG-pBABE (generated by Marc Rodriguez-Niedenfuhr), Cherry-FLAG-LPC, mCbx7-Cherry-FLAG-LPC, mCbx7T119A-Cherry-FLAG-LPC or mCbx7T119E-Cherry-FLAG-LPC (generated by Mooki Wu)) were packaged into amphotropic particles and used to infect TIG3 **(A)** and ESC **(B)** cells. 14 days post-infection infection, cells were lysed and protein was fractionated by SDS-PAGE. Immunoblotting was performed against FLAG, p16^{INK4a}, phospho-mCbx7(T119) and β-tubulin. Single asterisks indicate full-length Cherry-FLAG-tagged mCbx7 species. Double asterisks indicate full-length FLAG-tagged mCbx7 species. Images are representative of two biological repeats.

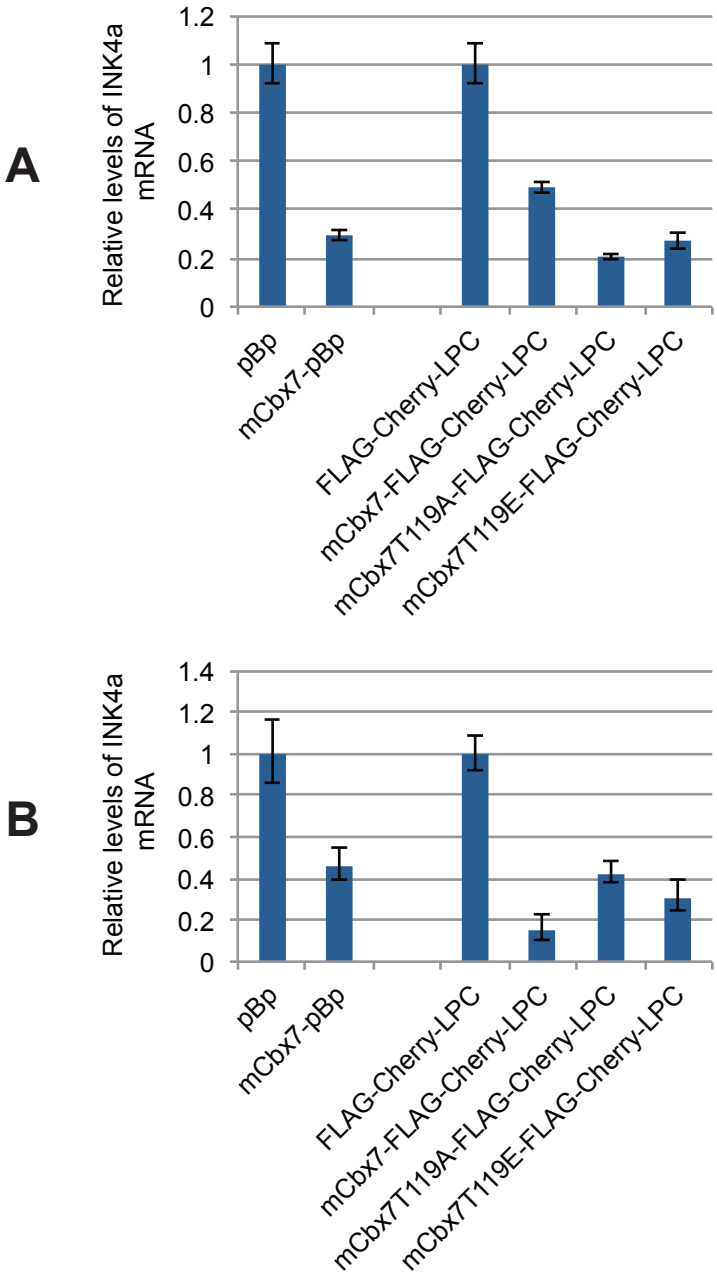

Figure 4.9 *INK4a* RNA levels in HDFs following expression of mCbx7 mutants

Retrovirus-based vectors (pBABE, mCbx7-FLAG-pBABE (generated by Marc Rodriguez-Niedenfuhr), Cherry-FLAG-LPC, mCbx7-Cherry-FLAG-LPC, mCbx7T119A-Cherry-FLAG-LPC or mCbx7T119E-Cherry-FLAG-LPC (generated by Mooki Wu)) were packaged into amphotropic particles and used to infect TIG3 **(A)** and ESC **(B)** cells. 14 days post-infection, cells were lysed, and the RNA was extracted and reverse transcribed. *INK4a* and *β-tubulin* cDNA was amplified by qPCR and CT values of *INK4a* were normalised to *β-tubulin*. The fold change of *INK4a* mRNA following the overexpression of mCbx7 (wild-type, T119A or T119E), relative to control samples is shown. Data correspond to the average and standard deviation of three technical replicates and are representative of two biological repeats.

Recent work in the laboratory has suggested that CBX proteins function within Polycomb bodies that contain multiple variants of PRC1, and that the genes encoding CBX proteins are themselves subject to regulation by PRC1 (O'Loghlen et al., 2012, Bracken et al., 2006, Pemberton et al.). Further experiments were therefore performed to assess whether the contribution of mCbx7-Thr119 phospho-mimicking and phospho-ablating mutants to $p16^{INKa}$ regulation was concomitant with the physical association of these mutants to *INK4a*. In human fibroblasts, endogenous PRC1 proteins have a well-characterised binding pattern across the *INK4a-ARF-INK4b* region as documented by chromatin immunoprecipitation (ChIP) and PCR with multiple primer sets (Maertens et al., 2009, Dietrich et al., 2007, Bracken et al., 2007, Pemberton et al.). An initial test was performed to confirm that mCbx7-FLAG expressed from the pBABE vector showed the expected binding pattern at *INK4a* following ChIP with anti-FLAG agarose (Figure 4.10A). Peak binding was observed with primer sets 5 and 7, which correspond to the first exon of *INK4a*, whereas binding was minimal at *ARF* and *INK4b*. No signal was detected with cells infected with the empty vector.

In cells expressing FLAG-Cherry-tagged wild-type mCbx7, T119A-mCbx7 and T119E-mCbx7 from in the LPC vector, very similar binding patterns were observed following ChIP with anti-FLAG agarose (Figure 4.10B). Although the enrichment relative to input was lower than observed with the pBABE vector, this applied to the wild-type construct and could reflect interference by the additional Cherry epitope in these constructs. These data suggest that the T119A and T119E mutations did not impair the ability of mCbx7 to associate with *INK4a* in either TIG3 or ESC cells.

Finally, the mCbx7-Thr119 phosphomimicking and phosphoablating mutants were assessed for their ability to extend the lifespan of cells in which they are expressed. Previous work in the laboratory had shown that wild-type mCbx7 has a substantial impact on replicative lifespan of ESC cells but only a marginal effect in TIG3 cells (Sharon Brookes, personal communication). The reasons for these differences remain unclear but were recapitulated in the experiments described in Figure 4.11. Importantly, the ability of the T119A and T119E mutants to delay senescence was indistinguishable from that of wild-type mCbx7.

Taken together, these data imply that a phosphorylation event at Thr119 of mCbx7 is unlikely to affect the ability of mCbx7 to function as a component of PRC1. It remains conceivable that phosphorylation of Thr119 alters a property of mCbx7 that was not assessed or is only apparent at specific target genes. However, the Bernstein lab have more recently looked at global changes in gene expression by microarray analyses and found no significant differences between the effects of mCbx7T119A, mCbx7T119E and wild-type mCbx7 proteins.

4.4 Conclusions

Data presented in this chapter suggest that mCbx7 can be phosphorylated by CK2 *in vitro*. However, the target residue could not be identified. This called into question the extent of *in vitro* CBX7 phosphorylation by CK2 and therefore the likelihood of CBX7 being an endogenous substrate of CK2. It also meant that it was not possible to mutate any identified CK2 target residues and test the function of phosphorylation. Both endogenous CBX7 and RING2 were shown to be phospho-proteins and this status was not altered by CK2 inhibition. This suggested CBX7 and RING2 are both substrates for other kinases.

A CK2-independent phosphorylation site of mCbx7 (Thr119) was identified by Emily Bernstein's laboratory and, in collaboration, we sought to investigate the functional implications of this phosphorylation. Specifically, our work tested the recruitment and activity of phospho-mimicking and phospho-ablating mCbx7 mutants. Data here indicate that phosphorylation of mCbx7 at Thr119 is not important for PRC1 repression of *INK4a*.

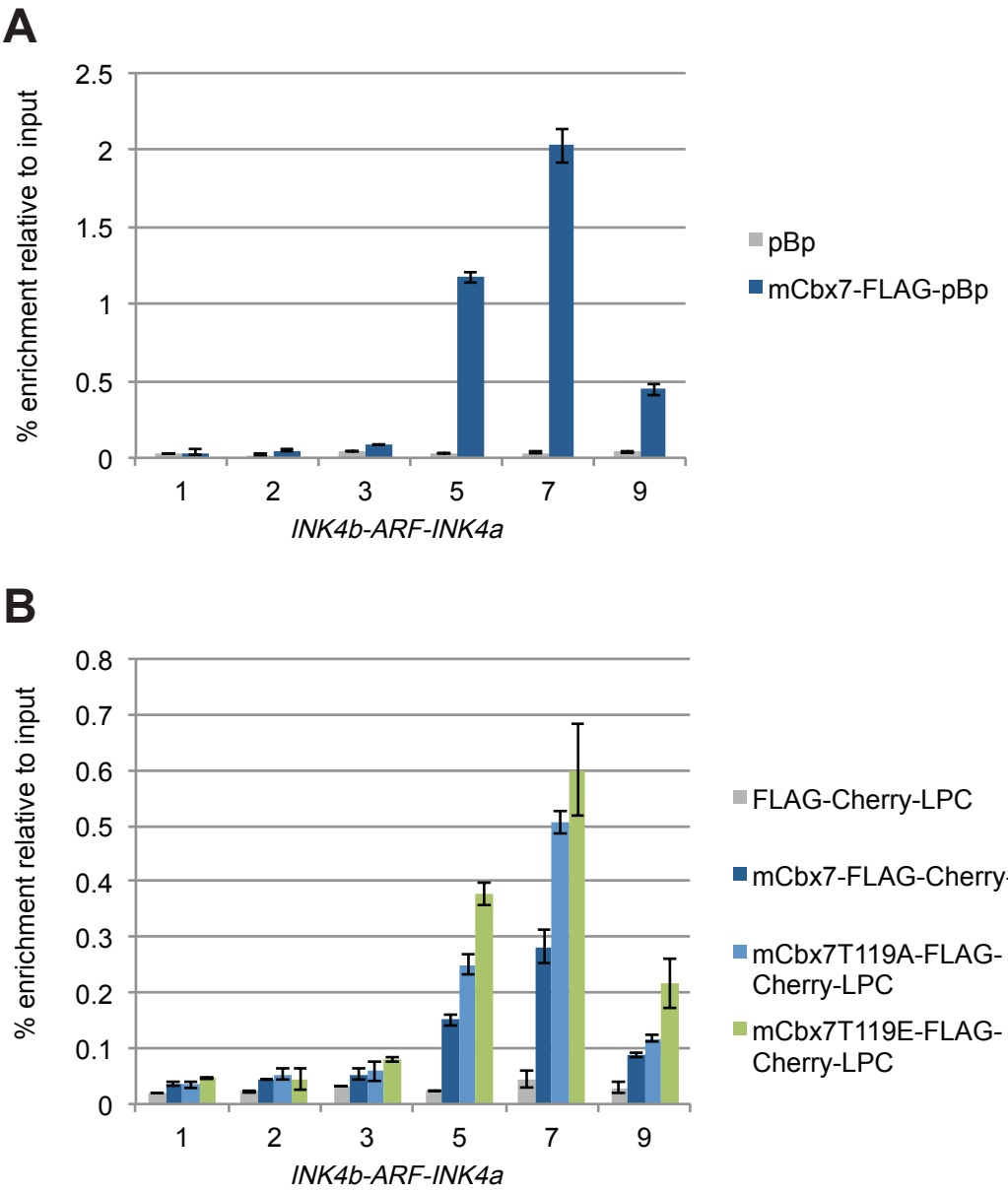
A
% enrichment relative to input
2.5
2
1.5
1
0.5
0
1
2
3
5
7
9
INK4b-ARF-INK4a
pBp
mCbx7-FLAG-pBp
B
% enrichment relative to input
0.8
0.7
0.6
0.5
0.4
0.3
0.2
0.1
0
1
2
3
5
7
9
INK4b-ARF-INK4a
FLAG-Cherry-LPC
mCbx7-FLAG-Cherry-LPC
mCbx7T119A-FLAG-Cherry-LPC
mCbx7T119E-FLAG-Cherry-LPC
C
Primer set positions for qPCR:
INK4b
ARF
INK4a
1
2
3
5
7
9

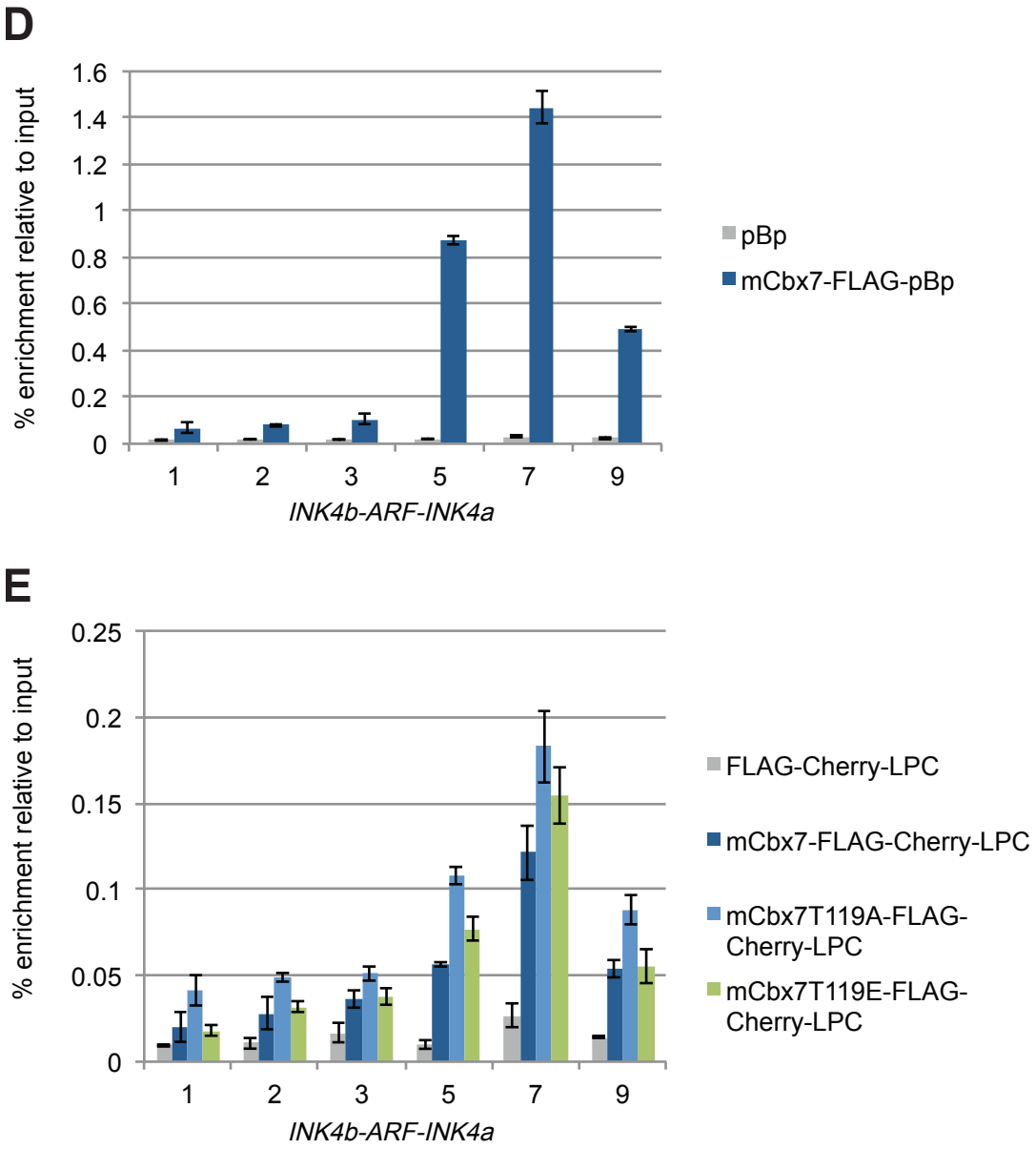

Figure 4.10 ChIP of mCbx7 (wild-type, T119A or T119E) at *INK4a-ARF-INK4b*

Retrovirus-based vectors (pBABE, mCbx7-FLAG-pBABE (generated by Marc Rodriguez-Niedenfuhr), Cherry-FLAG-LPC, mCbx7-Cherry-FLAG-LPC, mCbx7T119A-Cherry-FLAG-LPC or mCbx7T119E-Cherry-FLAG-LPC (generated by Mooki Wu)) were packaged into amphotropic particles and used to infect TIG3 **(A** and **B)** and ESC **(D** and **E)** cells. Cells were fixed 14-days post-infection and chromatin was subject to sonication and chromatin immunoprecipitation (ChIP) with anti-FLAG agarose (Thermoscientific). Purified DNA was isolated from bound protein and amplified by qPCR using primer sets at positions within the *INK4a-ARF-INK4b* locus (detailed in **C**). Graphs show the percentage enrichment of FLAG tagged protein relative to input DNA at the indicated primer sets. Data are representative of two biological repeats.

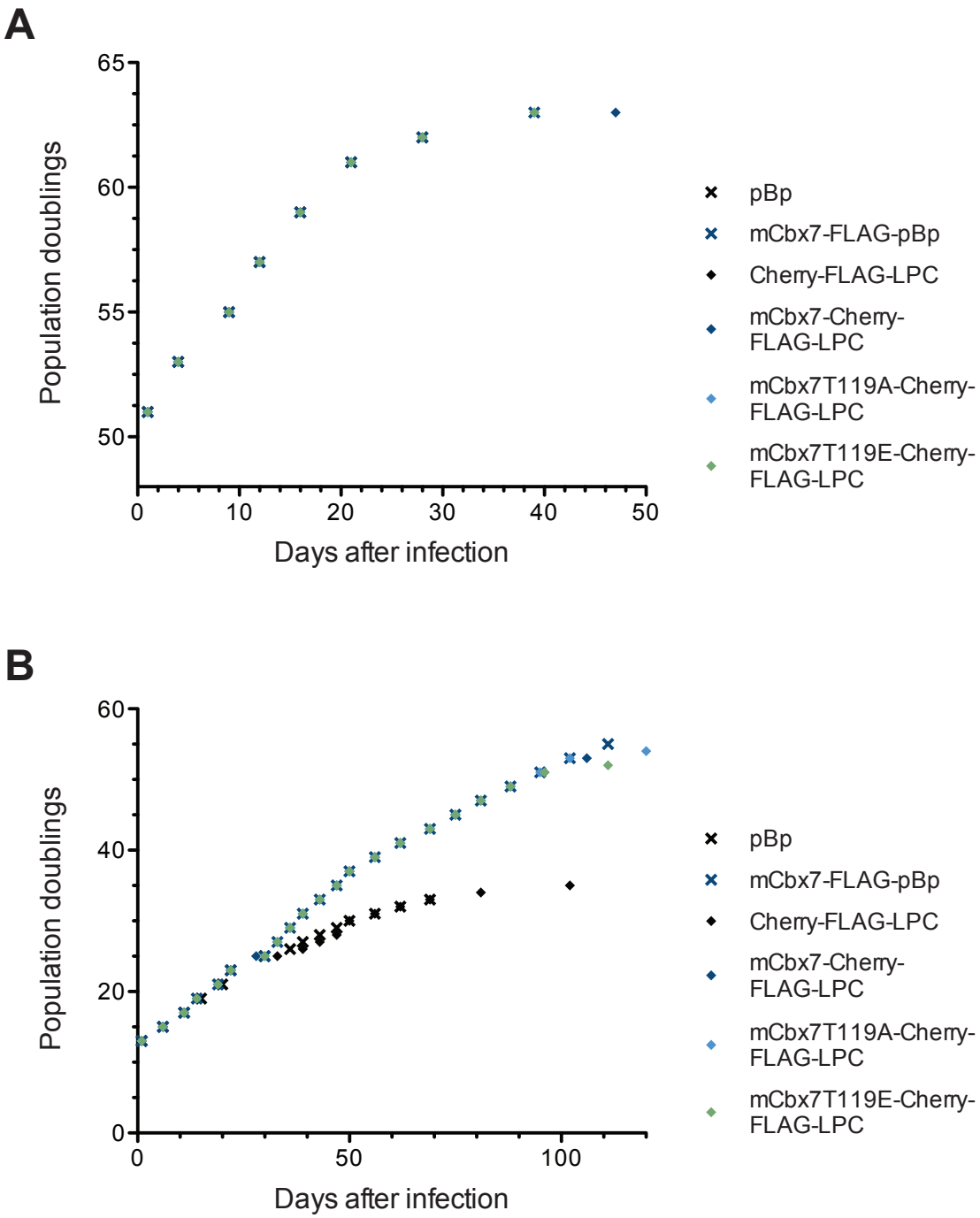

Figure 4.11 Life span chart of HDFs following expression of mCbx7 mutants

Retrovirus-based vectors (pBABE, mCbx7-FLAG-pBABE (generated by Marc Rodriguez-Niedenfuhr), Cherry-FLAG-LPC, mCbx7-Cherry-FLAG-LPC, mCbx7T119A-Cherry-FLAG-LPC or mCbx7T119E-Cherry-FLAG-LPC (generated by Mooki Wu)) were packaged into amphotropic particles and used to infect TIG3 **(A)** and ESC **(B)** cells. Population doublings were recorded until cells reached senescence. Graphs show cumulative population doublings as a function of time following infection.

Chapter 5. Importance of CK2 for PRC1 repression of target genes

5.1 Introduction

Chapters 3 and 4 have described attempts to identify sites in CBX7 that are phosphorylated by CK2 or other kinases, and to map domains or individual residues in CBX7 that are important for the interaction with CK2. The hope was that by identifying the critical residues, it might be possible to generate mutant versions of CBX7 that are either insensitive to or do not interact with CK2, and to use these in functional assays. If successful, this strategy would have enabled us to determine whether the presence of CK2 in the PRC1 complex reflects a role in transcriptional repression or the DNA damage response (DDR).

An alternative approach, which the laboratory has applied to other PRC1-associated proteins (USP7 and USP11 (Maertens et al., 2010), and MOV10 (El Messaoudi-Aubert et al., 2010)), would be to manipulate the levels or activity of CK2 and to assess the consequences for endogenous PRC1 function. The situation is of course complicated by the fact that CK2 is a tetramer of two catalytic subunits (α and α') and two β subunits. Although the latter are dubbed "regulatory" subunits, CK2 is constitutively active and the effect of the β-subunits on CK2 activity is substrate and context-dependent (Chapter 1.11.4). Manipulation of CK2 therefore requires either a reduction of CK2 protein levels or chemical inhibition of its catalytic activity. Interestingly, siRNA-mediated knockdown of CK2 catalytic subunits in human fibroblasts was reported to cause an increase in the proportion of senescence-associated β-galactosidase (SA-β-gal) positive cells. Furthermore, the same study showed that CK2 levels were reduced in senescent human fibroblasts (Ryu et al., 2006). These data suggested a link between CK2 levels and senescence, perhaps through some contribution to PRC1-mediated repression of *INK4a*.

5.2 CK2 levels at senescence

To confirm the report that CK2 levels are decreased in senescent cells (Ryu et al., 2006), Hs68 human fibroblasts were grown to replicative senescence and the levels of CK2 subunits were compared to those in proliferating Hs68 cells. The Hs68 cells achieved 67 population doublings and were judged to be senescent by several criteria. At 6 weeks after the final 1:2 split, the cultures had only reached ~50% confluency although cell viability was sustained. The cells had a large, flat morphology, single, prominent nucleoli, and stained positive for SA-β-gal activity (Figure 5.1). In addition, the cells expressed increased levels of $p16^{INK4a}$ and decreased levels of $p18^{INK4c}$ and CBX7 (Figure 5.1), changes that are typically seen at senescence (Acosta et al., 2008, Gagrica et al., 2012, Gil et al., 2004). Interestingly, the levels of both CK2α' and CK2β protein were decreased in senescent Hs68 cells, whereas those of CK2α remained constant. Two studies from Young-Seuk Bae's laboratory have demonstrated that mRNA and protein levels of CK2α and α' are decreased in senescent IMR90 cells, but expression of CK2β remains stable. The same work also showed that CK2α and CK2β protein levels were reduced in aged rat testis but only CK2β decreased in aged rat liver (levels of CK2α' were not reported) (Ryu et al., 2006, Kim et al., 2009). Taken together, the data suggest that there is a consistent reduction in the overall levels of CK2 subunits at senescence but that the effects on individual subunits might be context dependent.

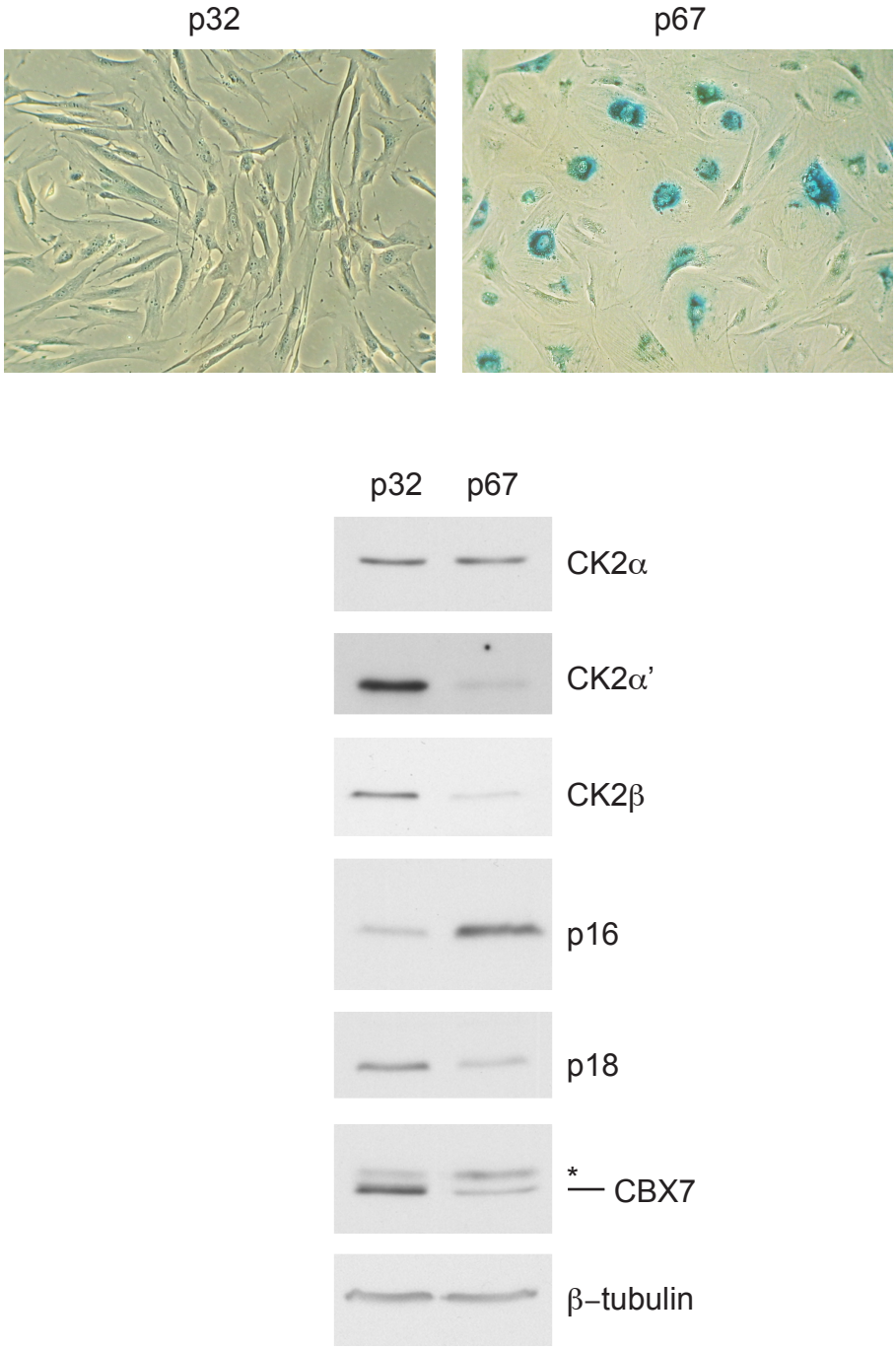

Figure 5.1 CK2 levels in senescent fibroblasts

Hs68 cells were harvested at PD32 and PD67. Equivalent amounts of cell lysate were fractionated by SDS-PAGE and immunoblotted with antibodies against $p16^{INK4a}$, $p18^{INK4c}$, CBX7, CK2α, CK2α' and CK2β and β-tubulin. The band denoted by an asterisk is believed to be a background immunoreactive band. Image is representative of two biological repeats.

5.3 Expression from *INK4a* following CK2 knockdown

To investigate whether long term knockdown of CK2 had a discernible effect on $p16^{INK4a}$ expression, short hairpin RNAs (shRNAs) were designed to individually target the CK2α, α' and β subunits (*CSNK2A1*, *CSNK2A2* and *CSNK2B* mRNA respectively). The relevant DNA sequences were cloned into the pRetroSuper vector (Chapter 2.1.4) and tested for their ability to knockdown the target CK2 subunit in transiently transfected 293T cells. The two most effective shRNAs for each subunit were then introduced into Hs68 human fibroblasts by retroviral infection. Figure 5.2 shows that levels of *CSNK2A1*, *CSNK2A2* and *CSNK2B* mRNA and CK2α, α' and β protein were reduced following expression of the corresponding shRNAs. However, none of the CK2 shRNAs caused an increase in the levels of *INK4a* mRNA compared to the control (luciferase shRNA), except for a very slight increase noted following the knockdown of *CSNK2A2* by shRNA2. If anything, a slight decrease in *INK4a* mRNA was observed, for example with both *CSNK2A1* shRNAs, *CSNK2A2* shRNA1 and *CSNK2B* shRNA2. These data are representative of two biological repeats and care was taken to ensure that the housekeeping gene *RPS17* was an appropriate control following CK2 knockdown in human fibroblasts. The levels of $p16^{INK4a}$ protein remained relatively unchanged following CK2 knockdown, in agreement with the RNA data. Exceptions to this were slight increases in $p16^{INK4a}$ protein levels following CK2α knockdown by *CSNK2A1* shRNA2 and CK2β knockdown by *CSNK2B* shRNA2.

As de-repression of *INK4a* is generally accompanied by the loss of H3K27me3 at the locus (Maertens et al., 2009, Barradas et al., 2009, Agger et al., 2007), Hs68 cells expressing shRNAs against *CSNK2A1* or luciferase (control shRNA) were fixed and a ChIP of H3K27me3 was performed. Figure 5.3 shows that enrichment of H3K27me3 across *INK4a-ARF-INK4b* did not appear to change following CK2 knockdown.

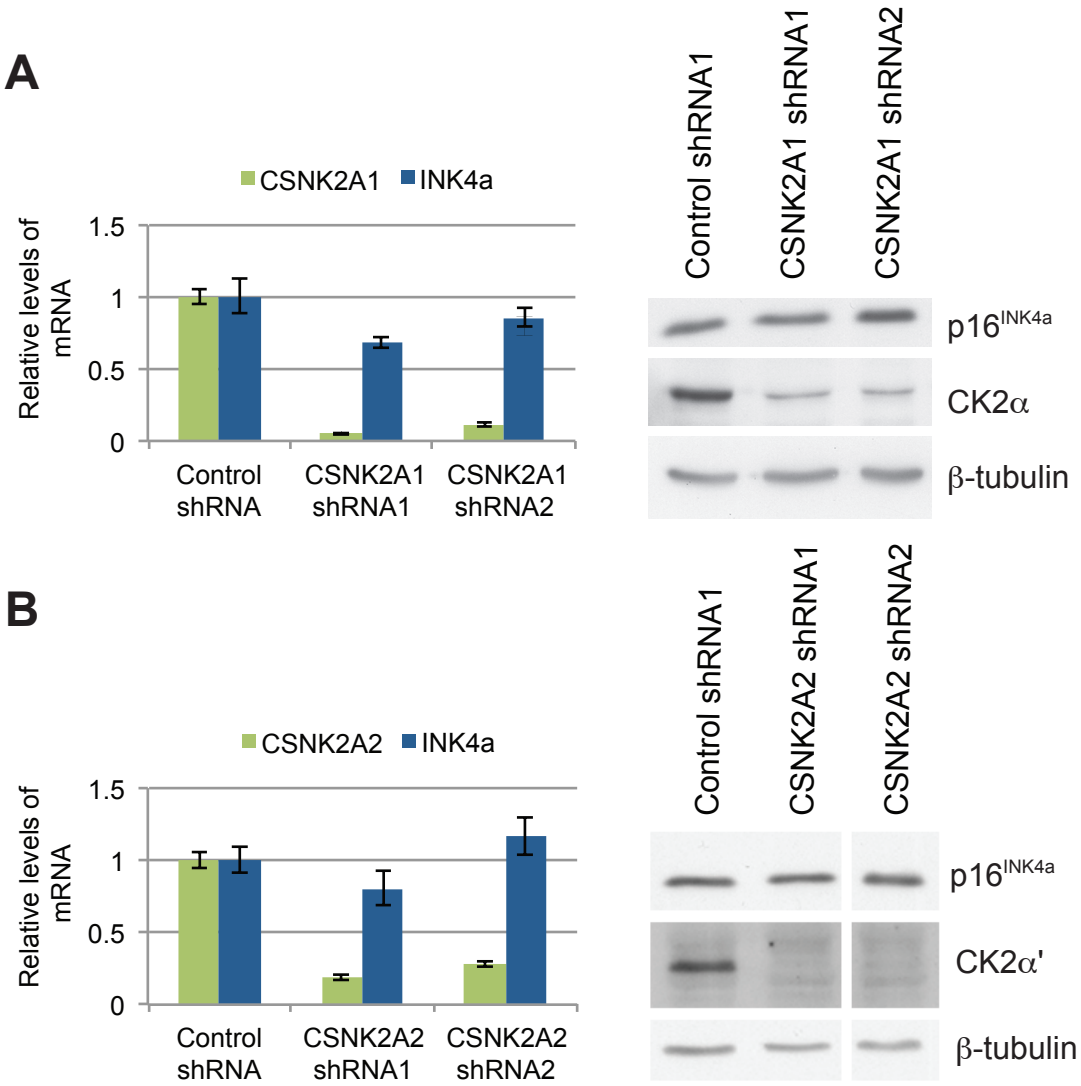
A
CSNK2A1
INK4a
Relative levels of mRNA
1.5
1
0.5
0
Control shRNA
CSNK2A1 shRNA1
CSNK2A1 shRNA2
Control shRNA1
CSNK2A1 shRNA1
CSNK2A1 shRNA2
p16INK4a
CK2α
β-tubulin
B
CSNK2A2
INK4a
Relative levels of mRNA
1.5
1
0.5
0
Control shRNA
CSNK2A2 shRNA1
CSNK2A2 shRNA2
Control shRNA1
CSNK2A2 shRNA1
CSNK2A2 shRNA2
p16INK4a
CK2α'
β-tubulin

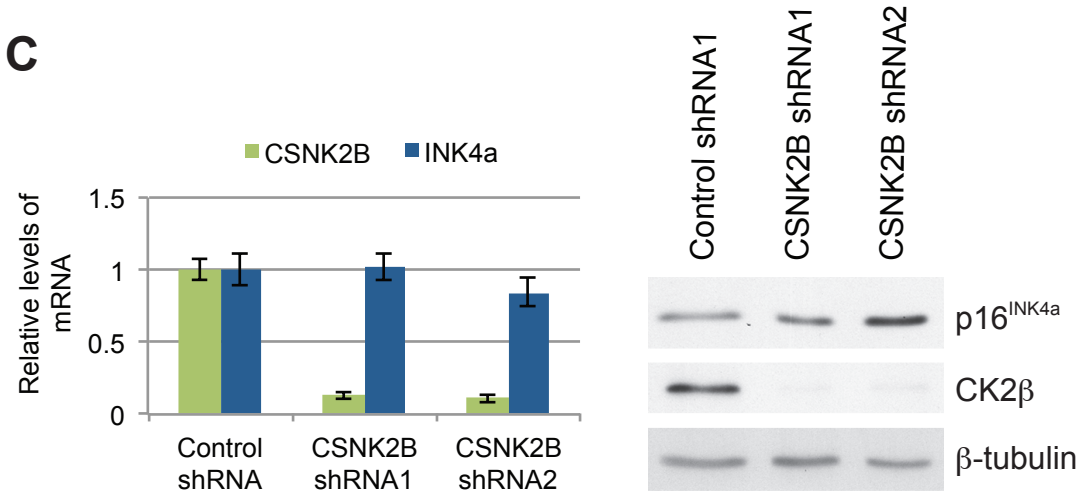

Figure 5.2 Levels of *INK4a* mRNA and p16^{INK4a} following CK2 knockdown

pRetroSuper plasmids encoding control shRNA (against luciferase) or shRNAs against *CSNK2A1* **(A)** *CSNK2A2* **(B)** or *CSNK2B* **(C)** (generated as detailed in materials and methods) were packaged into amphotropic particles and used to infect Hs68 cells. 14 days post-infection, cells were harvested. RNA was extracted and reverse transcribed. Gene of interest (GOI) (*INK4a, CSNK2A1, CSNK2A2, CSNK2B*) cDNA and *RPS17* cDNA was amplified by qPCR and CT values of the GOI were normalised to *RPS17*. The fold change of GOI mRNA following knockdown of *CSNK2A1*, *CSNK2A2* or *CSNK2B*, relative to control samples is shown. Data correspond to the average and standard deviation of three technical replicates and are representative of two biological repeats. For protein analysis, Hs68 cells were also harvested 14 days post-infection. Equivalent amounts of cell lysate were fractionated by SDS-PAGE and immunoblotted with antibodies against p16^{INK4a}, CK2α, CK2α' and CK2β and β-tubulin.

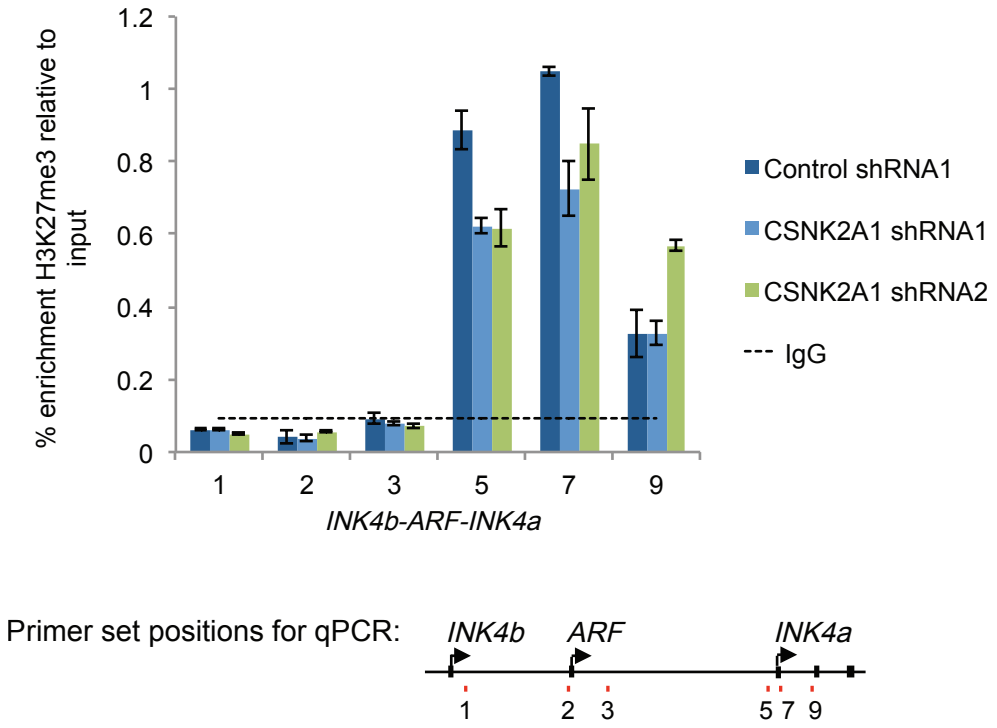

Figure 5.3 H3K27me3 enrichment at *INK4a-ARF-INK4b* following *CSNK2A1* knockdown

pRetroSuper plasmids encoding control shRNA (against luciferase) or shRNAs against *CSNK2A1* (generated as described in materials and methods) were packaged into amphotropic particles and used to infect Hs68 cells. 14 days post-infection, cells were fixed and chromatin was subject to sonication and chromatin immunoprecipitation (ChIP) using anti-H3K27me3 and Protein A agarose (Thermoscientific). Purified DNA was isolated from bound protein and amplified by qPCR using primer sets at positions within the *INK4a-ARF-INK4b* locus. Graph shows the percentage enrichment of H3K27me3 relative to input DNA at the indicated primer sets. Data are representative of two biological repeats.

5.4 Repression of PcG protein targets following CK2 inhibition

Although the shRNAs used to knockdown CK2 subunits were very effective, they did not completely eliminate protein expression. In addition, only one subunit at a time was targeted in any given population. It was therefore a concern that the residual CK2 activity following shRNA knockdown of one subunit would be sufficient for CK2 to still function effectively in PRC1. To address this issue, 4,5,6,7-Tetrabromobenzotriazole (TBB), a ATP/GTP-competitive inhibitor of CK2 (Sarno et al., 2001), was used to eliminate its catalytic activity. A limitation of this approach is that TBB treatment can cause a loss of cell viability and, as a result, is typically only applied to cells for 24 hours. Studies in the Jurkat human leukaemia cell line have shown that CK2-mediated phosphorylation of HS1, Max and Bid protects these proteins from caspase cleavage (Krippner-Heidenreich et al., 2001); (Desagher et al., 2001) (Ruzzene et al., 2002). This anti-apoptotic activity of CK2 could, at least in part, explain cell death following CK2 inhibition by TBB.

Human fibroblasts (FDF) were treated with 300μM TBB for 24 hours. Successful CK2 inhibition was indicated by detection of PARP cleavage. PARP cleavage is a result of the apoptotic program induced by CK2 inhibition (Figure 5.4). A sufficient proportion of the cells remained viable to allow an analysis of gene expression by qPCR. As changes in *INK4a* expression are rarely apparent at this time point, the analyses were conducted on a series of putative PRC1 target genes that had been identified in the lab by ChIP-seq and shRNA-mediated knockdown of CBX7. FDFs expressing either control or CBX7-specific shRNA that had been introduced by lentiviral infection (kindly provided by Sharon Brookes) were used as a control for these experiments, but in this case the RNA was extracted 10 days post infection. Figure 5.4 confirms that the levels of CBX7 mRNA were substantially reduced following expression of the CBX7 shRNA. As expected, the levels of *INK4a* and *TGFB2* mRNA increased, consistent with release from PRC1-mediated repression. However, CBX7 knockdown also caused a decrease in the levels of *GAS1* and *IGFBP5* mRNA. These changes are in line with recent RNAseq data suggesting that the knockdown of CBX7 can have both positive and negative effects on the expression of PRC1-occupied genes (Sharon Brookes, personal communication).

In contrast to the effects of CBX7 knockdown, the levels of *INK4a* and *GAS1* mRNA remained unchanged following TBB treatment while the levels of *TGFB2* were reduced. With the possible exception of *IGFBP5*, these data suggest that there is no correlation between the effects of CK2 inhibition and CBX7 knockdown. However, it is worth re-emphasising that the 24 hour restriction on TBB treatment limits the conclusions that can be drawn from such experiments. If CK2 inhibition did release PRC1-repression of the target genes, it is possible that a change in their expression would not be detected until later time points.

5.5 Conclusions

Data presented in this chapter confirm the relationship between decreasing CK2 levels and senescence. This relationship was interesting given that the *INK4a* gene is a target of PRC1 repression. However, both CK2 knockdown and inhibition experiments suggested that PRC1 regulation of *INK4a* is not affected by CK2 activity. Similarly, expression from other PRC1 target genes remained largely unaffected following CK2 inhibition. These data suggest that CK2 activity may not be relevant for PRC1 repression of target genes. However, it is important to note the significant limitations attached to CK2 knockdown and inhibition experiments. In light of these, the extent to which CK2 is important in PRC1 function remains uncertain.

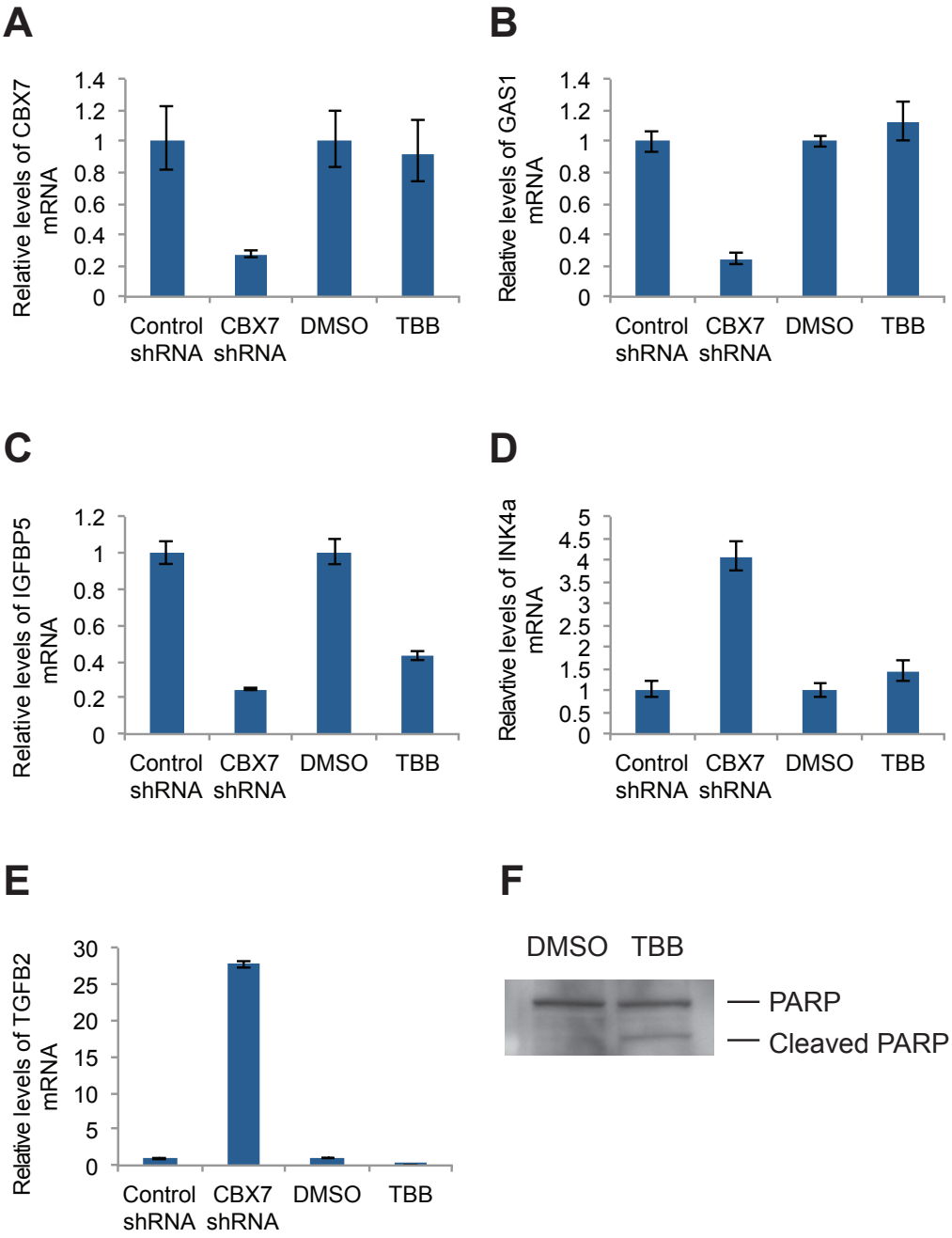

Figure 5.4 Expression of PRC1 target genes following CK2 inhibition

RNA was prepared from FDF cells expressing control or CBX7 shRNA, and from FDFs treated with DMSO (control) or the CK2 inhibitor, TBB. After reverse transcription, gene of interest (GOI) (*CBX7* **(A)**, *INK4a* **(B)**, *GAS1* **(C)**, I*GFBP5* **(D)**, *TGFB2* **(E)**) cDNA and *RPS17* cDNA was amplified by qPCR and CT values of the GOI were normalised to *RPS17*. The fold change of GOI mRNA following CBX7 knockdown or TBB treatment, relative to control samples is shown. Data correspond to the average and standard deviation of three technical replicates. **F)** FDFs treated with DMSO (control) or TBB, were lysed and equivalent amounts of lysate were fractionated by SDS-PAGE and immunoblotted with antibodies against PARP.

Chapter 6. PRC1 recruitment to double strand breaks

6.1 Introduction

Attempts to show that CK2 modulates the ability of PRC1 complexes to regulate transcription have proved equivocal. Although PcG proteins are classically associated with gene repression, they have recently been shown to localise at sites of DNA damage leading to the idea that they might also play a role in the DNA damage response (DDR). For example, Bmi1 null-MEFs show impaired recruitment of DDR proteins, such as 53BP1, at double-strand breaks (DSBs) and increased sensitivity to ionising radiation (Ismail et al., 2010). Interestingly, CK2 activity is important for both SSB and DSB repair. CK2 phosphorylation of the DDR proteins XRCC1, Rad51 and HP1β, affects their stability, their interaction with other DDR proteins and their interaction with DNA, respectively. Collectively, therefore, CK2 promotes effective DNA repair (Parsons et al., 2010, Yata et al., 2012, Ayoub et al., 2008).

Given reports of specific and prompt recruitment of PcG proteins to DSBs (Chou et al., 2010, Ismail et al., 2010, Facchino et al., 2010, Ginjala et al., 2011), we hypothesised that the interaction between PRC1 and CK2 could serve to localise CK2 at sites of DNA damage and thereby promote DNA repair. Alternatively, CK2 phosphorylation of a PRC1 protein during the DDR could be important for the mobilisation of PcG proteins to sites of DNA damage, either by affecting intra-molecular interactions of PRC1, interactions with other DDR proteins or with DNA itself. In an effort to test this latter hypothesis, we set about to establish a system whereby the genome-wide binding of PRC1 complexes could be assessed before and after inducing DSBs at predicted sites. Such a system could be used to determine the extent of PRC1 mobilisation during an extensive assault on DNA integrity. In addition, by manipulating CK2 activity in this system, the contribution of CK2 to the PRC1 response during DNA damage could be assessed.

6.2 Establishing an inducible DNA damage system in HDFs

To this end, we adopted an inducible DNA damage system based on a fusion between the *Asi*S1 restriction enzyme and a modified DNA binding domain from the oestrogen receptor. In cells that constitutively express the fusion protein, *Asi*S1 activity can be induced by addition of 4-hydroxy tamoxifen (4OHT). *Asi*SI is an 8bp endonuclease that cuts DNA at the consensus sequence GCGATCGC, which occurs at 1219 sites in the human genome (data not shown). A clone of U2OS cells that express the fusion protein (herein referred to as *Asi*SI-ER-HA-U2OS), along with the plasmid construct *Asi*SI-ER-HA-pBABE, were kindly provided by Gaelle Legube. The U2OS system was used by the Legube laboratory to map genome-wide enrichment of γH2AX at DSBs following 4OHT induction of *Asi*SI (Iacovoni et al., 2010).

The *Asi*SI-ER-HA-pBABE plasmid was packaged as a retroviral particle and used to infect the Hs68 strain of human fibroblasts. Hs68 cells were chosen because the binding sites for multiple PRC1 components have been mapped by ChIP-seq (Emma Anderton, personal communication) and because DNA repair pathways should be intact in normal human fibroblasts. Following drug selection, the infected cells were treated with 4OHT and analysed by immunofluorescence with antibodies against HA, to detect HA-tagged *Asi*S1, and γH2AX, to detect DSBs.

As shown in Figure 6.1, nuclear levels of HA-tagged *Asi*SI and the number of γH2AX foci increased significantly following addition of 4OHT to cells expressing the *Asi*SI-ER-HA fusion protein. This was evident in both the previously characterised *Asi*SI-ER-HA-U2OS cells and throughout the population of *Asi*SI-ER-HA-Hs68 cells. Importantly, only very low levels of nuclear HA and γH2AX signals were detected in these cells in the absence of 4OHT, levels equivalent to those seen in uninfected Hs68 cells, implying that the system was not leaky.

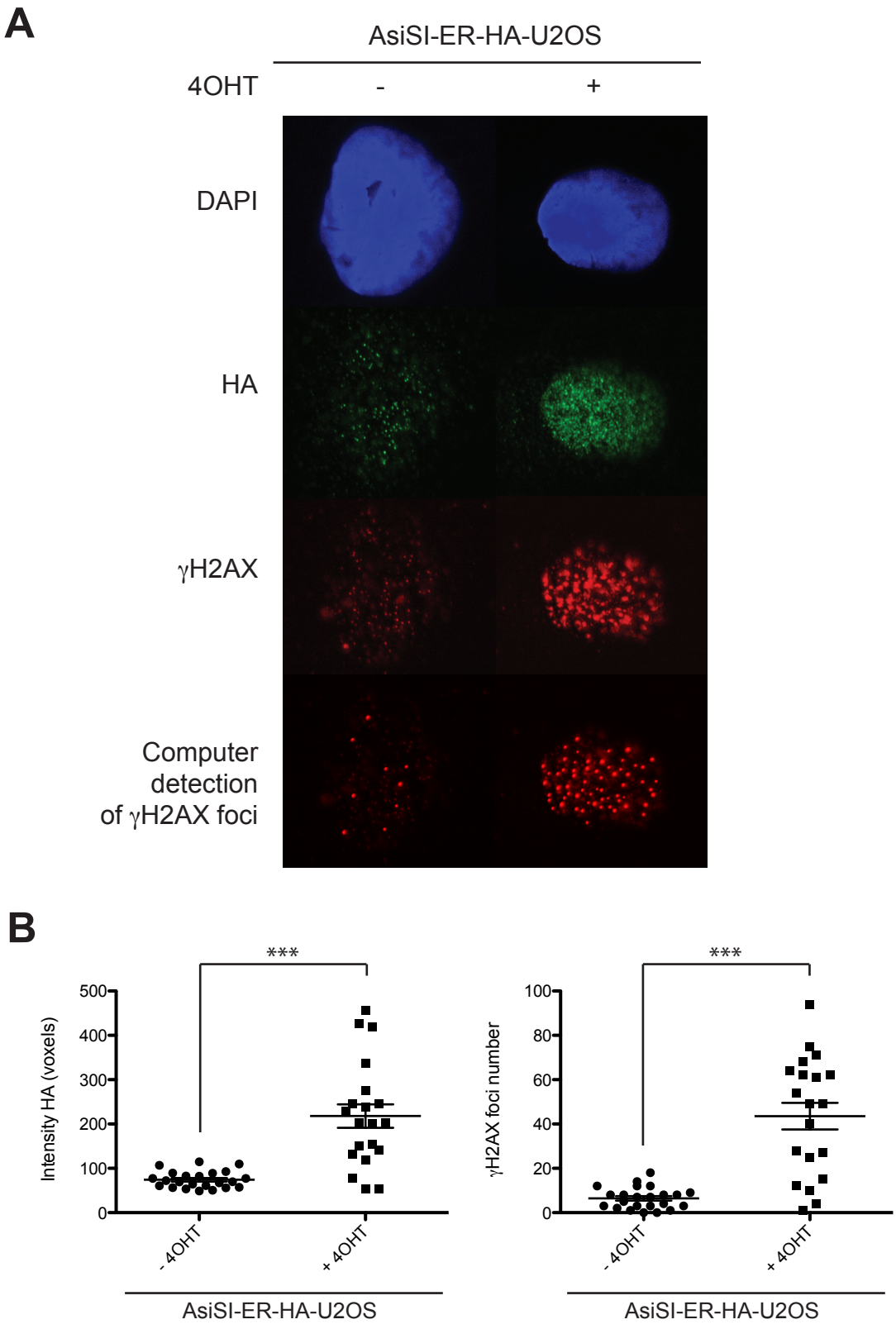
A
AsiSI-ER-HA-U2OS
4OHT
-
+
DAPI
HA
γH2AX
Computer detection of γH2AX foci
B
***
Intensity HA (voxels)
500
400
300
200
100
0
- 4OHT
+ 4OHT
AsiSI-ER-HA-U2OS
***
γH2AX foci number
100
80
60
40
20
0
- 4OHT
+ 4OHT
AsiSI-ER-HA-U2OS

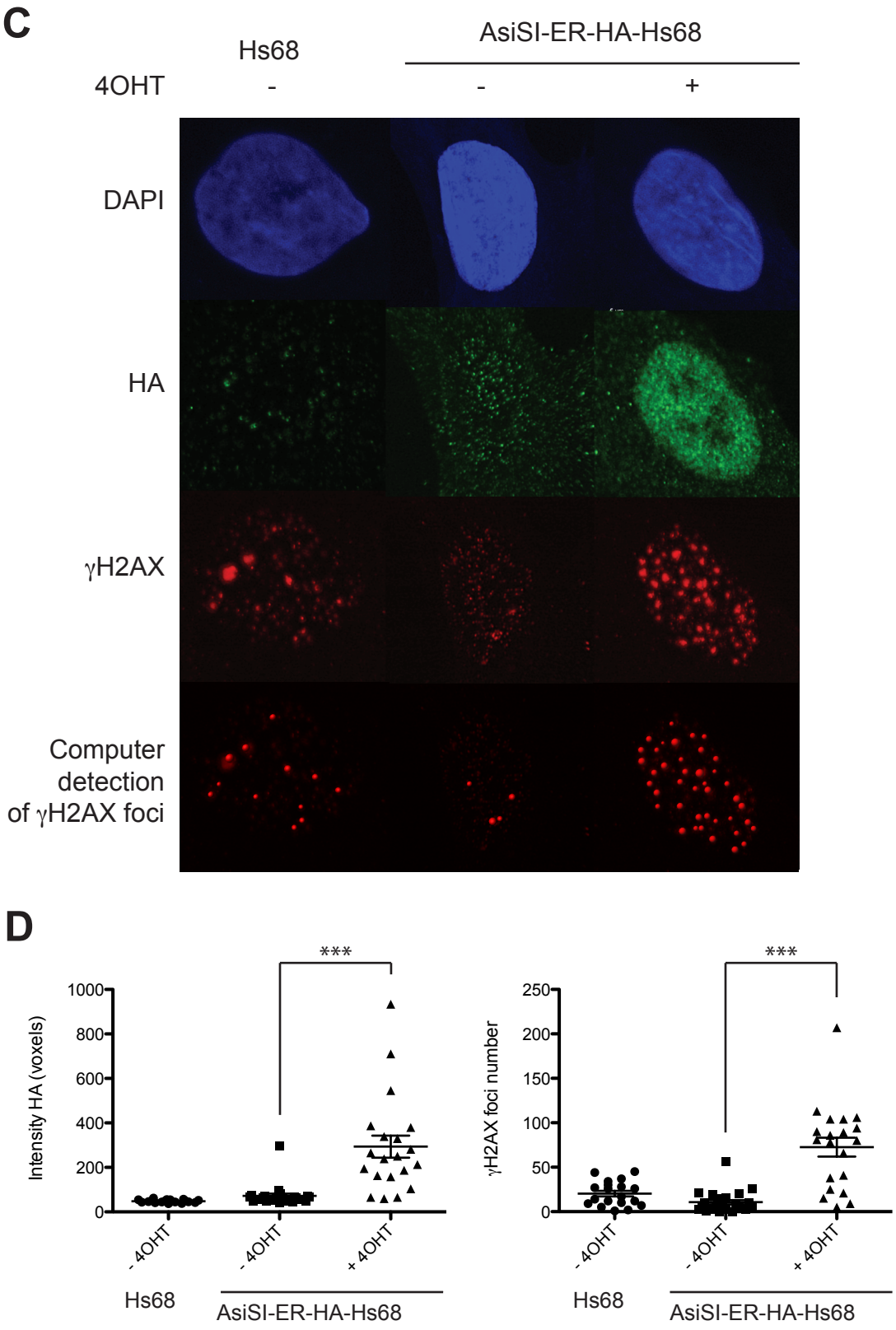

Figure 6.1 Immunofluorescence of γH2AX foci following 4OHT induction of DNA damage by *Asi*SI.

A) *Asi*SI-ER-HA-U2OS cells were co-stained with DAPI following incubation with antibodies against γH2AX (red) and HA epitope (green), before and after 4OHT treatment. Images were deconvoluted using Huygens Essential software and Imaris software was used to detect the number of γH2AX foci per nuclei. **B)** Quantification of HA intensity (voxels) and number of γH2AX foci in 20 representative *Asi*SI-HA-ER-U2OS nuclei before and after 4OHT treatment. A student's t-test was performed on the data using Prism 5.0 (GraphPad Software). A P value of >0.05 is considered statistically significant. *** indicates P<0.001. Error bars represent the standard deviation of the sample. **C)** Hs68 cells and *Asi*SI-ER-HA-Hs68 cells were co-stained with DAPI following incubation with antibodies against γH2AX (red) and HA epitope (green), before and after 4OHT treatment. Imaris software was used to detect the number of γH2AX foci per nuclei. **D)** Quantification of HA intensity (voxels) and number of γH2AX foci in 20 representative Hs68 and *Asi*SI-HA-ER-Hs68 nuclei before and after 4OHT treatment. A student's t-test was performed on the data using Prism 5.0 (GraphPad Software). A P value of >0.05 is considered statistically significant. *** indicates P<0.001. Error bars represent the standard deviation of the sample.

6.3 Co-localisation of PcG proteins at DSBs

Having validated 4OHT induction of DSB in cells expressing the *Asi*SI-ER-HA fusion protein, the system was used to assess recruitment of PcG proteins to DSBs. Fixed cells were immunostained with antibodies against CBX7, BMI1, RING2, 53BP1 and γH2AX and either Alexa Fluor 488 or Alexa Fluor 555-conjugated secondary antibodies. Nuclei were located by DAPI staining. To assess the degree of co-localisation between different antibody pairs, Z-stacked images of three representative nuclei were collected and the images were deconvoluted using Huygens Essential software. Co-localisation channels were generated using automatic thresholds in the region of interest (nucleus) as defined by the DAPI channel using Imaris software. Pearson's correlation coefficients (PCCs) were calculated, again using the Imaris software, to estimate the extent of co-localisation. PCCs can range from -1 to +1: -1 indicating a perfect negative linear relationship between two variables, 0 indicating no linear relationship between variables, and +1 indicating a perfect positive linear relationship between variables. The interpretation of intermediate PCCs can be quite varied in different studies. For the purpose of this investigation, we assume values between 0 and 0.09 to mean no

co-localisation, between 0.1 and 0.29 to mean weak co-localisation, between 0.3 and 0.7 to mean moderate co-localisation and between 0.7 and 1 to indicate strong co-localisation.

Following 4OHT treatment of *Asi*SI-ER-HA-U2OS cells, 53BP1 and γH2AX showed moderate co-localisation (Figure 6.2A-B). BMI1 and RING2 were mostly detected in large nuclear spots, as described previously for PRC1 components in U2OS cells (Alkema et al., 1997, Cmarko et al., 2003, Saurin et al., 1998, Hernandez-Munoz et al., 2005). Although there was a faint signal in the co-localisation channels for BMI1-γH2AX and RING2-γH2AX, the PCCs suggested that neither of these PcG proteins co-localised with γH2AX (Figure 6.2A-B). Co-localisation images and PCCs for BMI1-MEL18 and RING1-RING2 provided strong evidence for the co-localisation of these PRC1 proteins, giving confidence that the antibodies were appropriate for use in co-localisation studies (Figure 6.2C). Although the immunofluorescence signal for CBX7 appeared to be more dispersed compared to BMI1 and RING2, this could represent cross-reaction of the antiserum with another cellular protein(s), as there was no evidence for co-localisation with the PcG proteins. Even with the more diffuse staining, which would tend to bias the statistics towards a stronger correlation, only a weak co-localisation of CBX7 with γH2AX was suggested by the PCC.

Following 4OHT treatment of *Asi*SI-ER-HA-Hs68 cells, 53BP1 showed strong co-localisation with γH2AX (Figure 6.2D-E). The co-localisation channel signals and corresponding PCCs suggested a weak co-localisation of both BMI1 and CBX7 with γH2AX, with the caveat that the CBX7 result should be treated with caution (Figure 6.2D-E). RING2 could not be detected in Hs68 cells, although this might reflect a need for further optimisation of fixation, blocking and antibody incubation conditions. Interestingly, the distribution of BMI1 in Hs68 cells, in dispersed nuclear speckles, was very different from the large bodies seen in U2OS cells. Although most immunofluorescence studies on human PRC1 proteins have been carried out in U2OS or 293T cells, the difference between primary and transformed cells was noted in one of the first reports on RING1 localisation (Saurin et al., 1998) and clearly warrants further investigation.

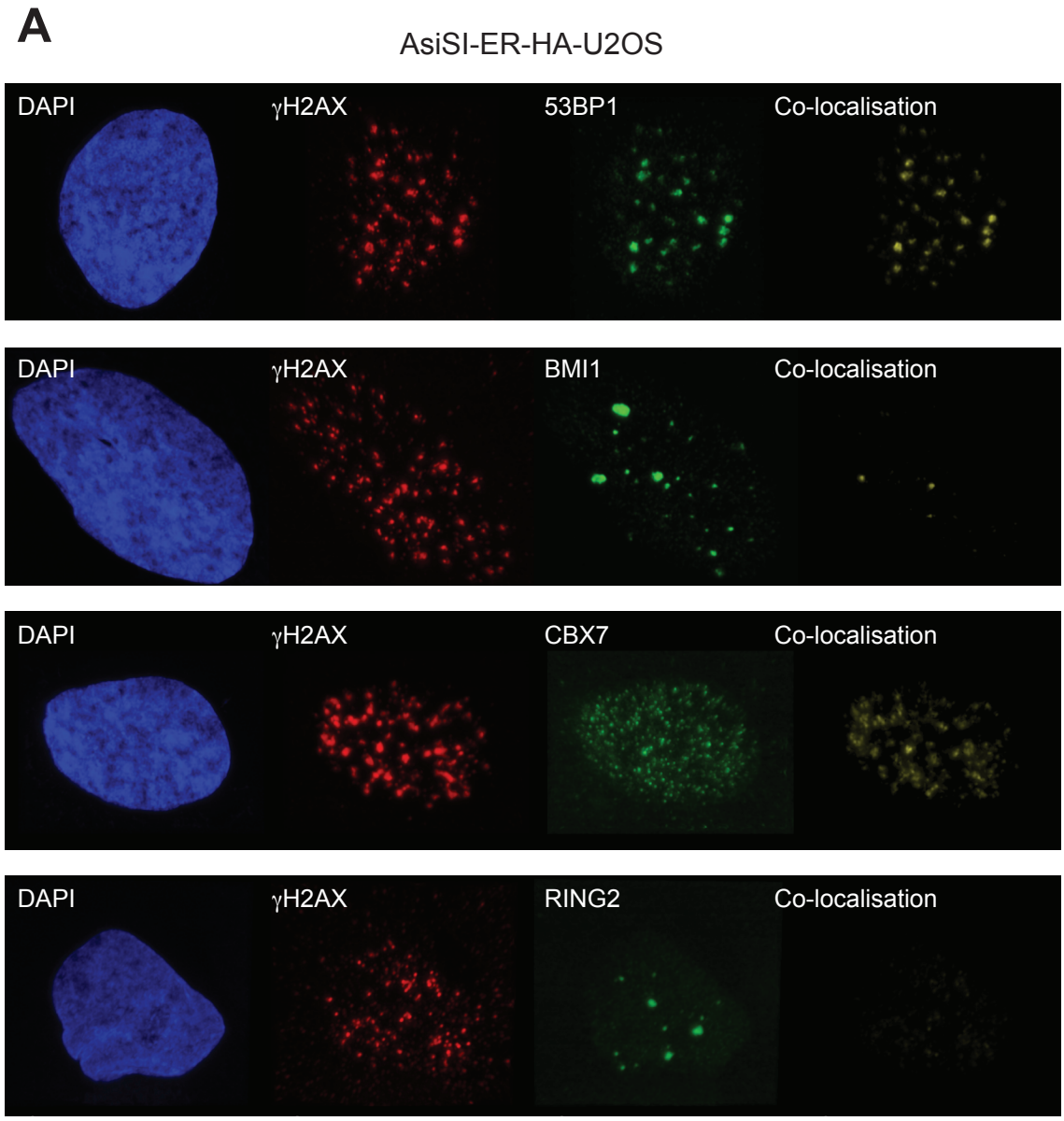
A
AsiSI-ER-HA-U2OS
DAPI
γH2AX
53BP1
Co-localisation
DAPI
γH2AX
BMI1
Co-localisation
DAPI
γH2AX
CBX7
Co-localisation
DAPI
γH2AX
RING2
Co-localisation

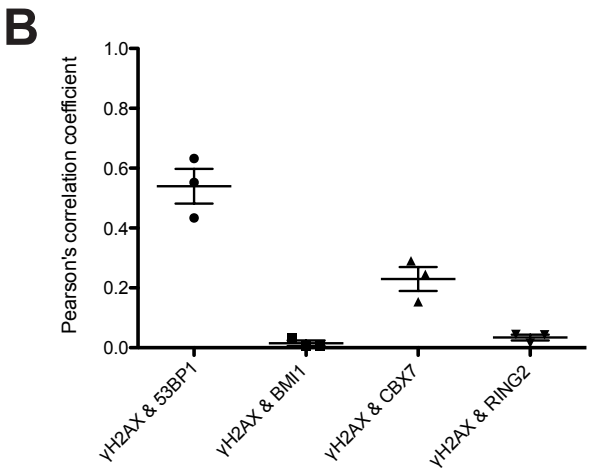
B
Pearson's correlation coefficient
1.0
0.8
0.6
0.4
0.2
0.0
γH2AX & 53BP1
γH2AX & BMI1
γH2AX & CBX7
γH2AX & RING2

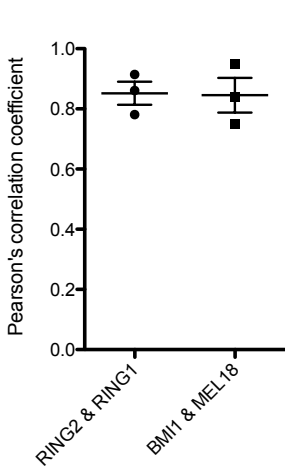
C
Pearson's correlation coefficient
1.0
0.8
0.6
0.4
0.2
0.0
RING2 & RING1
BMI1 & MEL18

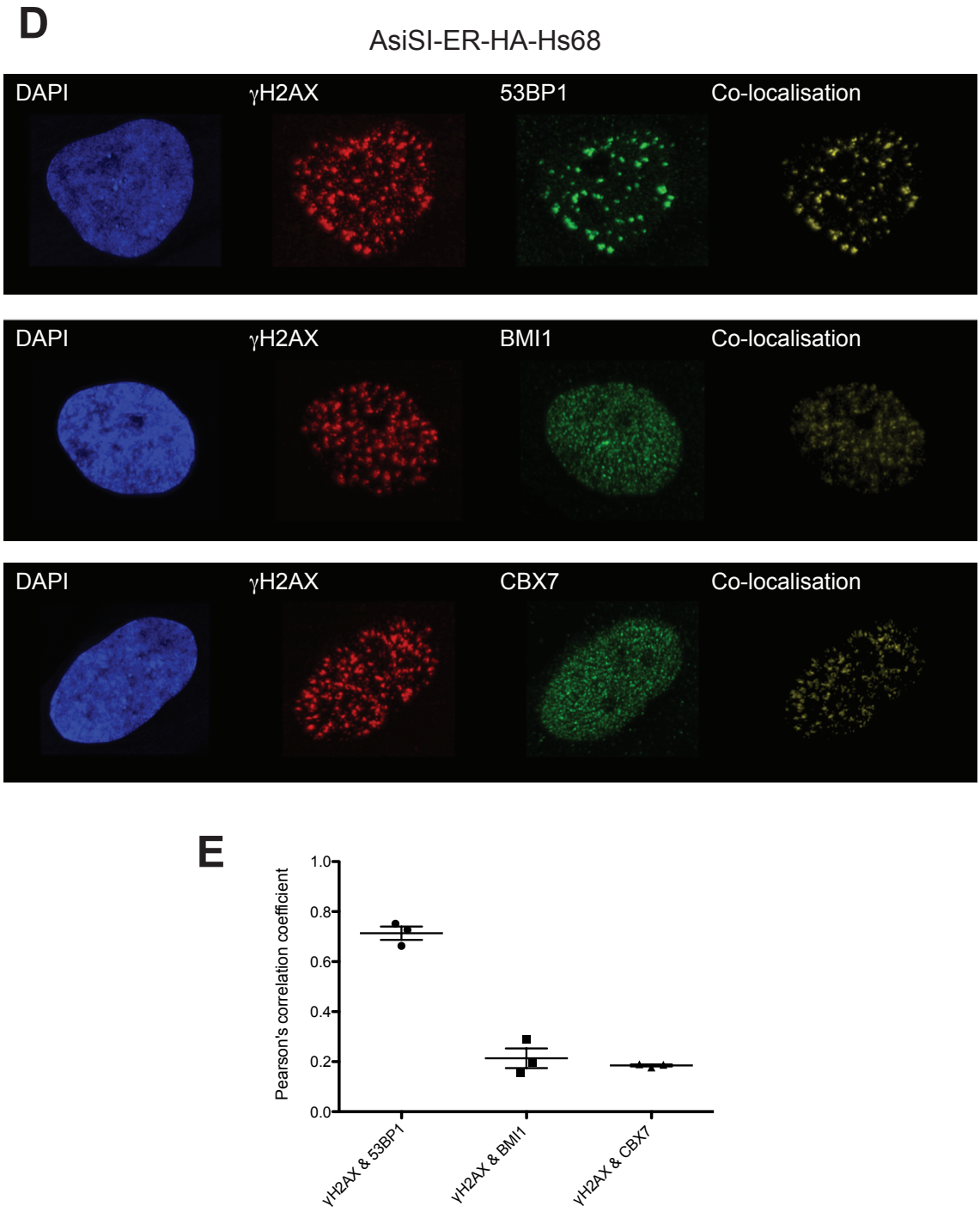

Figure 6.2 Detecting co-localisation of PcG proteins with γH2AX foci following 4OHT induction of DNA damage by *Asi*SI

A) U2OS *Asi*SI-ER-HA cells were co-stained with DAPI following incubation with antibodies against γH2AX (red) and 53BP1 or a PcG protein (BMI1, CBX7 or RING2) (green), before and after 4OHT treatment. Images were deconvoluted using Huygens Essential software and Imaris software was used to generate a co-localisation channel (yellow). **B-C)** PCC values for co-localisation of the indicated proteins in three representative nuclei. Error bars

represent the standard deviation of the sample. **D)** Hs68 cells and Hs68 *Asi*SI-ER-HA cells were co-stained with DAPI following incubation with antibodies against γH2AX (red) and 53BP1 or a PcG protein (BMI1 or CBX7) (green), before and after 4OHT treatment. Images were deconvoluted using Huygens Essential software and Imaris software was used to generate a co-localisation channel (yellow). **E)** PCC values for co-localisation of the indicated proteins in three representative nuclei. Error bars represent the standard deviation of the sample.

6.4 ChIP-seq analysis of CBX7 in HDFs following genome-wide DNA damage

Taken together, the immunofluorescence data suggested that the inducible system established in *Asi*SI-ER-HA-Hs68 cells was functioning as expected, as shown by the appearance of γH2AX foci and recruitment of 53BP1 following addition of 4OHT. However, the co-localisation of PcG proteins with γH2AX foci was questionable as only a weak correlation was observed with some antibodies. As an alternative approach, and to get a higher resolution picture of events occurring at *Asi*SI cut sites, chromatin was isolated from *Asi*SI-ER-HA-Hs68 cells before and after 4OHT treatment with a view to doing ChIP-seq analyses. For continuity with other aspects of the study, it was decided to focus initially on CBX7.

Although the anti-CBX7 antibody Ab21873 (Abcam) was not considered reliable for immunofluorescence, it has been thoroughly evaluated and shown to be effective for ChIP (Maertens et al., 2009, El Messaoudi-Aubert et al., 2010). Due to more recent batch-to-batch variation in its efficacy for ChIP experiments, we decided to generate our own antiserum against the same peptide used to generate Ab21873 (Chapter 2.4.5.1). This peptide, FREAQAAEGFFRDRSGKF, represented amino acids 234-251 at the C-terminus of CBX7. The IgG fraction of the antiserum generated against this peptide was purified, and is hereafter referred to as HCHA1. To test the specificity of HCHA1, FLAG tagged CBX2, CBX4, CBX6, CBX7 and CBX8 proteins were expressed in 293T cells, immunoprecipitated with anti-FLAG agarose, fractionated by SDS-PAGE, and immunoblotting was performed using HCHA1 (Figure 6.3). Although endogenous CBX7 from 293T cell lysate was not

detected by HCHA1, it clearly detected CBX7-FLAG and importantly, did not bind FLAG-tagged CBX4, 6 or 8. Anti-FLAG antibody failed to detect CBX2-FLAG from transiently transfected 293T lysates, suggesting expression of CBX2-FLAG in these cells was very low. The reactivity of HCHA1 with CBX2 has therefore not been evaluated, although as HCHA1 was generated against the same peptide as the commercial Ab21873 antibody, it should not cross-react. The efficacy of HCHA1 for ChIP of endogenous CBX7 was assessed. ChIP was performed using between 2.5 and 20µg HCHA1 per 500µg sonicated chromatin. A parallel ChIP was performed using 5µg Ab21873 (Abcam) from a batch that had been previously validated for ChIP of CBX7 (Emma Anderton, personal communication). ChIP of CBX7 at *INK4a* was as effective using HCHA1 as Ab21873 (Figure 6.4). The amount of HCHA1 antibody used did not noticeably affect the levels of CBX7 enrichment at the *INK4a*. Future ChIP experiments using HCHA1 were performed using 5µg of antibody per 500µg chromatin.

Chromatin from *Asi*SI-ER-HA-Hs68 cells, treated with or without 4OHT, was subjected to ChIP using the HCHA1 antibody. After confirmation that enrichment of CBX7 was observed at *INK4a-ARF-INK4b* (data not shown), the samples were submitted for massively parallel DNA sequencing on the Illumina GAII platform. This sequencing generated between 21 and 27 million 36bp reads that could be mapped to the hg19 release of the human genome. Equivalent data (between 20 and 24 million 36bp reads that could mapped to the hg19 release of the human genome) from ChIP of CBX7 using Ab21873 and chromatin from uninfected Hs68 cells had already been obtained by Emma Anderton. The ChIP-seq data showed that equivalent levels of CBX7 enrichment were observed genome-wide in both the untreated and 4OHT treated of AsSI-ER-HA-Hs68 cells, and that the patterns were indistinguishable from those in uninfected Hs68 cells. Examples of known CBX7-target genes (*INK4a*, *GATA6*, *DLX1*) are shown in Figure 6.5A-C. Thus, the induction of DSBs at *Asi*S1 sites did not appear to cause gross changes in the existing patterns of CBX7 binding.

The more telling question was whether CBX7 was recruited to *Asi*S1 sites following 4OHT treatment. Peaks identified by the MACS algorithm as showing significant CBX7 enrichment were scored for their position (+/- 10kb) relative to predicted

*Asi*S1 sites. Only one of these MACS peaks was found exclusively in 4OHT-treated *Asi*SI-HA-ER-Hs68 cells and not in the untreated or uninfected control cells (Figure 6.5D). As this is the only example out of 1219 potential *Asi*S1 sites, it has not been validated by conventional ChIP. At face value therefore, it appears that CBX7 is not recruited to DSBs generated by *Asi*S1 induction. As the *Asi*SI-HA-ER-Hs68 cells represent a mixed population it is conceivable that different subsets of *Asi*SI sites are cut in different cells, thereby diluting the apparent enrichment of CBX7 at each site. However, the immunostaining for γH2AX, which was performed on the same batch of cells as those used for the ChIP-seq analysis, suggests that a considerable proportion of the *Asi*S1 sites must be cut in each cell. Another possible explanation is that canonical PRC1 complexes are not recruited to DSBs; much of the existing literature focuses on BMI1 and RING2, which can participate in alternative complexes. In hindsight, it would have been useful to perform ChIP-seq with an antibody against a bona-fide DDR protein, such as 53BP1, or with RING2, for which we already have ChIP-seq data in uninfected Hs68 cells.

6.5 Conclusions

To investigate whether CK2 contributes to the non-canonical role of PRC1 in the DDR, a system was established to test PcG protein recruitment to DSBs. Specifically, the hope was be able to map genome-wide changes in PcG binding patterns by ChIP-seq following DNA damage. The sequence specific, inducible, DSB system was established and validated in Hs68 human fibroblasts. However, CBX7 recruitment to DSBs could not be detected by immunofluorescence or ChIP-seq. Furthermore, BMI1 and RING2, both previously reported to be recruited to DSBs, at best only showed weak co-localisation with DSBs as determined by PCC values.

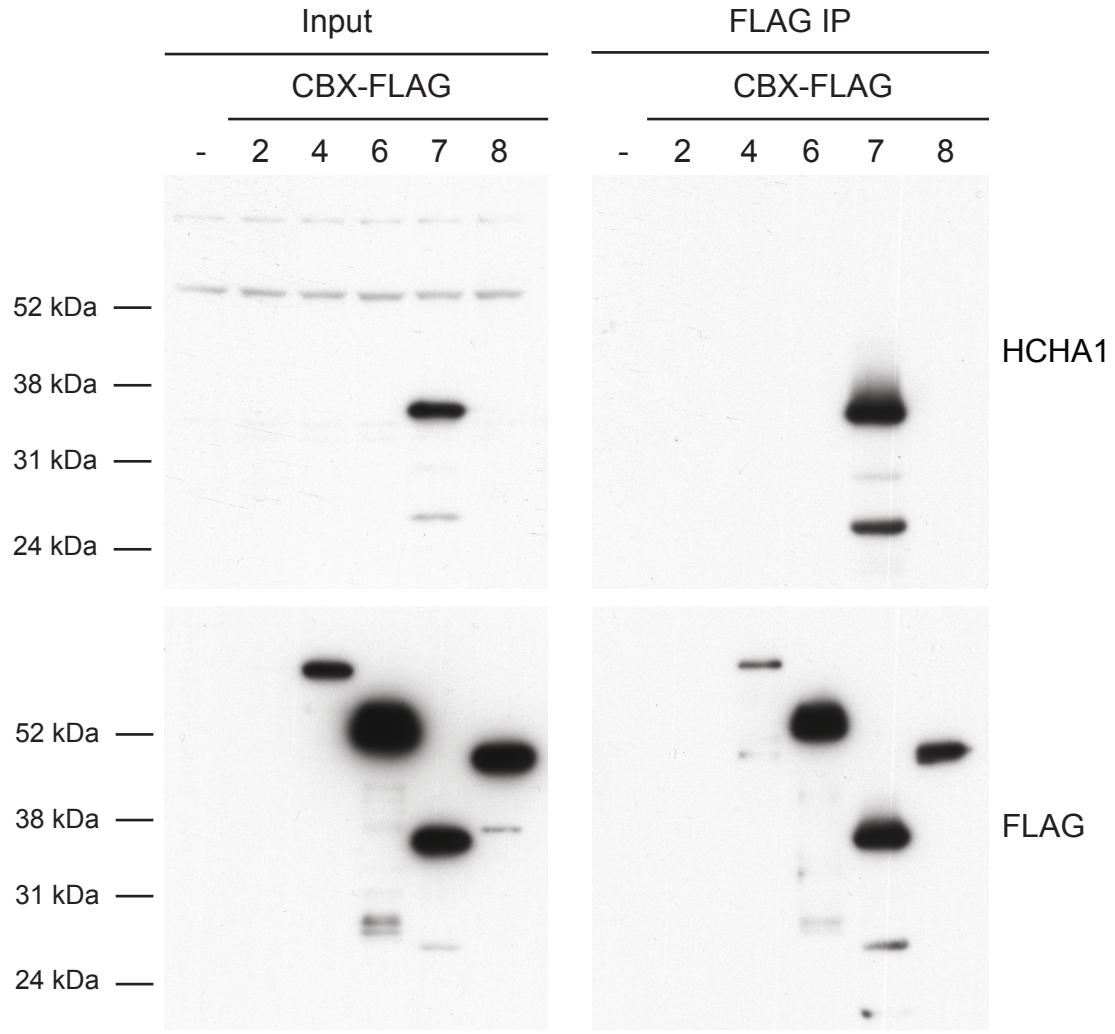

Figure 6.3 HCHA1 antibody detection of FLAG-tagged CBX7

pcDNA6 plasmids encoding FLAG-tagged CBX2, 4, 6, 7 or 8 were transfected into 293T cells using lipofectamine. After 24 hours cells were harvested and cell lysate was subject to immunoprecipitation (IP) using anti-FLAG M2 agarose (Sigma). Purified proteins were fractionated by SDS-PAGE alongside input samples equivalent to 1/10th volume of lysate used for the IP. Immunoblotting was performed against the FLAG-epitope (anti-FLAG) and CBX7 (HCHA1).

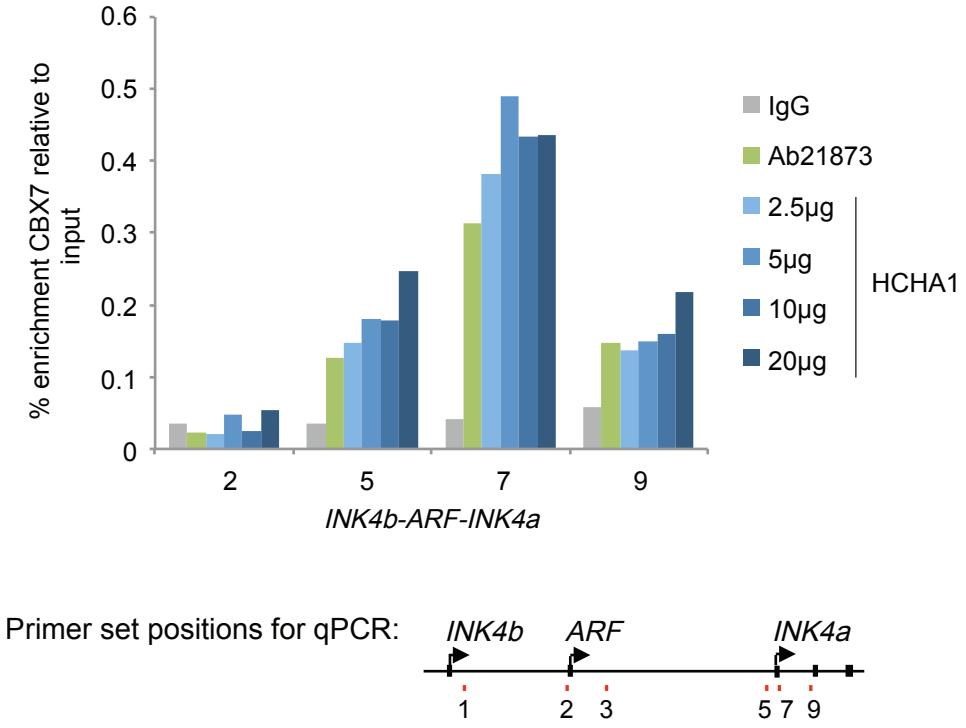

Figure 6.4 CBX7 enrichment across *INK4a-ARF-INK4b* following ChIP of CBX7 using Ab21873 or HCHA1 antibodies

Hs68 cells were fixed and chromatin was subject to sonication and chromatin immunoprecipitation (ChIP). ChIP was performed using Protein A agarose (Thermoscientific) and either 5µg Ab21873 (abcam) or between 2.5 and 20µg HCHA1 anti-CBX7 antibody, as indicated. Purified DNA was isolated from bound protein and amplified by qPCR using primer sets at positions within the *INK4a-ARF-INK4b* locus. Graphs show the percentage enrichment of CBX7 relative to input DNA at the indicated primer sets.

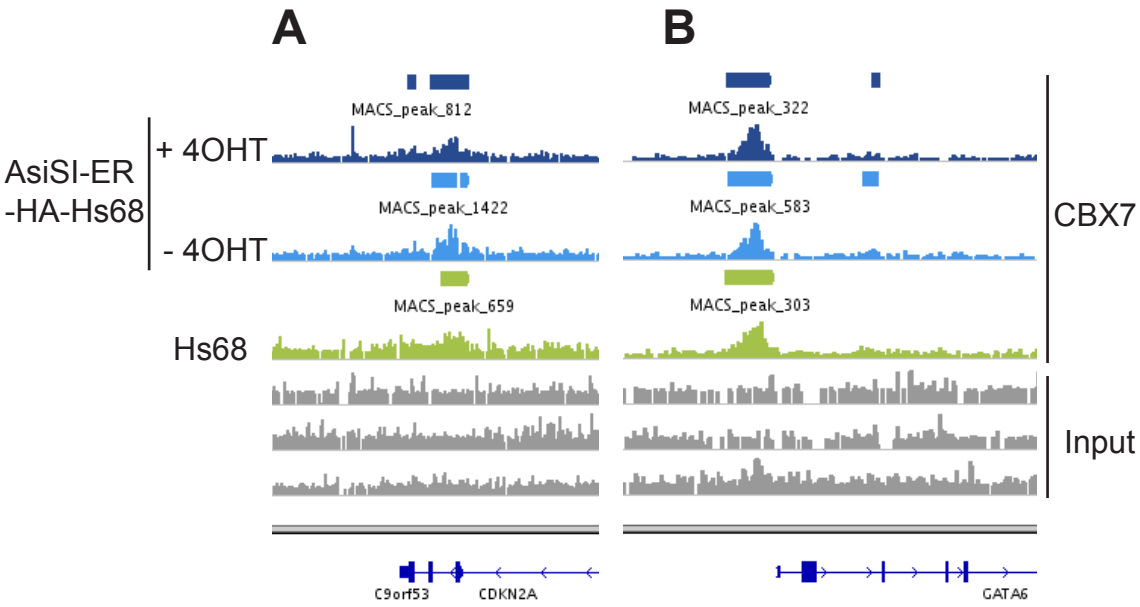
A
B
MACS_peak_812
MACS_peak_322
AsiSI-ER
-HA-Hs68
+ 4OHT
MACS_peak_1422
MACS_peak_583
- 4OHT
CBX7
MACS_peak_659
MACS_peak_303
Hs68
Input
C9orf53
CDKN2A
GATA6

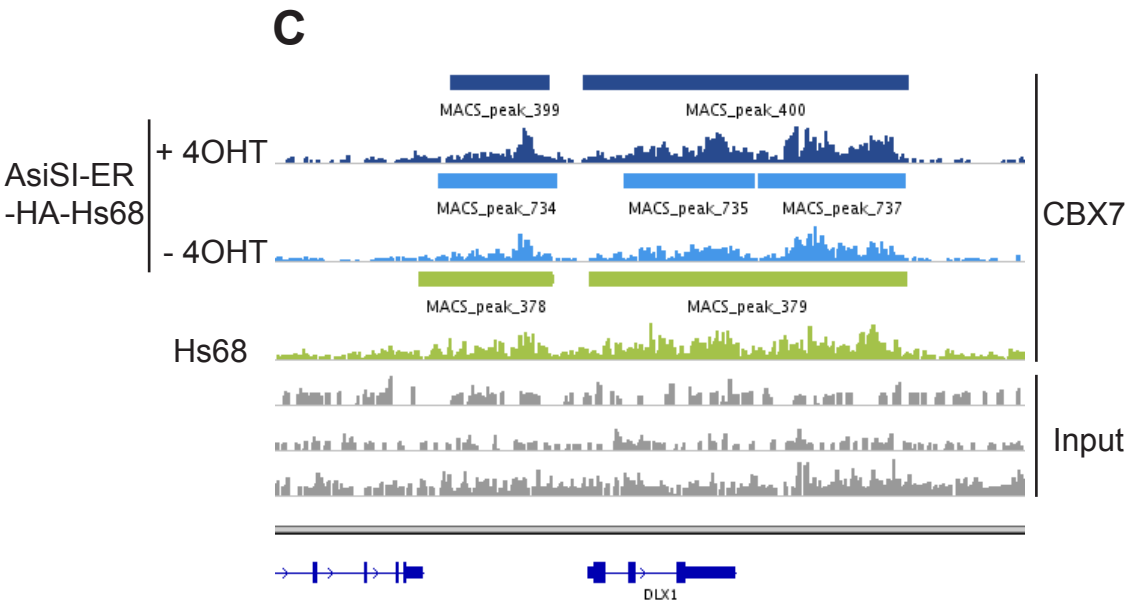
C
MACS_peak_399
MACS_peak_400
AsiSI-ER
-HA-Hs68
+ 4OHT
MACS_peak_734
MACS_peak_735
MACS_peak_737
- 4OHT
CBX7
MACS_peak_378
MACS_peak_379
Hs68
Input
DLX1

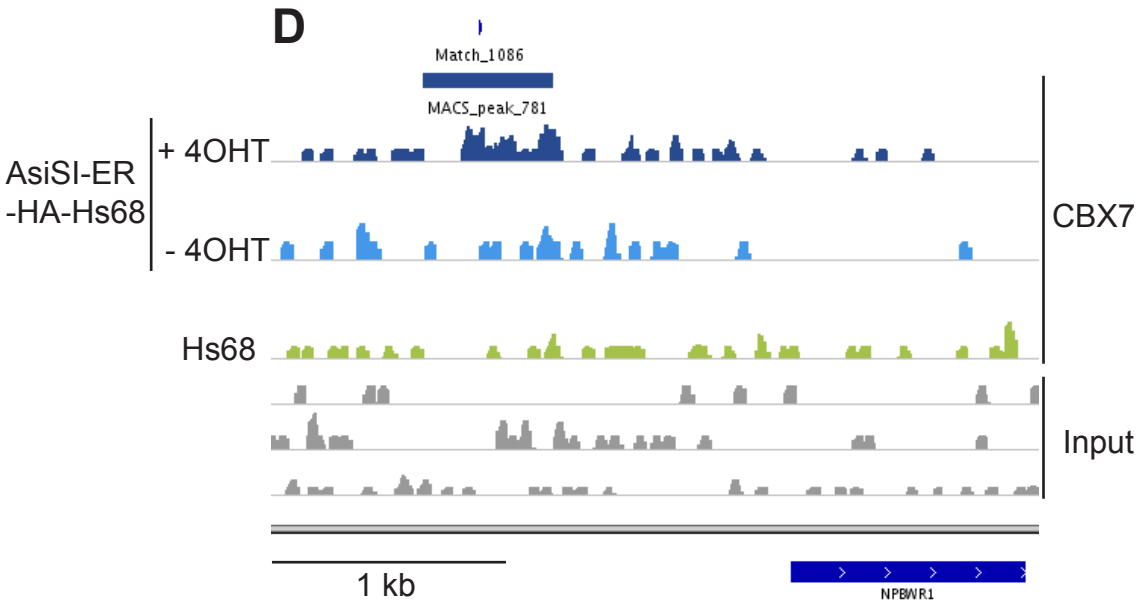

Figure 6.5 ChIP-seq analysis of CBX7 in HDFs before and after DNA damage

Profiles of DNA sequence tag densities at **A)** *INK4a-ARF-INK4b* **B)** *GATA6* **C)** *DLX1* and **D)** an *Asi*SI cut site, following ChIP-seq using anti-CBX7 (HCHA1). Profiles from *Asi*SI-ER-HA-Hs68 cells – 4OHT (light blue) and + 4OHT (dark blue) are shown, alongside data from uninfected Hs68 cells (green) (performed by Emma Anderton). Parallel analysis of input DNA is shown in grey. The genome organisation of each locus in **A-C)**, as represented in the UCSC genome browser, is shown below. The *Asi*SI cut site in **D)** is indicated above the CBX7 binding profile in *Asi*SI-ER-HA-Hs68 + 4OHT cells and denoted 'Match_1086'.

Chapter 7. Discussion

The aim of this thesis was to characterise the interaction of CK2 with PRC1 and to investigate the functional relevance of this association. We have found that CK2 can interact with all five CBX proteins and in the case of CBX7, this was shown to depend on residues within the conserved Pc box near the C-terminus. Mutations at these residues abrogated binding of mCbx7 to endogenous CK2. However these mutants were also unable to bind endogenous RING2. Consequently, these mutations could not be used to tease out the functional relevance of the CK2 interaction. We have shown that endogenous CBX7 is phosphorylated and that mCbx7 is phosphorylated by CK2 *in vitro*. However, we have been unable to identify the CK2 target residue of mCbx7 by mass spectrometry. Our data suggest that CK2 is not required for PRC1 repression of *INK4a* and evidence relating CBX7 phosphorylation to function remains equivocal. To investigate the hypothesis that CK2 could influence PRC1 protein function in the DDR, we established a system to induce sequence-specific DSBs in HDFs that express a tamoxifen-regulated version of the *Asi*S1 restriction enzyme. Staining for γ-H2AX and 53BP1 confirms that the system operates as expected. However, detection of PRC1 proteins by either immunofluorescence or genome-wide ChIP-seq suggests that they are not recruited to *Asi*S1 sites in this system and extensive DNA damage does not mobilise PRC1 complexes from known binding sites.

The following sections discuss the merits and weakness of the experimental data in relation to recently published findings and identify ways in which the investigation could be pursued in the future.

7.1 The interaction of CK2 with PRC1

As a starting point for further studies on the role of CK2 in the PRC1 complex, the interaction of CK2 with PRC1 components was confirmed by co-immunoprecipitation of the endogenous CK2 subunits with overexpressed CBX2, 4, 6, 7, and 8, and importantly, with endogenous RING2 (Figure 3.1). To our knowledge, this is the first report of an interaction between endogenous CK2 and

an endogenous PcG protein. The data provided confidence that the association could be physiologically relevant rather than an artificial consequence of over-expression. They are also consistent with a previous report that CK2α co-immunoprecipitates with overexpressed Ring1b (Sanchez et al., 2007) and more recent work showing that GST-tagged CK2α and β interact with overexpressed CBX4 and RING2 (Vandamme et al., 2011).

The other important criterion for physiological relevance is whether the auxiliary protein is present in complexes of an appropriate size. According to the gel filtration data, endogenous CK2 in 293T cells was present in high molecular weight fractions (Figure 3.2A), peaking at a size of approximately 550 kDa. This result is consistent with previous findings in mouse F9 cells (Guerra and Issinger, 1998), and suggests that CK2 is commonly associated with other proteins. The size range of CK2 complexes is consistent with that of endogenous PRC1 proteins although there is substantial variability in the sizes reported for different PCG proteins and in different studies (ranging from 400 kDa to over 2 mDa)(Gao et al., 2012, Sanchez et al., 2007, Vandamme et al., 2011, Tavares et al., 2012, Maertens et al., 2010). There are also discrepancies between the elution profiles of endogenous and ectopically expressed proteins (Figure 3.2B and (Vandamme et al., 2011)) suggesting that overexpressed PcG proteins may form additional interactions compared to their endogenous counterparts. Nevertheless, fractionation of immunoprecipitated CBX7-FLAG complexes showed that endogenous CK2 and RING2 co-purify with CBX7 in a complex greater than 669 kDa in size, consistent with that of a typical PRC1 complex (Figure 3.2B). A proper assessment of this issue would require co-immunoprecipitation of endogenous CK2 and PRC1 components either before or after gel filtration but the levels of the PcG proteins and the poor sensitivity of the detection methods precluded this approach.

Co-precipitation data do not indicate which component of the PRC1 complex is directly associated with CK2 but the peptide array data described here suggests that the principle contact is via the CBX protein. Recombinant CK2α bound strongly to a series of overlapping peptides that encompass the Pc box in the C-terminal domain of CBX7 (Figure 3.4). Neither the regulatory β subunits of CK2, nor any

other cellular proteins, were required for the interaction. It is also of note that ATP was absent from this system suggesting that the ability of CK2 to interact with these peptides is independent of CK2 kinase activity. Equivalent array data suggested that CK2α also binds to C-terminal peptides in CBX6 and CBX8, but not to RING2, HPH2 and BMI1 (Figure 3.3 and Figure 3.5). One caveat is that the signals detected on the latter peptide arrays were rather variable and less definitive. This could possibly reflect batch-to-batch variation in the recombinant CK2α obtained from a commercial supplier and, in retrospect, it might have been better to have produced our own recombinant CK2 in sufficient quantities to avoid this variable.

The findings are nevertheless consistent with recently published data demonstrating a direct interaction between CK2 and the C-terminus of CBX4 (specifically, the 290 amino acid isoform, which results from alternative splicing) (Vandamme et al., 2011). In this study, recombinant GST-CK2α and GST-CK2β, produced in bacteria, were shown to bind TAP-tagged CBX4, RING2 and BMI1 in 293T cell nuclear extract. However, when the binding was performed with *in vitro*-translated versions of CBX4, RING2 and BMI1, only CBX4 co-purified with CK2 and specifically, only with the β subunit. Binding assays performed with variants of CBX4 that either lacked the chromodomain (CBX4(68-290)) or the Pc domain (CBX4(1-269)), demonstrated that the Pc box of CBX4 (272-286) is important for its direct interaction with the regulatory β subunit of CK2.

In view of the peptide array data described here (Figure 3.4), it is curious that Vandamme and colleagues, did not detect binding between CBX4 and CK2α, as well as CK2β. It is conceivable that the GST-tag on the recombinant CK2α interfered with its ability to interact with CBX4. Another possibility is that CK2α and CK2β have different affinities for the Pc box of CBX4 and CBX7. However, this seems unlikely given the high conservation of the Pc domains of these proteins (Figure 3.7). It would be interesting to determine whether recombinant CK2β is able to bind the Pc box of CBX proteins in the context of a peptide array.

Although there is some evidence that the Pc box facilitates the self-association of Pc proteins (Reijnen et al., 1995), the best-characterised function of this domain is mediating the interaction of Pc proteins with RING2. The Pc box domains of CBX2, 4, 6, 7, and 8 all bind to the C-terminus of RING2 (C-RING2) with strong affinity. Interestingly the K_d values for these interactions vary from 9.2 nM (the most stable) for CBX7-C-RING2 to 180 nM for CBX6- and CBX8-C-RING2. The interaction stabilises the conformation of C-RING2 and induces structural constraints in the Pc box, which is largely disordered in the absence of C-RING2 (Wang et al., 2008). Intrinsically disordered protein regions can expand the repertoire of binding partners by allowing for the creation of distinct interaction surfaces for different binding partners (Fink, 2005). This inherent flexibility of the Pc box could therefore mediate CBX-binding to other proteins, such as CK2, in the absence of RING2. Alternatively, the conformation of the Pc box, induced by its interaction with RING2, could be required for CBX to interact with other proteins.

The crystal structure of the C-terminus of CBX7 bound to the C-terminal domain RING2 has been solved at a resolution of 1.7Å (PDB ID 3GS2, (Wang et al., 2010)). C-CBX7 has an antiparallel β-sheet structure that forms an extended, intermolecular β-sheet with the β-sheet region of C-RING2. Of note, Phe234 and surrounding residues in C-CBX7, including Val232, pack against a hydrophobic pocket in C-RING2 (Wang et al., 2010). It is not clear from the crystal structure, whether CK2 might be able to interact with CBX proteins that are complexed with RING2, or whether these interactions are likely to be mutually exclusive. As the peptide arrays and published data (Vandamme et al., 2011) imply that CK2 does not directly contact RING2, our ability to co-precipitate endogenous CK2 with RING2, suggests that the binding of CK2 and RING2 to CBX7 is not mutually exclusive. However, this hypothesis remains to be tested and it is conceivable that the interaction between CK2 and RING2 could be mediated by another protein.

The mutation array of the CBX7 Pc box region showed that four residues were critically important for the *in vitro* interaction with CK2α: Ile230, Val232, Thr233 and Phe234. As mentioned above, Phe234 and Val232 are known to mediate the interaction between CBX7 and RING2, Phe234 critically so. In contrast, Ile230 and Thr233 appeared to point away from the CBX7-RING2 interface and it was hoped

that alteration of these residues might yield a CBX7 mutant that would be specifically unable to bind CK2. Indeed, when the equivalent residues in mouse Cbx7 were changed to aspartic acid, the GST-mCbx7 fusion protein with all three residues mutated did not bind CK2. However, this CBX mutant was also unable to bind both RING2 and BMI1 (Figure 3.9). Interestingly, the binding of HPH2 did not appear to be disrupted by these mutations. This suggests that HPH2 interacts with CBX7 in a BMI1-RING2 independent manner and that the relevant residues in the Pc box of CBX7 are not important for the interaction with HPH2.

As BMI1 and RING2 are known to form a heterodimer (Buchwald et al., 2006, Li et al., 2006), the loss of BMI1 binding to the mCbx7 mutant was probably a consequence of the loss of RING2 binding. This illustrates an important limitation of the approach: as the binding assays were performed in the context of cell lysate, it is difficult to tell whether the failure of the mCbx7 mutant to interact with CK2 and RING2 reflects disruption of a direct contact with these proteins or of an interaction with a secondary protein that promotes the association of mCbx7 with CK2 and RING2. To investigate this further, it would be necessary to perform GST pull-down experiments with GST-tagged mCbx7 mutants and recombinant CK2 or recombinant RING2. Alternatively, these interactions could be tested amongst *in vitro*-translated versions of these proteins. Although this would be interesting, it would not shed light on whether it is theoretically possible to generate further variants of CBX7 that are specifically impaired for interacting with CK2 but not RING2.

The peptide array data indicated that, in addition to the CBX proteins, CK2 might directly bind RYBP (Figure 3.5). Although we have not demonstrated that CK2 binds full-length RYBP, this result is consistent with recent work by Gao and colleagues showing that CK2 co-purifies with TAP-tagged RYBP and YAF2 from 293T cells (Gao et al., 2012). Importantly, the data here suggest that the interaction between CK2 and RYBP involves a domain in RYBP that has a degree of homology with the Pc box of CBX proteins (Figure 3.5). Moreover, this domain is predicted to interact with RING2 via similar structural folds as CBX7 (Wang et al., 2010). This is interesting as it implies that the interaction domain of both CBX7 and RYBP with RING2 also mediates the interaction with CK2 in both complexes.

Whereas recruitment of the canonical PRC1 complex is in part dependent on PRC2 and H3K27me3, recruitment of the RYBP complex is not (Tavares et al., 2012). As both complexes contain Psc and Sce subunits, they can both function as E3 ubiquitin ligases. However, the balance of evidence suggests that H2A ubiquitination is largely carried out by the RYBP complex. The precise role of each complex has yet to be established but the association of CK2 in both complex types suggests its role is important for an aspect of PRC1 biology that is common to both.

7.2 Phosphorylation of CBX7 by CK2

The evidence that CK2 interacts directly with CBX7, and the presence of potential CK2 target sites in the CBX7 sequence, led us to investigate whether CBX7 is phosphorylated by CK2. The *in vitro* kinase assay, conducted using recombinant mCbx7 and commercial CK2 holoenzyme, showed clear incorporation of ^{32}P into mCbx7 (Figure 4.2). Importantly, the extent of labelling was comparable to that of a known CK2 target, Cdc37 (Figure 4.3) (Miyata and Nishida, 2005). It was therefore disappointing that MS analyses did not detect any phosphorylated residues in two separate experiments. Unfortunately, the samples were submitted at a time when the LRI Protein Analysis and Proteomics service was relocating from Lincoln's Inn Fields to Clare Hall laboratories, and subsequently undergoing a change in management. This caused a considerable delay in establishing an essentially negative result and, in retrospect, it might have been advisable to outsource the analysis.

A potential explanation for the inability of MS to identify phosphorylated residues in mCbx7 would be that the phosphorylation is substoichiometric. Prior enrichment of the phosphorylated forms, for example on PMAC resin (Chapter 4.2), might have alleviated the problem. However, if substoichiometric phosphorylation occurs at multiple sites in mCbx7, the MS analysis would remain challenging.

An equally plausible explanation would be that CBX7 is not a true substrate for CK2 *in vivo* and that the *in vitro* labelling of recombinant mCbx7 is non-specific.

This would be consistent with unpublished data from the Bernstein laboratory that was conveyed to us during the course of our investigations (Emily Bernstein, personal communication). They had performed affinity purification of TAP-tagged mCbx7, using a construct provided by us and used previously (Nicholls, 2006), and identified phosphorylated mCbx7 on Thr119 by MS analysis. This residue is not within a CK2 consensus, and no other phosphorylation events were detected. Moreover, in the experiments described in Chapter 4.2, inhibition of CK2 did not alter the status of CBX7 as a phosphorylated protein, as judged by retention on PMAC resin (Figure 4.6), implying that either CK2 does not phosphorylate CBX7 *in vivo* or, if it does, it is not the only kinase to do so.

In collaboration with the Bernstein laboratory, we investigated whether the phosphorylation status of Thr119 had any bearing on measurable properties of mCbx7. We were able to show that phosphomimicking and phosphoablating mutations of Thr119 do not affect the ability of mCbx7 to bind the *INK4a-ARF-INK4b* locus, to repress expression of $p16^{INK4a}$, or to extend the lifespan of HDFs (Figure 4.8-Figure 4.11). Although It was conceivable that phosphorylation of this residue could have gene-specific effects on PRC1-mediated repression, gene expression profiling revealed very few differences between the effects of the wild-type, T119A or T119E variants of Cbx7, (Emily Bernstein, personal communication). Together, these data suggest that Thr119 phosphorylation does not affect PRC1-repression of target genes.

The equivocal nature of the *in vitro* phosphorylation data precluded attempts to take a similar approach with candidate CK2 phosphorylation sites. However, as discussed above, one of the critical residues for the interaction between CBX7 and CK2 (Thr233 in the human protein, Thr140 in the mouse) is also a potential CK2 target site. Interestingly, substituting this residue with aspartic acid caused a modest reduction in ^{32}P-labelling by CK2 *in vitro* (Figure 4.3). This could suggest that Thr140 is indeed a CK2 target. However, given the acidic nature of the consensus sequence, it was somewhat surprising that aspartic acid substitutions caused the most severe disruption of the CK2-CBX7 interaction as judged by peptide arrays and GST pull-down approaches. Paradoxically, the mCbx7 variant with three aspartic acid substitutions in the Pc box domain (V137D, V139D and

T140D) appeared to be a more effective substrate in the *in vitro* kinase assay despite being impaired for binding to CK2 (Figure 4.3). A plausible explanation for the increased phosphorylation of this variant is that the mutations create a novel CK2 consensus site centred on Ser136. However, the data imply that the aspartic acid substitutions affect the stable binding of CK2 to mCbx7 but not its ability to phosphorylate mCbx7.

There are examples whereby the phosphorylation of a substrate by CK2 thereafter repels its interaction with CK2 (Filhol et al., 1992). However, this cannot explain the effects of aspartic acid substitutions on CK2 binding to the CBX7 peptide array as the binding assay was performed in the absence of ATP. Taken together, the data indicate that Val137, Val139 and Thr140 of mCbx7, and the equivalent residues in human CBX7, are important for the interaction with CK2 but this interaction is not required for the phosphorylation of mCbx7 *in vitro*. The data do not exclude the possibility that an interaction between CK2 and CBX7 is important for the phosphorylation of a CK2 target *in vivo*

Although the focus in this thesis was on CBX7, all mammalian PRC1 proteins contain multiple CK2 consensus sequences (Table 1.2). It might therefore be informative to apply an unbiased approach to identifying CK2 targets within PRC1. For example, TAP-purified PRC1 complexes could be used in a kinase assay with recombinant CK2 and, though the analyses might prove challenging, phosphorylated peptides could be identified by MS. In particular it will be important to investigate Sce proteins as CK2 substrates. MS has identified several phosphorylation sites in Mel18, one of which lies within a CK2 consensus. Furthermore, the phosphorylation of Mel18 has been suggested to affect H2A recognition, and consequential ubiquitination, by a Ring1b-Mel18 complex assayed *in vitro* (Elderkin et al., 2007).

7.3 Influence of CK2 on PRC1-repression of target genes

It has been challenging to ascertain whether CK2 activity influences the ability of PRC1 to function as a transcriptional repressor. The fact that CK2 is essential for

cell viability, and the shear number of CK2 substrates, means that it is difficult to identify whether a perceived change is direct or indirect. We employed two approaches to manipulate CK2 activity. The first was to use shRNAs to reduce the levels of individual CK2 subunits. Although the shRNAs were very effective there was always some residual CK2 protein in the cells and only one subunit was targeted in a given population of HDFs. Attempts to knock down all three CK2 subunits in the same cells were unsuccessful due to the loss of cell viability and it was clear that the combination of shRNAs had less substantial effects on each subunit as compared to the individual knockdowns.

In the event, the knockdown of single CK2 subunits did not significantly affect the expression of *INK4a* or cell proliferation (Figure 5.2 and data not shown) This contrasts with previous experience in the lab following shRNA-mediated knockdown of other PRC1 auxiliary proteins in HDFs. For example, knockdown of the ubiquitin-specific proteases, USP7 and USP11, and the RNA helicase, MOV10, was found to relieve PcG repression of *INK4a* and cause $p16^{INK4a}$-dependent senescence (El Messaoudi-Aubert et al., 2010, Maertens et al., 2010). USP7 and 11 are thought to promote repression of *INK4a* by their ability to regulate the turnover of BMI1 and MEL18 (Maertens et al., 2010).

The findings are also at odds with recent reports suggesting that siRNA-mediated knockdown of CK2 catalytic subunits in human mesenchymal stem cells and human fibroblasts can increase in the proportion of senescence-associated β-galactosidase (SA-β-gal) positive cells (Wang and Jang, 2009, Kim et al., 2009, Ryu et al., 2006). However, only one of these studies considered additional markers of cell-cycle arrest or senescence following CK2 knockdown. In this study Wang and colleagues showed that $p16^{INK4a}$ protein levels were unchanged three days after siRNA knockdown of CK2α' or CK2α in human mesenchymal stem cells. After six days, $p16^{INK4a}$ protein levels increased slightly following the knockdown of CK2α' but not CK2α (Wang and Jang, 2009). However, as this study relied on single siRNAs against each subunit there could have been off-target effects. Moreover, the fact that cells remain viable following knockdown of CK2 subunits, both in our own and the published studies, suggests that the cells have enough

residual CK2 activity to maintain phosphorylation of critical CK2 targets. To avoid the uncertainties associated with shRNA-based approaches, the alternative strategy was to treat cells with a chemical inhibitor of CK2, TBB. Although CK2 activity levels following TBB treatment were not measured directly, the cleavage of PARP indicated that CK2 was effectively inhibited. However, PARP-cleavage reflects engagement of an apoptotic program and highlights the substantial limitation of this approach. Studies in Jurkat human leukaemia cells have shown that inhibition of CK2 causes decreased phosphorylation of HS1, Max and Bid, a modification that protects these proteins from caspase-cleavage (Desagher et al., 2001, Krippner-Heidenreich et al., 2001, Ruzzene et al., 2002). Loss of cell viability under such conditions limits the conclusions that can be drawn but it was nonetheless surprising that the expression of most of the PRC1-target genes investigated did not change following TBB treatment of HDFs (Figure 5.4). These data suggest that inhibition of CK2 for 24 hours does not alter the ability of PRC1 to repress target loci. However, it is important to note that the documented changes in $p16^{INK4a}$ expression following knockdown of PRC1 components take place over a much longer time scale.

Although attempts to manipulate CK2 levels were problematic, it was clear that the endogenous levels of CK2 were reduced in senescent HDFs, albeit with differences between the subunits; CK2α and β subunits decreased substantially but α' levels remained constant (Figure 5.1). The decrease in CK2 levels at senescence has also been described in two studies from Young-Seuk Bae's laboratory. Together these studies suggested that both the mRNA and protein levels of CK2α and α' declined at senescence in IMR90 human fibroblasts, whereas expression of CK2β remained stable. They also demonstrated that CK2α and CK2β protein levels were reduced in aged rat testis but only CK2β decreased in aged rat liver; levels of CK2α' were not reported (Kim et al., 2009, Ryu et al., 2006). Taken together, the data suggest that the changes affecting individual CK2 subunits might be context dependent. Whether the changes contribute to, or are consequence of, senescence remains unclear.

7.4 PcG proteins in the DDR

Given the uncertainties regarding the role of CK2 in transcriptional regulation by PRC1 and the emerging evidence that both CK2 and PRC1 are implicated in the DDR, we were keen to establish a system in which we could assess the link between CK2 and PRC1 in the context of DNA damage. Having considered several possibilities, we adopted an inducible DNA damage system based on a fusion between the *Asi*S1 restriction enzyme and the tamoxifen-regulated ligand-binding domain of the estrogen receptor (ER). We validated this system in HDFs, and in the U2OS cell line in which it was originally reported, by demonstrating that the addition of 4OHT resulted in nuclear translocation of *Asi*SI and the induction of DSBs (as assessed by γH2AX foci) (Figure 6.1). Although we could show co-localisation of 53BP1 with γH2AX, and co-localisation of different PRC1 proteins, we were only able to show, at best, a weak co-localisation of PRC1 proteins with γH2AX.

The degree of protein co-localisation was determined using Pearson's correlation coefficient (PCC), which is generally considered the best statistical tool for assessing the co-localisation of proteins from microscopy data. However, PCC has limitations when applied to the issues relevant to this thesis. For example, if a subpopulation of BMI1 became co-localised with γH2AX following DNA damage, while the majority remained associated with chromatin at sites of gene repression, then the PCC will present an average of these separate states but may not adequately reflect either. Moreover, if the presence of repressive PRC1 complexes impaired DNA damage and/or γH2AX recruitment, then BMI1 and γH2AX would be predicted to have a negative PCC at PcG target loci; further decreasing the average PCC. Such a scenario may well exist if *Asi*SI does not cut at PcG target genes either because of steric hindrance or CpG methylation (Roberts et al., 2010, Vire et al., 2006, Mohammad et al., 2009).

Although several studies describe the detection of PRC1 proteins at sites of DNA damage by immunofluorescence, we are not aware of any relating to the induction of DSBs generated by an endonuclease. It is conceivable, therefore, that this type

of DNA damage does not elicit PRC1 recruitment, or does so to an extent that is not detectable by immunofluorescence. However, Ginjala and colleagues were able to demonstrate enrichment of BMI1 and CBX2 at a zinc-finger nuclease-site using ChIP in HeLa cells (Ginjala et al., 2011). In a separate, albeit less convincing study, YFP-tagged CBX4 was detected by ChIP at an I-*Sce*I cut site in MCF7 cells (Ismail et al., 2012). Curiously, the relatively modest enrichment (two-fold greater than IgG) was observed at a distance of 3kb and 4.5kb, but not adjacent to the cut site (Ismail et al., 2012).

The reason for adopting the inducible *Asi*SI system was to gain a more genome-wide impression of PRC1 recruitment at DSBs and we chose normal human fibroblasts as a cell system to avoid the genomic abnormalities associated with cancer cell lines. From on-going work in the laboratory, we also had a comprehensive picture of PRC1 binding profiles in the Hs68 strain of HDFs based on ChIP-seq analyses with antibodies against five different PRC1 components (unpublished results of Emma Anderton and Helen Pemberton). In the event, the ChIP-seq profiles for CBX7 before and after 4OHT treatment of *Asi*SI-ER-HA-Hs68 cells were essentially indistinguishable from one another and from the profiles observed in parental Hs68 cells. Importantly, with the exception of one site, CBX7 enrichment was not detected within 10kb of any *Asi*SI target sequences. As the immunofluorescence data suggested that a substantial proportion of the *Asi*SI sites must be cut in each cell following 4OHT treatment, we do not think that the lack of CBX7 enrichment at *Asi*SI sites reflects cleavage at different sites in different cells within the population.

It is possible that PRC1 recruitment to DSBs is much less stable than the chromatin interactions detected by our standard ChIP protocol. Interestingly, the recruitment kinetics of PRC1 proteins to DSBs seem to vary, depending on the context and the protein in question. For example, BMI1, CBX4 and RING2 are recruited to sites of microirradiation within 11 seconds; comparable to early DNA damage response proteins such as RNF8, NBS1 and MRE11 (Ismail et al., 2010). Recruitment of MEL18 to sites of DNA damage is also rapid (less than 5 minutes), but short-lived (less than 20 minutes) (Chou et al., 2010, Ginjala et al., 2011). In contrast, Ring1b, CBX4 and BMI1 remain detectable at DNA breaks for sustained periods (30

minutes, 4 hours and 24 hours respectively) following microirradiation (Ginjala et al., 2011, Chou et al., 2010, Ismail et al., 2010). Both our immunofluorescence observations and ChIP experiments were performed 4 hours after 4OHT treatment, when maximum γH2AX staining was observed by immunofluorescence. In contrast to microirradiation, we would expect the nuclease-generated DSBs to persist.

Another possibility that could explain the absence of CBX7 enrichment at *Asi*SI sites is that only a subset of PRC1 proteins are involved in the DDR. The recruitment of CBX7 to sites of microirradiation has only been shown by one study, which used ectopically expressed GFP-tagged CBX7 in HeLa cells (Chou et al., 2010). Although the focus on CBX7 provided continuity with other aspects of the work, it might be appropriate to extend the ChIP-seq analysis to additional PRC1 proteins such as RING2. RING2 has been heavily implicated in the DDR and we have the capacity to perform ChIP-seq for RING2 in HDFs.

One of the other reasons for establishing the *Asi*SI-inducible DNA damage system was to determine whether PRC1 recruitment at multiple DSBs would affect expression of PRC1-target genes. It has been suggested (Chou et al., 2010) that under conditions of persistent DNA damage, resulting for example from telomere erosion or oncogene-induced DNA replication stress, PRC1 recruitment to sites of DNA damage could mobilise PcG proteins from normal PRC1 targets, such as *INK4a,* leading to transcriptional derepression. With the same caveats as above, the CBX7 ChIP-seq data suggest that this hypothesis is not true. Another interesting way to investigate this hypothesis would be to perform ChIP-seq of PRC1 proteins in HDFs following artificial telomere uncapping by depletion of components that protect chromosome ends (d'Adda di Fagagna et al., 2003, Takai et al., 2003), or in HDFs that have undergone replicative senescence.

To our knowledge, there is no evidence that PRC1 proteins can be recruited to DSBs in HDFs. While a few of the studies exploring PcG proteins in the DDR have been conducted in MEFs and stem cells, the vast majority have used cancer cell lines, such as U2OS. It would therefore be interesting to determine whether recruitment of PRC1 to *Asi*SI sites could be demonstrated by ChIP in *Asi*SI-ER-HA-U2OS cells, instead of the HDF system. However, as the PRC1 targets in U2OS

cells are unknown, it is difficult to assess the quality of the ChIP samples prior to submission for DNA sequencing. For example, in a preliminary experiment, in which CBX7 ChIP was performed in *Asi*SI-ER-HA-U2OS cells before and after 4OHT treatment, it was not possible to detect CBX7 enrichment at *INK4a-ARF-INK4b* (data not shown). Additional PRC1 target genes will therefore need to be evaluated in U2OS cells before ChIP-seq analysis can be contemplated.

The *INK4a* locus is known to be hypermethylated in U2OS cells, which may explain the absence of CBX7 at this locus. It is also possible that the congregation of PRC1 proteins in PcG bodies in these cells distorts the binding profiles detected by ChIP. Indeed, in human tumour cells PcG proteins are predominantly found in a few, prominent foci, that associate with pericentromeric heterochromatin (Alkema et al., 1997, Saurin et al., 1998, Cmarko et al., 2003, Hernandez-Munoz et al., 2005), whereas, in human fibroblasts, these proteins are typically found in around 100 nuclear speckles that are evenly distributed throughout the nucleus (Voncken et al., 1999, Buchenau et al., 1998, Saurin et al., 1998). The immunofluorescence data in Chapter 6 are consistent with these studies. It is conceivable that the differences in PcG protein localisation between HDFs and human tumour cells may reflect changes in PRC1 function, PRC1 genome-wide binding or PRC1 protein interactions in tumour cells. This could have important implications for our understanding of PRC1 complex composition, which based largely on proteomic analysis of these proteins in cell lines. Of particular relevance to this thesis is that the interaction of CK2 with PRC1 proteins has only been demonstrated by us in 293T cells (El Messaoudi-Aubert et al., 2010, Nicholls, 2006) and by others in 293T cells (Dietrich et al., 2007, Gao et al., 2012), murine erythroleukemia (MEL) cells (Sanchez et al., 2007) and HeLa cells (Vandamme et al., 2011). It is therefore possible that CK2 is only relevant to PRC1 biology in abnormal contexts, such as tumorigenesis. It would be interesting to investigate this further by exploring whether an interaction of CK2 with PRC1 takes place in HDFs.

Chapter 8. Appendix

A

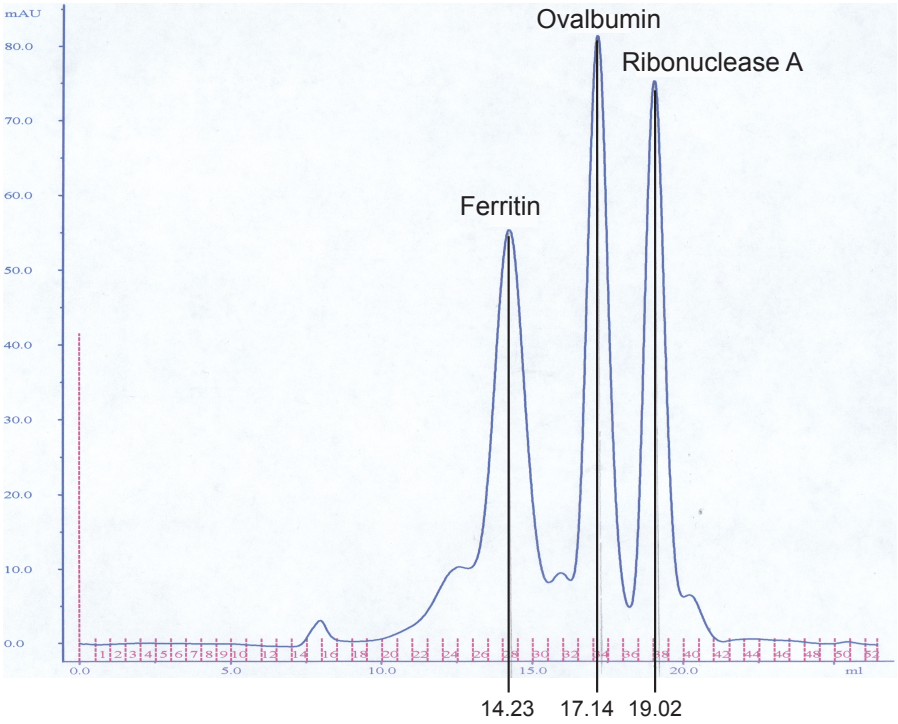

B

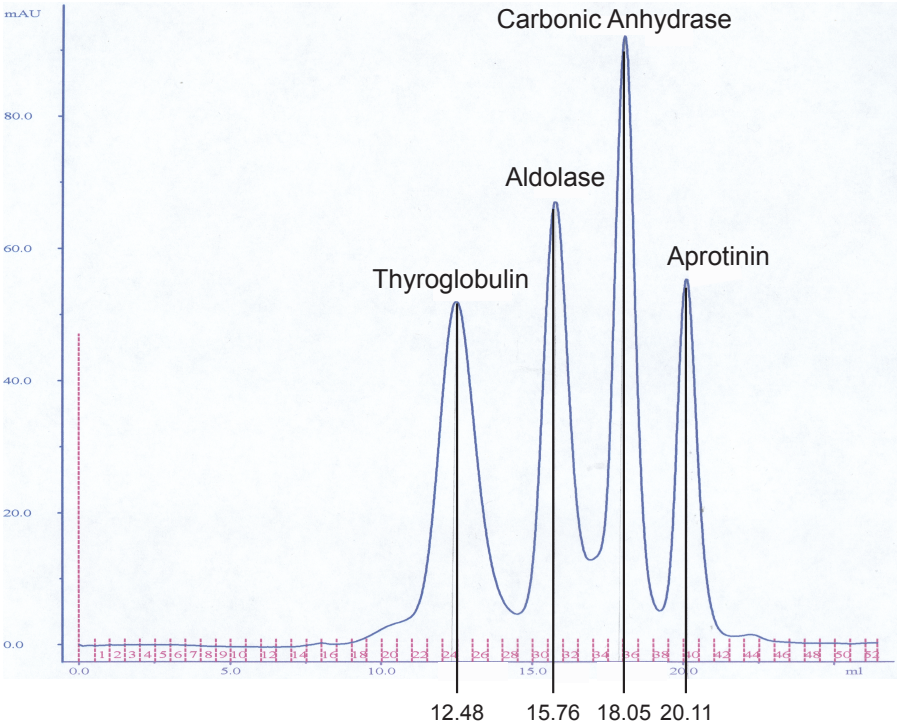

C

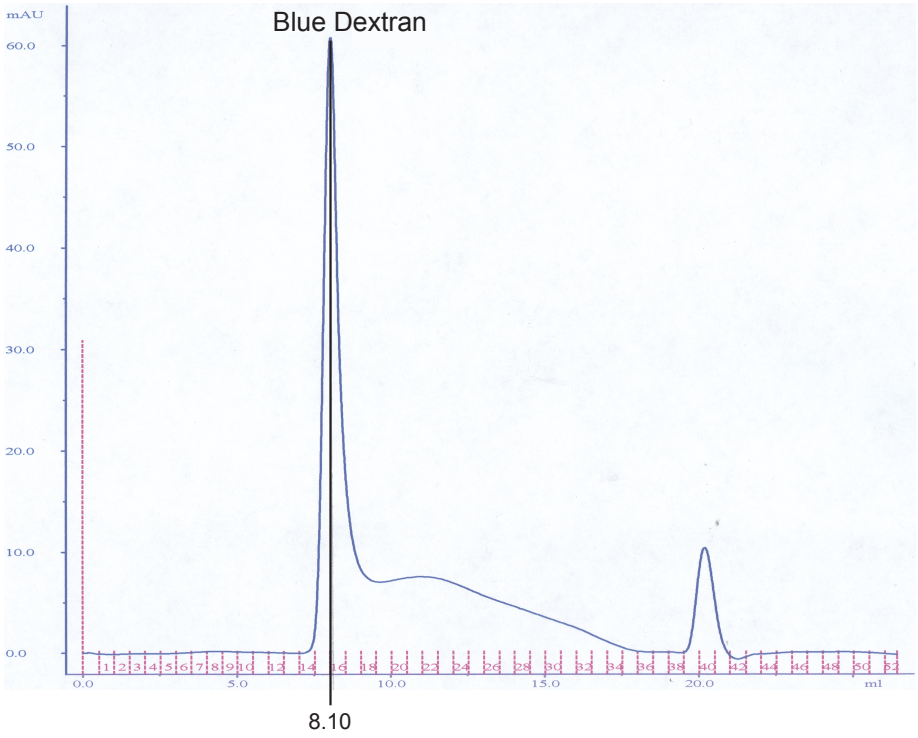

Figure 8.1 Calibration of Superose 6 column

A Superose 6 column (GE healthcare) to be used for gel filtration was calibrated using low molecular weight and high molecular weight standard proteins. Elution volumes were taken at the maximum absorbance of each respective protein and these are noted in the figure. **A)** A graph showing the absorbance of column flow-through following the application of mix A to the column (Aprotinin (1.5mg/ml), Carbonic Anhydrase (1.5mg/ml), Aldolase (2mg/ml) and Thyrogobulin (2.5mg/ml)). **B)** A graph showing the absorbance of column flow-through following the application of mix B to the column (Ribonuclease A (1.5mg/ml) Ovalbumin (2mg/ml) and Ferritin (0.15mg/ml)). **C)** A graph showing the absorbance of column flow-through following the application of Blue Dextran 2000 (0.5mg/ml) to the column. The elution volume of Blue Dextran is equal to the column void volume.

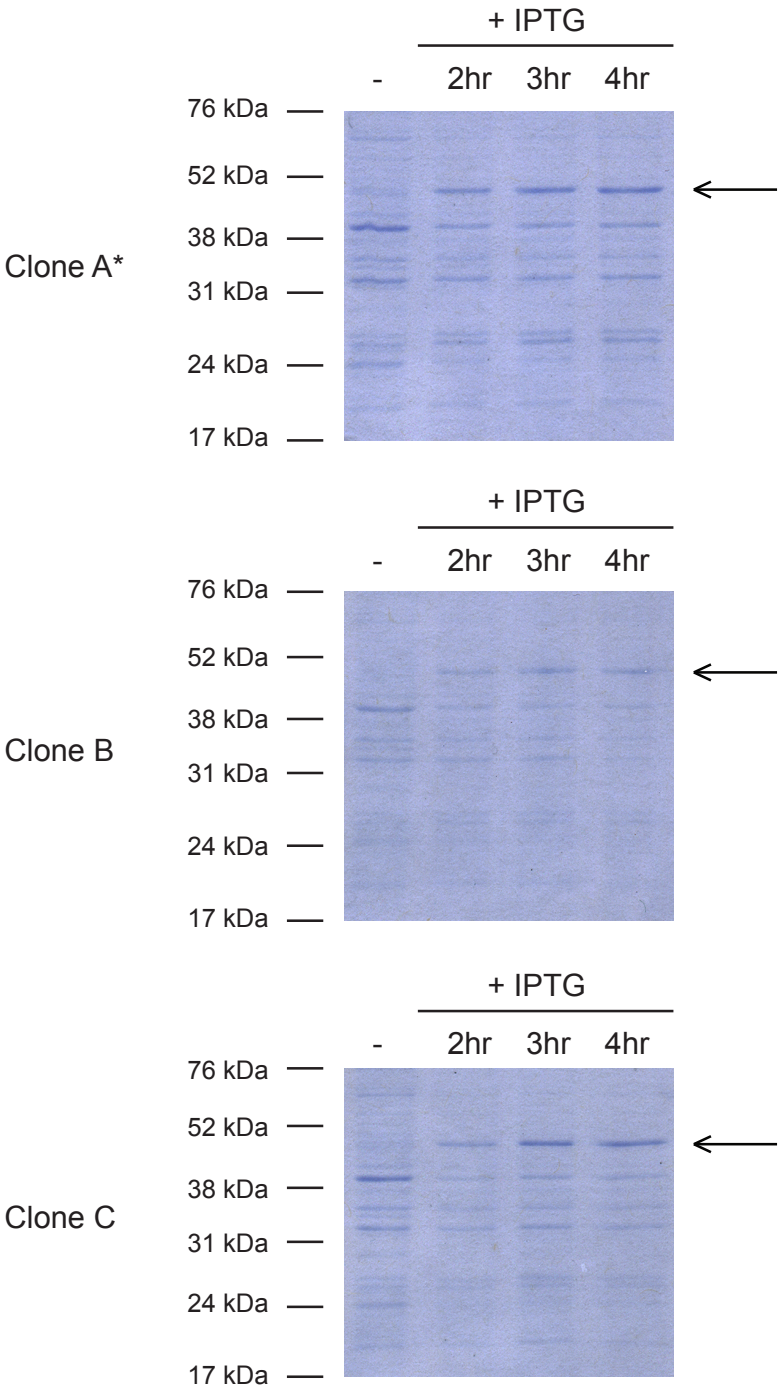

Figure 8.2 Bacterial expression of GST-mCbx7

Single colonies (clones A-C) of BL21 *E. coli* transformed with GST-mCbx7-pGEX-6P1 plasmid were grown to log phase, induced with IPTG for 2, 3 and 4 hours and then lysed. Protein lysates were fractionated by SDS-PAGE and proteins were subject to Coomassie staining overnight. Arrows indicate GST-mCbx7 protein expression following IPTG induction. Asterisk indicates the clone chosen for large-scale purification.

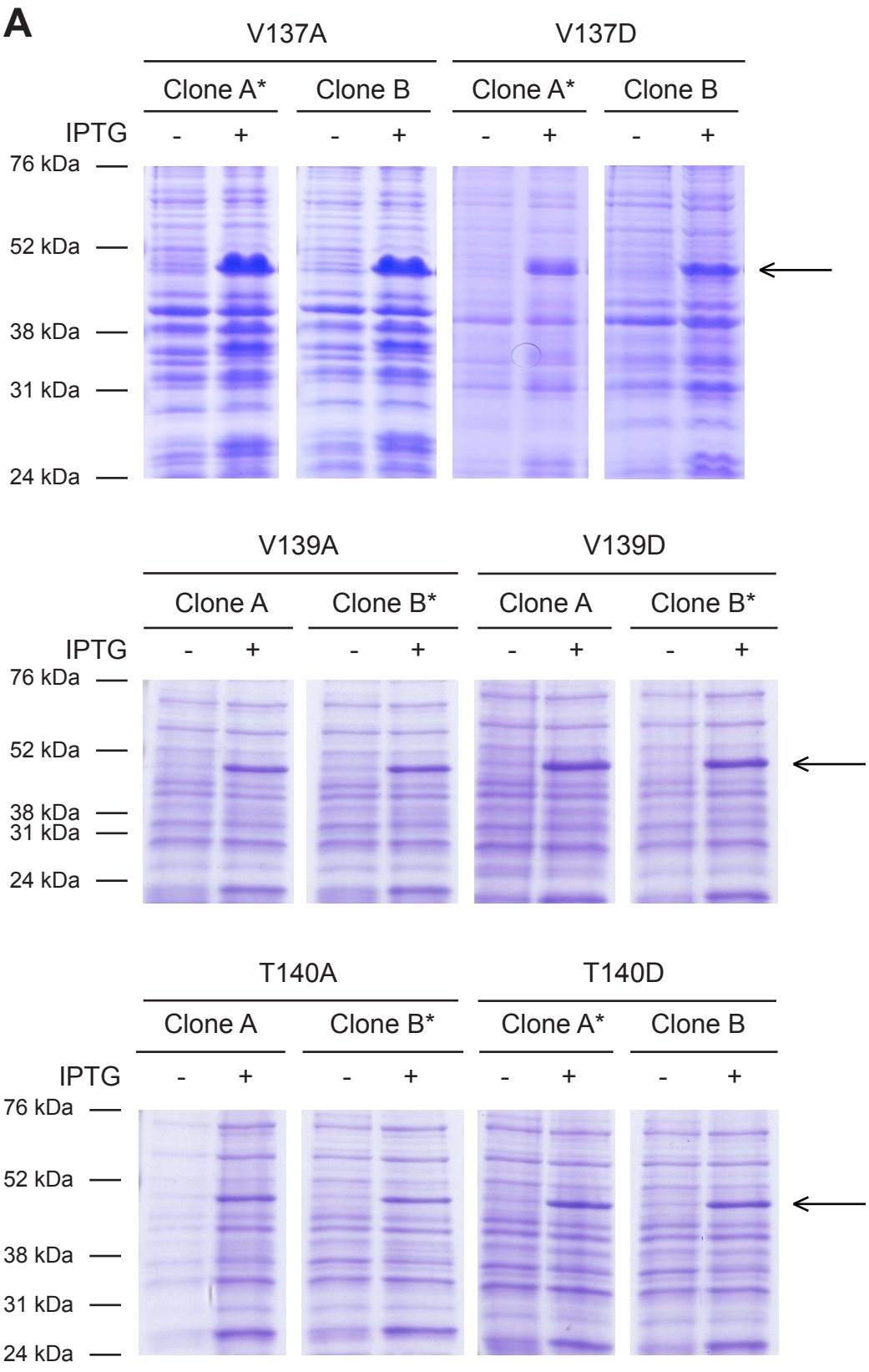
A
V137A
V137D
Clone A*
Clone B
Clone A*
Clone B
IPTG
- + - + - + - +
76 kDa
52 kDa
38 kDa
31 kDa
24 kDa
V139A
V139D
Clone A
Clone B*
Clone A
Clone B*
IPTG
- + - + - + - +
76 kDa
52 kDa
38 kDa
31 kDa
24 kDa
T140A
T140D
Clone A
Clone B*
Clone A*
Clone B
IPTG
- + - + - + - +
76 kDa
52 kDa
38 kDa
31 kDa
24 kDa

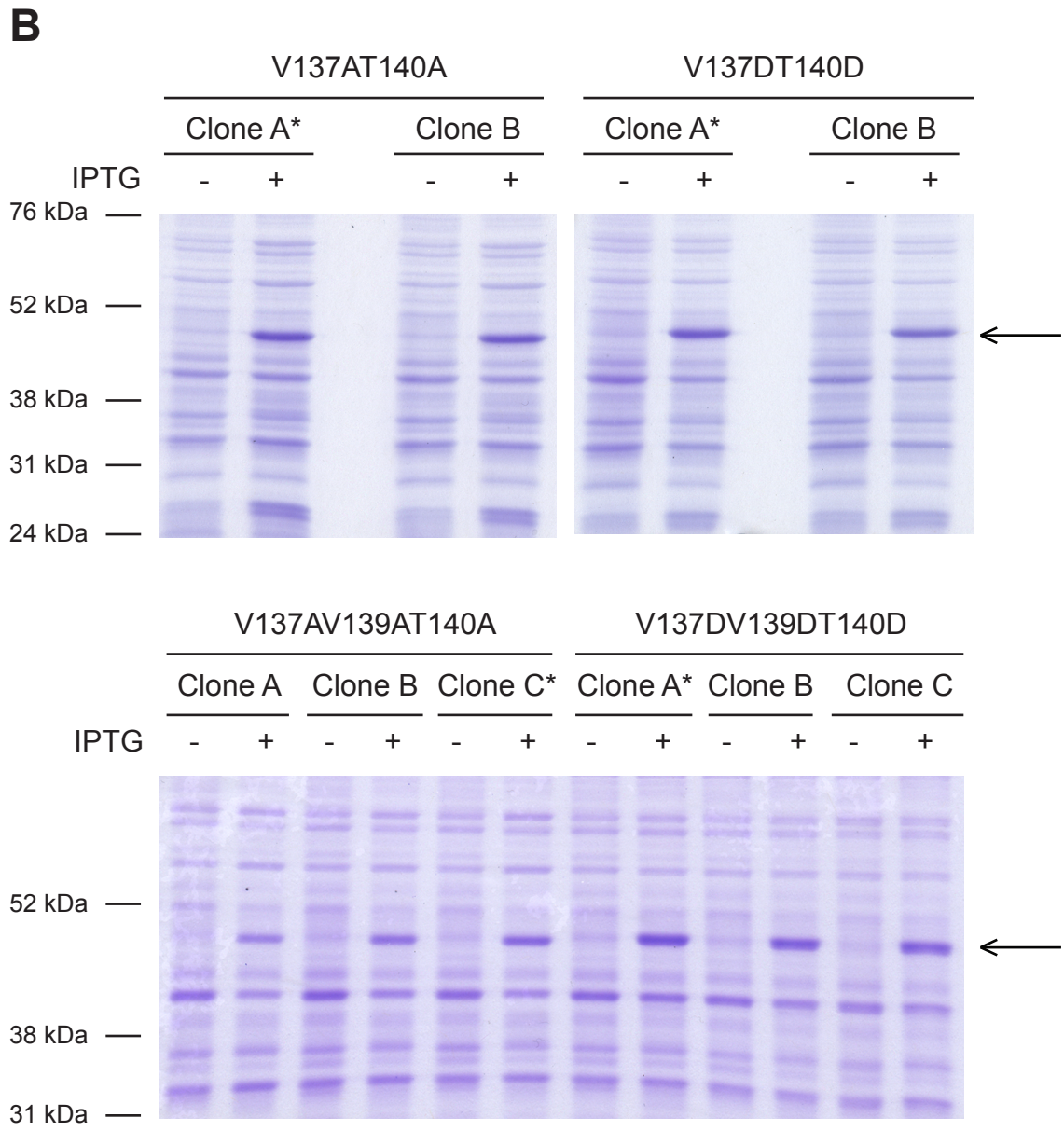

Figure 8.3 Bacterial expression of GST-mCbx7 point mutants

Single colonies (clones A-B or A-C) of BL21 *E. coli* transformed with the indicated GST-mCbx7-pGEX-6P1 mutant plasmid were grown to log phase, induced with IPTG for 3 hours and then lysed. Protein lysates were fractionated by SDS-PAGE and proteins were subject to Coomassie staining overnight. Arrows indicate GST-mCbx7 mutant protein expression following IPTG induction. Asterisks indicate the clones chosen for large-scale purification.

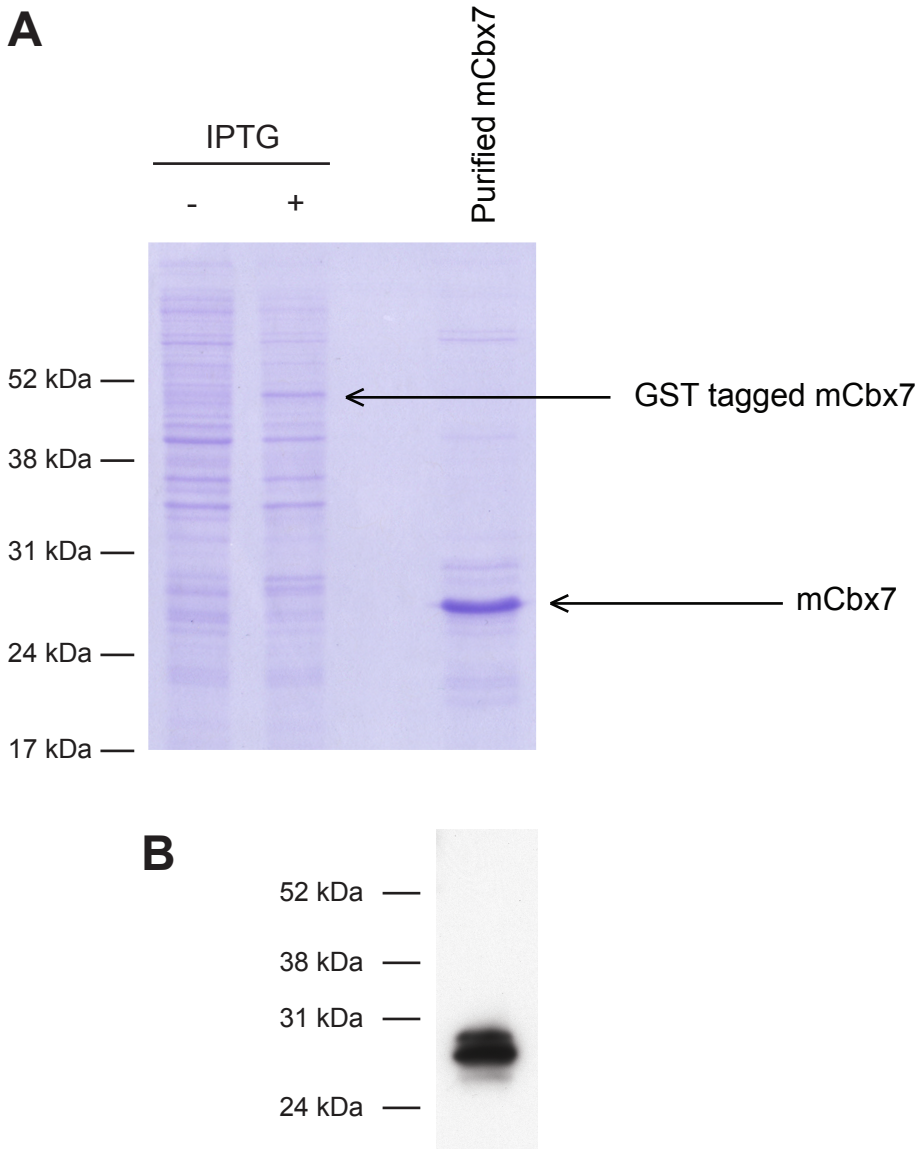

Figure 8.4 Purification of mCbx7

BL21 *E. coli* transformed with GST-mCbx7-pGEX-6P1 plasmid (Clone A, see Figure 8.2) were grown to log phase, induced with IPTG for 2 hours and then lysed. GST-mCbx7 was purified from lysate and PreScission protease (GE Healthcare) was used to cleave the GST-tag. A) Purified mCbx7 was fractionated by SDS-PAGE and proteins were subject to Coomassie staining overnight. Arrows indicate GST-mCbx7 protein expression following IPTG induction and the size of mCbx7 following GST-tag cleavage. B) Purified mCbx7 was fractionated by SDS-PAGE and immunoblotted with an antibody that recognises mCbx7.

Reference List

ACOSTA, J. C., O'LOGHLEN, A., BANITO, A., GUIJARRO, M. V., AUGERT, A., RAGUZ, S., FUMAGALLI, M., DA COSTA, M., BROWN, C., POPOV, N., TAKATSU, Y., MELAMED, J., D'ADDA DI FAGAGNA, F., BERNARD, D., HERNANDO, E. & GIL, J. 2008. Chemokine signaling via the CXCR2 receptor reinforces senescence. *Cell,* 133**,** 1006-18.

AGGER, K., CLOOS, P. A., CHRISTENSEN, J., PASINI, D., ROSE, S., RAPPSILBER, J., ISSAEVA, I., CANAANI, E., SALCINI, A. E. & HELIN, K. 2007. UTX and JMJD3 are histone H3K27 demethylases involved in HOX gene regulation and development. *Nature,* 449**,** 731-4.

AGUILO, F., ZHOU, M. M. & WALSH, M. J. 2011. Long noncoding RNA, polycomb, and the ghosts haunting INK4b-ARF-INK4a expression. *Cancer Res,* 71**,** 5365-9.

AKASAKA, T., TAKAHASHI, N., SUZUKI, M., KOSEKI, H., BODMER, R. & KOGA, H. 2002. MBLR, a new RING finger protein resembling mammalian Polycomb gene products, is regulated by cell cycle-dependent phosphorylation. *Genes Cells,* 7**,** 835-50.

AKHTAR, A., ZINK, D. & BECKER, P. B. 2000. Chromodomains are protein-RNA interaction modules. *Nature,* 407**,** 405-9.

ALCORTA, D. A., XIONG, Y., PHELPS, D., HANNON, G., BEACH, D. & BARRETT, J. C. 1996. Involvement of the cyclin-dependent kinase inhibitor p16 (INK4a) in replicative senescence of normal human fibroblasts. *Proc Natl Acad Sci U S A,* 93**,** 13742-7.

ALKEMA, M. J., BRONK, M., VERHOEVEN, E., OTTE, A., VAN 'T VEER, L. J., BERNS, A. & VAN LOHUIZEN, M. 1997. Identification of Bmi1-interacting proteins as constituents of a multimeric mammalian polycomb complex. *Genes Dev,* 11**,** 226-40.

ATSUTA, T., FUJIMURA, S., MORIYA, H., VIDAL, M., AKASAKA, T. & KOSEKI, H. 2001. Production of monoclonal antibodies against mammalian Ring1B proteins. *Hybridoma,* 20**,** 43-6.

AYOUB, N., JEYASEKHARAN, A. D., BERNAL, J. A. & VENKITARAMAN, A. R. 2008. HP1-beta mobilization promotes chromatin changes that initiate the DNA damage response. *Nature,* 453**,** 682-6.

BACHMANN, I. M., HALVORSEN, O. J., COLLETT, K., STEFANSSON, I. M., STRAUME, O., HAUKAAS, S. A., SALVESEN, H. B., OTTE, A. P. & AKSLEN, L. A. 2006. EZH2 expression is associated with high proliferation rate and aggressive tumor subgroups in cutaneous melanoma and cancers of the endometrium, prostate, and breast. *J Clin Oncol,* 24**,** 268-73.

BANNISTER, A. J., ZEGERMAN, P., PARTRIDGE, J. F., MISKA, E. A., THOMAS, J. O., ALLSHIRE, R. C. & KOUZARIDES, T. 2001. Selective recognition of methylated lysine 9 on histone H3 by the HP1 chromo domain. *Nature,* 410**,** 120-4.

BANTIGNIES, F., ROURE, V., COMET, I., LEBLANC, B., SCHUETTENGRUBER, B., BONNET, J., TIXIER, V., MAS, A. & CAVALLI, G. 2011. Polycomb-dependent regulatory contacts between distant Hox loci in Drosophila. *Cell,* 144**,** 214-26.

BARRADAS, M., ANDERTON, E., ACOSTA, J. C., LI, S., BANITO, A., RODRIGUEZ-NIEDENFUHR, M., MAERTENS, G., BANCK, M., ZHOU, M. M., WALSH, M. J., PETERS, G. & GIL, J. 2009. Histone demethylase JMJD3 contributes to epigenetic control of INK4a/ARF by oncogenic RAS. *Genes Dev,* 23**,** 1177-82.

BARTKOVA, J., REZAEI, N., LIONTOS, M., KARAKAIDOS, P., KLETSAS, D., ISSAEVA, N., VASSILIOU, L. V., KOLETTAS, E., NIFOROU, K., ZOUMPOURLIS, V. C., TAKAOKA, M., NAKAGAWA, H., TORT, F., FUGGER, K., JOHANSSON, F., SEHESTED, M., ANDERSEN, C. L., DYRSKJOT, L., ORNTOFT, T., LUKAS, J., KITTAS, C., HELLEDAY, T., HALAZONETIS, T. D., BARTEK, J. & GORGOULIS, V. G. 2006. Oncogene-induced senescence is part of the tumorigenesis barrier imposed by DNA damage checkpoints. *Nature,* 444**,** 633-7.

BEA, S., TORT, F., PINYOL, M., PUIG, X., HERNANDEZ, L., HERNANDEZ, S., FERNANDEZ, P. L., VAN LOHUIZEN, M., COLOMER, D. & CAMPO, E. 2001. BMI-1 gene amplification and overexpression in hematological malignancies occur mainly in mantle cell lymphomas. *Cancer Res,* 61**,** 2409-12.

BEISEL, C. & PARO, R. 2011. Silencing chromatin: comparing modes and mechanisms. *Nat Rev Genet,* 12**,** 123-35.

BERKOVICH, E., MONNAT, R. J., JR. & KASTAN, M. B. 2007. Roles of ATM and NBS1 in chromatin structure modulation and DNA double-strand break repair. *Nat Cell Biol,* 9**,** 683-90.

BERNSTEIN, B. E., MIKKELSEN, T. S., XIE, X., KAMAL, M., HUEBERT, D. J., CUFF, J., FRY, B., MEISSNER, A., WERNIG, M., PLATH, K., JAENISCH, R., WAGSCHAL, A., FEIL, R., SCHREIBER, S. L. & LANDER, E. S. 2006a. A bivalent chromatin structure marks key developmental genes in embryonic stem cells. *Cell,* 125**,** 315-26.

BERNSTEIN, E., DUNCAN, E. M., MASUI, O., GIL, J., HEARD, E. & ALLIS, C. D. 2006b. Mouse polycomb proteins bind differentially to methylated histone H3 and RNA and are enriched in facultative heterochromatin. *Mol Cell Biol,* 26**,** 2560-9.

BEROUKHIM, R., MERMEL, C. H., PORTER, D., WEI, G., RAYCHAUDHURI, S., DONOVAN, J., BARRETINA, J., BOEHM, J. S., DOBSON, J., URASHIMA, M., MC HENRY, K. T., PINCHBACK, R. M., LIGON, A. H., CHO, Y. J., HAERY, L., GREULICH, H., REICH, M., WINCKLER, W., LAWRENCE, M. S., WEIR, B. A., TANAKA, K. E., CHIANG, D. Y., BASS, A. J., LOO, A., HOFFMAN, C., PRENSNER, J., LIEFELD, T., GAO, Q., YECIES, D., SIGNORETTI, S., MAHER, E., KAYE, F. J., SASAKI, H., TEPPER, J. E., FLETCHER, J. A., TABERNERO, J., BASELGA, J., TSAO, M. S., DEMICHELIS, F., RUBIN, M. A., JANNE, P. A., DALY, M. J., NUCERA, C., LEVINE, R. L., EBERT, B. L., GABRIEL, S., RUSTGI, A. K., ANTONESCU, C. R., LADANYI, M., LETAI, A., GARRAWAY, L. A., LODA, M., BEER, D. G., TRUE, L. D., OKAMOTO, A., POMEROY, S. L., SINGER, S., GOLUB, T. R., LANDER, E. S., GETZ, G., SELLERS, W. R. & MEYERSON, M. 2010. The landscape of somatic copy-number alteration across human cancers. *Nature,* 463**,** 899-905.

BIBBY, A. C. & LITCHFIELD, D. W. 2005. The multiple personalities of the regulatory subunit of protein kinase CK2: CK2 dependent and CK2 independent roles reveal a secret identity for CK2beta. *Int J Biol Sci,* 1**,** 67-79.

BIGNELL, G. R., GREENMAN, C. D., DAVIES, H., BUTLER, A. P., EDKINS, S., ANDREWS, J. M., BUCK, G., CHEN, L., BEARE, D., LATIMER, C., WIDAA, S., HINTON, J., FAHEY, C., FU, B., SWAMY, S., DALGLIESH, G. L., TEH, B. T., DELOUKAS, P., YANG, F., CAMPBELL, P. J., FUTREAL, P. A. & STRATTON, M. R. 2010. Signatures of mutation and selection in the cancer genome. *Nature,* 463**,** 893-8.

BISCHOFF, N., OLSEN, B., RAAF, J., BRETNER, M., ISSINGER, O. G. & NIEFIND, K. 2011. Structure of the human protein kinase CK2 catalytic subunit CK2alpha' and interaction thermodynamics with the regulatory subunit CK2beta. *J Mol Biol,* 407**,** 1-12.

BLAYDES, J. P. & HUPP, T. R. 1998. DNA damage triggers DRB-resistant phosphorylation of human p53 at the CK2 site. *Oncogene,* 17**,** 1045-52.

BODNAR, A. G., OUELLETTE, M., FROLKIS, M., HOLT, S. E., CHIU, C. P., MORIN, G. B., HARLEY, C. B., SHAY, J. W., LICHTSTEINER, S. & WRIGHT, W. E. 1998. Extension of life-span by introduction of telomerase into normal human cells. *Science,* 279**,** 349-52.

BOHGAKI, T., BOHGAKI, M. & HAKEM, R. 2010. DNA double-strand break signaling and human disorders. *Genome Integr,* 1**,** 15.

BOLDYREFF, B., MEGGIO, F., PINNA, L. A. & ISSINGER, O. G. 1994. Protein kinase CK2 structure-function relationship: effects of the beta subunit on reconstitution and activity. *Cell Mol Biol Res,* 40**,** 391-9.

BONDARENKO, V. A., STEELE, L. M., UJVARI, A., GAYKALOVA, D. A., KULAEVA, O. I., POLIKANOV, Y. S., LUSE, D. S. & STUDITSKY, V. M. 2006. Nucleosomes can form a polar barrier to transcript elongation by RNA polymerase II. *Mol Cell,* 24**,** 469-79.

BOTHNER, B., LEWIS, W. S., DIGIAMMARINO, E. L., WEBER, J. D., BOTHNER, S. J. & KRIWACKI, R. W. 2001. Defining the molecular basis of Arf and Hdm2 interactions. *J Mol Biol,* 314**,** 263-77.

BOYER, L. A., PLATH, K., ZEITLINGER, J., BRAMBRINK, T., MEDEIROS, L. A., LEE, T. I., LEVINE, S. S., WERNIG, M., TAJONAR, A., RAY, M. K., BELL, G. W., OTTE, A. P., VIDAL, M., GIFFORD, D. K., YOUNG, R. A. & JAENISCH, R. 2006. Polycomb complexes repress developmental regulators in murine embryonic stem cells. *Nature,* 441**,** 349-53.

BRACKEN, A. P., DIETRICH, N., PASINI, D., HANSEN, K. H. & HELIN, K. 2006. Genome-wide mapping of Polycomb target genes unravels their roles in cell fate transitions. *Genes Dev,* 20**,** 1123-36.

BRACKEN, A. P., KLEINE-KOHLBRECHER, D., DIETRICH, N., PASINI, D., GARGIULO, G., BEEKMAN, C., THEILGAARD-MONCH, K., MINUCCI, S., PORSE, B. T., MARINE, J. C., HANSEN, K. H. & HELIN, K. 2007. The Polycomb group proteins bind throughout the INK4A-ARF locus and are disassociated in senescent cells. *Genes Dev,* 21**,** 525-30.

BRACKEN, A. P., PASINI, D., CAPRA, M., PROSPERINI, E., COLLI, E. & HELIN, K. 2003. EZH2 is downstream of the pRB-E2F pathway, essential for proliferation and amplified in cancer. *EMBO J,* 22**,** 5323-35.

BROOKES, S., ROWE, J., GUTIERREZ DEL ARROYO, A., BOND, J. & PETERS, G. 2004. Contribution of p16(INK4a) to replicative senescence of human fibroblasts. *Exp Cell Res,* 298**,** 549-59.

BROOKES, S., ROWE, J., RUAS, M., LLANOS, S., CLARK, P. A., LOMAX, M., JAMES, M. C., VATCHEVA, R., BATES, S., VOUSDEN, K. H., PARRY, D., GRUIS, N., SMIT, N., BERGMAN, W. & PETERS, G. 2002. INK4a-deficient human diploid fibroblasts are resistant to RAS-induced senescence. *EMBO J,* 21**,** 2936-45.

BROWN, J. L., MUCCI, D., WHITELEY, M., DIRKSEN, M. L. & KASSIS, J. A. 1998. The Drosophila Polycomb group gene pleiohomeotic encodes a DNA binding protein with homology to the transcription factor YY1. *Mol Cell,* 1**,** 1057-64.

BRUMMELKAMP, T. R., BERNARDS, R. & AGAMI, R. 2002. A system for stable expression of short interfering RNAs in mammalian cells. *Science,* 296**,** 550-3.

BUCHENAU, P., HODGSON, J., STRUTT, H. & ARNDT-JOVIN, D. J. 1998. The distribution of polycomb-group proteins during cell division and development in Drosophila embryos: impact on models for silencing. *J Cell Biol,* 141**,** 469-81.

BUCHOU, T., VERNET, M., BLOND, O., JENSEN, H. H., POINTU, H., OLSEN, B. B., COCHET, C., ISSINGER, O. G. & BOLDYREFF, B. 2003. Disruption of the regulatory beta subunit of protein kinase CK2 in mice leads to a cell-autonomous defect and early embryonic lethality. *Mol Cell Biol,* 23**,** 908-15.

BUCHWALD, G., VAN DER STOOP, P., WEICHENRIEDER, O., PERRAKIS, A., VAN LOHUIZEN, M. & SIXMA, T. K. 2006. Structure and E3-ligase activity of the Ring-Ring complex of polycomb proteins Bmi1 and Ring1b. *EMBO J,* 25**,** 2465-74.

CALDECOTT, K. W. 2008. Single-strand break repair and genetic disease. *Nat Rev Genet,* 9**,** 619-31.

CALES, C., ROMAN-TRUFERO, M., PAVON, L., SERRANO, I., MELGAR, T., ENDOH, M., PEREZ, C., KOSEKI, H. & VIDAL, M. 2008. Inactivation of the polycomb group protein Ring1B unveils an antiproliferative role in hematopoietic cell expansion and cooperation with tumorigenesis associated with Ink4a deletion. *Mol Cell Biol,* 28**,** 1018-28.

CAMPISI, J. & D'ADDA DI FAGAGNA, F. 2007. Cellular senescence: when bad things happen to good cells. *Nat Rev Mol Cell Biol,* 8**,** 729-40.

CAO, R., WANG, H., HE, J., ERDJUMENT-BROMAGE, H., TEMPST, P. & ZHANG, Y. 2008. Role of hPHF1 in H3K27 methylation and Hox gene silencing. *Mol Cell Biol,* 28**,** 1862-72.

CAO, R., WANG, L., WANG, H., XIA, L., ERDJUMENT-BROMAGE, H., TEMPST, P., JONES, R. S. & ZHANG, Y. 2002. Role of histone H3 lysine 27 methylation in Polycomb-group silencing. *Science,* 298**,** 1039-43.

CHANNAVAJHALA, P. & SELDIN, D. C. 2002. Functional interaction of protein kinase CK2 and c-Myc in lymphomagenesis. *Oncogene,* 21**,** 5280-8.

CHEN, M., LI, D., KREBS, E. G. & COOPER, J. A. 1997. The casein kinase II beta subunit binds to Mos and inhibits Mos activity. *Mol Cell Biol,* 17**,** 1904-12.

CHOU, D. M., ADAMSON, B., DEPHOURE, N. E., TAN, X., NOTTKE, A. C., HUROV, K. E., GYGI, S. P., COLAIACOVO, M. P. & ELLEDGE, S. J. 2010. A chromatin localization screen reveals poly (ADP ribose)-regulated recruitment of the repressive polycomb and NuRD complexes to sites of DNA damage. *Proc Natl Acad Sci U S A,* 107**,** 18475-80.

CHOW, J. & HEARD, E. 2009. X inactivation and the complexities of silencing a sex chromosome. *Curr Opin Cell Biol,* 21**,** 359-66.

CMARKO, D., VERSCHURE, P. J., OTTE, A. P., VAN DRIEL, R. & FAKAN, S. 2003. Polycomb group gene silencing proteins are concentrated in the perichromatin compartment of the mammalian nucleus. *J Cell Sci,* 116**,** 335-43.

COPPE, J. P., PATIL, C. K., RODIER, F., SUN, Y., MUNOZ, D. P., GOLDSTEIN, J., NELSON, P. S., DESPREZ, P. Y. & CAMPISI, J. 2008. Senescence-associated secretory phenotypes reveal cell-nonautonomous functions of oncogenic RAS and the p53 tumor suppressor. *PLoS Biol,* 6**,** 2853-68.

CORE, N., BEL, S., GAUNT, S. J., AURRAND-LIONS, M., PEARCE, J., FISHER, A. & DJABALI, M. 1997. Altered cellular proliferation and mesoderm patterning in Polycomb-M33-deficient mice. *Development,* 124**,** 721-9.

COSTES, S. V., PONOMAREV, A., CHEN, J. L., NGUYEN, D., CUCINOTTA, F. A. & BARCELLOS-HOFF, M. H. 2007. Image-based modeling reveals dynamic redistribution of DNA damage into nuclear sub-domains. *PLoS Comput Biol,* 3**,** e155.

CZERMIN, B., MELFI, R., MCCABE, D., SEITZ, V., IMHOF, A. & PIRROTTA, V. 2002. Drosophila enhancer of Zeste/ESC complexes have a histone H3 methyltransferase activity that marks chromosomal Polycomb sites. *Cell,* 111**,** 185-96.

D'ADDA DI FAGAGNA, F., REAPER, P. M., CLAY-FARRACE, L., FIEGLER, H., CARR, P., VON ZGLINICKI, T., SARETZKI, G., CARTER, N. P. & JACKSON, S. P. 2003. A DNA damage checkpoint response in telomere-initiated senescence. *Nature,* 426**,** 194-8.

DE NAPOLES, M., MERMOUD, J. E., WAKAO, R., TANG, Y. A., ENDOH, M., APPANAH, R., NESTEROVA, T. B., SILVA, J., OTTE, A. P., VIDAL, M., KOSEKI, H. & BROCKDORFF, N. 2004. Polycomb group proteins Ring1A/B link ubiquitylation of histone H2A to heritable gene silencing and X inactivation. *Dev Cell,* 7**,** 663-76.

DESAGHER, S., OSEN-SAND, A., MONTESSUIT, S., MAGNENAT, E., VILBOIS, F., HOCHMANN, A., JOURNOT, L., ANTONSSON, B. & MARTINOU, J. C. 2001. Phosphorylation of bid by casein kinases I and II regulates its cleavage by caspase 8. *Mol Cell,* 8**,** 601-11.

DI MICCO, R., FUMAGALLI, M., CICALESE, A., PICCININ, S., GASPARINI, P., LUISE, C., SCHURRA, C., GARRE, M., NUCIFORO, P. G., BENSIMON, A., MAESTRO, R.,

PELICCI, P. G. & D'ADDA DI FAGAGNA, F. 2006. Oncogene-induced senescence is a DNA damage response triggered by DNA hyper-replication. *Nature,* 444**,** 638-42.

DI MICCO, R., SULLI, G., DOBREVA, M., LIONTOS, M., BOTRUGNO, O. A., GARGIULO, G., DAL ZUFFO, R., MATTI, V., D'ARIO, G., MONTANI, E., MERCURIO, C., HAHN, W. C., GORGOULIS, V., MINUCCI, S. & D'ADDA DI FAGAGNA, F. 2011. Interplay between oncogene-induced DNA damage response and heterochromatin in senescence and cancer. *Nat Cell Biol,* 13**,** 292-302.

DIETRICH, N., BRACKEN, A. P., TRINH, E., SCHJERLING, C. K., KOSEKI, H., RAPPSILBER, J., HELIN, K. & HANSEN, K. H. 2007. Bypass of senescence by the polycomb group protein CBX8 through direct binding to the INK4A-ARF locus. *EMBO J,* 26**,** 1637-48.

DIMRI, G. P., LEE, X., BASILE, G., ACOSTA, M., SCOTT, G., ROSKELLEY, C., MEDRANO, E. E., LINSKENS, M., RUBELJ, I., PEREIRA-SMITH, O. & ET AL. 1995. A biomarker that identifies senescent human cells in culture and in aging skin in vivo. *Proc Natl Acad Sci U S A,* 92**,** 9363-7.

EL MESSAOUDI-AUBERT, S., NICHOLLS, J., MAERTENS, G. N., BROOKES, S., BERNSTEIN, E. & PETERS, G. 2010. Role for the MOV10 RNA helicase in polycomb-mediated repression of the INK4a tumor suppressor. *Nat Struct Mol Biol,* 17**,** 862-8.

ELDERKIN, S., MAERTENS, G. N., ENDOH, M., MALLERY, D. L., MORRICE, N., KOSEKI, H., PETERS, G., BROCKDORFF, N. & HIOM, K. 2007. A phosphorylated form of Mel-18 targets the Ring1B histone H2A ubiquitin ligase to chromatin. *Mol Cell,* 28**,** 107-20.

ELIA, M. C. & BRADLEY, M. O. 1992. Influence of chromatin structure on the induction of DNA double strand breaks by ionizing radiation. *Cancer Res,* 52**,** 1580-6.

ENDOH, M., ENDO, T. A., ENDOH, T., ISONO, K., SHARIF, J., OHARA, O., TOYODA, T., ITO, T., ESKELAND, R., BICKMORE, W. A., VIDAL, M., BERNSTEIN, B. E. & KOSEKI, H. 2012. Histone H2A Mono-Ubiquitination Is a Crucial Step to Mediate PRC1-Dependent Repression of Developmental Genes to Maintain ES Cell Identity. *PLoS Genet,* 8**,** e1002774.

ESKELAND, R., LEEB, M., GRIMES, G. R., KRESS, C., BOYLE, S., SPROUL, D., GILBERT, N., FAN, Y., SKOULTCHI, A. I., WUTZ, A. & BICKMORE, W. A. 2010. Ring1B compacts chromatin structure and represses gene expression independent of histone ubiquitination. *Mol Cell,* 38**,** 452-64.

ESTELLER, M., CORDON-CARDO, C., CORN, P. G., MELTZER, S. J., POHAR, K. S., WATKINS, D. N., CAPELLA, G., PEINADO, M. A., MATIAS-GUIU, X., PRAT, J., BAYLIN, S. B. & HERMAN, J. G. 2001. p14ARF silencing by promoter hypermethylation mediates abnormal intracellular localization of MDM2. *Cancer Res,* 61**,** 2816-21.

FACCHINO, S., ABDOUH, M., CHATOO, W. & BERNIER, G. 2010. BMI1 confers radioresistance to normal and cancerous neural stem cells through recruitment of the DNA damage response machinery. *J Neurosci,* 30**,** 10096-111.

FALCK, J., COATES, J. & JACKSON, S. P. 2005. Conserved modes of recruitment of ATM, ATR and DNA-PKcs to sites of DNA damage. *Nature,* 434**,** 605-11.

FAUST, M., JUNG, M., GUNTHER, J., ZIMMERMANN, R. & MONTENARH, M. 2001. Localization of individual subunits of protein kinase CK2 to the endoplasmic reticulum and to the Golgi apparatus. *Mol Cell Biochem,* 227**,** 73-80.

FAUST, M. & MONTENARH, M. 2000. Subcellular localization of protein kinase CK2. A key to its function? *Cell Tissue Res,* 301**,** 329-40.

FAUST, R. A., GAPANY, M., TRISTANI, P., DAVIS, A., ADAMS, G. L. & AHMED, K. 1996. Elevated protein kinase CK2 activity in chromatin of head and neck tumors: association with malignant transformation. *Cancer Lett,* 101**,** 31-5.

FAUST, R. A., NIEHANS, G., GAPANY, M., HOISTAD, D., KNAPP, D., CHERWITZ, D., DAVIS, A., ADAMS, G. L. & AHMED, K. 1999. Subcellular immunolocalization of protein kinase CK2 in normal and carcinoma cells. *Int J Biochem Cell Biol,* 31**,** 941-9.

FILHOL, O., BAUDIER, J., DELPHIN, C., LOUE-MACKENBACH, P., CHAMBAZ, E. M. & COCHET, C. 1992. Casein kinase II and the tumor suppressor protein P53 associate in a molecular complex that is negatively regulated upon P53 phosphorylation. *J Biol Chem,* 267**,** 20577-83.

FILHOL, O., NUEDA, A., MARTEL, V., GERBER-SCOKAERT, D., BENITEZ, M. J., SOUCHIER, C., SAOUDI, Y. & COCHET, C. 2003. Live-cell fluorescence imaging reveals the dynamics of protein kinase CK2 individual subunits. *Mol Cell Biol,* 23**,** 975-87.

FINK, A. L. 2005. Natively unfolded proteins. *Curr Opin Struct Biol,* 15**,** 35-41.

FISCHLE, W., WANG, Y., JACOBS, S. A., KIM, Y., ALLIS, C. D. & KHORASANIZADEH, S. 2003. Molecular basis for the discrimination of repressive methyl-lysine marks in histone H3 by Polycomb and HP1 chromodomains. *Genes Dev,* 17**,** 1870-81.

FORBES, S. A., BHAMRA, G., BAMFORD, S., DAWSON, E., KOK, C., CLEMENTS, J., MENZIES, A., TEAGUE, J. W., FUTREAL, P. A. & STRATTON, M. R. 2008. The Catalogue of Somatic Mutations in Cancer (COSMIC). *Curr Protoc Hum Genet,* Chapter 10**,** Unit 10 11.

FRANCIS, N. J., KINGSTON, R. E. & WOODCOCK, C. L. 2004. Chromatin compaction by a polycomb group protein complex. *Science,* 306**,** 1574-7.

FRANCIS, N. J., SAURIN, A. J., SHAO, Z. & KINGSTON, R. E. 2001. Reconstitution of a functional core polycomb repressive complex. *Mol Cell,* 8**,** 545-56.

FRANKE, A., DECAMILLIS, M., ZINK, D., CHENG, N., BROCK, H. W. & PARO, R. 1992. Polycomb and polyhomeotic are constituents of a multimeric protein complex in chromatin of Drosophila melanogaster. *EMBO J,* 11**,** 2941-50.

FUMAGALLI, M., ROSSIELLO, F., CLERICI, M., BAROZZI, S., CITTARO, D., KAPLUNOV, J. M., BUCCI, G., DOBREVA, M., MATTI, V., BEAUSEJOUR, C. M., HERBIG, U., LONGHESE, M. P. & D'ADDA DI FAGAGNA, F. 2012. Telomeric DNA

damage is irreparable and causes persistent DNA-damage-response activation. *Nat Cell Biol,* 14**,** 355-65.

GAGRICA, S., BROOKES, S., ANDERTON, E., ROWE, J. & PETERS, G. 2012. Contrasting behavior of the p18INK4c and p16INK4a tumor suppressors in both replicative and oncogene-induced senescence. *Cancer Res,* 72**,** 165-75.

GALANTY, Y., BELOTSERKOVSKAYA, R., COATES, J., POLO, S., MILLER, K. M. & JACKSON, S. P. 2009. Mammalian SUMO E3-ligases PIAS1 and PIAS4 promote responses to DNA double-strand breaks. *Nature,* 462**,** 935-9.

GAO, Z., ZHANG, J., BONASIO, R., STRINO, F., SAWAI, A., PARISI, F., KLUGER, Y. & REINBERG, D. 2012. PCGF homologs, CBX proteins, and RYBP define functionally distinct PRC1 family complexes. *Mol Cell,* 45**,** 344-56.

GAPANY, M., FAUST, R. A., TAWFIC, S., DAVIS, A., ADAMS, G. L. & AHMED, K. 1995. Association of elevated protein kinase CK2 activity with aggressive behavior of squamous cell carcinoma of the head and neck. *Mol Med,* 1**,** 659-66.

GEARHART, M. D., CORCORAN, C. M., WAMSTAD, J. A. & BARDWELL, V. J. 2006. Polycomb group and SCF ubiquitin ligases are found in a novel BCOR complex that is recruited to BCL6 targets. *Mol Cell Biol,* 26**,** 6880-9.

GIDEKEL, S., PIZOV, G., BERGMAN, Y. & PIKARSKY, E. 2003. Oct-3/4 is a dose-dependent oncogenic fate determinant. *Cancer Cell,* 4**,** 361-70.

GIL, J., BERNARD, D., MARTINEZ, D. & BEACH, D. 2004. Polycomb CBX7 has a unifying role in cellular lifespan. *Nat Cell Biol,* 6**,** 67-72.

GIL, J. & PETERS, G. 2006. Regulation of the INK4b-ARF-INK4a tumour suppressor locus: all for one or one for all. *Nat Rev Mol Cell Biol,* 7**,** 667-77.

GILBERT, N. & ALLAN, J. 2001. Distinctive higher-order chromatin structure at mammalian centromeres. *Proc Natl Acad Sci U S A,* 98**,** 11949-54.

GINJALA, V., NACERDDINE, K., KULKARNI, A., OZA, J., HILL, S. J., YAO, M., CITTERIO, E., VAN LOHUIZEN, M. & GANESAN, S. 2011. BMI1 is recruited to DNA breaks and contributes to DNA damage-induced H2A ubiquitination and repair. *Mol Cell Biol,* 31**,** 1972-82.

GLOTZER, M., MURRAY, A. W. & KIRSCHNER, M. W. 1991. Cyclin is degraded by the ubiquitin pathway. *Nature,* 349**,** 132-8.

GOLDBERG, M. L., COLVIN, R. A. & MELLIN, A. F. 1989. The Drosophila zeste locus is nonessential. *Genetics,* 123**,** 145-55.

GRANKOWSKI, N., BOLDYREFF, B. & ISSINGER, O. G. 1991. Isolation and characterization of recombinant human casein kinase II subunits alpha and beta from bacteria. *Eur J Biochem,* 198**,** 25-30.

GRIMAUD, C., BANTIGNIES, F., PAL-BHADRA, M., GHANA, P., BHADRA, U. & CAVALLI, G. 2006. RNAi components are required for nuclear clustering of Polycomb group response elements. *Cell,* 124**,** 957-71.

GUERRA, B. & ISSINGER, O. G. 1998. p53 and the ribosomal protein L5 participate in high molecular mass complex formation with protein kinase CK2 in murine teratocarcinoma cell line F9 after serum stimulation and cisplatin treatment. *FEBS Lett,* 434**,** 115-20.

GUERRA, B. & ISSINGER, O. G. 1999. Protein kinase CK2 and its role in cellular proliferation, development and pathology. *Electrophoresis,* 20**,** 391-408.

GUERRA, B., SIEMER, S., BOLDYREFF, B. & ISSINGER, O. G. 1999. Protein kinase CK2: evidence for a protein kinase CK2beta subunit fraction, devoid of the catalytic CK2alpha subunit, in mouse brain and testicles. *FEBS Lett,* 462**,** 353-7.

GUO, C., YU, S., DAVIS, A. T., WANG, H., GREEN, J. E. & AHMED, K. 2001. A potential role of nuclear matrix-associated protein kinase CK2 in protection against drug-induced apoptosis in cancer cells. *J Biol Chem,* 276**,** 5992-9.

GUPTA, R. A., SHAH, N., WANG, K. C., KIM, J., HORLINGS, H. M., WONG, D. J., TSAI, M. C., HUNG, T., ARGANI, P., RINN, J. L., WANG, Y., BRZOSKA, P., KONG, B., LI, R., WEST, R. B., VAN DE VIJVER, M. J., SUKUMAR, S. & CHANG, H. Y. 2010. Long non-coding RNA HOTAIR reprograms chromatin state to promote cancer metastasis. *Nature,* 464**,** 1071-6.

GUTIERREZ, L., OKTABA, K., SCHEUERMANN, J. C., GAMBETTA, M. C., LY-HARTIG, N. & MULLER, J. 2012. The role of the histone H2A ubiquitinase Sce in Polycomb repression. *Development,* 139**,** 117-27.

HAAF, T., GOLUB, E. I., REDDY, G., RADDING, C. M. & WARD, D. C. 1995. Nuclear foci of mammalian Rad51 recombination protein in somatic cells after DNA damage and its localization in synaptonemal complexes. *Proc Natl Acad Sci U S A,* 92**,** 2298-302.

HAGEMANN, C., KALMES, A., WIXLER, V., WIXLER, L., SCHUSTER, T. & RAPP, U. R. 1997. The regulatory subunit of protein kinase CK2 is a specific A-Raf activator. *FEBS Lett,* 403**,** 200-2.

HANAHAN, D. & WEINBERG, R. A. 2000. The hallmarks of cancer. *Cell,* 100**,** 57-70.

HANAHAN, D. & WEINBERG, R. A. 2011. Hallmarks of cancer: the next generation. *Cell,* 144**,** 646-74.

HARPER, J. W. & ELLEDGE, S. J. 2007. The DNA damage response: ten years after. *Mol Cell,* 28**,** 739-45.

HARTLERODE, A. J. & SCULLY, R. 2009. Mechanisms of double-strand break repair in somatic mammalian cells. *Biochem J,* 423**,** 157-68.

HAUPT, Y., ALEXANDER, W. S., BARRI, G., KLINKEN, S. P. & ADAMS, J. M. 1991. Novel zinc finger gene implicated as myc collaborator by retrovirally accelerated lymphomagenesis in E mu-myc transgenic mice. *Cell,* 65**,** 753-63.

HAYFLICK, L. & MOORHEAD, P. S. 1961. The serial cultivation of human diploid cell strains. *Exp Cell Res,* 25**,** 585-621.

HERNANDEZ-MUNOZ, I., TAGHAVI, P., KUIJL, C., NEEFJES, J. & VAN LOHUIZEN, M. 2005. Association of BMI1 with polycomb bodies is dynamic and requires PRC2/EZH2 and the maintenance DNA methyltransferase DNMT1. *Mol Cell Biol,* 25**,** 11047-58.

HIYAMA, E. & HIYAMA, K. 2007. Telomere and telomerase in stem cells. *Br J Cancer,* 96**,** 1020-4.

HONG, L., SCHROTH, G. P., MATTHEWS, H. R., YAU, P. & BRADBURY, E. M. 1993. Studies of the DNA binding properties of histone H4 amino terminus. Thermal denaturation studies reveal that acetylation markedly reduces the binding constant of the H4 "tail" to DNA. *J Biol Chem,* 268**,** 305-14.

HONG, Z., JIANG, J., LAN, L., NAKAJIMA, S., KANNO, S., KOSEKI, H. & YASUI, A. 2008. A polycomb group protein, PHF1, is involved in the response to DNA double-strand breaks in human cell. *Nucleic Acids Res,* 36**,** 2939-47.

HOREJSI, Z., TAKAI, H., ADELMAN, C. A., COLLIS, S. J., FLYNN, H., MASLEN, S., SKEHEL, J. M., DE LANGE, T. & BOULTON, S. J. 2010. CK2 phospho-dependent binding of R2TP complex to TEL2 is essential for mTOR and SMG1 stability. *Mol Cell,* 39**,** 839-50.

HUEN, M. S., GRANT, R., MANKE, I., MINN, K., YU, X., YAFFE, M. B. & CHEN, J. 2007. RNF8 transduces the DNA-damage signal via histone ubiquitylation and checkpoint protein assembly. *Cell,* 131**,** 901-14.

IACOVONI, J. S., CARON, P., LASSADI, I., NICOLAS, E., MASSIP, L., TROUCHE, D. & LEGUBE, G. 2010. High-resolution profiling of gammaH2AX around DNA double strand breaks in the mammalian genome. *EMBO J,* 29**,** 1446-57.

IIMOTO, D. S., MASLIAH, E., DETERESA, R., TERRY, R. D. & SAITOH, T. 1990. Aberrant casein kinase II in Alzheimer's disease. *Brain Res,* 507**,** 273-80.

ISMAIL, I. H., ANDRIN, C., MCDONALD, D. & HENDZEL, M. J. 2010. BMI1-mediated histone ubiquitylation promotes DNA double-strand break repair. *J Cell Biol,* 191**,** 45-60.

ISMAIL, I. H., GAGNE, J. P., CARON, M. C., MCDONALD, D., XU, Z., MASSON, J. Y., POIRIER, G. G. & HENDZEL, M. J. 2012. CBX4-mediated SUMO modification regulates BMI1 recruitment at sites of DNA damage. *Nucleic Acids Res,* 40**,** 5497-510.

ITAHANA, K., ZOU, Y., ITAHANA, Y., MARTINEZ, J. L., BEAUSEJOUR, C., JACOBS, J. J., VAN LOHUIZEN, M., BAND, V., CAMPISI, J. & DIMRI, G. P. 2003. Control of the replicative life span of human fibroblasts by p16 and the polycomb protein Bmi-1. *Mol Cell Biol,* 23**,** 389-401.

IWAMA, A., OGURO, H., NEGISHI, M., KATO, Y., MORITA, Y., TSUKUI, H., EMA, H., KAMIJO, T., KATOH-FUKUI, Y., KOSEKI, H., VAN LOHUIZEN, M. & NAKAUCHI, H. 2004. Enhanced self-renewal of hematopoietic stem cells mediated by the polycomb gene product Bmi-1. *Immunity,* 21**,** 843-51.

JACKSON, S. P. & BARTEK, J. 2009. The DNA-damage response in human biology and disease. *Nature,* 461**,** 1071-8.

JACOBS, J. J., KIEBOOM, K., MARINO, S., DEPINHO, R. A. & VAN LOHUIZEN, M. 1999a. The oncogene and Polycomb-group gene bmi-1 regulates cell proliferation and senescence through the ink4a locus. *Nature,* 397**,** 164-8.

JACOBS, J. J., SCHEIJEN, B., VONCKEN, J. W., KIEBOOM, K., BERNS, A. & VAN LOHUIZEN, M. 1999b. Bmi-1 collaborates with c-Myc in tumorigenesis by inhibiting c-Myc-induced apoptosis via INK4a/ARF. *Genes Dev,* 13**,** 2678-90.

JENUWEIN, T. & ALLIS, C. D. 2001. Translating the histone code. *Science,* 293**,** 1074-80.

KALLIN, E. M., CAO, R., JOTHI, R., XIA, K., CUI, K., ZHAO, K. & ZHANG, Y. 2009. Genome-wide uH2A localization analysis highlights Bmi1-dependent deposition of the mark at repressed genes. *PLoS Genet,* 5**,** e1000506.

KAMB, A., GRUIS, N. A., WEAVER-FELDHAUS, J., LIU, Q., HARSHMAN, K., TAVTIGIAN, S. V., STOCKERT, E., DAY, R. S., 3RD, JOHNSON, B. E. & SKOLNICK, M. H. 1994. A cell cycle regulator potentially involved in genesis of many tumor types. *Science,* 264**,** 436-40.

KAMIJO, T., ZINDY, F., ROUSSEL, M. F., QUELLE, D. E., DOWNING, J. R., ASHMUN, R. A., GROSVELD, G. & SHERR, C. J. 1997. Tumor suppression at the mouse INK4a locus mediated by the alternative reading frame product p19ARF. *Cell,* 91**,** 649-59.

KAMMINGA, L. M., BYSTRYKH, L. V., DE BOER, A., HOUWER, S., DOUMA, J., WEERSING, E., DONTJE, B. & DE HAAN, G. 2006. The Polycomb group gene Ezh2 prevents hematopoietic stem cell exhaustion. *Blood,* 107**,** 2170-9.

KANG, T. W., YEVSA, T., WOLLER, N., HOENICKE, L., WUESTEFELD, T., DAUCH, D., HOHMEYER, A., GEREKE, M., RUDALSKA, R., POTAPOVA, A., IKEN, M., VUCUR, M., WEISS, S., HEIKENWALDER, M., KHAN, S., GIL, J., BRUDER, D., MANNS, M., SCHIRMACHER, P., TACKE, F., OTT, M., LUEDDE, T., LONGERICH, T., KUBICKA, S. & ZENDER, L. 2011. Senescence surveillance of pre-malignant hepatocytes limits liver cancer development. *Nature,* 479**,** 547-51.

KANHERE, A., VIIRI, K., ARAUJO, C. C., RASAIYAAH, J., BOUWMAN, R. D., WHYTE, W. A., PEREIRA, C. F., BROOKES, E., WALKER, K., BELL, G. W., POMBO, A., FISHER, A. G., YOUNG, R. A. & JENNER, R. G. 2010. Short RNAs are transcribed from repressed polycomb target genes and interact with polycomb repressive complex-2. *Mol Cell,* 38**,** 675-88.

KELLER, D. M., ZENG, X., WANG, Y., ZHANG, Q. H., KAPOOR, M., SHU, H., GOODMAN, R., LOZANO, G., ZHAO, Y. & LU, H. 2001. A DNA damage-induced p53 serine 392 kinase complex contains CK2, hSpt16, and SSRP1. *Mol Cell,* 7**,** 283-92.

KELLIHER, M. A., SELDIN, D. C. & LEDER, P. 1996. Tal-1 induces T cell acute lymphoblastic leukemia accelerated by casein kinase IIalpha. *EMBO J,* 15**,** 5160-6.

KENNISON, J. A. 1995. The Polycomb and trithorax group proteins of Drosophila: trans-regulators of homeotic gene function. *Annu Rev Genet,* 29**,** 289-303.

KHORASANIZADEH, S. 2004. The nucleosome: from genomic organization to genomic regulation. *Cell,* 116**,** 259-72.

KIM, C. A., GINGERY, M., PILPA, R. M. & BOWIE, J. U. 2002. The SAM domain of polyhomeotic forms a helical polymer. *Nat Struct Biol,* 9**,** 453-7.

KIM, E. K., KANG, J. Y., RHO, Y. H., KIM, Y. S., KIM, D. S. & BAE, Y. S. 2009. Silencing of the CKII alpha and CKII alpha' genes during cellular senescence is mediated by DNA methylation. *Gene,* 431**,** 55-60.

KING, R. W., GLOTZER, M. & KIRSCHNER, M. W. 1996. Mutagenic analysis of the destruction signal of mitotic cyclins and structural characterization of ubiquitinated intermediates. *Mol Biol Cell,* 7**,** 1343-57.

KLEER, C. G., CAO, Q., VARAMBALLY, S., SHEN, R., OTA, I., TOMLINS, S. A., GHOSH, D., SEWALT, R. G., OTTE, A. P., HAYES, D. F., SABEL, M. S., LIVANT, D., WEISS, S. J., RUBIN, M. A. & CHINNAIYAN, A. M. 2003. EZH2 is a marker of aggressive breast cancer and promotes neoplastic transformation of breast epithelial cells. *Proc Natl Acad Sci U S A,* 100**,** 11606-11.

KLYMENKO, T., PAPP, B., FISCHLE, W., KOCHER, T., SCHELDER, M., FRITSCH, C., WILD, B., WILM, M. & MULLER, J. 2006. A Polycomb group protein complex with sequence-specific DNA-binding and selective methyl-lysine-binding activities. *Genes Dev,* 20**,** 1110-22.

KOLAS, N. K., CHAPMAN, J. R., NAKADA, S., YLANKO, J., CHAHWAN, R., SWEENEY, F. D., PANIER, S., MENDEZ, M., WILDENHAIN, J., THOMSON, T. M., PELLETIER, L., JACKSON, S. P. & DUROCHER, D. 2007. Orchestration of the DNA-damage response by the RNF8 ubiquitin ligase. *Science,* 318**,** 1637-40.

KOTAKE, Y., NAKAGAWA, T., KITAGAWA, K., SUZUKI, S., LIU, N., KITAGAWA, M. & XIONG, Y. 2011. Long non-coding RNA ANRIL is required for the PRC2 recruitment to and silencing of p15(INK4B) tumor suppressor gene. *Oncogene,* 30**,** 1956-62.

KREK, W., MARIDOR, G. & NIGG, E. A. 1992. Casein kinase II is a predominantly nuclear enzyme. *J Cell Biol,* 116**,** 43-55.

KRIMPENFORT, P., QUON, K. C., MOOI, W. J., LOONSTRA, A. & BERNS, A. 2001. Loss of p16Ink4a confers susceptibility to metastatic melanoma in mice. *Nature,* 413**,** 83-6.

KRIPPNER-HEIDENREICH, A., TALANIAN, R. V., SEKUL, R., KRAFT, R., THOLE, H., OTTLEBEN, H. & LUSCHER, B. 2001. Targeting of the transcription factor Max during apoptosis: phosphorylation-regulated cleavage by caspase-5 at an unusual glutamic acid residue in position P1. *Biochem J,* 358**,** 705-15.

KU, M., KOCHE, R. P., RHEINBAY, E., MENDENHALL, E. M., ENDOH, M., MIKKELSEN, T. S., PRESSER, A., NUSBAUM, C., XIE, X., CHI, A. S., ADLI, M., KASIF, S., PTASZEK, L. M., COWAN, C. A., LANDER, E. S., KOSEKI, H. & BERNSTEIN, B. E. 2008. Genomewide analysis of PRC1 and PRC2 occupancy identifies two classes of bivalent domains. *PLoS Genet,* 4**,** e1000242.

KUILMAN, T., MICHALOGLOU, C., VREDEVELD, L. C., DOUMA, S., VAN DOORN, R., DESMET, C. J., AARDEN, L. A., MOOI, W. J. & PEEPER, D. S. 2008. Oncogene-induced senescence relayed by an interleukin-dependent inflammatory network. *Cell,* 133**,** 1019-31.

KUZMICHEV, A., NISHIOKA, K., ERDJUMENT-BROMAGE, H., TEMPST, P. & REINBERG, D. 2002. Histone methyltransferase activity associated with a human multiprotein complex containing the Enhancer of Zeste protein. *Genes Dev,* 16**,** 2893-905.

KYBA, M. & BROCK, H. W. 1998. The SAM domain of polyhomeotic, RAE28, and scm mediates specific interactions through conserved residues. *Dev Genet,* 22**,** 74-84.

LACHNER, M., O'CARROLL, D., REA, S., MECHTLER, K. & JENUWEIN, T. 2001. Methylation of histone H3 lysine 9 creates a binding site for HP1 proteins. *Nature,* 410**,** 116-20.

LAGAROU, A., MOHD-SARIP, A., MOSHKIN, Y. M., CHALKLEY, G. E., BEZSTAROSTI, K., DEMMERS, J. A. & VERRIJZER, C. P. 2008. dKDM2 couples histone H2A ubiquitylation to histone H3 demethylation during Polycomb group silencing. *Genes Dev,* 22**,** 2799-810.

LANDESMAN-BOLLAG, E., CHANNAVAJHALA, P. L., CARDIFF, R. D. & SELDIN, D. C. 1998. p53 deficiency and misexpression of protein kinase CK2alpha collaborate in the development of thymic lymphomas in mice. *Oncogene,* 16**,** 2965-74.

LANZUOLO, C., ROURE, V., DEKKER, J., BANTIGNIES, F. & ORLANDO, V. 2007. Polycomb response elements mediate the formation of chromosome higher-order structures in the bithorax complex. *Nat Cell Biol,* 9**,** 1167-74.

LARAMAS, M., PASQUIER, D., FILHOL, O., RINGEISEN, F., DESCOTES, J. L. & COCHET, C. 2007. Nuclear localization of protein kinase CK2 catalytic subunit (CK2alpha) is associated with poor prognostic factors in human prostate cancer. *Eur J Cancer,* 43**,** 928-34.

LAVIN, M. F. 2007. ATM and the Mre11 complex combine to recognize and signal DNA double-strand breaks. *Oncogene,* 26**,** 7749-58.

LEE, B. Y., HAN, J. A., IM, J. S., MORRONE, A., JOHUNG, K., GOODWIN, E. C., KLEIJER, W. J., DIMAIO, D. & HWANG, E. S. 2006a. Senescence-associated beta-galactosidase is lysosomal beta-galactosidase. *Aging Cell,* 5**,** 187-95.

LEE, J. H. & PAULL, T. T. 2005. ATM activation by DNA double-strand breaks through the Mre11-Rad50-Nbs1 complex. *Science,* 308**,** 551-4.

LEE, M. G., VILLA, R., TROJER, P., NORMAN, J., YAN, K. P., REINBERG, D., DI CROCE, L. & SHIEKHATTAR, R. 2007. Demethylation of H3K27 regulates polycomb recruitment and H2A ubiquitination. *Science,* 318**,** 447-50.

LEE, T. I., JENNER, R. G., BOYER, L. A., GUENTHER, M. G., LEVINE, S. S., KUMAR, R. M., CHEVALIER, B., JOHNSTONE, S. E., COLE, M. F., ISONO, K., KOSEKI, H., FUCHIKAMI, T., ABE, K., MURRAY, H. L., ZUCKER, J. P., YUAN, B., BELL, G. W., HERBOLSHEIMER, E., HANNETT, N. M., SUN, K., ODOM, D. T., OTTE, A. P., VOLKERT, T. L., BARTEL, D. P., MELTON, D. A., GIFFORD, D. K., JAENISCH, R. & YOUNG, R. A. 2006b. Control of developmental regulators by Polycomb in human embryonic stem cells. *Cell,* 125**,** 301-13.

LEHMANN, L., FERRARI, R., VASHISHT, A. A., WOHLSCHLEGEL, J. A., KURDISTANI, S. K. & CAREY, M. 2012. Polycomb Repressive Complex 1 (PRC1) Disassembles RNA Polymerase II Preinitiation Complexes. *J Biol Chem*.

LESSARD, J. & SAUVAGEAU, G. 2003. Bmi-1 determines the proliferative capacity of normal and leukaemic stem cells. *Nature,* 423**,** 255-60.

LEUNG, C., LINGBEEK, M., SHAKHOVA, O., LIU, J., TANGER, E., SAREMASLANI, P., VAN LOHUIZEN, M. & MARINO, S. 2004. Bmi1 is essential for cerebellar development and is overexpressed in human medulloblastomas. *Nature,* 428**,** 337-41.

LEVINE, S. S., WEISS, A., ERDJUMENT-BROMAGE, H., SHAO, Z., TEMPST, P. & KINGSTON, R. E. 2002. The core of the polycomb repressive complex is compositionally and functionally conserved in flies and humans. *Mol Cell Biol,* 22**,** 6070-8.

LEWIS, P. H. 1947. Melanogaster- New mutants: Report of Pamela H. Lewis. *Dros. Inform. Serv,* 21**,** 69.

LI, P. F., LI, J., MULLER, E. C., OTTO, A., DIETZ, R. & VON HARSDORF, R. 2002. Phosphorylation by protein kinase CK2: a signaling switch for the caspase-inhibiting protein ARC. *Mol Cell,* 10**,** 247-58.

LI, Z., CAO, R., WANG, M., MYERS, M. P., ZHANG, Y. & XU, R. M. 2006. Structure of a Bmi-1-Ring1B polycomb group ubiquitin ligase complex. *J Biol Chem,* 281**,** 20643-9.

LITCHFIELD, D. W. 2003. Protein kinase CK2: structure, regulation and role in cellular decisions of life and death. *Biochem J,* 369**,** 1-15.

LITCHFIELD, D. W., BOSC, D. G. & SLOMINSKI, E. 1995. The protein kinase from mitotic human cells that phosphorylates Ser-209 on the casein kinase II beta-subunit is p34cdc2. *Biochim Biophys Acta,* 1269**,** 69-78.

LITCHFIELD, D. W., LUSCHER, B., LOZEMAN, F. J., EISENMAN, R. N. & KREBS, E. G. 1992. Phosphorylation of casein kinase II by p34cdc2 in vitro and at mitosis. *J Biol Chem,* 267**,** 13943-51.

LONIE, A., D'ANDREA, R., PARO, R. & SAINT, R. 1994. Molecular characterisation of the Polycomblike gene of Drosophila melanogaster, a trans-acting negative regulator of homeotic gene expression. *Development,* 120**,** 2629-36.

LOOIJENGA, L. H., STOOP, H., DE LEEUW, H. P., DE GOUVEIA BRAZAO, C. A., GILLIS, A. J., VAN ROOZENDAAL, K. E., VAN ZOELEN, E. J., WEBER, R. F., WOLFFENBUTTEL, K. P., VAN DEKKEN, H., HONECKER, F., BOKEMEYER, C., PERLMAN, E. J., SCHNEIDER, D. T., KONONEN, J., SAUTER, G. & OOSTERHUIS, J. W. 2003. POU5F1 (OCT3/4) identifies cells with pluripotent potential in human germ cell tumors. *Cancer Res,* 63**,** 2244-50.

LORCH, Y., LAPOINTE, J. W. & KORNBERG, R. D. 1987. Nucleosomes inhibit the initiation of transcription but allow chain elongation with the displacement of histones. *Cell,* 49**,** 203-10.

LORENZ, P., PEPPERKOK, R., ANSORGE, W. & PYERIN, W. 1993. Cell biological studies with monoclonal and polyclonal antibodies against human casein kinase II subunit beta demonstrate participation of the kinase in mitogenic signaling. *J Biol Chem,* 268**,** 2733-9.

LOU, D. Y., DOMINGUEZ, I., TOSELLI, P., LANDESMAN-BOLLAG, E., O'BRIEN, C. & SELDIN, D. C. 2008. The alpha catalytic subunit of protein kinase CK2 is required for mouse embryonic development. *Mol Cell Biol,* 28**,** 131-9.

LOWE, S. W. & SHERR, C. J. 2003. Tumor suppression by Ink4a-Arf: progress and puzzles. *Curr Opin Genet Dev,* 13**,** 77-83.

LU, K. P. & ZHOU, X. Z. 2007. The prolyl isomerase PIN1: a pivotal new twist in phosphorylation signalling and disease. *Nat Rev Mol Cell Biol,* 8**,** 904-16.

MAERTENS, G. N., EL MESSAOUDI-AUBERT, S., ELDERKIN, S., HIOM, K. & PETERS, G. 2010. Ubiquitin-specific proteases 7 and 11 modulate Polycomb regulation of the INK4a tumour suppressor. *EMBO J,* 29**,** 2553-65.

MAERTENS, G. N., EL MESSAOUDI-AUBERT, S., RACEK, T., STOCK, J. K., NICHOLLS, J., RODRIGUEZ-NIEDENFUHR, M., GIL, J. & PETERS, G. 2009. Several distinct polycomb complexes regulate and co-localize on the INK4a tumor suppressor locus. *PLoS One,* 4**,** e6380.

MAILAND, N., BEKKER-JENSEN, S., FAUSTRUP, H., MELANDER, F., BARTEK, J., LUKAS, C. & LUKAS, J. 2007. RNF8 ubiquitylates histones at DNA double-strand breaks and promotes assembly of repair proteins. *Cell,* 131**,** 887-900.

MARIN, O., MEGGIO, F., MARCHIORI, F., BORIN, G. & PINNA, L. A. 1986. Site specificity of casein kinase-2 (TS) from rat liver cytosol. A study with model peptide substrates. *Eur J Biochem,* 160**,** 239-44.

MARIN, O., MEGGIO, F. & PINNA, L. A. 1999a. Structural features underlying the unusual mode of calmodulin phosphorylation by protein kinase CK2: A study with synthetic calmodulin fragments. *Biochem Biophys Res Commun,* 256**,** 442-6.

MARIN, O., MEGGIO, F., SARNO, S., CESARO, L., PAGANO, M. A. & PINNA, L. A. 1999b. Tyrosine versus serine/threonine phosphorylation by protein kinase casein kinase-2. A study with peptide substrates derived from immunophilin Fpr3. *J Biol Chem,* 274**,** 29260-5.

MARTEL, V., FILHOL, O., NUEDA, A., GERBER, D., BENITEZ, M. J. & COCHET, C. 2001. Visualization and molecular analysis of nuclear import of protein kinase CK2 subunits in living cells. *Mol Cell Biochem,* 227**,** 81-90.

MARTIN, E. C. & ADLER, P. N. 1993. The Polycomb group gene Posterior Sex Combs encodes a chromosomal protein. *Development,* 117**,** 641-55.

MASER, R. S., MONSEN, K. J., NELMS, B. E. & PETRINI, J. H. 1997. hMre11 and hRad50 nuclear foci are induced during the normal cellular response to DNA double-strand breaks. *Mol Cell Biol,* 17**,** 6087-96.

MEGGIO, F., MARCHIORI, F., BORIN, G., CHESSA, G. & PINNA, L. A. 1984. Synthetic peptides including acidic clusters as substrates and inhibitors of rat liver casein kinase TS (type-2). *J Biol Chem,* 259**,** 14576-9.

MEGGIO, F., MARIN, O. & PINNA, L. A. 1994. Substrate specificity of protein kinase CK2. *Cell Mol Biol Res,* 40**,** 401-9.

MEGGIO, F. & PINNA, L. A. 2003. One-thousand-and-one substrates of protein kinase CK2? *Faseb J,* 17**,** 349-68.

MESSENGER, M. M., SAULNIER, R. B., GILCHRIST, A. D., DIAMOND, P., GORBSKY, G. J. & LITCHFIELD, D. W. 2002. Interactions between protein kinase CK2 and Pin1. Evidence for phosphorylation-dependent interactions. *J Biol Chem,* 277**,** 23054-64.

MESSMER, S., FRANKE, A. & PARO, R. 1992. Analysis of the functional role of the Polycomb chromo domain in Drosophila melanogaster. *Genes Dev,* 6**,** 1241-54.

MICHAEL, D. & OREN, M. 2003. The p53-Mdm2 module and the ubiquitin system. *Semin Cancer Biol,* 13**,** 49-58.

MICHALOGLOU, C., VREDEVELD, L. C., SOENGAS, M. S., DENOYELLE, C., KUILMAN, T., VAN DER HORST, C. M., MAJOOR, D. M., SHAY, J. W., MOOI, W. J. & PEEPER, D. S. 2005. BRAFE600-associated senescence-like cell cycle arrest of human naevi. *Nature,* 436**,** 720-4.

MILLER, J. C., HOLMES, M. C., WANG, J., GUSCHIN, D. Y., LEE, Y. L., RUPNIEWSKI, I., BEAUSEJOUR, C. M., WAITE, A. J., WANG, N. S., KIM, K. A., GREGORY, P. D., PABO, C. O. & REBAR, E. J. 2007. An improved zinc-finger nuclease architecture for highly specific genome editing. *Nat Biotechnol,* 25**,** 778-85.

MIN, J., ZHANG, Y. & XU, R. M. 2003. Structural basis for specific binding of Polycomb chromodomain to histone H3 methylated at Lys 27. *Genes Dev,* 17**,** 1823-8.

MINC, E., ALLORY, Y., WORMAN, H. J., COURVALIN, J. C. & BUENDIA, B. 1999. Localization and phosphorylation of HP1 proteins during the cell cycle in mammalian cells. *Chromosoma,* 108**,** 220-34.

MISTELI, T. & SOUTOGLOU, E. 2009. The emerging role of nuclear architecture in DNA repair and genome maintenance. *Nat Rev Mol Cell Biol,* 10**,** 243-54.

MIYATA, Y. & NISHIDA, E. 2005. CK2 binds, phosphorylates, and regulates its pivotal substrate Cdc37, an Hsp90-cochaperone. *Mol Cell Biochem,* 274**,** 171-9.

MOHAMMAD, H. P., CAI, Y., MCGARVEY, K. M., EASWARAN, H., VAN NESTE, L., OHM, J. E., O'HAGAN, H. M. & BAYLIN, S. B. 2009. Polycomb CBX7 promotes initiation of heritable repression of genes frequently silenced with cancer-specific DNA hypermethylation. *Cancer Res,* 69**,** 6322-30.

MOHD-SARIP, A., VENTURINI, F., CHALKLEY, G. E. & VERRIJZER, C. P. 2002. Pleiohomeotic can link polycomb to DNA and mediate transcriptional repression. *Mol Cell Biol,* 22**,** 7473-83.

MOHN, F., WEBER, M., REBHAN, M., ROLOFF, T. C., RICHTER, J., STADLER, M. B., BIBEL, M. & SCHUBELER, D. 2008. Lineage-specific polycomb targets and de novo DNA methylation define restriction and potential of neuronal progenitors. *Mol Cell,* 30**,** 755-66.

MOLOFSKY, A. V., PARDAL, R., IWASHITA, T., PARK, I. K., CLARKE, M. F. & MORRISON, S. J. 2003. Bmi-1 dependence distinguishes neural stem cell self-renewal from progenitor proliferation. *Nature,* 425**,** 962-7.

MOREY, L., PASCUAL, G., COZZUTO, L., ROMA, G., WUTZ, A., BENITAH, S. A. & DI CROCE, L. 2012. Nonoverlapping functions of the Polycomb group Cbx family of proteins in embryonic stem cells. *Cell Stem Cell,* 10**,** 47-62.

MORGENSTERN, J. P. & LAND, H. 1990. Advanced mammalian gene transfer: high titre retroviral vectors with multiple drug selection markers and a complementary helper-free packaging cell line. *Nucleic Acids Res,* 18**,** 3587-96.

MULLER, J., HART, C. M., FRANCIS, N. J., VARGAS, M. L., SENGUPTA, A., WILD, B., MILLER, E. L., O'CONNOR, M. B., KINGSTON, R. E. & SIMON, J. A. 2002. Histone methyltransferase activity of a Drosophila Polycomb group repressor complex. *Cell,* 111**,** 197-208.

MULLER, J. & KASSIS, J. A. 2006. Polycomb response elements and targeting of Polycomb group proteins in Drosophila. *Curr Opin Genet Dev,* 16**,** 476-84.

NAKAYAMA, J., RICE, J. C., STRAHL, B. D., ALLIS, C. D. & GREWAL, S. I. 2001. Role of histone H3 lysine 9 methylation in epigenetic control of heterochromatin assembly. *Science,* 292**,** 110-3.

NARITA, M., NUNEZ, S., HEARD, E., NARITA, M., LIN, A. W., HEARN, S. A., SPECTOR, D. L., HANNON, G. J. & LOWE, S. W. 2003. Rb-mediated heterochromatin formation and silencing of E2F target genes during cellular senescence. *Cell,* 113**,** 703-16.

NECHAEV, S. & ADELMAN, K. 2011. Pol II waiting in the starting gates: Regulating the transition from transcription initiation into productive elongation. *Biochim Biophys Acta,* 1809**,** 34-45.

NICHOLLS, J. 2006. Investigating protein complexes that are involved in the function and regulation of the human INK4a/ARF locus. *University of London Thesis*.

NICHOLS, W. W., MURPHY, D. G., CRISTOFALO, V. J., TOJI, L. H., GREENE, A. E. & DWIGHT, S. A. 1977. Characterization of a new human diploid cell strain, IMR-90. *Science,* 196**,** 60-3.

NIEFIND, K., GUERRA, B., ERMAKOWA, I. & ISSINGER, O. G. 2001. Crystal structure of human protein kinase CK2: insights into basic properties of the CK2 holoenzyme. *EMBO J,* 20**,** 5320-31.

NIEFIND, K., PUTTER, M., GUERRA, B., ISSINGER, O. G. & SCHOMBURG, D. 1999. GTP plus water mimic ATP in the active site of protein kinase CK2. *Nat Struct Biol,* 6**,** 1100-3.

NISHIKAWA, S., JAKT, L. M. & ERA, T. 2007. Embryonic stem-cell culture as a tool for developmental cell biology. *Nat Rev Mol Cell Biol,* 8**,** 502-7.

NOBORI, T., TAKABAYASHI, K., TRAN, P., ORVIS, L., BATOVA, A., YU, A. L. & CARSON, D. A. 1996. Genomic cloning of methylthioadenosine phosphorylase: a purine metabolic enzyme deficient in multiple different cancers. *Proc Natl Acad Sci U S A,* 93**,** 6203-8.

O-CHAROENRAT, P., RUSCH, V., TALBOT, S. G., SARKARIA, I., VIALE, A., SOCCI, N., NGAI, I., RAO, P. & SINGH, B. 2004. Casein kinase II alpha subunit and C1-inhibitor are independent predictors of outcome in patients with squamous cell carcinoma of the lung. *Clin Cancer Res,* 10**,** 5792-803.

O'HAGAN, H. M., MOHAMMAD, H. P. & BAYLIN, S. B. 2008. Double strand breaks can initiate gene silencing and SIRT1-dependent onset of DNA methylation in an exogenous promoter CpG island. *PLoS Genet,* 4**,** e1000155.

O'LOGHLEN, A., MUNOZ-CABELLO, A. M., GASPAR-MAIA, A., WU, H. A., BANITO, A., KUNOWSKA, N., RACEK, T., PEMBERTON, H. N., BEOLCHI, P., LAVIAL, F., MASUI, O., VERMEULEN, M., CARROLL, T., GRAUMANN, J., HEARD, E., DILLON, N., AZUARA, V., SNIJDERS, A. P., PETERS, G., BERNSTEIN, E. & GIL, J. 2012. MicroRNA regulation of Cbx7 mediates a switch of Polycomb orthologs during ESC differentiation. *Cell Stem Cell,* 10**,** 33-46.

OHM, J. E., MCGARVEY, K. M., YU, X., CHENG, L., SCHUEBEL, K. E., COPE, L., MOHAMMAD, H. P., CHEN, W., DANIEL, V. C., YU, W., BERMAN, D. M., JENUWEIN, T., PRUITT, K., SHARKIS, S. J., WATKINS, D. N., HERMAN, J. G. & BAYLIN, S. B. 2007. A stem cell-like chromatin pattern may predispose tumor suppressor genes to DNA hypermethylation and heritable silencing. *Nat Genet,* 39**,** 237-42.

OHTA, H., SAWADA, A., KIM, J. Y., TOKIMASA, S., NISHIGUCHI, S., HUMPHRIES, R. K., HARA, J. & TAKIHARA, Y. 2002. Polycomb group gene rae28 is required for sustaining activity of hematopoietic stem cells. *J Exp Med,* 195**,** 759-70.

OHTANI, N., ZEBEDEE, Z., HUOT, T. J., STINSON, J. A., SUGIMOTO, M., OHASHI, Y., SHARROCKS, A. D., PETERS, G. & HARA, E. 2001. Opposing effects of Ets and Id proteins on p16INK4a expression during cellular senescence. *Nature,* 409**,** 1067-70.

OLOVNIKOV, A. M. 1971. [Principle of marginotomy in template synthesis of polynucleotides]. *Dokl Akad Nauk SSSR,* 201**,** 1496-9.

OLSEN, B. B., RASMUSSEN, T., NIEFIND, K. & ISSINGER, O. G. 2008. Biochemical characterization of CK2alpha and alpha' paralogues and their derived holoenzymes: evidence for the existence of a heterotrimeric CK2alpha'-holoenzyme forming trimeric complexes. *Mol Cell Biochem,* 316**,** 37-47.

ORPHANIDES, G., LEROY, G., CHANG, C. H., LUSE, D. S. & REINBERG, D. 1998. FACT, a factor that facilitates transcript elongation through nucleosomes. *Cell,* 92**,** 105-16.

ORTEGA, S., MALUMBRES, M. & BARBACID, M. 2002. Cyclin D-dependent kinases, INK4 inhibitors and cancer. *Biochim Biophys Acta,* 1602**,** 73-87.

PAN, M. R., PENG, G., HUNG, W. C. & LIN, S. Y. 2011. Monoubiquitination of H2AX protein regulates DNA damage response signaling. *J Biol Chem,* 286**,** 28599-607.

PARK, I. K., QIAN, D., KIEL, M., BECKER, M. W., PIHALJA, M., WEISSMAN, I. L., MORRISON, S. J. & CLARKE, M. F. 2003. Bmi-1 is required for maintenance of adult self-renewing haematopoietic stem cells. *Nature,* 423**,** 302-5.

PARRINELLO, S., SAMPER, E., KRTOLICA, A., GOLDSTEIN, J., MELOV, S. & CAMPISI, J. 2003. Oxygen sensitivity severely limits the replicative lifespan of murine fibroblasts. *Nat Cell Biol,* 5**,** 741-7.

PARSONS, J. L., DIANOVA, II, FINCH, D., TAIT, P. S., STROM, C. E., HELLEDAY, T. & DIANOV, G. L. 2010. XRCC1 phosphorylation by CK2 is required for its stability and efficient DNA repair. *DNA Repair (Amst),* 9**,** 835-41.

PASINI, D., BRACKEN, A. P., HANSEN, J. B., CAPILLO, M. & HELIN, K. 2007. The polycomb group protein Suz12 is required for embryonic stem cell differentiation. *Mol Cell Biol,* 27**,** 3769-79.

PAVLETICH, N. P. 1999. Mechanisms of cyclin-dependent kinase regulation: structures of Cdks, their cyclin activators, and Cip and INK4 inhibitors. *J Mol Biol,* 287**,** 821-8.

PEMBERTON, H., ANDERTON, E., PATEL, P., BROOKES, S., STOCK, J., RODRIGUEZ-NIEDENFUHR, M., CHANDLER, H., RACEK, T., DE BREED, L., STEWART, A., MATTHEWS, N. & PETERS, G. Submitted. Multiple variants of Polycomb repressive complex 1 (PRC1) congregate at common sites in the human genome.

PEPPERKOK, R., LORENZ, P., ANSORGE, W. & PYERIN, W. 1994. Casein kinase II is required for transition of G0/G1, early G1, and G1/S phases of the cell cycle. *J Biol Chem,* 269**,** 6986-91.

PEPPERKOK, R., LORENZ, P., JAKOBI, R., ANSORGE, W. & PYERIN, W. 1991. Cell growth stimulation by EGF: inhibition through antisense-oligodeoxynucleotides demonstrates important role of casein kinase II. *Exp Cell Res,* 197**,** 245-53.

PETERS, A. H., MERMOUD, J. E., O'CARROLL, D., PAGANI, M., SCHWEIZER, D., BROCKDORFF, N. & JENUWEIN, T. 2002. Histone H3 lysine 9 methylation is an epigenetic imprint of facultative heterochromatin. *Nat Genet,* 30**,** 77-80.

PETRUK, S., SEDKOV, Y., RILEY, K. M., HODGSON, J., SCHWEISGUTH, F., HIROSE, S., JAYNES, J. B., BROCK, H. W. & MAZO, A. 2006. Transcription of bxd noncoding RNAs promoted by trithorax represses Ubx in cis by transcriptional interference. *Cell,* 127**,** 1209-21.

PIERRE, F., CHUA, P. C., O'BRIEN, S. E., SIDDIQUI-JAIN, A., BOURBON, P., HADDACH, M., MICHAUX, J., NAGASAWA, J., SCHWAEBE, M. K., STEFAN, E., VIALETTES, A., WHITTEN, J. P., CHEN, T. K., DARJANIA, L., STANSFIELD, R., BLIESATH, J., DRYGIN, D., HO, C., OMORI, M., PROFFITT, C., STREINER, N., RICE, W. G., RYCKMAN, D. M. & ANDERES, K. 2011. Pre-clinical characterization of CX-4945, a potent and selective small molecule inhibitor of CK2 for the treatment of cancer. *Mol Cell Biochem,* 356**,** 37-43.

POLO, S. E. & JACKSON, S. P. 2011. Dynamics of DNA damage response proteins at DNA breaks: a focus on protein modifications. *Genes Dev,* 25**,** 409-33.

PRAY-GRANT, M. G., DANIEL, J. A., SCHIELTZ, D., YATES, J. R., 3RD & GRANT, P. A. 2005. Chd1 chromodomain links histone H3 methylation with SAGA- and SLIK-dependent acetylation. *Nature,* 433**,** 434-8.

PYERIN, W. & ACKERMANN, K. 2003. The genes encoding human protein kinase CK2 and their functional links. *Prog Nucleic Acid Res Mol Biol,* 74**,** 239-73.

QUELLE, D. E., ZINDY, F., ASHMUN, R. A. & SHERR, C. J. 1995. Alternative reading frames of the INK4a tumor suppressor gene encode two unrelated proteins capable of inducing cell cycle arrest. *Cell,* 83**,** 993-1000.

RASTELLI, L., CHAN, C. S. & PIRROTTA, V. 1993. Related chromosome binding sites for zeste, suppressors of zeste and Polycomb group proteins in Drosophila and their dependence on Enhancer of zeste function. *EMBO J,* 12**,** 1513-22.

REIJNEN, M. J., HAMER, K. M., DEN BLAAUWEN, J. L., LAMBRECHTS, C., SCHONEVELD, I., VAN DRIEL, R. & OTTE, A. P. 1995. Polycomb and bmi-1 homologs are expressed in overlapping patterns in Xenopus embryos and are able to interact with each other. *Mech Dev,* 53**,** 35-46.

REYA, T., MORRISON, S. J., CLARKE, M. F. & WEISSMAN, I. L. 2001. Stem cells, cancer, and cancer stem cells. *Nature,* 414**,** 105-11.

RINGROSE, L., EHRET, H. & PARO, R. 2004. Distinct contributions of histone H3 lysine 9 and 27 methylation to locus-specific stability of polycomb complexes. *Mol Cell,* 16**,** 641-53.

RINGROSE, L. & PARO, R. 2004. Epigenetic regulation of cellular memory by the Polycomb and Trithorax group proteins. *Annu Rev Genet,* 38**,** 413-43.

RINN, J. L., KERTESZ, M., WANG, J. K., SQUAZZO, S. L., XU, X., BRUGMANN, S. A., GOODNOUGH, L. H., HELMS, J. A., FARNHAM, P. J., SEGAL, E. & CHANG, H. Y. 2007. Functional demarcation of active and silent chromatin domains in human HOX loci by noncoding RNAs. *Cell,* 129**,** 1311-23.

ROBERTS, R. J., VINCZE, T., POSFAI, J. & MACELIS, D. 2010. REBASE--a database for DNA restriction and modification: enzymes, genes and genomes. *Nucleic Acids Res,* 38**,** D234-6.

ROUET, P., SMIH, F. & JASIN, M. 1994. Introduction of double-strand breaks into the genome of mouse cells by expression of a rare-cutting endonuclease. *Mol Cell Biol,* 14**,** 8096-106.

RUAS, M. & PETERS, G. 1998. The p16INK4a/CDKN2A tumor suppressor and its relatives. *Biochim Biophys Acta,* 1378**,** F115-77.

RUZZENE, M., PENZO, D. & PINNA, L. A. 2002. Protein kinase CK2 inhibitor 4,5,6,7-tetrabromobenzotriazole (TBB) induces apoptosis and caspase-dependent degradation of haematopoietic lineage cell-specific protein 1 (HS1) in Jurkat cells. *Biochem J,* 364**,** 41-7.

RYU, S. W., WOO, J. H., KIM, Y. H., LEE, Y. S., PARK, J. W. & BAE, Y. S. 2006. Downregulation of protein kinase CKII is associated with cellular senescence. *FEBS Lett,* 580**,** 988-94.

SANCHEZ, C., SANCHEZ, I., DEMMERS, J. A., RODRIGUEZ, P., STROUBOULIS, J. & VIDAL, M. 2007. Proteomics analysis of Ring1B/Rnf2 interactors identifies a novel complex with the Fbxl10/Jhdm1B histone demethylase and the Bcl6 interacting corepressor. *Mol Cell Proteomics,* 6**,** 820-34.

SANCHEZ-ELSNER, T., GOU, D., KREMMER, E. & SAUER, F. 2006. Noncoding RNAs of trithorax response elements recruit Drosophila Ash1 to Ultrabithorax. *Science,* 311**,** 1118-23.

SANTOS-ROSA, H., SCHNEIDER, R., BERNSTEIN, B. E., KARABETSOU, N., MORILLON, A., WEISE, C., SCHREIBER, S. L., MELLOR, J. & KOUZARIDES, T. 2003. Methylation of histone H3 K4 mediates association of the Isw1p ATPase with chromatin. *Mol Cell,* 12**,** 1325-32.

SARNO, S., REDDY, H., MEGGIO, F., RUZZENE, M., DAVIES, S. P., DONELLA-DEANA, A., SHUGAR, D. & PINNA, L. A. 2001. Selectivity of 4,5,6,7-tetrabromobenzotriazole, an ATP site-directed inhibitor of protein kinase CK2 ('casein kinase-2'). *FEBS Lett,* 496**,** 44-8.

SAURIN, A. J., SHAO, Z., ERDJUMENT-BROMAGE, H., TEMPST, P. & KINGSTON, R. E. 2001. A Drosophila Polycomb group complex includes Zeste and dTAFII proteins. *Nature,* 412**,** 655-60.

SAURIN, A. J., SHIELS, C., WILLIAMSON, J., SATIJN, D. P., OTTE, A. P., SHEER, D. & FREEMONT, P. S. 1998. The human polycomb group complex associates with pericentromeric heterochromatin to form a novel nuclear domain. *J Cell Biol,* 142**,** 887-98.

SCHLESINGER, Y., STRAUSSMAN, R., KESHET, I., FARKASH, S., HECHT, M., ZIMMERMAN, J., EDEN, E., YAKHINI, Z., BEN-SHUSHAN, E., REUBINOFF, B. E., BERGMAN, Y., SIMON, I. & CEDAR, H. 2007. Polycomb-mediated methylation on Lys27 of histone H3 pre-marks genes for de novo methylation in cancer. *Nat Genet,* 39**,** 232-6.

SCHMITT, S., PRESTEL, M. & PARO, R. 2005. Intergenic transcription through a polycomb group response element counteracts silencing. *Genes Dev,* 19**,** 697-708.

SCHOEFTNER, S. & BLASCO, M. A. 2009. A 'higher order' of telomere regulation: telomere heterochromatin and telomeric RNAs. *EMBO J,* 28**,** 2323-36.

SCHOEFTNER, S., SENGUPTA, A. K., KUBICEK, S., MECHTLER, K., SPAHN, L., KOSEKI, H., JENUWEIN, T. & WUTZ, A. 2006. Recruitment of PRC1 function at the initiation of X inactivation independent of PRC2 and silencing. *EMBO J,* 25**,** 3110-22.

SCHUETTENGRUBER, B., MARTINEZ, A. M., IOVINO, N. & CAVALLI, G. 2011. Trithorax group proteins: switching genes on and keeping them active. *Nat Rev Mol Cell Biol,* 12**,** 799-814.

SCHWARTZ, Y. B., KAHN, T. G., NIX, D. A., LI, X. Y., BOURGON, R., BIGGIN, M. & PIRROTTA, V. 2006. Genome-wide analysis of Polycomb targets in Drosophila melanogaster. *Nat Genet,* 38**,** 700-5.

SCOTT, C. L., GIL, J., HERNANDO, E., TERUYA-FELDSTEIN, J., NARITA, M., MARTINEZ, D., VISAKORPI, T., MU, D., CORDON-CARDO, C., PETERS, G., BEACH, D. & LOWE, S. W. 2007. Role of the chromobox protein CBX7 in lymphomagenesis. *Proc Natl Acad Sci U S A,* 104**,** 5389-94.

SCULLY, R., CHEN, J., PLUG, A., XIAO, Y., WEAVER, D., FEUNTEUN, J., ASHLEY, T. & LIVINGSTON, D. M. 1997. Association of BRCA1 with Rad51 in mitotic and meiotic cells. *Cell,* 88**,** 265-75.

SERRANO, M., LIN, A. W., MCCURRACH, M. E., BEACH, D. & LOWE, S. W. 1997. Oncogenic ras provokes premature cell senescence associated with accumulation of p53 and p16INK4a. *Cell,* 88**,** 593-602.

SHAO, Z., RAIBLE, F., MOLLAAGHABABA, R., GUYON, J. R., WU, C. T., BENDER, W. & KINGSTON, R. E. 1999. Stabilization of chromatin structure by PRC1, a Polycomb complex. *Cell,* 98**,** 37-46.

SHARPLESS, N. E. 2005. INK4a/ARF: a multifunctional tumor suppressor locus. *Mutat Res,* 576**,** 22-38.

SHARPLESS, N. E., RAMSEY, M. R., BALASUBRAMANIAN, P., CASTRILLON, D. H. & DEPINHO, R. A. 2004. The differential impact of p16(INK4a) or p19(ARF) deficiency on cell growth and tumorigenesis. *Oncogene,* 23**,** 379-85.

SHERR, C. J. 2000. The Pezcoller lecture: cancer cell cycles revisited. *Cancer Res,* 60**,** 3689-95.

SHERR, C. J. & ROBERTS, J. M. 1999. CDK inhibitors: positive and negative regulators of G1-phase progression. *Genes Dev,* 13**,** 1501-12.

SING, A., PANNELL, D., KARAISKAKIS, A., STURGEON, K., DJABALI, M., ELLIS, J., LIPSHITZ, H. D. & CORDES, S. P. 2009. A vertebrate Polycomb response element governs segmentation of the posterior hindbrain. *Cell,* 138**,** 885-97.

SLIFER, E. H. 1942. A mutant stock of Drosophila with extra sex-combs. *J. exp. Xool.,* 90**,** 31-40.

SNIPPERT, H. J. & CLEVERS, H. 2011. Tracking adult stem cells. *EMBO Rep,* 12**,** 113-22.

SPARMANN, A. & VAN LOHUIZEN, M. 2006. Polycomb silencers control cell fate, development and cancer. *Nat Rev Cancer,* 6**,** 846-56.

STEWART, G. S. 2009. Solving the RIDDLE of 53BP1 recruitment to sites of damage. *Cell Cycle,* 8**,** 1532-8.

STOCK, J. K., GIADROSSI, S., CASANOVA, M., BROOKES, E., VIDAL, M., KOSEKI, H., BROCKDORFF, N., FISHER, A. G. & POMBO, A. 2007. Ring1-mediated

ubiquitination of H2A restrains poised RNA polymerase II at bivalent genes in mouse ES cells. *Nat Cell Biol,* 9**,** 1428-35.

STRUHL, K. 1998. Histone acetylation and transcriptional regulatory mechanisms. *Genes Dev,* 12**,** 599-606.

TAKAI, H., SMOGORZEWSKA, A. & DE LANGE, T. 2003. DNA damage foci at dysfunctional telomeres. *Curr Biol,* 13**,** 1549-56.

TAVARES, L., DIMITROVA, E., OXLEY, D., WEBSTER, J., POOT, R., DEMMERS, J., BEZSTAROSTI, K., TAYLOR, S., URA, H., KOIDE, H., WUTZ, A., VIDAL, M., ELDERKIN, S. & BROCKDORFF, N. 2012. RYBP-PRC1 complexes mediate H2A ubiquitylation at polycomb target sites independently of PRC2 and H3K27me3. *Cell,* 148**,** 664-78.

TAWFIC, S., YU, S., WANG, H., FAUST, R., DAVIS, A. & AHMED, K. 2001. Protein kinase CK2 signal in neoplasia. *Histol Histopathol,* 16**,** 573-82.

TRIMARCHI, J. M., FAIRCHILD, B., WEN, J. & LEES, J. A. 2001. The E2F6 transcription factor is a component of the mammalian Bmi1-containing polycomb complex. *Proc Natl Acad Sci U S A,* 98**,** 1519-24.

TROJER, P., CAO, A. R., GAO, Z., LI, Y., ZHANG, J., XU, X., LI, G., LOSSON, R., ERDJUMENT-BROMAGE, H., TEMPST, P., FARNHAM, P. J. & REINBERG, D. 2011. L3MBTL2 protein acts in concert with PcG protein-mediated monoubiquitination of H2A to establish a repressive chromatin structure. *Mol Cell,* 42**,** 438-50.

UZIEL, T., LERENTHAL, Y., MOYAL, L., ANDEGEKO, Y., MITTELMAN, L. & SHILOH, Y. 2003. Requirement of the MRN complex for ATM activation by DNA damage. *EMBO J,* 22**,** 5612-21.

VAKOC, C. R., MANDAT, S. A., OLENCHOCK, B. A. & BLOBEL, G. A. 2005. Histone H3 lysine 9 methylation and HP1gamma are associated with transcription elongation through mammalian chromatin. *Mol Cell,* 19**,** 381-91.

VAN ATTIKUM, H. & GASSER, S. M. 2009. Crosstalk between histone modifications during the DNA damage response. *Trends Cell Biol,* 19**,** 207-17.

VAN KEMENADE, F. J., RAAPHORST, F. M., BLOKZIJL, T., FIERET, E., HAMER, K. M., SATIJN, D. P., OTTE, A. P. & MEIJER, C. J. 2001. Coexpression of BMI-1 and EZH2 polycomb-group proteins is associated with cycling cells and degree of malignancy in B-cell non-Hodgkin lymphoma. *Blood,* 97**,** 3896-901.

VAN LOHUIZEN, M., VERBEEK, S., SCHEIJEN, B., WIENTJENS, E., VAN DER GULDEN, H. & BERNS, A. 1991. Identification of cooperating oncogenes in E mu-myc transgenic mice by provirus tagging. *Cell,* 65**,** 737-52.

VANDAMME, J., VOLKEL, P., ROSNOBLET, C., LE FAOU, P. & ANGRAND, P. O. 2011. Interaction proteomics analysis of polycomb proteins defines distinct PRC1 complexes in mammalian cells. *Mol Cell Proteomics,* 10**,** M110 002642.

VARAMBALLY, S., DHANASEKARAN, S. M., ZHOU, M., BARRETTE, T. R., KUMAR-SINHA, C., SANDA, M. G., GHOSH, D., PIENTA, K. J., SEWALT, R. G., OTTE, A. P.,

RUBIN, M. A. & CHINNAIYAN, A. M. 2002. The polycomb group protein EZH2 is involved in progression of prostate cancer. *Nature,* 419**,** 624-9.

VINCENZ, C. & KERPPOLA, T. K. 2008. Different polycomb group CBX family proteins associate with distinct regions of chromatin using nonhomologous protein sequences. *Proc Natl Acad Sci U S A,* 105**,** 16572-7.

VIRE, E., BRENNER, C., DEPLUS, R., BLANCHON, L., FRAGA, M., DIDELOT, C., MOREY, L., VAN EYNDE, A., BERNARD, D., VANDERWINDEN, J. M., BOLLEN, M., ESTELLER, M., DI CROCE, L., DE LAUNOIT, Y. & FUKS, F. 2006. The Polycomb group protein EZH2 directly controls DNA methylation. *Nature,* 439**,** 871-4.

VONCKEN, J. W., SCHWEIZER, D., AAGAARD, L., SATTLER, L., JANTSCH, M. F. & VAN LOHUIZEN, M. 1999. Chromatin-association of the Polycomb group protein BMI1 is cell cycle-regulated and correlates with its phosphorylation status. *J Cell Sci,* 112 (Pt 24)**,** 4627-39.

WANG, D. & JANG, D. J. 2009. Protein kinase CK2 regulates cytoskeletal reorganization during ionizing radiation-induced senescence of human mesenchymal stem cells. *Cancer Res,* 69**,** 8200-7.

WANG, G., UNGER, G., AHMAD, K. A., SLATON, J. W. & AHMED, K. 2005. Downregulation of CK2 induces apoptosis in cancer cells--a potential approach to cancer therapy. *Mol Cell Biochem,* 274**,** 77-84.

WANG, H., WANG, L., ERDJUMENT-BROMAGE, H., VIDAL, M., TEMPST, P., JONES, R. S. & ZHANG, Y. 2004a. Role of histone H2A ubiquitination in Polycomb silencing. *Nature,* 431**,** 873-8.

WANG, L., BROWN, J. L., CAO, R., ZHANG, Y., KASSIS, J. A. & JONES, R. S. 2004b. Hierarchical recruitment of polycomb group silencing complexes. *Mol Cell,* 14**,** 637-46.

WANG, R., ILANGOVAN, U., ROBINSON, A. K., SCHIRF, V., SCHWARZ, P. M., LAFER, E. M., DEMELER, B., HINCK, A. P. & KIM, C. A. 2008. Structural transitions of the RING1B C-terminal region upon binding the polycomb cbox domain. *Biochemistry,* 47**,** 8007-15.

WANG, R., TAYLOR, A. B., LEAL, B. Z., CHADWELL, L. V., ILANGOVAN, U., ROBINSON, A. K., SCHIRF, V., HART, P. J., LAFER, E. M., DEMELER, B., HINCK, A. P., MCEWEN, D. G. & KIM, C. A. 2010. Polycomb group targeting through different binding partners of RING1B C-terminal domain. *Structure,* 18**,** 966-75.

WATSON, J. D. 1972. Origin of concatemeric T7 DNA. *Nat New Biol,* 239**,** 197-201.

WIDSCHWENDTER, M., FIEGL, H., EGLE, D., MUELLER-HOLZNER, E., SPIZZO, G., MARTH, C., WEISENBERGER, D. J., CAMPAN, M., YOUNG, J., JACOBS, I. & LAIRD, P. W. 2007. Epigenetic stem cell signature in cancer. *Nat Genet,* 39**,** 157-8.

WOO, C. J., KHARCHENKO, P. V., DAHERON, L., PARK, P. J. & KINGSTON, R. E. 2010. A region of the human HOXD cluster that confers polycomb-group responsiveness. *Cell,* 140**,** 99-110.

XU, X., TOSELLI, P. A., RUSSELL, L. D. & SELDIN, D. C. 1999. Globozoospermia in mice lacking the casein kinase II alpha' catalytic subunit. *Nat Genet,* 23**,** 118-21.

YAMANE, K. & KINSELLA, T. J. 2005. CK2 inhibits apoptosis and changes its cellular localization following ionizing radiation. *Cancer Res,* 65**,** 4362-7.

YAP, K. L., LI, S., MUNOZ-CABELLO, A. M., RAGUZ, S., ZENG, L., MUJTABA, S., GIL, J., WALSH, M. J. & ZHOU, M. M. 2010. Molecular interplay of the noncoding RNA ANRIL and methylated histone H3 lysine 27 by polycomb CBX7 in transcriptional silencing of INK4a. *Mol Cell,* 38**,** 662-74.

YATA, K., LLOYD, J., MASLEN, S., BLEUYARD, J. Y., SKEHEL, M., SMERDON, S. J. & ESASHI, F. 2012. Plk1 and CK2 act in concert to regulate Rad51 during DNA double strand break repair. *Mol Cell,* 45**,** 371-83.

YU, M., MAZOR, T., HUANG, H., HUANG, H. T., KATHREIN, K. L., WOO, A. J., CHOUINARD, C. R., LABADORF, A., AKIE, T. E., MORAN, T. B., XIE, H., ZACHAREK, S., TANIUCHI, I., ROEDER, R. G., KIM, C. F., ZON, L. I., FRAENKEL, E. & CANTOR, A. B. 2012. Direct recruitment of polycomb repressive complex 1 to chromatin by core binding transcription factors. *Mol Cell,* 45**,** 330-43.

ZENG, X., CHEN, S. & HUANG, H. 2011. Phosphorylation of EZH2 by CDK1 and CDK2: a possible regulatory mechanism of transmission of the H3K27me3 epigenetic mark through cell divisions. *Cell Cycle,* 10**,** 579-83.

ZHANG, C., VILK, G., CANTON, D. A. & LITCHFIELD, D. W. 2002. Phosphorylation regulates the stability of the regulatory CK2beta subunit. *Oncogene,* 21**,** 3754-64.

ZHANG, R., CHEN, W. & ADAMS, P. D. 2007. Molecular dissection of formation of senescence-associated heterochromatin foci. *Mol Cell Biol,* 27**,** 2343-58.